



# Rock Slope Stability 2021

## Symposium Rock Slope Stability 2021

November 17 and 18, 2021



Chutes de Blocs  
Risques Rocheux  
Ouvrages de Protection



# Table of contents

<b>List of sponsors</b>	<b>4</b>
<b>Site investigation and rockfall hazard modelling</b>	<b>1</b>
Assessment of the stability of the Bonifacio cliff in the Citadel sector, Thoraval Alain . . . . .	1
Contribution of Artificial Intelligence models for the management of rockfall risks, Chanut Marie-Aurélie [et al.] . . . . .	4
Effect of sample size on the prediction of survival probability of brittle spheres, Buzzi Olivier [et al.] . . . . .	6
Estimating rockfall release scenarios based on a simple rockfall frequency tool, Moos Christine [et al.] . . . . .	9
Joint inversion of electrical resistivity and P-wave velocity data to evaluate the damage degree of supporting pillars in an underground cave, Burgundy (France), Car- rier Aurore [et al.] . . . . .	11
Mapping release areas and mobility of rockfall and rock avalanches in the French Alps high mountain, Cathala Maëva [et al.] . . . . .	13
Modelling Rotational Drag in Rockfall Dynamics, Munch Jessica [et al.] . . . . .	15
Presentation of a methodology for determining rockfall hazard, Halbwegs Camille [et al.] . . . . .	17
Prédiction de scénarios d'embâcle avec le modèle de couche-mince ShalTOP, Levy Clara [et al.] . . . . .	19
Results of Real Scale Block Shape/Mass Experiments, Chant Sura, Switzer- land, Caviezel Andrin [et al.] . . . . .	21

Slope instabilities of the Larzac Plateau: the Pégairolles-de-l’Escalette rotational landslide, Elkharrat Kévin [et al.] . . . . .	23
Small scale rock fall experiments and statistical laws for run-out, Daudon Dominique [et al.] . . . . .	25
TLS- and inventory-based Magnitude – Frequency relationship for rockfall in Montserrat and Castellfollit de la Roca, Janeras Marc [et al.] . . . . .	27
<b>Monitoring techniques</b>	<b>29</b>
Comparison of the effectiveness of the InSAR method in rocky areas and forested areas, Abbasimaedeh Pouyan [et al.] . . . . .	29
Inventory of ground instabilities on the western Mediterranean coast of Morocco (case of the region between Tetouan and Jebha), Tribak Haytam [et al.] . . . . .	32
Maintenance préventive et suivi non-destructif des ancrages rocheux Les outils issus des essais dynamiques et de leur corrélation aux essais statiques, Horb Corinne	34
Modelling Rock Wall Permafrost to Understand Rock Slope Failure, Magnin Florence [et al.] . . . . .	38
Monitoring unstable slopes with passive RFID, Le Breton Mathieu [et al.] . . . . .	40
Understanding the triggering processes of landslides with induced polarization, Vaudelet Pierre [et al.] . . . . .	42
<b>Rockfall trajectory analysis</b>	<b>44</b>
Determining realistic rockfall runout zones using simulated reach probability maps, Dorren Luuk [et al.] . . . . .	44
ELANA (Energy Line Angle Normalized Area): un outil d’aide à la cartographie de la propagation des chutes de blocs basée sur la méthode de la ligne d’énergie à différentes échelles, Levy Clara [et al.] . . . . .	47
Influence of scrubs on rockfall dynamics, Ringenbach Adrian [et al.] . . . . .	49
Objective comparison of block propagation models using the Platrock platform, Bourrier Franck [et al.] . . . . .	51
RAMMS Model Updates – Soil Scarring, Trees and Rotational Stability, Christen Marc [et al.] . . . . .	53

Unusual Debris Characteristics from the February 17, 2006, Guinsaigon, Leyte, Philippines, Rockslide, Gutierrez Marte . . . . .	55
<b>Risk management</b>	<b>57</b>
A rockfall risk database for the French Alps, Eckert Nicolas [et al.] . . . . .	57
Coastal cliff landslide susceptibility in Essaouira - Morocco, Khouz Abdellah . . .	60
Digitization and Building Information Modeling of rockfall protection's work-sites, Galandrin Clément [et al.] . . . . .	63
FEEDBACK ON THE 4D MONITORING AND ASSESSMENT OF ROCK-FALL AND HANGING GLACIER STABILITY (Taconnaz bassin, Chamonix, France), Berthet Johan [et al.] . . . . .	65
Feedback on four exemplary early warning systems for landslides, Coccia Stella .	67
Harmonisation des méthodes de calcul et de justification des soutènements des talus instables – Etude du cas de la route entre Marrakech et Ouarzazate, Jabri Imane [et al.] . . . . .	69
Quantitative rockfall risk analysis for railway using 2D block propagation simulations, Farvacque Manon . . . . .	71
Seeking improvements to landslide operational management through case studies, Chollier Pauline [et al.] . . . . .	74
<b>Protection structures</b>	<b>76</b>
5 MJ energy impact test on a slender reinforced soil embankment, Korini Oltion [et al.] . . . . .	76
A new method for the design of rockfall fences by surrogate modelling, Dugelas Loic [et al.] . . . . .	79
An innovative Early Warning System for rockfall and debris flow protection structures, Grimod Alberto . . . . .	81
Assessment of the robustness of a numerical model of Bloc Armé® rockfall protection walls considering high energies impacts on real-scale structures, Furet Agathe [et al.] . . . . .	83
Bringing certified rockfall barriers to their realistic limits, Hofmann Helene [et al.]	85

DEM Modelling of the ELITE rockfall flexible barrier: a new net model introducing sliding, Dugelas Loic [et al.] . . . . .	87
Forest flexible fences: increasing their energy capacity, Olmedo Ignacio [et al.] . .	89
High energy impacts for assessing the Bloc Armé® technology as rockfall protection, Furet Agathe [et al.] . . . . .	91
Monitoring debris flow flexible fences for design purposes, Olmedo Ignacio [et al.]	93
Numerical modelling of full-scale rockfall protection structures under dynamic impact using discrete element method, Rafiee Ali [et al.] . . . . .	96
Simulation des essais d'arrachement des ancrages passifs par une méthode au module de réaction axial, Serratrice Jean François . . . . .	98
<b>Case studies</b>	<b>100</b>
Application of a high-frequency radar for early warning of a rock-fall hazard in the Pitztal valley, Schöffl Tobias [et al.] . . . . .	100
Innovative rockfall alarm system with automatic road closure at Axenstrasse, Switzerland, Stähly Severin [et al.] . . . . .	103
Rock slope cutting works near fragile speleothems: Choranche case study (Vercors, France), Bottelin Pierre [et al.] . . . . .	105
Temperature distribution in a permafrost-affected rock ridge from conductivity and induced polarization tomography, Duvillard Pierre-Allain . . . . .	107
<b>Keynotes</b>	<b>110</b>
30 years of Rockfall Engineering research at PoliTO, De Biagi Valerio . . . . .	110
Inspection, assessment and maintenance of rock slopes and excavated caverns of hydroelectric schemes for safety and sustainability, Quirion Marco . . . . .	114
The Cliets, two major rockfalls at the Arly river (2014, 2019, Savoie, France), Lescurier Anne [et al.] . . . . .	116
<b>Author Index</b>	<b>117</b>

# List of sponsors



**GEOBRUGG**

Safety is our nature - fidèles à ce principe directeur, Geobrugg développe et fabrique des solutions de protection depuis 1951. Les filets en fil d'acier haute résistance et les services correspondants surveillent et protègent contre les risques naturels tels que les chutes de pierres, les glissements de terrain, les laves torrentielles, les avalanches ou l'érosion côtière. Ils assurent la sécurité dans les mines et les tunnels, ainsi que sur les pistes de sport automobile, dans l'industrie et dans les installations d'essai. Grâce à l'expérience, à l'esprit de recherche, à la formation interne continue et à l'étroite collaboration avec les instituts de recherche, Geobrugg à l'origine d'innovations et de normes industrielles.



**GINGER CEBTP**

Ginger CEBTP, filiale de la branche construction du groupe Ginger, est leader en France pour l'ingénierie des sols, les essais sur les matériaux et la santé des ouvrages et des bâtiments. Il intervient en tant que bureau d'études auprès de tous les acteurs de la construction dans l'accompagnement des projets des plus simples aux plus complexes. Ginger CEBTP compte aujourd'hui plus de 1000 collaborateurs présents sur toute la France et à l'Ile de la Réunion. Tout au long du cycle de vie d'un ouvrage quel qu'il soit, Ginger CEBTP offre une prise en charge globale des missions d'expertises en se positionnant sur une chaîne de valeur unique : PRÉLEVER – ANALYSER – DIAGNOSTIQUER – RECOMMANDER



**Région Auvergne-Rhône-Alpes**

Avec ses 7,9M d'habitants Auvergne-Rhône-Alpes est la 1re région industrielle française (500000 emplois) et 2e région exportatrice de France. Son économie est avant tout tertiaire, mais aussi industrielle.



**INRAE**

INRAE, l'institut national de recherche pour l'agriculture, l'alimentation et l'environnement, est le premier organisme de recherche mondial spécialisé sur ces trois domaines scientifiques. Relever ces défis en proposant par la recherche, l'innovation et l'appui aux politiques publiques

de nouvelles orientations pour transformer durablement l'agriculture, l'alimentation et l'environnement, telle est son ambition. Grâce à la richesse de ses collectifs de recherche, INRAE met en oeuvre une recherche finalisée, associant science fondamentale et appliquée, approches disciplinaires et interdisciplinaires. L'institut s'appuie sur un dispositif d'infrastructures de recherche et d'unités expérimentales unique en Europe. INRAE adopte résolument les démarches de science ouverte et participative associant toujours plus les citoyens.

# Site investigation and rockfall hazard modelling

## Modeling of the stability of the Bonifacio cliff in the Citadel sector

Alain THORAVAL<sup>1</sup>, Christian FRANCK, Stella Coccia, Baptiste VIGNEROT<sup>2</sup>

**Keywords:** cliff stability, geomechanics, fracture, Bonifacio, 3DEC, UDEC

### ABSTRACT IN ENGLISH

The work presented in this paper is part of the hazard and risk assessment study related to the Citadel of Bonifacio (department of Southern Corsica) located partly on a cliff overhanging up to 20 m. The objective was to provide elements for improving the qualification and quantification of the “massive collapse” hazard.

### ABSTRACT IN FRENCH

Les travaux présentés dans cet article s'inscrivent dans le cadre de l'étude d'évaluation des dangers et des risques liés à la Citadelle de Bonifacio (département de la Corse du Sud) située en partie sur une falaise surplombant jusqu'à 20 m. L'objectif était de fournir des éléments permettant d'améliorer la qualification et la quantification de l'aléa « effondrement massif ».

## 1 INTRODUCTION

A hazard and risk assessment study, related to the Citadel of Bonifacio (department of Southern Corsica) located partly on a cliff overhanging up to 20 m, has been conducted at the request of the DDTM of Southern Corsica and with the help of BRGM and Cerema. The objective was to provide elements for improving the qualification and quantification of the “massive collapse” hazard in order to better assess, in a second step, the level of risk regarding public safety issues raised by such a major hazard. In the framework of this study the cliff was also instrumented to observe its evolution in real time for several years.

## 2 DESCRIPTION OF THE EVALUATION PROCESS

The selected rupture scenarios, already described by Cerema (2013), assume a predominant role of the overhang (the extension of which increases over time through erosion) and of the discontinuities which cut the cliff. They combine mechanisms considering: a tilting, then a detachment by rupture in traction of the overhanging part; landslides along discontinuities present in the cliff; a compression rupture of the foot of the cliff.

In order to verify the relevance of these scenarios and to help quantifying the hazard in the Citadel sector, various models have been produced. The models are based on the following data acquired in parts 1 and 2 of the study:

- geometry of the cliff face: Lidar measurements were carried out by Ineris using two laser scanners;
- geology: core drillings F1, F2 and F3, coordinated by the BRGM, making it possible to establish a simplified geological log with 4 lithologies L1, L2, L3 and L4 (the last one containing a softer geomechanical layer L4deg);
- fractures: HD photogrammetry (performed by the BRGM) showing the discontinuities of the model. The cliff is crossed by a vertical fracture oriented approximately N110, and vertical fractures oriented N20;
- geomechanical characteristics: determination of the geomechanical properties of the rockmass (from samples from the vertical borehole F3) done by Cerema

The modeling work was done in close collaboration with the Committee of Experts (EC) throughout the project. The discussions made it possible to gradually refine the objectives and the calculation assumptions, so that the results could be useful for the appraisal given the uncertainties of the available data.

## 3 DESCRIPTION OF THE MODELS

Preliminary models have been computed for an area near the Citadel, called Sutta-Rocca. This area is not crossed a priori, by any major fracture. The objective of these models was to assess the impact of the overhang (without the influence of any discontinuities) on the stability of the cliff. The models show that in its current state, the cliff is stable with a significant safety factor (greater than 3) even assuming an extension of the overhang of a few meters. The zones showing rupture (traction) remain very localized near the cliff front in the least resistant geological unit (L4deg) at the base of the cliff.

---

<sup>1</sup> THORAVAL Alain, Ineris, Nancy, FRANCE (ISO 3166-2:FR), alain.thoraval@ineris.fr

<sup>2</sup> Coordinateur du projet, rattaché au BRGM

Regarding the modeling carried out for the Citadel area, we first assessed the impact of the N110° fracture (without taking into account the N20°E fracture). We then observed that additional tensile ruptures appear in the L4 geological unit (located above L4deg) near the fracture. However, the safety factor obtained (with 3D models) remains higher than 3, whether the N110°E fracture is considered or not.

Secondly, we sought to assess the impact of the N20°E fracture on the stability of the Citadel area. Such a fracture was observed on the cliff near the parapet of the Place du Marché at the level of the geological unit L2 and L3. Apart from this case of the proven position of the N20°E (known as the N20min scenario), two hypothetical positions of the N20°E were studied, one at the level of the first bordering house on the Place du Marché (N20int scenario), the other beyond Place Manichella (scenario N20max), as well as an extension through the unit L1 or the other formations.

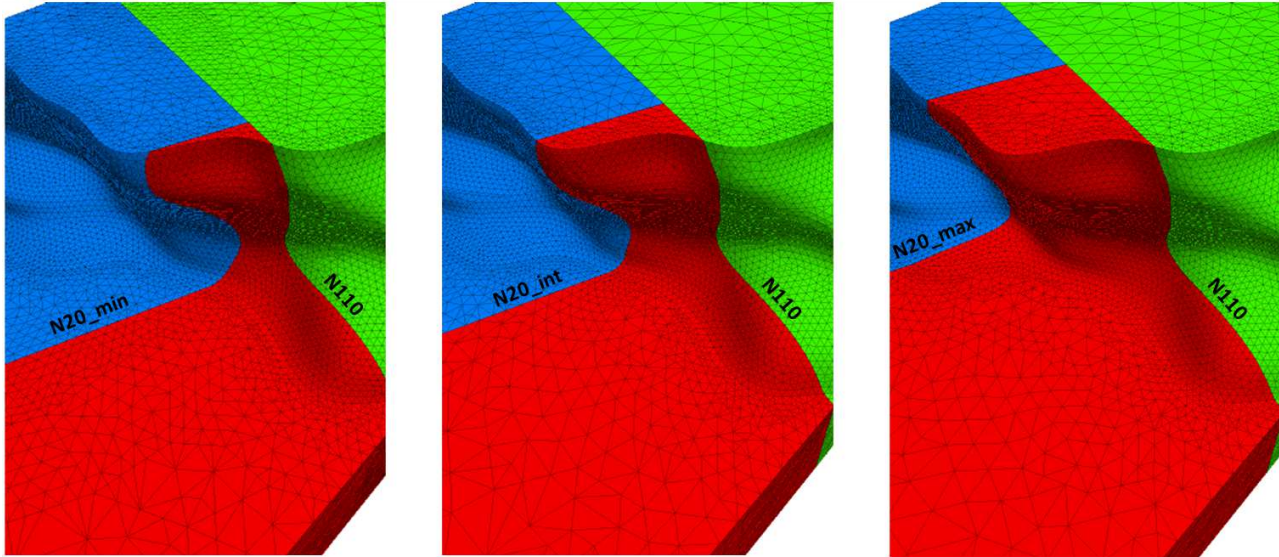


Figure 1: Cutting of 3D models with N110 and N20 fractures

Results show that the hypothesis in which the N20°E fracture would cut through all the units leads to a geometrically unstable model, and therefore is not plausible, except in the case where the N20°E fracture is at the "maximum" offset location, that is including Manichella square. In this case, the cliff would remain stable in all cases, whatever the extension of the N20°E fracture is, with a comfortable safety factor greater than 1.6.

If we consider that the fracture N20°E is in a "minimal" offset position, near the parapet of the Place du Marché, or "intermediate" one, at the level of the first bordering house on the Place du Marché, the safety factor is lower, all the more if we assume a possible extension of the N20°E fracture through the L1 unit to the surface.

## CONCLUSION

The models carried out have enabled us to improve our understanding of the failure mechanisms likely to develop within the cliff. We evaluated in each case the safety factor in the current state given the uncertainties about the geomechanical characteristics, the location and the extension of the N20 fractures. The main conclusion is that the block cut by the N110 and N20 fractures could become geometrically unstable by considering a so-called "minimal" or "intermediate" location of the N20 fracture.

Up to now, the evaluation of the impact of the overhang extension (sea cliff erosion) was carried out in a simplified way (2D). In the presence of a fracture, the 2D approach is no longer valid, given the high dependency of the results to the cross-section choice. A complementary 3D approach would be necessary to study the impact of the extension of the fractured overhang extension under the Citadel.

## REFERENCES

- Cerema (2013) Réalisation de la carte multi-aléas « mouvement de terrain » et « hydraulique » dans les secteurs à enjeux de la commune de Bonifacio. N° d'affaire 10R000046.
- Itasca Consulting Group, Inc. (1994) 3DEC 3-Dimensional Distinct Element Code, Version 1.5: Volume I : User's Manual.
- Thoraval Alain (2020) Amélioration de la connaissance de l'aléa « effondrement en grande masse » - Secteur de la citadelle, falaise de Bonifacio, rapport Ineris référencé Ineris-175501-2081373, septembre.

## Contribution of Artificial Intelligence models for the management of rockfall risks

Marie-Aurélié Chanut (corresponding author)<sup>1</sup>, Clara Lévy<sup>2</sup>, Lucas Meignan<sup>3</sup>, Muriel Gasc<sup>1</sup>, Abdourrahmane Atto<sup>4</sup>, Nickolas Stelzenmuller<sup>3</sup>, Guilherme Cunha de Barros-Santos<sup>1,2,3</sup>, Hermann Courteille<sup>4</sup>, Emmanuel Trouvé<sup>4</sup>, Sylvie Galichet<sup>4</sup>, Nicolas Meger<sup>4</sup>

**Keywords:** rockfall, climatic factors, risk management, Artificial Intelligence (AI) models

### ABSTRACT IN ENGLISH:

This paper proposes a methodology to evaluate the suitability of AI models to describe rockfalls triggered by several factors, such as meteorological and geological conditions. So, we aim to train neural networks with all relevant and available data that could effectively predict rockfalls. To achieve this goal, we have already selected appropriate sites, collected data at high temporal and spatial resolution, and we propose some relevant models for this task. Ultimately, this type of model could assist in the operational management of infrastructure, especially during major climatic events.

### ABSTRACT IN FRENCH:

Cette communication présente une méthodologie pour évaluer la pertinence des modèles type IA à décrire des chutes de blocs déclenchées par des facteurs multiples, tels que les conditions météorologiques et géologiques. Ainsi, nous voulons entraîner des modèles IA à prédire la probabilité de chute de pierres en partant des données pertinentes et disponibles. Pour atteindre ce but, nous présentons ici les sites d'études sélectionnés, les caractéristiques des données recueillies à haute résolution temporelle et spatiale, et enfin des typologies de réseaux de neurones appropriés. A terme, ce type de modèle représenterait un outil supplémentaire pour le management des infrastructures, particulièrement lors d'événements climatiques majeurs.

The role of climatic factors (precipitation, temperature variations and freeze/thaw cycles) in the triggering of rockfalls was evidenced in numerous publications (e.g. Hemstetter and Garambois, 2009; Delonca et al, 2014; D'amato et al, 2016). The quantification of this triggering role remains a difficult task for specific sites, challenging the operational management of infrastructures during major climatic events (road closures in connection with weather forecasts, deployment of monitoring, etc.). Classical multi-scale and multi-physical models integrate thermal, hydric and mechanical couplings to provide a coherent understanding and reliable prediction of phenomena and their impacts. In addition to these physical models, the approach proposed in this paper aims at learning from the data themselves to build predictive models of rockfalls using AI methods. The prediction of landslide behavior using such methods have been recently developed (Ma et al., 2018) while the use of AI for the prediction of rockfalls is still limited due to the scarcity of documented events.

## 1 SITES AND DATA

Two sites with documented rockfall events together with measurements of meteorological factors (precipitation, temperature or snowmelt) were selected in France: the RN1 road in La Réunion (974) and the Saint-Eynard cliff near Grenoble (38). In La Réunion (Figure 1), we study the rockfalls that reached the road using the database fed by RN1 management services where date, mass and location of the events are referenced. At the Saint-Eynard cliff site, we focus on the failure of the rocks from the cliff using seismic monitoring of rockfall collapses and high-frequency monitoring of topographic changes (at least every day) thanks to laser scans or photogrammetric acquisitions. In this latter case, we need data pre-processing to accurately date and describe rockfall events. At first level, rockfall events are daily recorded with locations, masses and meteorological data such as rains. Hereafter, other data will be integrated in the analysis such as geology, topography, and the presence of protective structures.

We perform initial tests of our methodology using event-rich databases from specific sites, in order to facilitate training and validation of the AI models and sites where the correlation between rockfalls and climatic factors has already been shown statistically. The generalization of other sites could be carried out in a second step.

1 Cerema, Team GeoCoD, 25 avenue François Mitterrand, 69674 Bron, France; [marie-aurelie.chanut@cerema.fr](mailto:marie-aurelie.chanut@cerema.fr); [muriel.gasc@cerema.fr](mailto:muriel.gasc@cerema.fr); [guilherme.cunha-de-barros-santos@cerema.fr](mailto:guilherme.cunha-de-barros-santos@cerema.fr)

2 BRGM, 45100 Orleans, France; [c.levy@brgm.fr](mailto:c.levy@brgm.fr)

3 Géolithe, 181, rue des Bécasses, 38920 Crolles, France; [lucas.meignan@geolithe.com](mailto:lucas.meignan@geolithe.com); [nickolas.stelzenmuller@geolithe.com](mailto:nickolas.stelzenmuller@geolithe.com)

4 Université Savoie Mont-Blanc, LISTIC, BP 80439 -Annecy le Vieux - 74944 Annecy; [emmanuel.trouve@univ-smb.fr](mailto:emmanuel.trouve@univ-smb.fr); [abdourrahmane.atto@univ-smb.fr](mailto:abdourrahmane.atto@univ-smb.fr); [nicolas.meger@univ-smb.fr](mailto:nicolas.meger@univ-smb.fr); [hermann.courteille@univ-smb.fr](mailto:hermann.courteille@univ-smb.fr); [sylvie.galichet@univ-smb.fr](mailto:sylvie.galichet@univ-smb.fr)

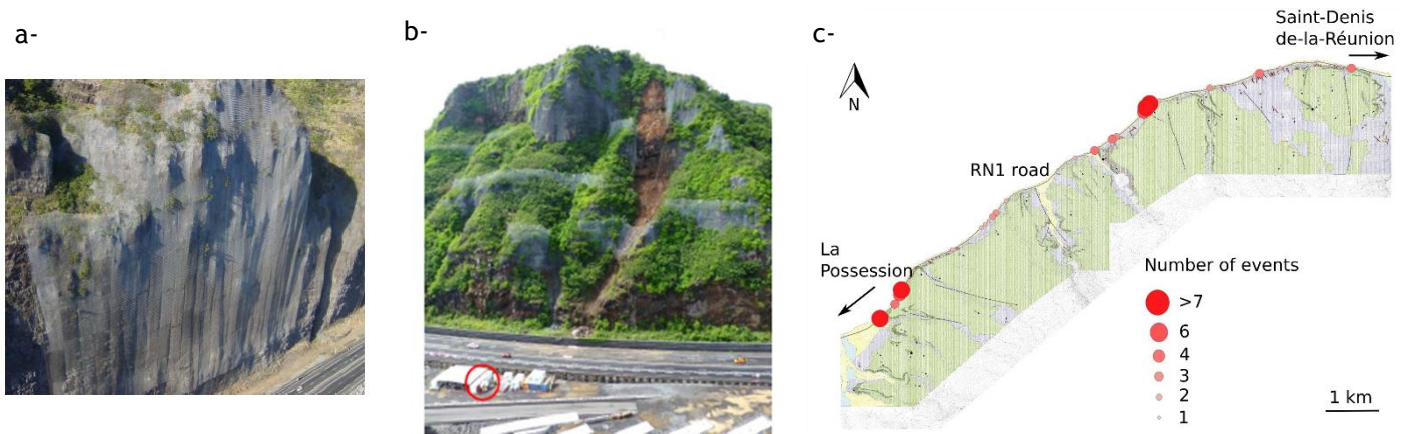


Figure 1: The RN1 Road in La Réunion : a- an example of the cliff overhanging the road, (b) a rockfall event, (c) rockfalls distribution along the RN1

## 2 METHODOLOGY TO CALIBRATE AND EVALUATE AI MODELS

Machine learning and its deep learning branch seem to be promising ways to induce predictive models of risk from the data itself. As previously mentioned, rockfalls are discrete events that are highly correlated with weather events which exhibit seasonal patterns. Therefore, we want to model the intensity of the point process (rate of falls during a period  $\Delta t$ ) with respect to exogenous variables such as rain, geological area ... A good challenger in such task could be Spiking Neural Networks (SNNs). Several calibrations of the neural networks are planned: first, a baseline with only dates and events, then others with external data and expertise (meteorological data, geology and topography) to improve performance. This approach will allow us to characterize more precisely the data and the minimum number of rockfall events needed to generate a relevant AI model. In addition, the validated results will be compared to the results of physical and statistical models.

## CONCLUSION

With the use of AI models, we expect to be able to identify more precisely the cause and effect relationships within complex data (rockfalls, meteorological, geological, topographic data) and to predict the evolution of the risk of rockfall according to meteorological conditions with sufficient confidence for the operational management of infrastructure. In particular, an application integrating meteorological forecasts would allow infrastructure managers to anticipate monitoring, protection or closure measures for the infrastructure.

## ACKNOWLEDGEMENTS

The authors would like to gratefully acknowledge the FEREC Fondation for funding this work. This work was carried out within the framework of the national C2ROP project and we thank the SNCF, CD 38 and CD 73 for their support and the CR La Réunion for sharing their data.

## REFERENCES

- D'Amato, J., Hantz, D., Guerin, A., Jaboyedoff, M., Baillet, L., Mariscal, A., (2016) Influence of meteorological factors on rockfall occurrence in a middle mountain limestone cliff. *Natural Hazards and Earth System Sciences*, 16, 719–735
- Delonca, A., Gunzburger, Y., and Verdel, T (2014) Statistical correlation between meteorological and rockfall databases, *Nat. Hazards Earth Syst. Sci.*, 14, 1953–1964.
- Hemstetter, A., Garambois, S., (2010) Seismic monitoring of Séchilienne rockslide (French Alps): Analysis of seismic signals and their correlation with rainfalls, *Journal of Geophysical Research: Earth Surface*, 115 (F3)
- Ma, J., Tang, H., Wen, T., and Liu, X. (2018) A hybrid approach for prediction of changes in landslide rates based on clustering and a decision tree, *Int. Arch. Photogramm. Remote Sens. Spatial Inf. Sci.*, XLII-3/W4, 335–341.

## Effect of sample size on the prediction of survival probability of brittle spheres

Olivier BUZZI<sup>1</sup>, Davide GUCCIONE<sup>2</sup>, Klaus THOENI<sup>3</sup>, Stephen FITYUS<sup>4</sup>, Anna GIACOMINI<sup>5</sup>

**Keywords:** rockfall, fragmentation, survival probability, statistical variability

Fragmentation of rocks during rockfall events is poorly understood and rarely modelled because it is a very complex phenomenon influenced by many factors. A novel model was recently proposed by the Authors (Guccione et al., 2021) to predict the survival probability (SP) of brittle spheres upon impact from the statistical analysis of Brazilian test results. The objective of this study is to assess how the size of the specimens tested in indirect tension in order provide the input data for the model influences the prediction of SP. To do so, Brazilian test data pertaining to different disc sizes will be used to predict the SP of 100 mm spheres and the different predictions will be compared.

### ABSTRACT IN ENGLISH:

This study deals with the prediction of likelihood of rock fragmentation at impact in the context of rockfall. In particular, the sensitivity of a recent predictive model developed by the authors to specimen size is investigated. The extensive test results show some influence of specimen size, although the predictions still fall very close to the experimental data.

### ABSTRACT IN FRENCH:

Cette étude traite de la prédiction de la probabilité de fragmentation des roches à l'impact. La sensibilité d'un récent modèle à la taille des échantillons testés est étudiée. Les résultats des tests montrent une certaine influence de la taille des échantillons, bien que les prédictions restent très proches des données expérimentales.

## 1 A MODEL TO PREDICT THE SURVIVAL PROBABILITY OF BRITTLE SPHERES IN DROP TESTS

The model is described in its entirety in Guccione et al. (2021) so, for a matter of conciseness, only its key aspects are recalled here. The model relies on the analogy between fragmentation at impact and failure in indirect tension (Brazilian test). To apply the model, the results of Brazilian tests are first analysed in terms of cumulative distribution of work required to fail the specimens in indirect tension (noted  $W_{BT}$ ). Then, for each value of  $W_{BT}$ , a corresponding SP value can be computed as one minus the cumulative frequency pertaining to work  $W_{BT}$ . The full SP curve (Weibull function) for  $W_{BT}$  can then be derived. Once this is done, the scale and shape parameters,  $W_{BT}^{cr}$  and  $m_{BT-W}$ , can be found. The SP of brittle spheres in drop tests is then predicted via another two Weibull parameters: a shape parameter  $m_E$  taken equal to  $m_{BT-W}$  and a scale parameter  $E_k^{cr}$  defined as:

$$E_k^{cr} = W_{BT}^{cr} \cdot C_{size} \cdot C_{shape} \cdot C_{rate} \quad (1)$$

where  $C_{size}$ ,  $C_{shape}$  and  $C_{rate}$  are conversion factors used to account for the difference in size, shape and loading rate between the specimens tested in Brazilian test and the spheres used in drop tests.  $C_{size}$  and  $C_{rate}$  are derived from Hertz's contact theory (Guccione et al., 2021). The equations of the conversion factors are not given here, for a matter of space. The SP for the brittle spheres in drop test corresponding to a given value of kinetic energy,  $SP(E_k)$  in %, is then expressed as:

$$SP(E_k) = (37 + 100 \cdot m_E / e) - E_k (100 \cdot m_E / e / E_k^{cr}) \quad (2)$$

Although the SP is expressed as a function of Weibull parameters, it was found that a linear relationship (Eq. 2) better matches

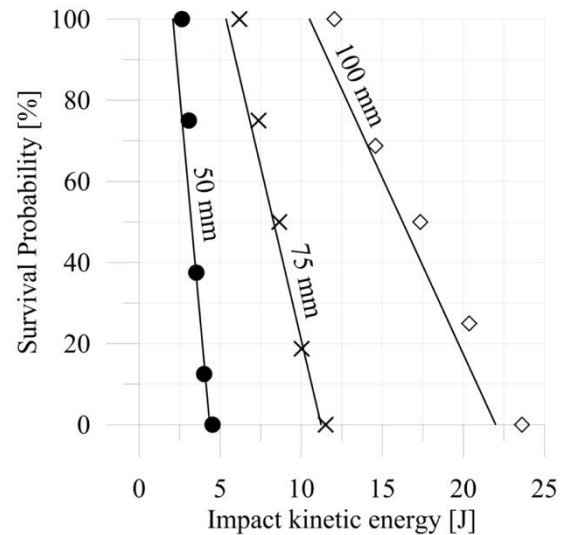


Figure 1: Experimental SP for 50 mm (circles), 75 mm (crosses) and 100 mm (diamonds) mortar spheres and model prediction for the same diameters (lines)

<sup>1</sup> BUZZI Olivier, University of Newcastle, Callaghan, NSW, Australia, [Olivier.buzzi@newcastle.edu.au](mailto:Olivier.buzzi@newcastle.edu.au)

<sup>2</sup> GUCCIONE Davide, University of Newcastle, Callaghan, NSW, Australia, [Davide.Guccione@uon.edu.au](mailto:Davide.Guccione@uon.edu.au)

<sup>3</sup> THOENI Klaus, University of Newcastle, Callaghan, NSW, Australia, [Klaus.Thoeni@newcastle.edu.au](mailto:Klaus.Thoeni@newcastle.edu.au)

<sup>4</sup> FITYUS Stephen, University of Newcastle, Callaghan, NSW, Australia, [Stephen.Fityus@newcastle.edu.au](mailto:Stephen.Fityus@newcastle.edu.au)

<sup>5</sup> GIACOMINI Anna, University of Newcastle, Callaghan, NSW, Australia, [Anna.Giacomini@newcastle.edu.au](mailto:Anna.Giacomini@newcastle.edu.au)

experimental observations (Guccione et al., 2021). The model was validated against experimental values of SP in drop tests for spheres having diameters of 50mm, 75mm and 100 mm using the fragmentation cell developed by Guccione et al. (2021). Figure 1 compares the experimental SP data to the model prediction for three different sphere diameters (see Guccione et al., 2021 for more details about the validation).

## 2 RESULTS

56 discs of 21mm, 53mm, 76mm in diameter and 20 discs of 154mm and 302mm in diameter were cast using the same mortar than that used for the experimental tests presented in Figure 1. The discs were cured for 4 weeks under a wet hessian before being fan-dried for 5 weeks. The discs were tested in indirect tension following the ISRM recommended method (1978). After each test, the area under the force-displacement curve, from beginning of loading to failure, was calculated in order to infer the amount of work required to reach failure. Table 1 shows, for each disc size, the results of the series of Brazilian tests, which constitutes the majority of model inputs (other inputs are the materials moduli and Poisson’s ratios and impact time in drop tests), the conversion factors and the model outputs, pertaining to the SP of 100 mm spheres in drop tests. Data in Table 1 indicate that the amount of work required to fail the specimens in indirect tension ( $W_{BT}^{cr}$ ) increases significantly with specimen diameter: there are three orders of magnitude between the lowest and highest values of work. As for the shape parameter  $m_{BT-W}$  (which indicates how flat the cumulative distribution of  $W_{BT}$  is), no clear correlation was found with specimen size, unlike what was suggested in Guccione et al. (2021).  $m_{BT-W}$  is taken as the shape parameter of the predicted SP ( $m_E$ ) as per Eq. (1).

**Table 1: Results of Brazilian tests for each specimen diameter (D) and thickness (T) and model outputs: time to failure ( $t_{BT}$ ), scale parameters for Weibull distribution of force ( $F_{BT}^{cr}$ ) and work ( $W_{BT}^{cr}$ ), shape parameters for Weibull distribution of force ( $m_{BT-F}$ ) and work ( $m_{BT-W}$ ), conversion factors ( $C_{size}$ ,  $C_{shape}$  and  $C_{rate}$ ), scale parameter ( $E_k^{cr}$ ), shape parameter ( $m_E$ ) and gradient (Grad., per Eq. 2) for the predicted survival probability of 100 mm spheres.**

Size [mm]		Results of Brazilian tests (model inputs)					Survival probability model outputs					
D	T	$W_{BT}^{cr}$	$m_{BT-W}$	$F_{BT}^{cr}$	$m_{BT-F}$	$t_{BT}$	$C_{shape}$	$C_{size}$	$C_{rate}$	$m_E$	$E_k^{cr}$	Grad.
21	12	0.04 J	3.54	0.78 kN	5.3	10 s	4.23	24.86	1.29	3.54	5.6 J	-23.1
53	27	0.54 J	4.91	5.40 kN	6.47	25 s	4.23	4.04	1.41	4.91	12.5 J	-14.4
76	39	0.94 J	3.24	10.45 kN	6.12	35 s	4.23	1.84	1.45	3.24	10.6 J	-11.2
154	77	12.7 J	3.14	36.7 kN	5.76	30 s	4.23	0.40	1.43	3.14	30.8 J	-3.8
302	149	45.8 J	3.94	101 kN	6.53	40 s	4.23	0.08	1.47	3.94	25.8 J	-5.6

The following can be observed regarding the conversion factors: the variations of time at failure ( $t_{BT}$ ) between specimens is a result of different loading rates and the higher  $t_{BT}$ , the higher  $C_{rate}$ . Given that the predictions of SP pertain to 100 mm spheres, all discs smaller than 100 mm in diameter have a  $C_{size} > 1$  while those larger than 100 mm have a  $C_{size} < 1$ . Finally,  $C_{shape}$  is constant because it is not diameter dependent. The combination of the three conversion factors (as per Eq. 1) has reduced the initial wide range of  $W_{BT}^{cr}$  (3 orders of magnitudes) to only a factor 5.5 between the lowest  $E_k^{cr}$  value (5.6J) and the highest one (30.8J). The slope and position of the predicted SPs plotted in Figure 2 appear to be sensitive to the diameter of the specimens used for the Brazilian tests. The slope of the SP depends both on  $E_k^{cr}$  (which increases with specimen diameter) and  $m_{BT-W}$  which does not seem to be size dependent (see Table 1). The experimental data fall in between the predicted SPs, which confirms the good predictive ability of the model.

## CONCLUSION

A novel model was recently proposed by the authors to predict the survival probability of brittle spheres in drop tests from statistical data of Brazilian tests. The results presented in this abstract highlight a slight dependence of the prediction on the size of the specimens used for the Brazilian tests and confirm the predictive ability of the model. It is important to bear in mind that the results are linked to the distribution of internal cracks, which can be very different in actual rocks and in spheres cast using mortar.

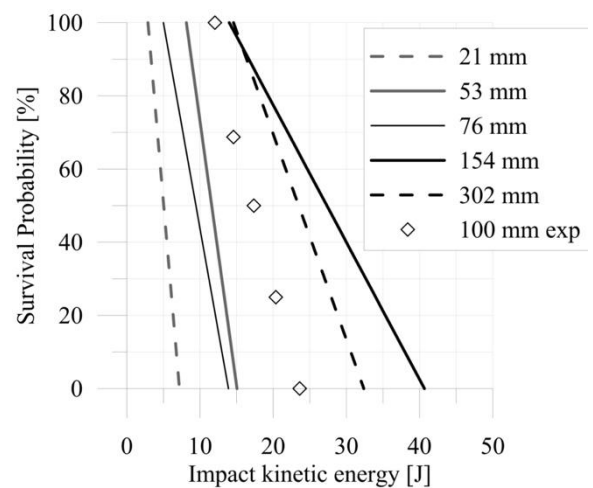


**Figure 2: Survival probability in drop tests for 100 mm spheres, predicted from the model developed by Guccione et al. (2021) and using the inputs of Table 1, for different diameters of specimens tested in indirect tension (Brazilian tests).**

## REFERENCES

Guccione D, Buzzi O., Thoeni K., Fityus S., Giacomini A. (2021) Predicting the fragmentation survival probability of brittle spheres upon impact from statistical distribution of material properties, *International Journal of Rock Mechanics and Mining Sciences*, <https://doi.org/10.1016/j.ijrmms.2021.104768>.

# Estimating rockfall release scenarios based on a simple rockfall frequency model

Christine MOOS (corresponding author)<sup>1</sup>, Zeno BONTOGNALI<sup>2</sup>, Luuk DORREN<sup>3</sup>, Michel JABOYEDOFF<sup>4</sup>,  
Didier HANTZ<sup>5</sup>

**Keywords:** rockfall frequency, rockfall risk, power law, block size distribution

## 1 INTRODUCTION

A realistic quantification of rockfall risk is crucial for an effective and efficient prevention of damages. Although rockfall trajectory models allow for an increasingly precise calculation of rockfall runout zones, the estimation of realistic block and event volumes as well as their release frequencies remain a major challenge. They are often based on a rough estimation of a set of scenarios which represent different event magnitudes (release volumes) and return periods, based on geological surveys of the rock cliff and (scarce) inventory data. Based on the analysis of the rockfall frequency and magnitude of a wide range of rock cliffs, Hantz et al. (2020) proposed a power law based model for the determination of rockfall magnitude-frequency aiming at a more objective approach for practitioners. The objective of this study was to apply and test the proposed model at 8 different sites in the Swiss Alps.

## 2 ROCKFALL FREQUENCY MODEL

The frequency of rockfall events (one or several blocks releasing simultaneously) for a given volume  $V$  is described by a power law following Hantz et al. (2016):

$$F(V) = AV^{-B} \quad (1)$$

The integration of this function over the frequency corresponds to the erosion rate  $W$  of the cliff for a volume range between  $V_1$  and  $V_2$  (minimum and maximum considered volumes):

$$W = \int_F V dF = AB/(1-B) [V_2^{(1-B)} - V_1^{(1-B)}] \quad (2)$$

$F(V)$  is the number of events with a volume  $\geq V$  per year and ha. The parameters  $A$  and  $B$  depend on the rock structure and are derived based on a scale and as a function of the main layer distance as proposed in Hantz et al. (2020).

The frequency of single falling blocks also follows a power law, but with differing parameters (Hantz et al. 2016):

$$f(v) = av^{-b} \quad (3)$$

with  $f(v)$  being the frequency of blocks with a volume  $\geq v$  per year and ha. The parameter  $b$  depends on the block size distribution (and thus the fracture properties of the rock) and  $a$  is the number of blocks with a volume  $\geq 1\text{m}^3$  per year and ha (Hantz et al. 2020).

As with the frequency of events, this equation can be integrated to derive the erosion rate of the cliff (Hantz et al. 2020):

$$W' = \int_f V df = a/(1-b) v_2^{(1-b)} - a/(1-b) v_1^{(1-b)} \quad (4)$$

## 3 DATA AND METHODS

We selected 8 rockfall cliffs at 7 sites in the Swiss Alps of different sizes and with different geological settings, for which detailed hazard analyses from engineering companies or cantonal authorities were available. For each site, we sampled deposited blocks in the field to derive the block size distribution and the corresponding parameter  $b$  based on

<sup>1</sup> MOOS Christine, Interdisciplinary Centre for Mountain Research, University of Lausanne, Sion, CH, christine.moos@unil.ch

<sup>2</sup> BONTOGNALI Zeno, Egli Engineering AG, Bern / St. Gallen, CH, bontognali@naturgefahr.ch

<sup>3</sup> DORREN Luuk, Bern University of Applied Sciences – HAFL, Zollikofen, CH, luuk.dorren@bfh.ch

<sup>4</sup> JABOYEDOFF Michel, Risk Group, University of Lausanne, Lausanne, CH, michel.jaboyedoff@unil.ch

<sup>5</sup> HANTZ Didier ISTERre, University of Grenoble Alps, Grenoble, FR, Didier.hantz@univ-grenoble-alpes.fr

a power law fitting using the least-squares method. The parameters A and B were determined according to Hantz et al. (2020). By equating the two erosion rates (Eq. 2, 4), the parameter a can be calculated with the following equation:

$$a = W(1-b) / (v_2^{(1-b)} - v_1^{(1-b)}) \times 1/b \quad (5)$$

Based on the defined parameters A, B, a and b, the frequency of blocks and events can be determined for the total rock cliff by multiplying equations 1 and 3 with the cliff area (Area). We compared the derived block volume ranges for return periods defined by the Swiss natural hazard risk concept (RP = 10, 30, 100 and 300 years) with existing rockfall scenarios from hazard assessments and finally analysed the influence of the parameters A, B, a and  $v_2$  on the rockfall frequency.

## 4 RESULTS

Block volume distributions of all sites could be well fitted by power law distributions (Figure 1). The fitted b values ranged from 0.69 to 1.69. The calculated block volumes for the predefined scenarios were all significantly larger than the estimated volumes of the hazard assessments and mostly also larger than the expert-based maximum block volumes. The overall calculated rockfall frequencies for blocks with a volume  $\geq 0.05 \text{ m}^3$ , however, were in a realistic range compared to empirical data. The sensitivity analysis revealed a particularly strong influence of parameter B on the modelled frequency.

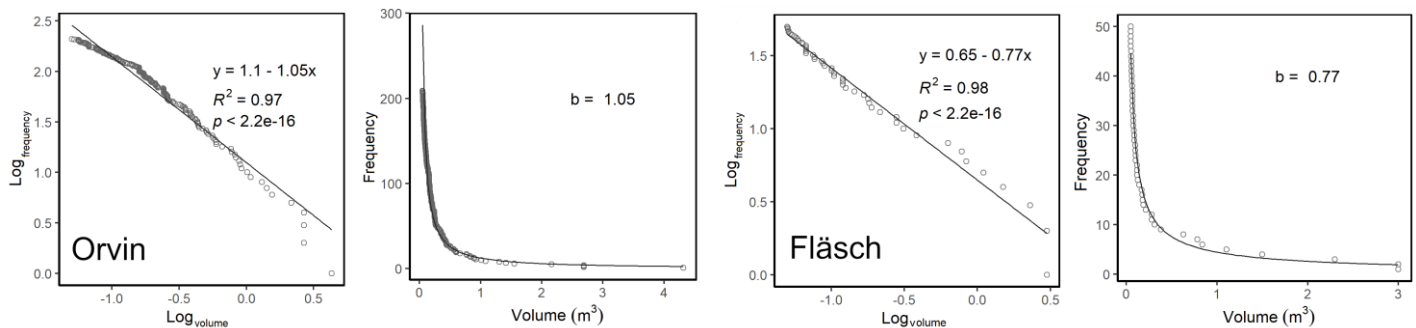


Figure 1: block volume distribution and fitted power law for the sites “Orvin” and “Tasch” (left plots in logarithmic scale).

## 5 CONCLUSIONS

The method proposed in this study allows for a more objective and consistent estimation of rockfall scenarios and thus has the potential to substantially improve the mostly opaque determination of rockfall scenarios. The results further show that the block volume scenarios for pre-defined return periods strongly depend on the considered cliff size, which does not appear to be consistently taken into account in current hazard assessments. However, the sensitivity analysis revealed a large uncertainty regarding the estimation of parameter B, which generally appeared to be too low at our case study sites. This indicates that the study should be extended to additional sites and the estimation of parameter B has to be optimised to come up with a consistent and transparent method to estimate rockfall frequencies in practice.

## REFERENCES

- Hantz D., Colas B., Dewez T., Levy C., Reossetti J., Guerin A., Jaboyedoff M. 2020. Caractérisation quantitative des aléas rocheux de départ diffus. Rapport de Recherche C2ROP, 15 p.
- Hantz D., Vengeon J.M., Dussauge-Peisser C. 2003. An historical, geomechanical and probabilistic approach to rockfall hazard assessment. *Natural Hazards and Earth System Science* 3(6): 693-701.
- Hantz D., Ventroux Q., Rossetti J., Berger F. 2016. A new approach of diffuse rockfall hazard. In: Aversa S., Cascini L., Picarelli L., Scavia C. (Ed.): *Landslides and engineered slopes. Experience, theory and practice: proceedings of the 12<sup>th</sup> International Symposium on Landslides, Napoli (IT), 12-19 June 2016.* CRC Press, Boca Raton, 1063-1067.

## Joint inversion of electrical resistivity and P-wave velocity data to evaluate the damage degree of supporting pillars in an underground cave, Burgundy (France)

Aurore CARRIER (corresponding author)<sup>1</sup>, Pierre BOTTELIN<sup>2</sup>, Lambert FAVRE<sup>3</sup>, Alexandre MATHY<sup>4</sup>

**Keywords:** joint inversion, structural health, electrical resistivity tomography, refraction seismics, clustering, geophysics

### ABSTRACT IN ENGLISH:

This study reveals the benefit of the use of refraction seismic and electrical resistivity joint inversion for the evaluation of structural health of supporting pillars in an underground cave. Results reveal contrasted resistivity and velocity areas related to fracturation degree and rock weathering. The use of petrophysical joint inversion gives access to rock, water, and air fraction. The results appear to be consistent with visual observations and drilling logs. The final automatic clustering of the resulting models enables to build resistivity/velocity groups and to determine a proxy of the damage condition.

### ABSTRACT IN FRENCH:

La présente étude démontre les apports de l'utilisation de l'inversion jointe des données de résistivité électrique et de sismique refraction pour l'évaluation du degré d'endommagement de piliers porteurs dans une cave souterraine. Les résultats montrent des variations de vitesse et de résistivité associées à des variations du taux de fracturation et du contenu en eau. L'utilisation d'un modèle pétrophysique pour joindre l'inversion permet d'avoir accès à la fraction de roche, d'eau et d'air. Les résultats sont en accord avec les observations visuelles faites sur le terrain ainsi qu'avec les observations et mesures réalisées sur les carottes. La création automatique de groupes vitesse/résistivité par une approche de clustering permet de déterminer une variable d'endommagement.

## 1 INTRODUCTION AND SETTINGS

Evaluating the damage degree of rocks is a key parameter to assess rock stability. Up to now if damage can easily be assessed on rock samples, its estimation at the field scale remains challenging. The spatial repartition of damage into rock volumes is a key to understand the stability of rock masses and their evolution through time.

Geophysical methods have proven to be useful to image the physical parameters of rock pillars (Fargier 2017). Commonly, geophysical studies consider the joint interpretation of different geophysical methods results such as electrical resistivity tomography, refraction seismics tomography and ground penetrating radar, each technique suffering from its own intrinsic ambiguities. More recently, the possibilities of joint inverting several geophysical datasets to improve model resolution and consistency have been studied and provides promising results (Gallardo and Meju 2004, Gunther and Rucker 2006, Coutant 2012, Hellman 2017, Wagner 2019). In this study the use of a petrophysical law relating inversion parameters is explored.

The studied underground carry is located in Burgundy (France) and consists in a set of chambers and pillars. Cracking processes have been detected and lead to a careful study of the carry stability. Numerical stability studies as well as laboratory analysis have been performed. Rock strength appeared very variable and the need to evaluate damage appears as a key to prioritize reinforcement works and to ensure the carry safety and integrity.

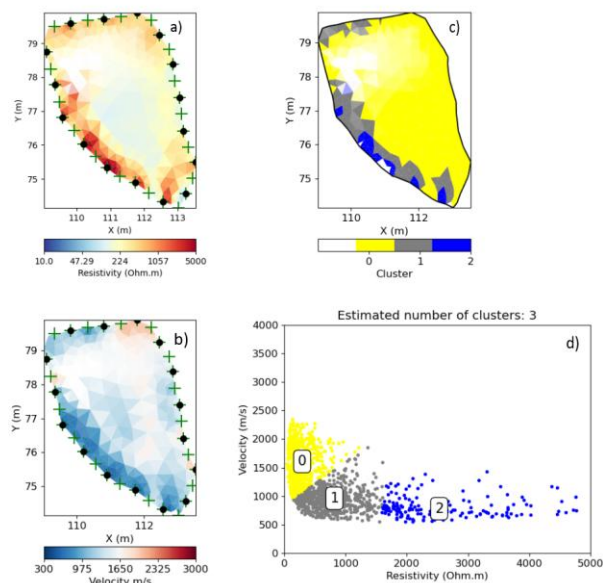


Figure 1 Resistivity (a) and velocity (b) models obtained from petrophysical joint inversion. Spatial distribution of the velocity/resistivity clusters (c) and velocity/resistivity distribution and clustering results (d).

<sup>1</sup> CARRIER Aurore, ADRGT, Grenoble, France, a.carrier@adrgt.org

<sup>2</sup> BOTTELIN Pierre, ADRGT, Grenoble, France, p.bottelin@adrgt.org

<sup>3</sup> FABRE Lambert, SAGE, Grenoble, France, l.fabre@sage-ingenierie.com

<sup>4</sup> MATHY Alexandre, SAGE, Grenoble, France, a.mathy@sage-ingenierie.com<sup>11</sup>

## 2 METHODOLOGY

Electrical Resistivity Tomography (ERT) and Refraction Seismic Tomography (RST) data have been acquired around three supporting pillars as horizontal cross-sections. The sensors have been placed at 1 m above the ground. The precise shape of the pillars as well as the precise location of the sensors is determined thanks to a high-resolution Lidar.

ERT and RST data are inverted through a petrophysical joint inversion process (Wagner 2019). Because no clay is present, the combined use of Archie's (experimentally based petrophysical law relating in-situ electrical conductivity, porosity and fluid saturation) and Wyllie's (empirical time average relationship considering the observed time as the sum of the traveltimes through the volumetric fractional thicknesses of the solid matrix and pore fluids) laws enabled to build a simplified three phase petrophysical model. This model is implemented in the inversion process to better constrain resistivity and velocity models.

Final velocity and resistivity models are interpreted together using an automatic clustering classification method.

## 3 RESULTS

The petrophysical joint inversion enables to build petrophysically consistent velocity and resistivity models. The results are consistent with visual observations, drilling logs and laboratory results. Highly damaged areas are consistent with high resistivity and low velocity areas. The healthy inner core consists in water saturated limestones and is associated to high velocity and low resistivity areas. The clustering classification enables to clearly identify and quantify the damaged areas. On this basis a pillar quality estimator can be established to prioritize safety work on the pillars.

## CONCLUSION

This study confirms that the joint use of refraction seismic and electrical resistivity data through a petrophysical joint inversion process enables to better constrain the velocity and resistivity models. The use of an automatic classification on the resulting models enables to quantify the damage degree associated to each pillar and is a good help for working decisions.

## REFERENCES

- Coutant, O., Bernard, M., Beauducel, F., Nicollin, F., Bouin, M., Roussel, S., 2012. Joint inversion of P-wave velocity and density, application to La Soufrière of Guadeloupe hydrothermal system. *Geophysical Journal International* 191, 723-742.
- Fargier, Y., Antoine, R., Dore, L., Lopes, S. P., & Fauchard, C. (2017). 3D assessment of an underground mine pillar by combination of photogrammetric and geoelectric methods. *Geophysics*, 82(4), E143-E153.
- Gallardo, L.A., Meju, M.A., 2004. Joint two-dimensional dc resistivity and seismic travel time inversion with cross-gradients constraints. *Journal of Geophysical Research: Solid Earth* 109.
- Gunther, T., Rucker, C., 2006. A new joint inversion approach applied to the combined tomography of dc resistivity and seismic refraction data, in: *Symposium on the Application of Geophysics to Engineering and Environmental Problems 2006*, Society of Exploration Geophysicists. pp. 1196-1202.
- Hellman, K., Ronczka, M., Günther, T., Wennermark, M., Rucker, C., & Dahlin, T. (2017). Structurally coupled inversion of ERT and refraction seismic data combined with cluster-based model integration. *Journal of Applied Geophysics*, 143, 169-181.
- Wagner, F. M., Mollaret, C., Günther, T., Kemna, A., & Hauck, C. (2019). Quantitative imaging of water, ice and air in permafrost systems through petrophysical joint inversion of seismic refraction and electrical resistivity data. *Geophysical Journal International*, 219(3), 1866-1875.

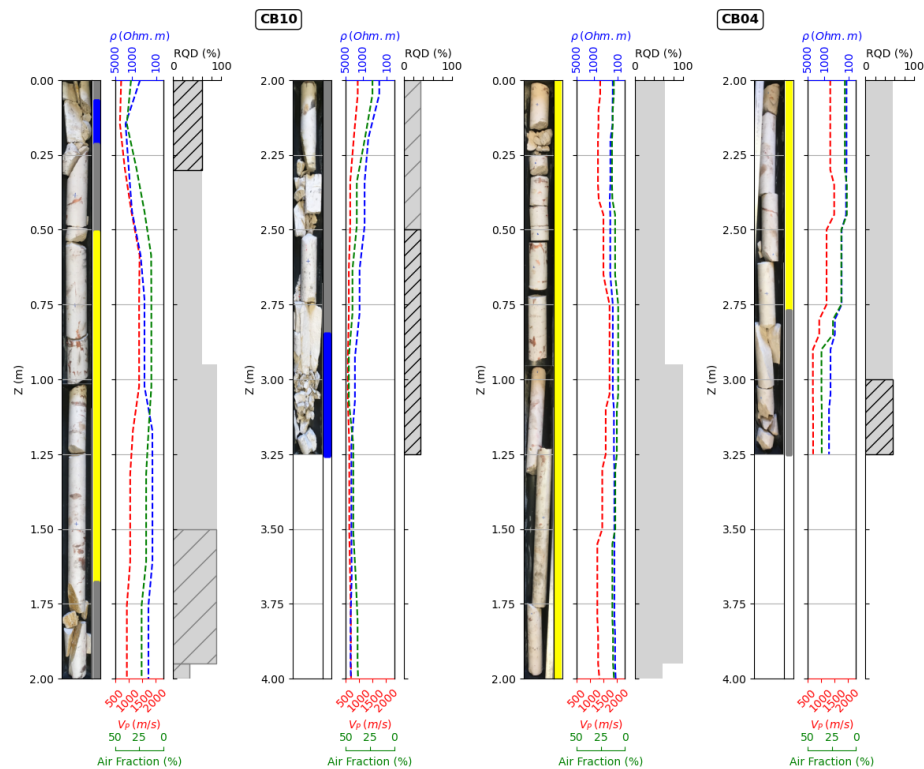


**Figure 2** Drilling cores versus RQD, velocity, resistivity, fracture fraction and cluster id logs extracted from petrophysical joint inversion. Black to grey striped : observed fractured and moderately fractured samples.

## Mapping release areas and mobility of large rock slide and rock avalanches in the French Alps high mountain

Maëva CATHALA<sup>1,2</sup>, Florence MAGNIN<sup>1</sup>, Ludovic RAVANEL<sup>1</sup>, Frederic BERGER<sup>3</sup>, Philip DELINE<sup>1</sup>

**Keywords:** large rock slide, rock avalanche, mobility index, mapping, GIS, high mountain, permafrost.

### ABSTRACT IN ENGLISH:

High mountain environments have been increasingly affected by rock slope failures such as large rock slides and rock avalanches over the past three decades (Huggel *et al.*, 2012). These hazards constitute a threat for population and infrastructure which highlights the need to improve knowledge about the distribution, characteristics and propagation of these processes. The aims of this study are (i) to identify the topography and permafrost conditions that are most prone to trigger a large rock slide or rock avalanche, and (ii) to characterize their mobility. To do so, two inventories were compiled; one from rock avalanches listed in the literature and another corresponding to a GIS database of large rock slides documented in the Alps. The relation between the volume and mobility of the events is investigated. Then, the results will be used in statistical models to identify potential release areas and to map the large rock slide or rock avalanche mobility.

### ABSTRACT IN FRENCH :

Les environnements de haute montagne sont de plus en plus affectés par des éboulements en masse et des écroulements en grande masse (Huggel *et al.*, 2012), ce qui constitue une menace pour les populations et les infrastructures. Les buts de cette étude sont (i) d'identifier les zones de départ potentielles d'éboulements en masse ou d'écroulements en grande masse, et (ii) de cartographier leur mobilité dans les environnements glaciaires et périglaciaires. Pour ce faire, deux inventaires ont été réalisés ; l'un à partir d'écroulements en grande masse répertoriés dans la littérature et l'autre correspondant à une base de données SIG d'éboulements en masse inventoriés dans les Alpes. La relation entre le volume et la mobilité de ces événements est étudiée. Les résultats sont ensuite utilisés dans des modèles statistiques pour identifier les zones de départ potentielles et pour cartographier la mobilité d'un éboulement en masse ou d'un écroulement en grande masse.

## 1 LARGE ROCK SLIDES AND ROCK AVALANCHES INVENTORIES

An inventory of 60 rock avalanches  $> 0.5 \text{ Mm}^3$  that occurred in high mountains worldwide was extracted from the available literature (Deline *et al.*, 2015; Sosio *et al.*, 2012; Schneider *et al.*, 2011). 31 are located in the USA, 11 in Canada, and the others in Iceland, Italy, Nepal, New Zealand, Pakistan, Peru, Russia and Switzerland. They all travelled onto clean- or debris-covered glaciers.

A second database was created with 24 large rock slides that occurred between 1997 and 2020 in the French Alps and

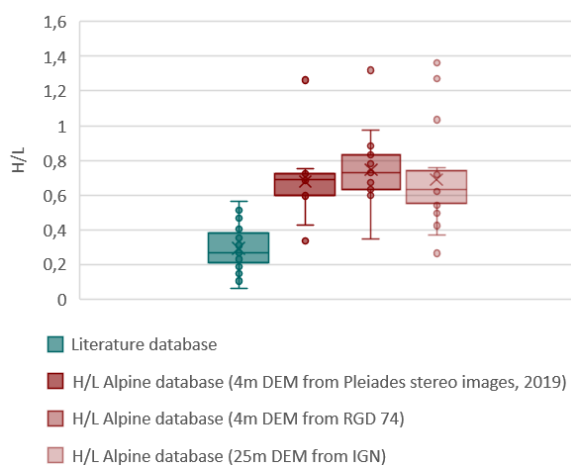


**Figure 1: Mobility of rock avalanches (blue) and large rock slides (red).**

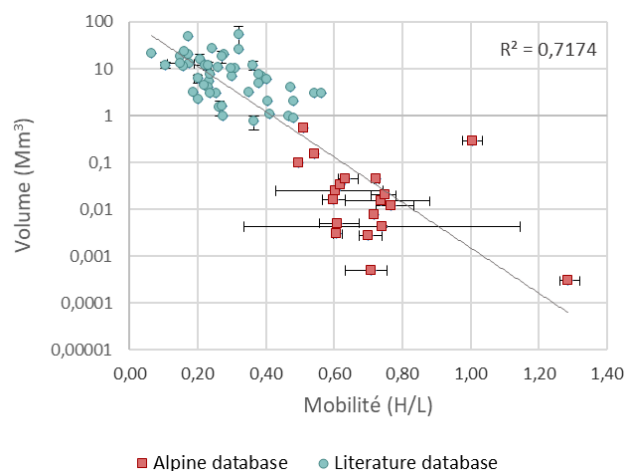


**Figure 2: H/L ratio vs. volumes. The lower the H/L ratio, the higher the mobility.**

<sup>1</sup> Edytem laboratory – UMR 5204 – Savoie Mont Blanc University, Le Bourget du Lac, France.

<sup>2</sup> Alpes Ingé, Saint-Vincent-de-Mercuze, France. maeva.cathala@univ-smb.fr

<sup>3</sup> INRAE, Saint-Martin-d'Hères, France

on the Italian side of the Mont Blanc massif (MBM), with volume ranging from 300 to  $535 \times 10^3 \text{ m}^3$ . 18 large rock slides are located in the MBM, and the others in the Berrio Blanc, Vanoise, Écrins, and Ubaye massifs. All the starting and stopping points of these events are georeferenced in a GIS database. As for the previous inventory, they mostly travelled onto clean- and debris-covered glaciers, with some onto snow or sediments.

Two criteria can be analysed and compared in each database: (i) the mobility of the event (H/L ratio) and (ii) its volume. To characterize the runout path and the mobility of the large rock slides from the GIS Alpine database, three DEMs (Digital Elevation Models) were used: one with a medium resolution (25m) which covers the entire French Alps (IGN), and two 4m-DEM which cover only the MBM (one from RGD 74 and one compiled from 2019 Pleiades images).

The GIS large rock slide database is also used to determine potential release areas, by identifying the topography and permafrost conditions that are most prone to trigger a large rock slide.

## 2 PRELIMINARY RESULTS: CHARACTERISATION OF THE MOBILITY FOR EACH DATABASE

Rock avalanches from the literature database are characterized by a high mobility (Figure 1). The H/L ratio is 0.29 (+/- 0.12) in average. The large rock slides in the Alps have a lower mobility, with an average H/L ratio of 0.68 (4m DEM from Pleiades stereo images), 0.74 (4m DEM from RGD 74) and 0.69 (25m DEM from IGN).

As demonstrated in the literature, the difference of mobility between the two processes is partly explained by the volume difference. Figure 2 shows that mobility increases as the volume of the event is getting higher, with a volume threshold between large rock slide and rock avalanche of c.  $1 \times 10^6 \text{ m}^3$ .

## 3 DISCUSSION

### 3.1 Implications of the results

The results will be used to calibrate statistical models to map the potential release areas and the mobility of the large rock slides and rock avalanches. Indeed, by analysing the frequency of the events according to their volume, it is possible to determine mobility thresholds (based on the H/L ratio) below which a large rock slide or rock avalanches cannot propagate. These thresholds can be directly used in a GIS scheme to calculate the areas potentially reachable by these processes (Figure 3). Such mapping at a regional scale is in progress.

### 3.2 Limits of the results

This study correlates the large rock slide and rock avalanche mobility with their volume, but other parameters need to be considered. The role of the substratum (e.g. rock, sediment types) and the snow appears also essential to characterize mobility on the runout path and could be integrate to this study.

## CONCLUSION

This study shows a strong correlation between the volume of the large rock slides and rock avalanches, confirming the literature. In addition, the results will be used to calibrate GIS models to map at regional scale (i) the potential release areas, and (ii) the areas potentially reachable, and point out hot spots where more detailed analysis would be required to estimate the possible risks.

## ACKNOWLEDGEMENTS

The authors thank Suvrat Kaushik for building the Pleiades 4 m DEM used in this study. The study received the financial support of *Alpes Ingé*.

## REFERENCES

- Deline, P., Hewitt, K., Reznichenko, N. and Shugar, D., (2015). Chapter 9 - Rock Avalanches onto Glaciers, in *Landslide Hazards, Risks and Disasters*, edited by J. F. Shroder and T. Davies, pp. 263–319, Academic Press, Boston. <https://doi.org/10.1016/B978-0-12-396452-6.00009-4>.
- Huggel, C., Allen, S., Deline, P., Fischer, L., Noetzli, J., Raveland, L., (2012). Ice thawing, mountains falling - are alpine rock slope failures increasing? *Geol. Today* 28 (3):98–104.
- Schneider, D., Huggel, C., Haeberli, W. and Kaitna, R., (2011). Unraveling driving factors for large rock–ice avalanche mobility, *Earth Surface Processes and Landforms*, 36(14), 1948–1966, <https://doi.org/10.1002/esp.2218>.
- Sosio, R., Crosta, G. B., Chen, J. H. and Hungr, O., (2012). Modelling rock avalanche propagation onto glaciers, *Quaternary Science Reviews*, 47, 23–40.

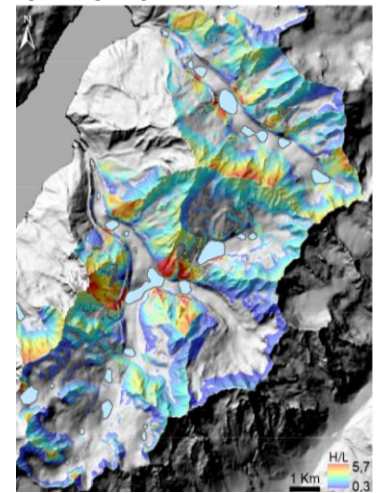


Figure 3: Example of mapping using a mobility threshold ( $H/L > 0.3$ ) to determine which potential release area could impact a lake in case of large rock slide in the Mer de Glace and Argentière glacier basins (MBM).

## Modelling Rotational Drag in Rockfall Dynamics

Jessica MUNCH, Andrin CAVIEZEL, Marc CHRISTEN, Adrian RINGENBACH, Guang LU and Perry BARTELT<sup>1</sup>

**Keywords:** Rockfall dynamics, trajectory modelling, drag, rotations, rebound, RAMMS

### 1 INTRODUCTION

When falling, a rock goes through airborne phases separated by ground interaction phases. In this work we focus on rock-ground interactions and present a method to calculate the rotational drag acting on rocks as they penetrate ground substrates. The method is general in that it can be applied to rocks of general shape and size, with known translational resultant velocity  $\mathbf{V}_V$  and rotational speed  $\mathbf{V}_\Omega$ . We use it for rockfall trajectory analysis, to model changes of rotation during the rock-ground interaction process. Modelling the correct rotational speed is essential to predict gyroscopic forces, or how rock features, such as edges and sharp corners penetrate and scar the ground surface. This process controls how rocks rebound and therefore jump heights, runout and dispersion, an important problem in rockfall mitigation.

### 2 ROCK PENETRATION, DRAG FORCES AND TORQUES

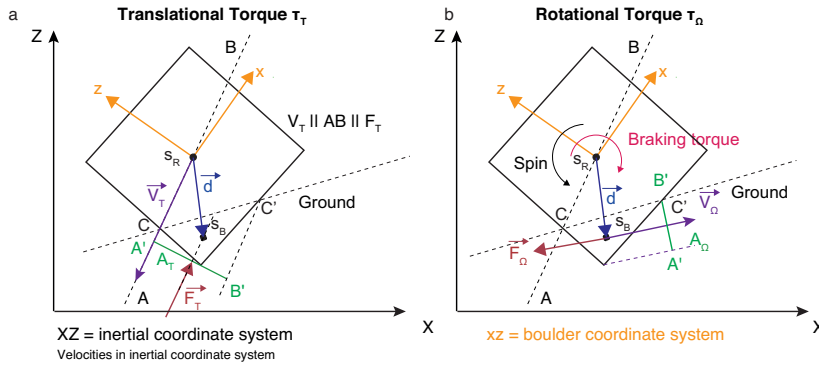


**Figure 1:** During the ground-rock interaction the translational movement of a rock into the ground creates a rotational drag because the rock has only partially penetrated the ground surface.

velocity  $\mathbf{V}_V = (V_x, V_y, V_z)$ . We define a line  $(AB)$ , parallel to  $\mathbf{V}_T$ , and a line  $(A'B')$  perpendicular to  $\mathbf{V}_V$  (Fig. 1). The drag force  $\mathbf{F}_V$  associated with the rock's penetration into the ground is parallel and opposite in direction to  $\mathbf{V}_V$ :  $\mathbf{F}_V \parallel (AB)$ ; the drag force  $\mathbf{F}_\Omega$  associated with the rock's rotation is perpendicular to  $\mathbf{V}_\Omega$  i.e.  $\mathbf{F}_\Omega \parallel (A'B')$ . The  $(x, y, z)$  location of the center-of-mass (COM)  $\mathbf{s}_R$  of the rock is known relative to the ground in the inertial coordinate system. Knowing the location of the ground surface with respect to the rock's location, it is possible to define the volume of the rock below the ground surface and to find the location of the COM  $\mathbf{s}_B$  of this submerged volume. The torque arm for both the translational and rotational drag forces is defined by  $\mathbf{d} = \mathbf{s}_R - \mathbf{s}_B$ . We then find the velocity  $\mathbf{V}_\Omega$  at the submerged COM in the direction of  $(A'B')$ .

The projection of the line  $(C'C)$  (intersection plane separating the emerged and submerged volumes of the rock) on the line  $(A'B')$  gives the ground area  $A_V$  resisting the translational penetration; the projection of  $(C'C)$  on  $(AB)$  gives the approximate area  $A_\Omega$  resisting the rotational movement.

The translational drag forces can then be found:  $\mathbf{F}_V = 0.5 \cdot \rho_{ground} \cdot C_d \cdot \mathbf{V}_V \cdot \mathbf{V}_V \cdot A_V$  and  $\mathbf{F}_\Omega = 0.5 \cdot \rho_{ground} \cdot C_d \cdot \mathbf{V}_\Omega \cdot \mathbf{V}_\Omega \cdot A_\Omega$  where  $C_d$  is the drag coefficient, representing ratio between the characteristic volumes of the rock and the scar (Lu et al., 2019). The corresponding torques are  $\boldsymbol{\tau}_V = -\mathbf{F}_V \times \mathbf{d}$  and  $\boldsymbol{\tau}_\Omega = -\mathbf{F}_\Omega \times \mathbf{d}$ . The minus sign ensures that the torques act against the translational and rotational velocities.

The total rotational drag acting on a rock penetrating the ground surface results from two separate torques: one arising from the translational penetration of the rock into the ground (Torque  $\boldsymbol{\tau}_V$ , Fig. 1a) and one arising from the rotational spin of the rock as it scars the ground surface (Torque  $\boldsymbol{\tau}_\Omega$ , Fig. 1b). The sum of  $\boldsymbol{\tau}_V$  and  $\boldsymbol{\tau}_\Omega$  provides the total drag resistance  $\mathbf{T}$ .

We consider the rock to be a rigid body approaching the ground with

### 3 RESULTS AND DISCUSSION

We apply this model to a rockfall which occurred along the Lago di Poschiavo in February 2021. The numerical modelling is performed using RAMMS::Rockfall software (Leine et al. 2014), where the above described model is implemented. The rock-ground interactions are divided into two phases, a scarring phase followed by a rebound phase. The non-smooth mechanics for the rebound phase are explained in (Lu et al., 2019). To assess the influence of drag forces on the motion of the rock, we perform rockfall simulations on different ground types varying the drag coefficient.

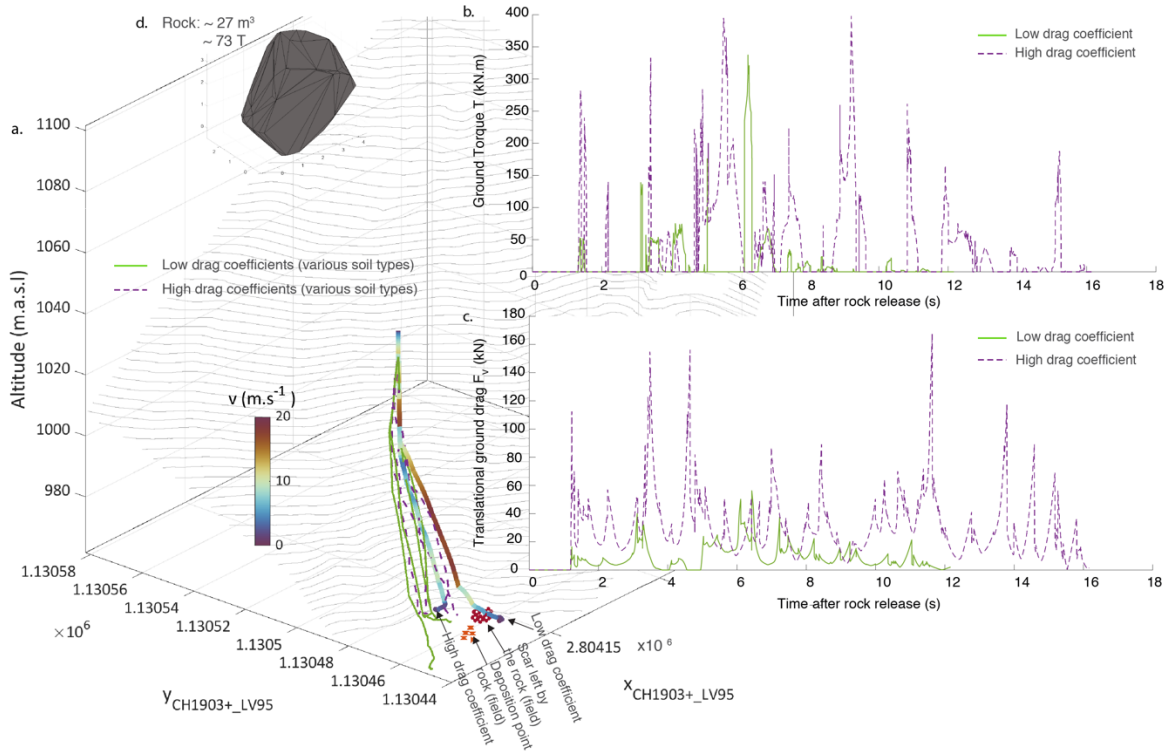


**Figure 2:** a. Trajectories for rocks falling on different grounds (soft to extra hard). Green lines indicate simulations done with a drag coefficient of 0.5, purple dotted lines simulations with a drag coefficient of 10. 2 trajectories, both of rocks falling on a soft ground, are coloured with the translational velocity, the “low drag coefficient” corresponds to  $C_d=0.5$  and “high drag coefficient” to  $C_d=10$ . Their translational ground drag and ground torque are given in panels b. and c. respectively. The rock used for the simulations is shown in panel d. The location of the rock and its last scar are given in the orange and red areas.

The results with variable drag coefficients show that whatever the ground type, the higher the  $C_d$ , the shorter the rock trajectory (Fig. 2. a.). We also note that the deposition points are coherent with field observations (Fig. 2. a. – GNSS points). The translational ground drag is stronger for simulations with high drag coefficient (Fig. 2. c.), which fits with the translational velocity evolution (Fig. 2. a., colored trajectories for high and low drag coefficients). The torque values are consistent with the translational ground drag, the rock’s dimensions, and the rockfall setting (Fig. 2. b.).

### CONCLUSION

A rotational drag is introduced when the rock penetrates the soil scarring layer. In RAMMS the combination of ground drag in the scarring layer with hard contact rebound mechanics facilitates the realistic modelling of the rock ground interaction. More data in different soil types will be gathered to calibrate the rotational drag model in future.

### REFERENCES

- Leine, Remco I, Andreas Schweizer, Marc Christen, James Glover, P Bartelt, and Werner Gerber. 2014. 'Simulation of rockfall trajectories with consideration of rock shape', *Multibody System Dynamics*, 32: 241-71.
- Lu, Guang, Andrin Caviezol, Marc Christen, Sophia E Demmel, Adrian Ringenbach, Yves Bühler, Claire E Dinneen, Werner Gerber, and Perry Bartelt. 2019. 'Modelling rockfall impact with scarring in compactable soils', *Landslides*, 16: 2353-67.

## Presentation of a methodology for determining rockfall hazard

Camille HALBWACHS<sup>1</sup> Jean-Philippe JARRIN<sup>2</sup>

**Keywords:** Rockfall, Methodology

**Summary :** An innovative methodology is presented for determining rockfall hazard based on the estimation of the annual probability of reaching an issue, allowing to evaluate the hazard quantitatively, in contrast to qualitative evaluations used by most engineering consultants in France. The application of this methodology to various sites is shown to determine the hazard more finely, leading to better advices to authorities on mitigation measures.

### Genèse : Pourquoi proposer une nouvelle méthodologie de qualification de l'aléa éboulement rocheux

Nous travaillons sur les problématiques d'éboulement rocheux et de définition de l'aléa résultant depuis plus de 25 ans. La plupart des bureaux d'étude (y compris Géolithe jusqu'à récemment) s'appuient sur des méthodologies internes et généralement basées sur le guide technique édité par le LCPC en Juin 2004.

Ces méthodologies n'abordent le sujet des aléas que de manière qualitative et non quantitative. Il est dès lors difficile d'établir une correspondance entre un niveau d'aléa résultant qualifié de "Très Elevé", "Elevé", "Moyen", etc. avec une probabilité annuelle d'atteinte de l'enjeu étudié et de ce fait difficile pour les maîtres d'ouvrage d'apprécier ces niveaux d'aléa ou de comparer entre elles des études de différents bureaux d'études. Certaines méthodologies (comme la méthode MEZAP par exemple) permettent de qualifier l'aléa de manière quantitative. Cependant, cette méthode présente une limite d'utilisation quant aux seuils utilisés pour qualifier les niveaux d'aléa. En effet, elle qualifie un aléa résultant de "Très Elevé" pour une probabilité d'atteinte annuelle de l'enjeu supérieure à  $10^{-3}$ . En termes de période de retour, cela signifie un enjeu atteint en moyenne tous les 1000 ans. Cette qualification peut avoir un sens dans le cadre d'un zonage réglementaire, pour la définition des zones constructibles (PPR), mais ne paraît pas adaptée pour l'étude d'enjeux spécifiques, notamment linéaires tels que des routes de montagnes, construites dans des secteurs très fortement soumis aux phénomènes d'éboulement rocheux.

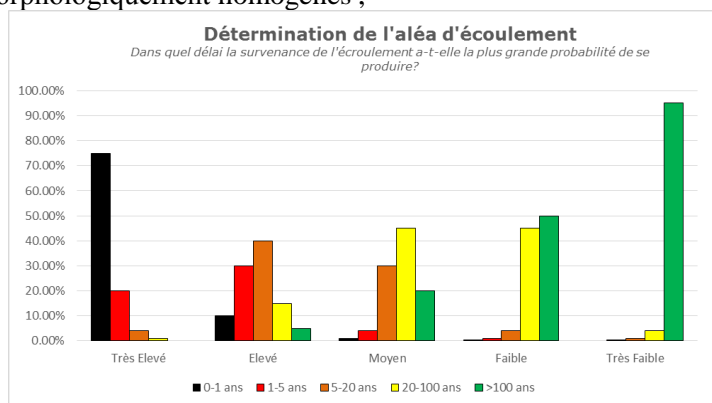
La méthodologie développée par Géolithe a été pensée pour répondre aux besoins des maîtres d'ouvrage :

- 1- Comparaison des secteurs d'un même itinéraire ou d'itinéraires d'un même réseau ;
- 2- Estimation du nombre d'événements susceptibles d'atteindre les enjeux dans un délai donné (généralement de l'ordre de quelques décennies à 1 siècle maximum) ;
- 3- Qualification du type de phénomènes (pierres, blocs, masses, grandes masses, etc.) ;
- 4- Choix d'un principe de sécurisation cohérent/pertinent en fonction des phénomènes et de leur fréquence, y compris en termes de maintenance future des ouvrages de sécurisation mis en œuvre.

### Présentation de la méthodologie

Le déroulement méthodologique permettant d'aboutir à ce résultat est le suivant :

- 1- Subdivision de la zone d'étude en secteurs morphologiquement homogènes ;
- 2- Diagnostic : Recensement et caractérisation des instabilités en paroi (volume initial, volume résiduel, niveau d'aléa d'écroulement). L'aléa d'écroulement est défini, sur la base de l'analyse des facteurs déclenchants, comme la probabilité de survenance de l'écroulement dans un délai donné. Il est déterminé selon les histogrammes présentés ci-dessous, qui indiquent la répartition de la probabilité de déclenchement dans différentes gammes de délais. Par exemple l'aléa d'écroulement qualifié de "Elevé" présente une probabilité d'un écroulement dans l'année de 10 %, d'un écroulement dans les 5 ans de 40 %, d'un écroulement dans les 20 ans de 80 %, etc.



<sup>1</sup> HALBWACHS Camille, GEOLITHE, Crolles, FR, camille.halbwachs@geolithe.com

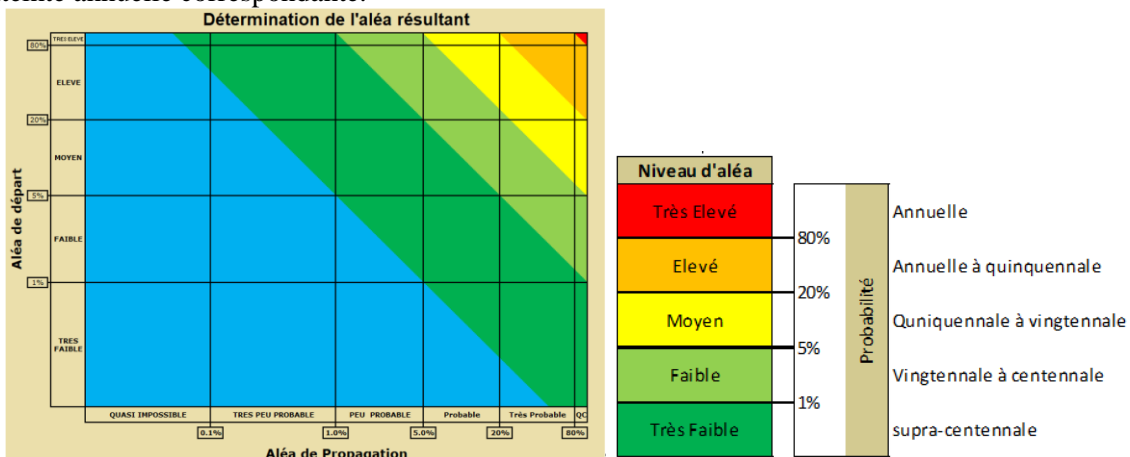
<sup>2</sup> JARRIN Jean Philippe, GEOLITHE, Crolles, FR, jp.jarrin@geolithe.com

- 3- Tri des instabilités par classe de volume (pierres < 0.1m<sup>3</sup>; blocs 0.1 à 2 m<sup>3</sup> ; masses 2 à 20 m<sup>3</sup>, Grandes masses 20 à 100 m<sup>3</sup>, très grandes masses > 100 m<sup>3</sup>) ;
- 4- Pour chaque classe de volume d'instabilité, dans un secteur donné, répartition en pourcentage, de l'ensemble des compartiments recensés dans les différents niveaux d'aléa d'écroulement (TE, E, M, F et TF). *Exemple :*

Secteur	Classe d'instabilité	Nbre de compartiments relevés	Incertitude diagnostic	Nbre compartiments réels estimés	Aléa d'écroulement									
					Très Elevé		Elevé		Moyen		Faible		Très Faible	
					%	Nbre	%	Nbre	%	Nbre	%	Nbre	%	Nbre
2	Pierres	1	-	150	35%	53	35%	53	20%	30	10%	15	0%	0
	Blocs	13	30%	17	15%	3	54%	10	31%	6	0%	0	0%	0
	Masses	4	10%	5	25%	2	0%	0	75%	4	0%	0	0%	0
	Grandes Masses	4	0%	4	0%	0	0%	0	50%	2	50%	2	0%	0
	Très Grandes Masses	1	0%	1	0%	0	0%	0	0%	0	100%	1	0%	0

- 5- Cette répartition permet de calculer, pour chaque classe d'instabilité, la probabilité annuelle qu'au moins un événement se déclenche, qui définit l'aléa de départ. Afin de permettre la comparaison de secteurs entre eux, cet aléa de départ est calculé pour un linéaire de référence défini à 30 mètres.
- 6- Classiquement, l'étude de la propagation est réalisée à l'aide de simulations trajectographiques. Les valeurs seuils de probabilité de propagation permettant la détermination du niveau d'aléa de propagation sont choisies de manière à présenter une pertinence statistique vis-à-vis du nombre de simulations généralement réalisées (souvent de l'ordre de 10 000 à 100 000).
- 7- Le croisement entre l'aléa de départ et l'aléa de propagation permet d'aboutir à l'aléa résultant (probabilité annuelle d'atteinte de l'enjeu par un phénomène d'éboulement rocheux). Cette probabilité est calculée par multiplication de la probabilité annuelle de déclenchement d'un phénomène à l'échelle de la zone de départ et de la probabilité de propagation. En fonction de la morphologie du secteur, et notamment de la possibilité de concentrer ou au contraire de disperser les trajectoires, un terme correctif ajuste ce calcul. Le graphique ci-dessous synthétise les niveaux d'aléa que nous proposons ainsi que les probabilités d'atteinte annuelle correspondante.

Aléa de propagation		Probabilité
Quasi Certain	80%	
Très Probable	20%	
Probable	5%	
Peu probable	1%	
Très Peu Probable	0.10%	
Quasi Impossible		



On observe que les probabilités annuelles considérées induisent des périodes de retour facilement appréhendables par les maîtres d'ouvrage et du même ordre de grandeur que la durée de vie des ouvrages de sécurisation usuellement mis en œuvre.

### Conclusions

Après utilisation de cette méthodologie sur plusieurs études, nous constatons une plus grande finesse dans l'estimation de l'aléa résultant qu'avec les méthodes utilisées antérieurement. Les résultats nous permettent d'être également plus fins sur les solutions proposées et sur l'estimation des coûts de maintenance. Elle nous pousse, ainsi que les maîtres d'ouvrage, à nous interroger sur la notion de risque acceptable et sur le bon équilibre coût (investissement + maintenance) / sécurisation en fonction des enjeux. Le dimensionnement des ouvrages ne se fait ainsi pas forcément en fonction de l'événement le plus important, mais en fonction de l'événement susceptible de se produire dans le délai de référence choisi par le maître d'ouvrage.

### Références bibliographiques

- LCPC (Laboratoire Central des Ponts et Chaussées) 2004. Les études spécifiques d'aléa lié aux éboulements rocheux.
- Projet National C2ROP. Caractérisation de l'aléa éboulement rocheux – Etat de l'art – Bron : Cerema, 2020. Collection : Connaissances. ISBN :978-2-37180-470-8
- MEZAP – Méthodologie d'Evaluation du Zonage de l'Alea chute de Pierres - En cours de Publication.

## Prédiction de scénarios d'embâcle avec le modèle de couche-mince SHALTOP

Clara Levy<sup>1</sup>, Bastien Colas<sup>2</sup>, Anne Mangeney<sup>3</sup>, Caritg Severine<sup>1</sup>, Thierry Baudin<sup>1</sup>, Elizabeth Le Goff<sup>1</sup>, Pierre Azemard<sup>4</sup>, Cécile Guitet<sup>5</sup>, Rémy Martin<sup>5</sup>

**Keywords:** modèle couche-mince, glissement, embâcle, prédiction, calibration

Un mouvement de versant lent de près de 40 Mm<sup>3</sup> est constaté au sein d'une vallée alpine. Afin de prendre en compte ce risque pour l'aménagement et les infrastructures existantes (route et voie ferrées notamment), l'étude de scénarios de rupture brutale, avec le comblement du fond de vallée et embâcle de la rivière s'écoulant au pied de versant, a été engagée. Nous modélisons la propagation des glissements potentiels et la création d'embâcles avec le modèle de couche mince SHALTOP développé par l'IPGP et LAMA. Afin de paramétrer ces simulations, la stratégie a été d'estimer la valeur optimale des paramètres pour des éboulements historiques documentés en contextes similaires.

### 1 DÉFINITION DES SCÉNARIOS D'EMBÂCLE

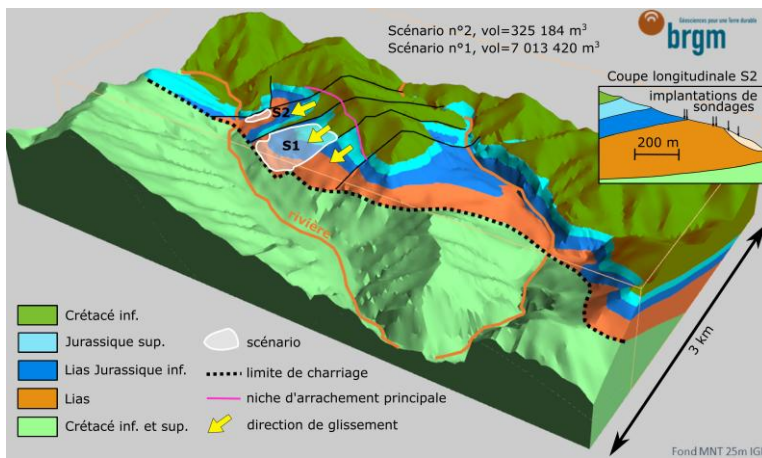


Figure 1: modèle géologique 3D du versant instable et coupe du scénario S2

L'étude débute avec la caractérisation géologique et géotechnique du versant. Un modèle géologique 3D est établi avec Geomodeller (Fig. 1); il prend en compte : 1) les données de déplacement in situ et celles obtenues par traitement d'images satellites, 2) la géologie locale déduite des observations et mesures de terrain et des photo-interprétations, 3) les données de forages. Une surveillance de la déformation du versant est mise en place depuis plusieurs années sur le site. Le versant est constitué d'une nappe de charriage avec des formations sédimentaires allochtones du Trias au Crétacé inférieur, reposant sur du Crétacé autochtone. La niche d'arrachement principale affecte 3 compartiments de formations allochtones, individualisés par des failles subverticales héritées de l'ouverture du bassin

Vocontien au Crétacé inf., ayant joué lors des déformations associées au charriage. Les matériaux mobilisés sont du calcaire massif (J. sup.) des marno-calcaires (J. inf.) et des marnes (Lias). Les déplacements historiques montrent une dynamique individualisée par compartiment. Deux scénarios de rupture (S1 et S2, Fig. 1) affectant chacun un compartiment sont retenus pour évaluer le risque d'embâcle. Ils ont été définis à partir du modèle géologique 3D avec une géométrie des surfaces de rupture contrainte par les données de forages et d'observations in-situ. La formation d'embâcle a été évaluée par modélisation de la propagation des glissements potentiels avec le modèle de couche mince SHALTOP (Bouchut et Westdickenberg, 2004; Mangeney et al., 2007 ; Peruzzetto et al., 2021), détaillé ci-dessous.

### 2 CALIBRATION DU MODELE DE PROPAGATION

SHALTOP a été utilisé pour reproduire aussi bien des écoulements granulaires en laboratoire que des éboulements et glissements de terrain de volumes très variables (Mangeney et al. 2007, Lucas et al. 2014, etc.). Certains travaux ont permis de quantifier l'augmentation de la mobilité des glissements avec leur volume, dont Lucas et al. (2014) qui proposent une loi empirique où la friction basale suit une loi de Coulomb, avec un angle de friction  $\phi$  constant mais dont la valeur dépend empiriquement du volume de l'évènement (Fig. 2). La Figure 2 illustre aussi la dispersion naturelle qui existe par rapport à ce comportement moyen (ligne rouge en Fig. 2) qui s'explique notamment parce que la friction au niveau de la surface basale dépend de la nature des matériaux, de la teneur en eau au moment de la propagation, etc. La difficulté pour l'utilisateur est donc de choisir une valeur adéquate pour ce paramètre  $\mu = \tan(\phi)$  afin de faire les meilleures prédictions de propagation possibles. La stratégie utilisée ici est d'estimer la valeur optimum de ce paramètre  $\mu$  pour des éboulements historiques bien documentés en contextes similaires (géologie, mode de déclenchement, etc.) afin d'ajuster la loi empirique moyenne au cas étudié. Des glissements historiques dans la même vallée et affectant les mêmes formations géologiques que les scénarios S1 et S2 ont été recherchés : 1) dans

<sup>1</sup> LEVY Clara, BRGM, Orléans, FRANCE (ISO 3166-2), c.levy@brgm.fr

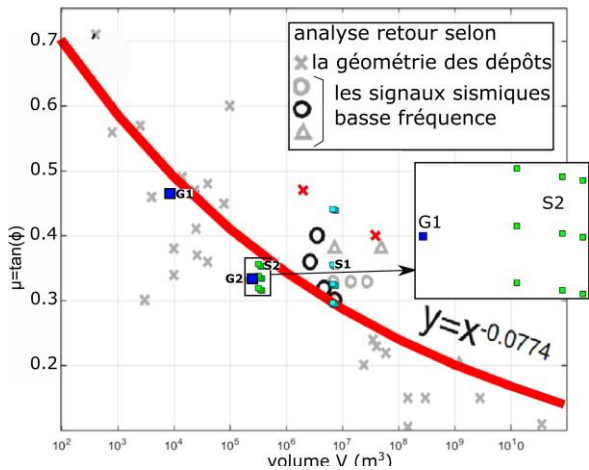
<sup>2</sup> COLAS Bastien, BRGM, Montpellier, FRANCE (ISO 3166-2), b.colas@brgm.fr

<sup>3</sup> MANGENEY Anne, IPGP, Paris, FRANCE (ISO 3166-2), mangeney@ipgp.fr

<sup>4</sup> AZEMARD Pierre, CEREMA, Aix en Provence, FRANCE (ISO 3166-2), pierre.azemard@cerema.fr

<sup>5</sup> GUITET Cécile, ONF-RTM, Nice, FRANCE (ISO 3166-2), cecile.guitet@onf.fr

les archives, 2) à partir des orthophotographies historiques disponibles sur le site de l'IGN remonterletemps.ign.fr et sur Google Earth, 3) à partir de recherches internet sur les glissements qui se sont produits dans la région. Six glissements historiques ont ainsi pu être mis en évidence, mais l'analyse en retour et en particulier la reconstruction des géométries avant glissement n'a été possible que pour deux d'entre eux affectant les marnes (G1 et G2 en Fig. 2).



Pour chaque simulation de G1 et G2, on compare la géométrie des dépôts avec les informations connues sur le glissement (forme des dépôts, hauteur du barrage, etc.) afin de qualifier si la simulation reproduit correctement le phénomène. L'angle  $\phi$  optimum est de  $18,5^\circ$  pour G1 et  $25^\circ$  pour G2, soit des angles qui valent 89% et 95% de la valeur prédite par la loi empirique  $\mu=V^{-0,0774}$  (avec V le volume de l'évènement) de  $20,9^\circ$  pour G1 et  $26,5^\circ$  pour G2.

### 3 SIMULATIONS PREDICTIVES DES EMBLÂCLES

Le scénario S2 mobilisant des marnes, comme G1 et G2, sera modélisé par analogie avec des angles de frottement valant 85%, 90% et 95% de la valeur prédite par la loi  $\mu=V^{-0,0774}$ , ce qui permet de prendre en compte à la fois l'influence des matériaux et du volume sur la valeur de  $\phi$ . Pour le scénario S1 cette analogie n'est pas transposable car il affecte principalement le calcaire jurassique beaucoup plus résistant et pour lequel nous ne disposons pas d'exemple historique. Il est donc difficile de choisir une valeur adaptée pour  $\phi$ . Aussi, nous avons utilisé des angles de friction sur une gamme de valeur plus large, en prenant en compte que : 1)  $\phi$  pour ce scénario devrait être a priori plus élevé que celui choisi pour S2 car les matériaux sont plus résistants ; 2) les

Figure 2: Valeurs optimums du coefficient de friction  $\mu=\tan(\phi)$  suivant une loi de Coulomb pour reproduire la géométrie des dépôts ou les signaux sismiques de plusieurs glissements et éboulements, d'après Lucas et al. 2014. Malgré la dispersion des valeurs, on observe un comportement moyen (ligne rouge  $\mu=V^{-0,0774}$ ) montrant l'augmentation de la mobilité des glissements avec leur volume. Coefficients choisis pour les simulations des scénarios S1 (carrés cyans) et S2 (carrés verts), ainsi que ceux ayant permis de reproduire au mieux les glissements historiques (carrés bleus).

experts estiment probable que S1 se produise le long d'une surface de rupture extrêmement rugueuse en forme d'escalier. L'angle de friction  $\phi$  pour S1 devrait donc être a priori plus élevé que le comportement moyen observé par Lucas et al. (2014). Pour ces simulations prédictives, nous avons utilisé des angles de friction à 100%, 110% et 120% de l'angle prédit par la loi  $\mu=V^{-0,0774}$ , ainsi que des valeurs d'angle dans les plus hautes utilisées pour reproduire des éboulements historiques (croix rouges, Fig. 2). Plusieurs volumes de masse instable sont testés pour les 2 scénarios afin de prendre en compte l'incertitude sur leur géométrie (zoom, Fig. 2).

### CONCLUSION

Pour toutes les simulations de S1 et S2, les matériaux se sont majoritairement écoulés dans la vallée en créant un embâcle, avec des hauteurs de barrage entre 3 et 6 m pour S2 et entre 8 et 35 m pour S1. Les dépôts sont en partie remontés sur le versant opposé et atteignent la route et la voie ferrée pour toutes les simulations de S1 et pour les

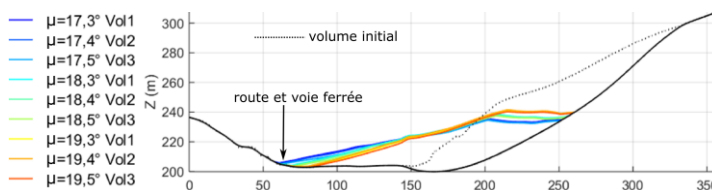


Figure 3 : variabilité du profil longitudinal des dépôts obtenus pour les simulations du scénario S2

simulations de S2 avec  $\phi > 17,5^\circ$ . La pente des dépôts peut être assimilée à une pente régulière pour les simulations de S1 avec  $\phi > 23^\circ$  et pour S2 avec  $\phi > 19^\circ$ . La proportion de matériaux éboulés qui contribue de manière effective au barrage (matériaux dans le lit de rivière vs matériaux restés dans le versant) est de 100% pour S2 et varie entre 37 et 84% pour S1. Ces résultats sont comparables aux observations de Ermini et Casagli (2003) de barrages naturels générés par glissements.

### REFERENCES

Bouchut, F., and M. Westdickenberg (2004), Gravity driven shallow water models for arbitrary topography, *Communications in Mathematical Sciences*, 2(3), 359–389.  
 Ermini, L., and N. Casagli (2003), Prediction of the behaviour of landslide dams using a geomorphological dimensionless index, *Earth Surface Processes and Landforms*, 28(1), 31–47.  
 Lucas, A., A. Mangeney, and J. P. Ampuero (2014), Frictional velocity-weakening in landslides on earth and on other planetary bodies, *Nature communications*, 5.  
 Mangeney, A., L. Tsimring, D. Volfson, I. Aranson, and F. Bouchut (2007), Avalanche mobility induced by the presence of an erodible bed and associated entrainment, *GRL*, 34(22), L22,401.  
 Peruzzetto, M., A. Mangeney, F. Bouchut, G. Grandjean, C. Levy, Y. Thiery, and A. Lucas (2021), Topography curvature effects in thin-layer models for gravity-driven flows without bed erosion, *in prep.*

## Results of Real Scale Block Shape/Mass Experiments, Chant Sura, Switzerland

Andrin CAVIEZEL<sup>1</sup>, Adrian RINGENBACH<sup>1</sup>, Sophia DEMMEL<sup>1</sup>, Yves BÜHLER<sup>1</sup>, Marc CHRISTEN<sup>1</sup>,  
Guillaume MEYRAT<sup>1</sup>, Nora KREBS<sup>1</sup>, and Perry BARTELT<sup>1</sup>

**Keywords:** rockfall, single block experiments, induced rockfall, shape, data set, numerical model calibration

An accurate rockfall hazard assessment relies on one key factor: Determining the longitudinal and lateral spread kinematics for a rock of a specific shape and mass from a given rockfall release area. The underlying physical problem is to accurately calculate the dissipation of translational and rotational energy during the short rock-ground interactions, for a specific and usually highly inhomogeneous mountain terrain. An accurate calibration of these dissipation processes is prerequisite for a functioning numerical rockfall trajectory model. Here we present the results of a multi-year rockfall experimental campaign performed at the Swiss Chant Sura test site. The data set quantifies the influence of rock shape and mass on longitudinal runout as well as lateral spreading. The results serve as a foundation for the systematic calibration of advanced rockfall simulation programs. More importantly, the results contradict several common practices in rockfall hazard assessment.

Une évaluation précise des risques de chute de pierres repose sur un facteur clé: la détermination de la cinématique de propagation longitudinale et latérale pour une roche d'une forme et d'une masse spécifiques à partir d'une zone de libération d'éboulements donnée. Le problème physique sous-jacent est de calculer avec précision la dissipation de l'énergie de translation et de rotation lors des courtes interactions roche-sol, pour un terrain montagneux spécifique et généralement très inhomogène. Un étalonnage précis de ces processus de dissipation est une condition préalable pour un modèle de trajectoire numérique fonctionnel. Nous présentons ici les résultats d'une campagne expérimentale de chute de pierres réalisée sur plusieurs années sur le site d'essai suisse de Chant Sura. L'ensemble de données quantifie l'influence de la forme et de la masse de la roche sur propagation longitudinale ainsi que sur la propagation latérale. Les résultats servent de base à calibration systématique des programmes avancés de simulation des chutes de pierres. Plus important encore, les résultats contredisent plusieurs pratiques courantes dans l'évaluation des risques de chute de pierres.

### 1 THE CHANT SURA EXPERIMENTAL CAMPAIGN

Over the course of three summer seasons, we performed comprehensive repetitive single block induced rockfall experiments for two shape classes - cubic and wheel - and four weight classes - 45, 200, 800 and 2670 kg - at the Chant Sura slope (46.74625°N, 9.96720°E) located on the Flüelapass, Switzerland (Fig. 1). The resulting data set hence is termed the *Chant Sura Experimental Campaign* (CSEC). The complete data set comprises 183 runs distributed on the perfectly symmetric, fabricated EOTA blocks, the norm rock of the European Organization for Technical Assessment used in standardised rock fence testing procedures in official European Technical Approval Guidelines in the above-mentioned weight and shape classes. In-situ sensor nodes, so called StoneNodes, allow tracking of internal rotations and accelerations, high-resolution synchronized videogrammetry enables a-posteriori trajectory reconstruction. Detailed information about the experimental setup, used sensors and post-processing procedures as well as the used sensors can be found in Caviezel *et al.*, (2019, 2020) and references therein.

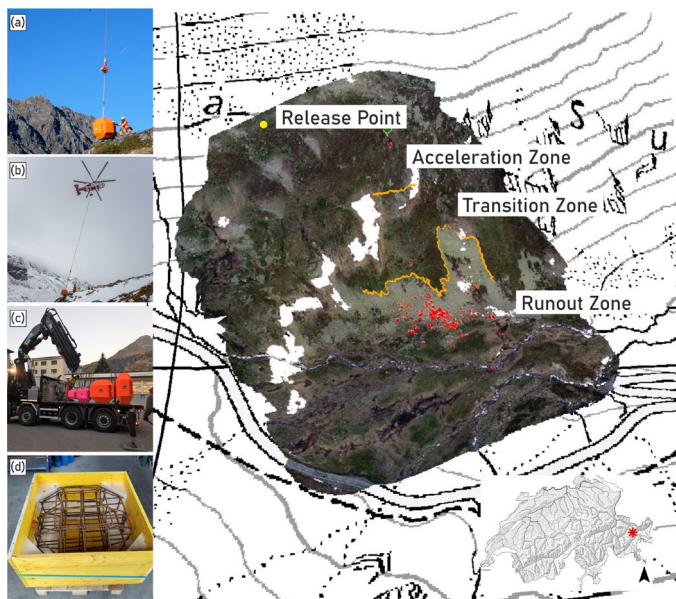


Figure 1: The Chant Sura test site located on Flüelapass, Switzerland, with its geographic location depicted in lower right corner. The images shows a UAS-derived ortho-photo draped over the digital elevation model on top of a swisstopo map (Source: Federal Office of Topography).

The release platform (yellow dot), the entire set of deposited rocks (red markers), the acceleration zone above the cliff, the transition zone between cliff and scree line and runout zone/scree are labelled.

- a) Arrival of a cubic EOTA 2670 kg rock to the release platform.
- b) Slings of heavy rocks by a Kamov KA 32 A12 helicopter.
- c) A subset of the used rocks prepared for transport: EOTA<sub>111</sub> (200/800/2670 kg) and an EOTA<sub>221</sub> (2670 kg) from left to right.
- d) Steel reinforcement cage of a wheel-shaped EOTA block to ensure maximal ruggedness and lifetime.

<sup>1</sup> Caviezel Andrin, WSL Institute for Snow and Avalanche Research SLF, Davos Dorf, CH, caviezel@slf.ch

## 2 FOUR-DIMENSIONAL TRAJECTORY RECONSTRUCTION

If data availability allowed, complete four dimensional trajectory construction has been performed. Figure 2 shows six out of 82 reconstructed trajectories of the CSEC data ensemble plotted over the contour plot of the UAS generated high-resolution digital elevation model. Three trajectories for each shape class – equant and platy – along with its rock shape proxy are depicted. The translational kinematic information is visualized via a velocity scaled, perceptually uniform colouring of the trajectories. StoneNode sensor stream availability is given to 66% for accelerometer data, internal rotations were successfully measured for 63% of the runs. Analysis of deposition points patterns, sensor streams and kinematic contributes to a complete picture and derivation of key messages for single block rockfall events. The data set shows that translational kinematic behaviour remains rather uniform over shape and mass classes, rotational kinematics obviously scale with moment of inertia. The rock shape heavily influences the depositional pattern. While lateral spreading decreases for equant rocks with increasing masses, wheel shaped rocks feature the opposite dependency, a fact ringing the alarm bells for any hazard assessment engineer.

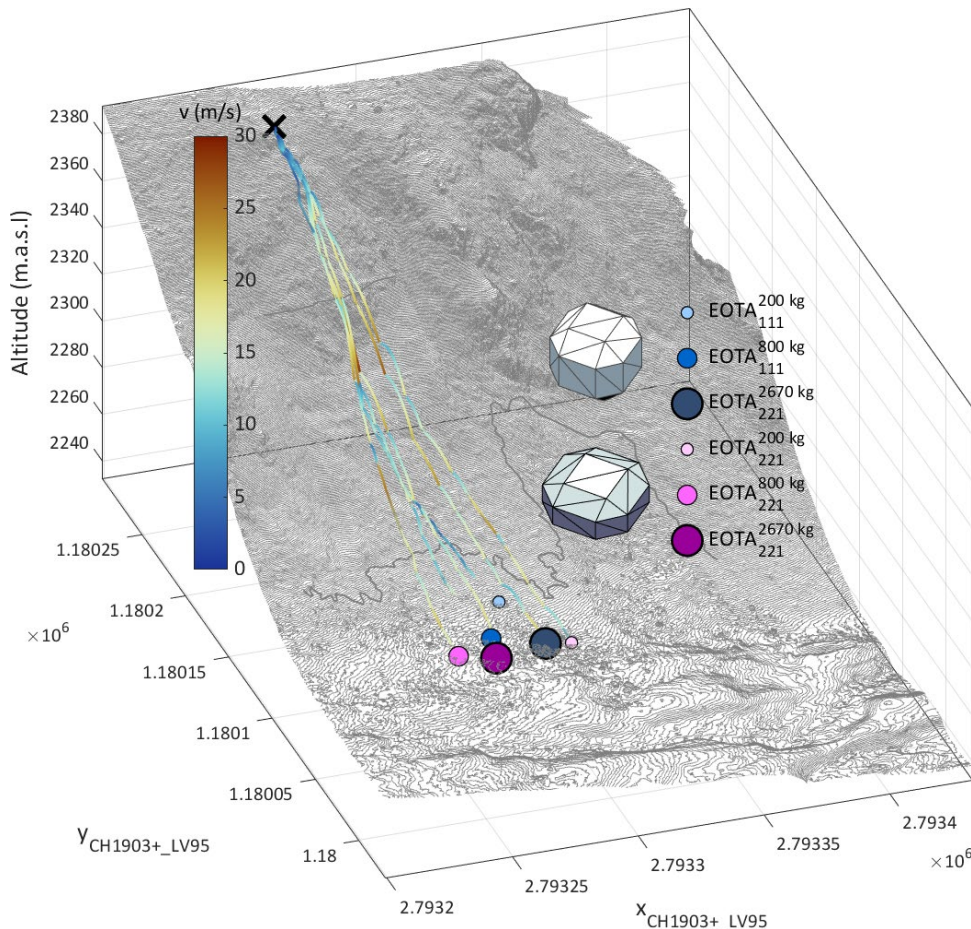


Figure 2: Six selected reconstructed trajectories out of the CSEC ensemble. Blue markers represent equant  $EOTA_{111}$  rocks varying from 200 kg (light blue) to 2670 kg (dark blue). The wheel shaped  $EOTA_{221}$  deposition points are represented with masses from 200 kg (light magenta) to 2670 kg (dark magenta). The translational kinematics are visualised with a velocity scaled, perceptually uniform, colouring of the trajectories.

## CONCLUSION

The key message of the CSEC is to incorporate shape effects in state-of-the-art numerical models but equally in rockfall hazard assessments. Using this data set – as it will be made publicly available - allows the rockfall modelling community to (re-)evaluate existing or newly developed models, as it is continuously done for RAMMS::ROCKFALL (Leine, 2021). Leaving calibration routines on oversimplified assumptions and data sources behind, it could serve as calibration landmark for any numerical model and ultimately lead to more accurate hazard assessment and larger safety margins for societies in rockfall prone environments.

## REFERENCES

- Caviezel, A. *et al.* (2019) Reconstruction of four-dimensional rockfall trajectories using remote sensing and rock-based accelerometers and gyroscopes, *Earth Surface Dynamics.*, 7, 199–210.
- Caviezel, A. *et al.* (2021) Disentangling of Energy Dissipation Mechanisms for Rockfall Hazard Assessment, *Nature Communications*, (under review)
- Leine, R. *et al.* (2021), Stability of rigid body motion through an extended Intermediate Axis Theorem: application to rockfall simulation, *Multibody System Dynamics*, (accepted)

## Slope instabilities of the Larzac Plateau: the Pégairolles-de-l'Escalette rotational landslide

Kévin Elkharrat<sup>1</sup>, Catherine Homberg<sup>2</sup>, Sara Lafuerza<sup>3</sup>, Muriel Gasc<sup>4</sup>

**Keywords:** landslides, rotational, Larzac, slope instabilities

### ABSTRACT IN FRENCH :

Le plateau du Larzac est affecté par plusieurs mouvements de terrain, allant du basculement à des grands mouvements de versant rotationnels, évoluant dans la série sédimentaire allant des grès du Ladinien aux carbonates de l'Hettangien. Ce travail se concentre sur le glissement rotationnel de Pégairolles-de-l'Escalette, afin d'identifier des scénarios de rupture permettant d'expliquer son activité actuelle. Les observations de terrain montrent que le massif est découpé par deux familles de discontinuités en plus de la stratigraphie. Le Rock Mass Rating (Bieniawski, 1993) est utilisé in-situ afin d'obtenir des paramètres mécaniques pour le massif carbonaté. Les modélisations à l'équilibre limite montrent que c'est essentiellement le niveau piézométrique et les niveaux de faiblesses mécaniques qui gouvernent ces instabilités.

### INTRODUCTION

The Larzac carbonate plateau extending from Millau (Aveyron) to Lodève (Hérault) is subjected to various slope instabilities, from rock toppling, to large rotational landslides. Our study focusses on the deep-seated landslide located on the right bank of the Lergue river, close to Pégairolles-de-l'Escalette village and the A75 highway (Fig. 1). Its activity, with a low slip rate of 3 mm/year, has been characterized through in situ (borehole) geophysical monitoring (Denchick et al., 2019).

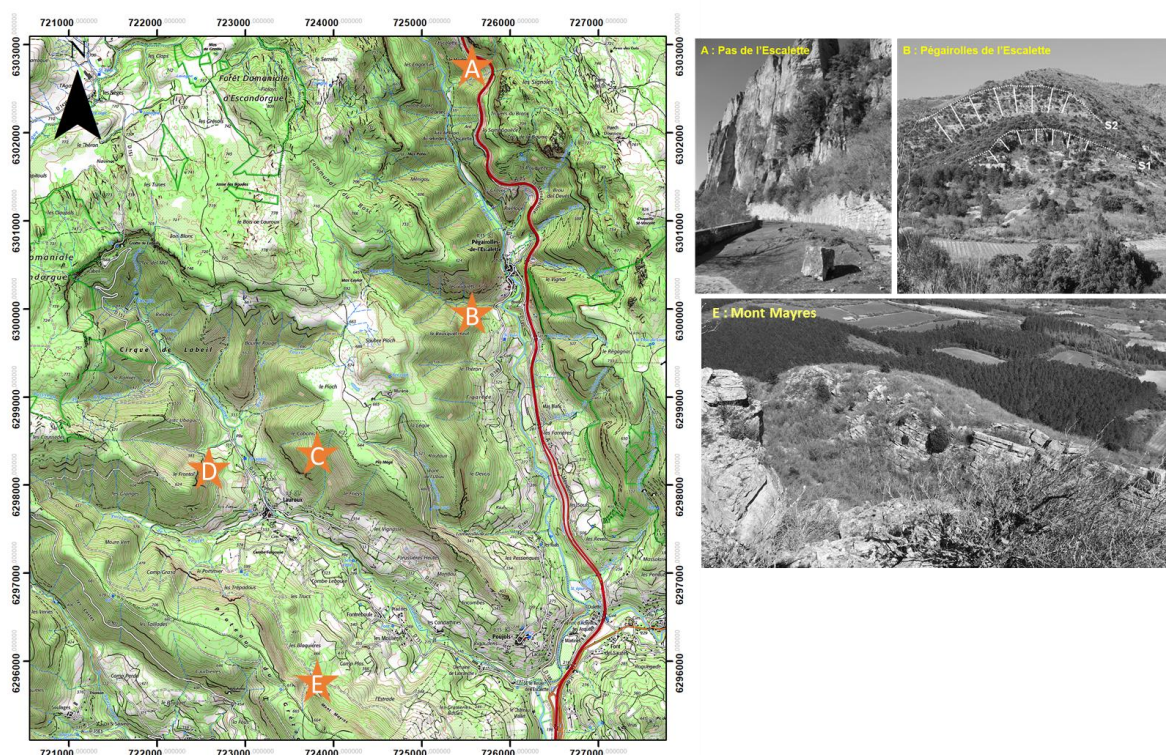


**Figure 1:** geological mapping illustrating the location of the different landslides or rocks toppling, A: Pas de l'Escalette, B: Pégairolles-de-l'Escalette, C: Le Cabanis, D: Le Frontal and E: Mont Mayres

<sup>1</sup> ELKHARRAT Kévin, Sorbonne Université, Paris, France, kevin.elkharrat@sorbonne-universite.fr

<sup>2</sup> HOMBERG Catherine, Sorbonne Université, Paris, France, catherine.homberg@sorbonne-universite.fr

<sup>3</sup> LAFUERZA Sara, Sorbonne Université, Paris, France, sara.lafuerza@sorbonne-universite.fr

<sup>4</sup> GASC Muriel, Cerema, Aix-en-Provence, France, Muriel.Gasc@cerema.fr

The geologic model of the landslide is given in Fig. 2. The rotational slide involves sedimentary rocks from Ladinian (Triassic) sandstone to Hettangian (Jurassic) carbonates and includes several slides surfaces. The presence of similar landslides in the area (Fig. 1), suggest a common (causal) factor.

## 1 AIM OF THE STUDY

The goal of our work is to find the failure scenario accounting for the current activity of the sliding mechanism. For this purpose, several failure scenarios are proposed from field data and evaluated through 2D slope stability simulation based on through 2D slope stability simulation based on the strength reduction analysis approach (implemented in OPTUM G2 software).

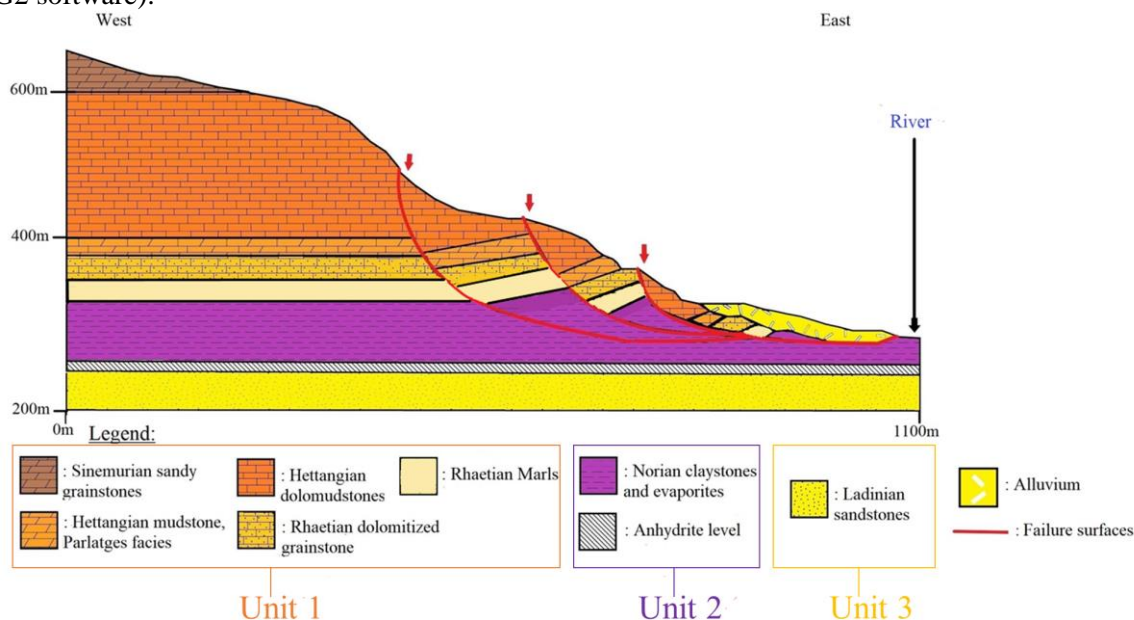


Figure 2: Geological cross-section of the Pégairolles-de-l'Escalette landslide. This geological model has been simplified for the numerical simulations into three lithological units (Unit1: Late Triassic sandstones and Jurassic carbonates, Unit 2: Triassic clays and Unit 3: Triassic sandstones). Location of the deep-seated failure surfaces are given after Denchick *et al.* (2019).

## 2 RESULTS

Field data, that include geomorphological mapping, measurements of the fractures network, and Rockschmidt (Unconfined Compressive Strength, UCS) measurements of the geological units, show that upper units are cut by a dense network of discontinuities. Three families are present: bedding planes, subvertical NNW-SSE joints and subvertical WSW-ENE joints. Using these data, we applied a Rock Mass Rating (Bieniawski, 1993) analysis to propose failure scenarios based on the Hoek-Brown and Mohr-Coulomb failure criterion for the carbonates rocks. Due to the lack of outcrops of Norian clays, UCS values were obtained from literature (Hoek, 1990). Borehole information available informs about anhydrite intercalated in Norian clays (Denchik *et al.*, 2019). The five failure scenarios tested were based on a trilayer geological model: carbonates overlying claystones overlying sandstones. These scenarios illustrate the role of joints, anhydrite levels and water table on the slope stability.

## CONCLUSION

These numerical simulations demonstrate the importance of considering both joints and weak mechanical levels like anhydrite bed, but also the main role of water table as key parameters governing slope instabilities in heterogeneous rock medium like sedimentary rocks.

## REFERENCES

- Bieniawski, Z. T. (1993) Classification of Rock Masses for Engineering: The RMR System and Future Trends, in *Rock Testing and Site Characterization*. Elsevier, pp. 553–573. doi: 10.1016/B978-0-08-042066-0.50028-8.
- Denchik, N. *et al.* (2019) In-situ geophysical and hydro-geochemical monitoring to infer landslide dynamics (Pégairolles-de-l'Escalette landslide, France), *Engineering Geology*, 254, pp. 102–112. doi: 10.1016/j.enggeo.2019.04.009.
- Hoek, E. (1990) Estimating Mohr-Coulomb Friction and Cohesion Values from the Hoek-Brown Failure Criterion, *Int. J. Rock Mech. Min. Sci. & Geomech. Abstr.*, 27(3), pp. 227–229.

## Small scale rock fall experiments and statistical laws for run-out

Dominique DAUDON (corresponding author)<sup>1</sup>, Vincent COUALLIER<sup>2</sup>, Frédérique LEBLANC<sup>3</sup>

**Keywords:** rockfall, small scale experiment, statistical analysis, censored data, Weibull distribution, extreme quantiles

### 1 SMALL SCALE RUN-OUT EXPERIMENTS ON BI-PLANAR SLOPES

Full-scale boulder fall experiments are hard to organize as demonstrated in the last C2ROP program (Bourrier 2020). Consequently, the lack of full documented data creates difficulties in evaluating the hazard and assessment of risks in the management of territories. Factors such as shape, initial velocity, initial orientation, and number of the blocks have great influences in the run-out (named  $X$ ) of the falling rocks, leading to difficulties to forecast the run-out zoning. Inspired by the sites of “Millau, Mizoen, and C2ROP” (Bourrier 2020, Cuervo 2015, Garcia 2020), a simple scaled experimental model was designed (Figure 1a), and tested with repetitive launches of various blocks and substrates on a bi-planar academic slope of  $45^\circ$  (adjustable from  $20^\circ$  to  $55^\circ$ ), with a free fall of 20 cm (adjustable from 10 to 30 cm). The actual database is available for 4 types of substrates (sand, wood, various rough substrates) and various blocks (set of 28 blocks essentially, repeated 50 times such as, parallelepiped, cubic and multi-faced dices, plastic or mineral material). The final location of blocks has been acquired by pictures (Figure 1b), and analyzed in term of position of the gravity center of each block of the run-out zone (60 cmx50 cm). A SQL database has been elaborated (Piras 2019) in order to have pertinent and liable statistical analysis directly on the  $X$  position of bloc's gravity center (Figure 1c). Results are translated by means of statistical and probabilistic work. This first study explores simple statistical laws that could be used by risk managers and experts to estimate quickly the probabilistic distribution of run-out distances in gravitational risks crisis managements. Further similitude studies are needed to apply the concept at realistic scales of engineering problems.

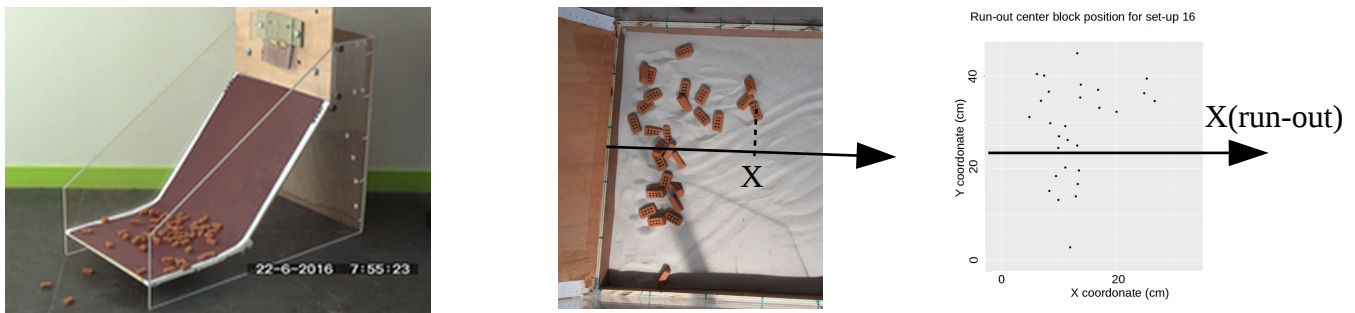


Figure 1: a) small experiment with sand paper substratum and cooked brick “block”

b) a launch of 28 blocks on sand

c) run-out point's coordinates obtained

### 2 STATISTICAL ANALYSIS

#### 2.1 Data description and their modelization

We analyzed 50 repetitive launches of 28 blocs, 14 bloc and 42 blocks by varying run-out surface, shapes ... The study is done only on a part of the database (sand boxe and wood plate). The  $X$  distance where modelized as a non-symmetric distribution law since we obviously observe a largest concentration of blocks with small run-out (small  $X$  values). Among the parametric models available for this problem was chosen the classical Weibull distribution characterized by two parameters (shape and scale) as it was demonstrated to be flexible enough (Mahfoud 2020) and permitted to estimate the survival function (probability of  $X$  exceeds a positive value  $t$ ) and more importantly the quantile function (to estimate extreme runout distances associated with small probability) with censored data. The

<sup>1</sup> UGA,CNRS, 3SR,Grenoble, <sup>3</sup>UGA, CNRS, LJK; <sup>1,3</sup> prénom.nom@univ-grenoble-alpes.fr ; <sup>2</sup> vincent.couallier@u-bordeaux.fr

Kaplan-Meyer non parametric estimator of the survival function was also provided for comparison. The experiment had a full factorial design with six factors: the set-up, characterized by factors slope (45°), type of material, kind of objects (brick and multiface dices), height of free fall (20 cm), and the number of launched blocks (n=14, 28 or 42). Fifty repetitions were carried out for each treatment.

## 2.2 Estimation of the survival function

The statistical fitting of the survival functions showed that the Weibull distribution fits correctly the data. The effects of the censorship rate and small sample sizes were analyzed with respect to their impact on confidence intervals.

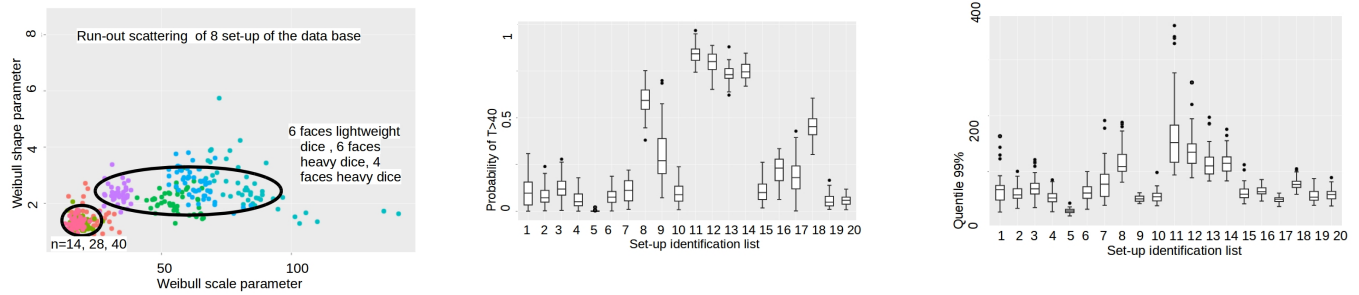


**Figure 2 : a) internal variability or similarity for 8 set-up b) boxplots of estimated probability that  $X > 40$  according to each setup c) boxplots of 99% estimated quantile according to each setup**

We have shown that the dispersion of the runout distances, and thus the extremes quantiles, differently depend on some factors defining the setup: for example, n has less effect than block shapes (Figure 2 a).

The parameters of the adjusted law being estimated for each launch, we can next compute any statistic related to it, for example the probability that an object exceeds any value t (Figure 2b; t=40; Figure 2c : 99% quantile). Without surprise the largest estimated survival function in t=40 occurs for setups where heavy dices with 6 or 8 faces were used. Therefore, the associated 99% quantiles are also the biggest one.

## CONCLUSIONS

This preliminary study shows importance of faces number and weight for estimating probability of runout distances or quantiles, and less importance on some others such as a limited number of block up to 40 specimens. The dependence of blocks' runouts within each launch is asserted by the effect of the sample size n. Weibull distribution law seems to be pertinent to qualify the run-out distribution. Further work will include an enrichment of the database with other levels of main factors (design of experiment), estimation of the extreme quantiles when no or few extreme observations are available (to be linked with the censorship rate), definition of a model explaining quantiles in terms of levels of the main factors, by regression methods.

**Aknowlegments:** thanks to IDEX UGA "Excellence training period program" and "CDP Risk program" for founding the training periods of A.Mafhoud, B. Bataihl, A.Piras and W.Ardati .

## REFERENCES

- Bourier(2020). Toe, D.; Garcia, B.; Baroth, J.; Lambert,S.(2020). Experimental investigations on complex block propagation for the assessment of propagation models quality. Landslides.10.1007/s10346-020-01469-5.
- Cuervo (2015). ; Daudon, D.; Richefeu, V. ; Villard, P. ; Lorentz, J. (2015). Discrete Element Modeling of a Rockfall in the South of the "Massif Central", France. 1657-1661. 10.1007/978-3-319-09057-3\_294.
- Garcia (2020). Richefeu, V.; Baroth, J.; Daudon, D. ;Villard, P. (2020). Collision of Shaped Boulders With Sand Substrate Investigated by Experimental, Stochastic, and Discrete Approaches. Journal of Geophysical Research: Earth Surface. 125. 10.1029/2019JF005500.
- Piras(2019). Internship report (supported by stages d'excellence de l'UGA). Chute de blocs rocheux : organisation et analyse statistique de données acquises sur modèle réduit.
- Mahfoud (2020). Master's thesis. Boulder rockfalls run-outs statistical analysis of data collected on a scale model.

## TLS- and inventory-based Magnitude – Frequency relationship for rockfall in Montserrat and Castellfollit de la Roca

Marc JANERAS<sup>1,2</sup>, Oriol PEDRAZA<sup>1</sup>, Nieves LANTADA<sup>2</sup>, Amparo NUÑEZ<sup>2</sup>, Didier HANTZ<sup>3</sup>, Joan PALAU<sup>1</sup>

**Keywords:** magnitude, cumulated frequency, rockfall, hazard assessment

Hazard scenarios are defined by a representative event of a certain magnitude, which corresponds to a frequency of occurrence or annual probability. In rockfall, scenario magnitude is identified by the total volume detached. Therefore, in diffuse hazard assessment it is crucial to fit this relationship magnitude/frequency, called McF, where cumulated frequency is quoted in spatial & temporal terms. Inventories are the classical source of data to deal with this objective. Last decade, TLS or digital photogrammetry monitoring came to offer a complementary approach. The samples obtained by the two methods have a specific coverage and each has its own lack of information that can be compensated together.

### 1 CASE SITES AND DATA

#### 1.1 Montserrat massif of conglomerate (M)

Montserrat Mountain is an isolated massif formed mainly by layers of conglomerate, and a characteristic relief of rocky walls and needles very attractive for climbing. It is placed at 50 km NW from Barcelona, in Catalonia, NE of Spain. The interest for this case is the rockfall risk on infrastructures and buildings to be managed according to natural and cultural heritage preservation besides the touristic activities. TLS available data cover more than 12 years of surveys in several scanner stations at different altitude and aspect of the mountain slopes (Table 1) (Janeras *et al.*, 2017). The historical and observational inventory has 205 events recorded from 1546 to present, ranging from 0.001 to 2160 m<sup>3</sup>.

#### 1.2 Castellfollit de la Roca basaltic cliff (C)

Castellfollit de la Roca is a country-side village placed at 50 km NW from Girona city, in Catalonia. The interest for this case comes from the risk caused by the rocky cliff retreat, since the town is placed at its top. The cliff is formed by columnar basalt of ancient lava flows in this inactive volcanic area, where the whole cliff become a high value landscape heritage. TLS available data cover near 12 years of surveys in 3 scanner stations and points of view of part of the cliff (Table 1) (Abellán *et al.*, 2011). Available inventory data cover 43 years from 1976 to 2018 and recorded 17 events from 1 to 1500 m<sup>3</sup>.

Table 1: Collected data with TLS surveys and McF regression.

Sample	Area (hm <sup>2</sup> )	Period (years)	No. of surveys	Sampling (hm <sup>2</sup> ·year)	No. of events	Volume min (m <sup>3</sup> )	Volume max (m <sup>3</sup> )	A <sub>st</sub>	B	R <sup>2</sup>
M: Degotalls_N+E	3.06	12.56	24	38.42	357	3.0E-04	7.9E+02	0.392	0.527	0.977
M: Monastery	3.57	8.79	23	31.39	162	2.0E-04	4.8E-01	0.097	0.652	0.875
M: Rack railway	1.83	3.36	8	6.15	19	1.6E-03	1.7E-01	0.104	0.656	0.986
M: Collbató Caves	2.32	3.82	7	8.86	21	6.0E-04	1.7E-01	0.180	0.464	0.943
Montserrat_ALL	10.78	7.87		84.82	397	5.0E-03	5.0E+01	0.166	0.640	0.987
C: Upper lava flow	2.40	11.86	5	28.47	194	5.3E-04	6.0E+00	0.333	0.472	0.970
C: Lower Lava flow	0.24	8.53	5	2.05	91	3.1E-04	3.8E+00	1.134	0.534	0.974
Castellfollit_ALL	2.64	11.56		30.52	240	2.0E-03	3.2E+00	0.391	0.490	0.995

The temporal and spatial coverage of each sample can be expressed in hm<sup>2</sup>·year, according to the surveyed outcrop surface and the period. The larger a component or another, the more appropriate is the analysis of spatial or temporal variability.

### 2 MAGNITUDE-FREQUENCY RELATIONSHIP

#### 2.1 Magnitude range

TLS and inventory data cover different volume ranges, according to sampling coverage (in time and space) and systematic detection capabilities. Therefore, the combination of both data allows to reach the maximum representativeness of the McF relation expressed by a potential law for the spatial & temporal cumulated frequency F<sub>st</sub> for detached volume equal or larger than V<sub>i</sub>, with unitary activity A<sub>st</sub> and distribution coefficient B:

$$F_{st}(V \geq V_i) = A_{st} \cdot V_i^{-B} \quad (1)$$

<sup>1</sup> Institut Cartogràfic i Geològic de Catalunya (ICGC), Barcelona, ES, [marc.janeras@icgc.cat](mailto:marc.janeras@icgc.cat), 

<sup>2</sup> Universitat Politècnica de Catalunya (UPC), Barcelona, ES

<sup>3</sup> Institut des Sciences de la Terre (ISTerre) – Université Grenoble Alpes (UGA), Saint-Martin-d'Hères, FR

Power law fitting corresponds to the assumption of scale-invariant behaviour. Montserrat data suggest that as rockfall mechanism changes, this hypothesis can become wrong, and the fitting can be scale-variant for different volume ranges. Statistical distribution of volume in the lowest limit is clearly affected by the detection capability of each surveying method and the surveying frequency, so the well-known roll-over effect is observed. Similarly, in the upper limit apparent scale-variant effects are observed in highest volumes due to several effects on extreme values recorded in the sampling, certainly limited. To overcome both distortions, different filtering techniques are applied in order to fit the power law for the central part.

## 2.2 Spatial variability

At massif scale, results of the power laws agree with the values obtained by previous similar work in France (Hantz *et al.*, 2020). Parameter B can be correlated with rock mass quality, where not only fracture density seems relevant, but the intercalation of hard and soft rock layers also could play a role (Table 1). In the same massif and lithology (Figure 1), at outcrop scale both parameters  $A_{st}$  and, in some reverse way, B show a fairly large variability that must be analysed more in detail, as it may become relevant for hazard zoning.

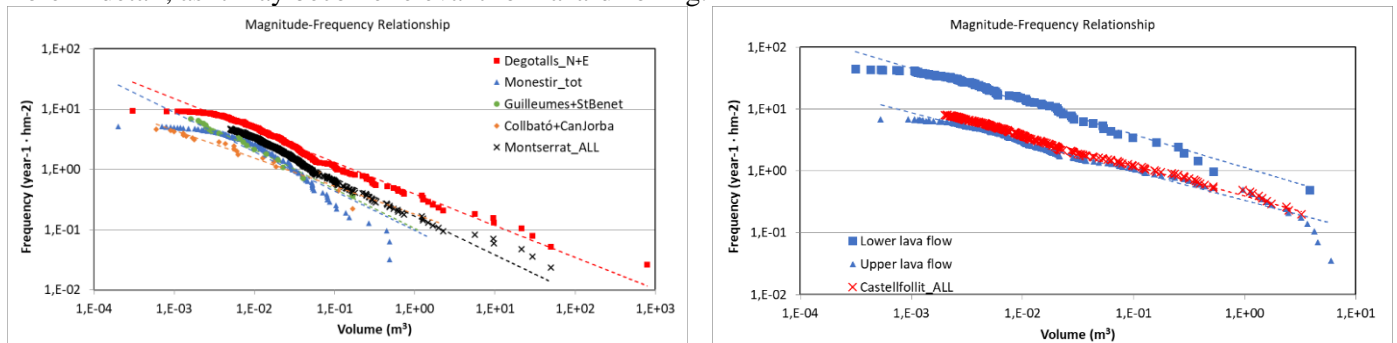


Figure 1: Magnitude – cumulated Frequency power law fitting for different samples in Montserrat (left) and Castellfollit de la Roca (right).

## 2.3 Temporal variability

As known, hazard is variable in time according to episodes of detaching actions, like rainfall. This rockfall activity along time is reflected to different values of  $A_{st}$  & B parameters for each sub-sampling in yearly periods (Figure 2). The effects of stabilization works, progressive rupture episodes and other changes in the wall can be seen reflected in these parameters over time. Also, from this variability is deduced the convenience of five years minimum duration of sampling so as not to be excessively subject to particular periods.

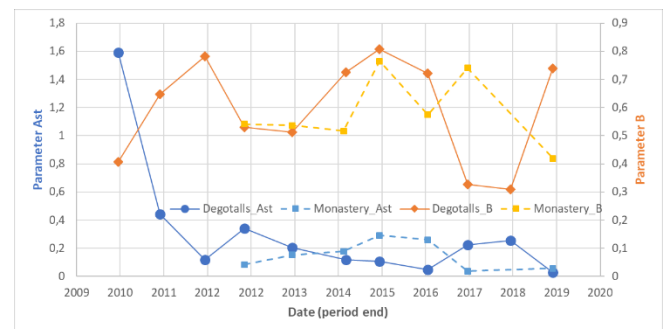


Figure 2: Time variability of  $A_{st}$  & B parameters in Montserrat.

## CONCLUSION

Rockfall inventory combined with monitoring with TLS allow an adequate hazard of detachment assessment as a basis for quantitative risk analysis, insofar as they allow to define scenarios of a certain magnitude to which to assign an annual probability of occurrence.

## ACKNOWLEDGEMENTS

This work is being carried out in the framework of the research project ‘Advances in rockfall quantitative risk analysis, QRA’, acronym GeoRisk, funded by the Spanish Ministry of Economy & Competitiveness and the Agencia Estatal de Investigación (AEI) with grant number PID2019-103974RB-I00/AEI/10.13039/501100011033. TLS data were processed by the RiskNat research group of the University of Barcelona.

## REFERENCES

- Abellán, A., Vilaplana, J.M., Calvet, J., García-Sellés, D., Asensio, E. (2011) Rockfall monitoring by Terrestrial Laser Scanning - Case study of the basaltic rock face at Castellfollit de la Roca (Catalonia, Spain). *Natural Hazards and Earth System Science*, 11, 829-841. doi:10.5194/nhess-11-829-2011.
- Hantz, D., Colas, B., Dewez, T., Lévy, C., Rossetti, J.P., Guerin, A., Jaboyedoff, M. (2020) Caractérisation quantitative des aléas rocheux de départ diffus. *Revue Française de Géotechnique*, 163, 2. doi:10.1051/geotech/2020011.
- Janeras M., Jara, J.A., Royán, M.J., Vilaplana, J.M., Aguasca, A., Fàbregas, X., Gili, J.A., Buxó, P. (2017) Multi-technique approach to rockfall monitoring in the Montserrat massif (Catalonia, NE Spain). *Engineering Geology*, 219 (2017) 4–20. doi:10.1016/j.enggeo.2016.12.010.

# Monitoring techniques

## Comparison of the effectiveness of the InSAR method in rocky areas and forested areas

Pouyan Abbasimaedeh<sup>1\*</sup>, Hugues Vincent<sup>2</sup>, Thibault Colette<sup>3</sup>, Abdeljalil Nahli<sup>4</sup>, Maxime Tatin<sup>5</sup>, Vincent Lamour<sup>6</sup>  
<sup>1,2,3,4,5,6</sup> 9 rue Léon Blum 91120 Palaiseau, Cementys Co., France

**Keywords:** InSAR, Slope Sliding, Movement, Rock Slope, Satellite

### 1 PURPOSE

Landslides and slope sliding are among the most common geological hazards which represents a major threat to human life, infrastructure and natural environment in most mountainous and rocky areas with steep slopes. Many methods have been used for mapping and monitoring ground and slope surfaces displacement (Krainer and Mostler, 2000, Krainer and He, 2006, Bauer et al., 2003, Käab, 2002).

During the last few decades, satellite-based interferometric synthetic aperture radar (InSAR) has become an important tool for mapping and monitoring a variety of displacement processes (Massonnet and Feigl, 1998). Depending on the revisit period of the SAR satellite, InSAR can monitor relative ground displacement on a scale of millimetres to centimetres (Berardino et al., 2002; Henderson et al., 2011, Chaussard et al., 2014, Massonnet et al., 1995, Liu and Danskin, 2001, Fialko et al., 2004). Temporal decorrelation is one of the main limitations of InSAR technology and particularly over vegetated areas, where decorrelation increases with the amount of vegetation cover because the scatters of the plants sensibly change over time.

In this research, we focused on the performance and effectiveness of InSAR monitoring in two different regions in rocky and vegetated coverage areas located in different geographical regions. We used the same configuration on InSAR sensitivity analysis and will compare the result of the density of reference points, noises, atmosphere and filtering effects and the density of losses points in both areas. Also, we will assess the quality of stability analysis in vegetated coverage and without coverage slopes. The first case study focuses on the measurements of sidewalls for Masjed Soleyman Dam in Iran and the second case is the Romanche valley area in the southern part of France.

### 2 STUDY AREAS

The Masjed Soleyman rockfill dam is constructed on Karun River in Khuzestan province in the southwest of Iran, 25.5km from Masjed Soleyman city. The dam has a maximum height of 177m, width of 700m at the foundation level and crest length of 492m. It is made of a central impervious core and upstream and downstream resting on the Bakhtiyari geological formation which is marked by a hard conglomerate and very thin clay intercalation. This study is focused on left side walls which have rocky material and covered by shotcrete concrete. This area has been rehabilitated by Pars Soil and Water Co. and fully stabilized using added strand anchorage and mono-bars.

Romanche valley area is located in the department of Isere and the Auvergne-Rhône-Alpes region in France. Romanche valley area is located on the road which links Grenoble to the ski resorts of Oisans. Romanche valley is mainly covered with forests (700 ha) but also with Lake Luitel (17 ha) and a river (the Romanche). It is an active area of landslides of Mont-Sec which forms the extreme south of the Belledonne range.

### 3 RESULTS

The rate of displacement and settlement of the rocky and vegetated coverage area have been evaluated by InSAR method with an emphasis on time series analysis. The result of this research is mainly focused on the density of detected reference points by interferometric analysis from satellite images in the study areas (Fig. 1). Reference points with low noise and compatible frequency were selected automatically by the image processing procedure to find the exact settlement and uplift amounts. In this step, the image processor will consider the range of noise and range of frequency between neighbour points and will select the points with a considerable amount of coordination.

Results show that the number of detected reference points by InSAR in rocky slopes and concrete face areas are considerably greater compared with detected reference points in the vegetated coverage area. Besides, it is observed that at least 80% of the detected reference points had been ignored after time history analysis in the vegetated coverage area by the image processor. Obtained results show that the precise movement control of high vegetated coverage area, due to high image noise and lack of natural reflectors can hardly be done.

1 Abbasimaedeh, Pouyan, PhD in Geotechnical Engineering, Director of Geotechnical R&D, pouyanAbbasimaedeh@cementys.com

2 PhD in Structural Engineering, Head of R&D Department

3 Topographic measurement expert

4 PhD student in Geodetic Engineering

5 PhD in Civil Engineering, Executive Vice President - Technical Director

6 CEO



Figure 1: Results of the Romanche valley area, France (left) and Masjed Soleyman Dam, Iran (Right)  
The comparison result with another monitoring project in a Bridge located in Saudi Arabia showed the higher accuracy for the point measurement in a comparison with the general measurement (Fig. 2).

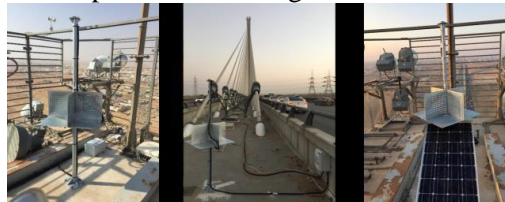


Figure 2: Co-located CRs and GNSS antennas installed on the bridge in Saudi Arabia (Nahli et. Al. 2020; 2018)

## CONCLUSION

Two different areas with different surface coverage have been evaluated by InSAR analysis in this study. An area is covered by rock and concrete shotcrete while another region is covered by vegetated skin and mature forest. Obtained results show that the rocky area has an acceptable number of natural reference points and their density is adequate for and accurate InSAR analysis in the study area. Obtained results also showed that due to detecting a lot of amount of high noisy points in vegetated skin areas, most of reference points had been ignored in final time history analysis by InSAR method. Consequently, using artificial reflector have been suggested by Cementys company to receive an accurate result in both special structure and the selected area.

## REFERENCES

- Bauer, A., Paar, G., Kaufmann, V. (2003). Terrestrial laser scanning for rock glacier monitoring. In: Proceedings of the 8th international conference on permafrost, Zürich. 55–60.
- Chaussard, E., S. Wdowinski, E. Cabral- Cano, and F. Amelung. (2014), Land subsidence in central Mexico detected by ALOS InSAR time- series, *Remote Sens. Environ.* 140, 94– 106.
- Massonnet, K.L. (1998). Feigl Radar interferometry and its application to changes in the Earth's surface *Rev. Geophys.* 36 (4), 441-500.
- Fialko, Y. (2004). Probing the mechanical properties of seismically active crust with space geodesy: Study of the co-seismic deformation due to the 1992 Mw 7.3 Landers (southern California) earthquake. *J.Geophys.Res.*109.
- Henderson, I.H.C., Saintot, A. (2011). Regional spatial variations in rockslide distribution from structural geology ranking: an example from Storfjorden, western. Norway. *Slope Tectonics.* Geological Society, London, Special Publications, 351, 79 – 95.
- Ka'ab, A., Huggel, C., Paul, F., Wessels, R., Raup, B., Kieffer, H., Kargel, J. (2002). Glacier monitoring from ASTER imagery: Accuracy and Applications, in *Proceedings of EARSeL-LISSIG Workshop Observing our Cryosphere from Space*, 2002.
- Krainer, K., He, X. (2006). Flow velocities of active rock glaciers in the Austrian Alps, *Geografiska Annaler: Series A, Phys. Geography.* 88, 267–280.
- Krainer, K., Mostler, W. (2002). Hydrology of active rock glaciers; Examples from the Austrian Alps. *Arctic, Antarctic, and Alpine Research.* 34(2), 142-149.
- Lu, Z., W. Danskin. (2001), InSAR analysis of natural recharge to define the structure of a ground- water basin, San Bernardino, California, *Geophys. Res. Lett.* 28(13), 2661– 2664.
- Massonnet, D., M. Rossi, C. Carmona, F. Adragna, G. Peltzer, K. L. Feigl, and T. Rabaute. (1993). The displacement field of the Landers earthquake mapped by radar interferometry, *Nature.* 364, 138– 142.
- Nahli, A., Simonetto, E., Merrien-Soukatchoff, V., Durand, F., Rangeard, D. (2018). Sentinel-1 for monitoring tunnel excavations in Rennes, France, *Procedia Computer Science*, 138, 393-400.
- Nahli, A., Simonetto, E., Tatin, M., Durand, S., Morel, L., and Lamour, V. (2020). ON THE COMBINATION OF PSINSAR AND GNSS TECHNIQUES FOR LONG-TERM BRIDGE MONITORING, *Int. Arch. Photogram. Remote Sens. Spatial Inf. Sci.* 325–332.
- P, Berardino., G. Fornaro., R. Lanari., E. Sansosti. (2002). A new algorithm for surface deformation monitoring based on small baseline differential SAR interferograms *IEEE TGRS.* 40 (11), 2375-2383.

## **Inventory of ground instabilities on the western Mediterranean coast of Morocco (case of the region between Tetouan and Jebha)**

Haytam TRIBAK<sup>1 2 3</sup>, Muriel GASC-BARBIER<sup>2</sup>, Abdelkader EL GAROUANI<sup>3</sup>

**Keywords:** ground instabilities, remote sensing, GIS, inventory, Moroccan Rif

### **ABSTRACT IN ENGLISH:**

The mountainous geosystem of the Moroccan Rif is considered to be one of the regions most sensitive to ground instabilities in the world. In order to carry out, for example, a land use plan or to initiate more in-depth scientific research studies in a given region, an inventory mapping the instabilities is necessary. The latter, will be the object of the present work, and will be generated from space remote sensing tools, mainly thanks to the Google Earth Professional program, also through direct observations in the field. GIS tools will then come for digital processing. The results obtained correspond to inventory maps mentioning the distribution, typology and extent of ground instabilities.

### **ABSTRACT IN FRENCH:**

Le géosystème montagneux du Rif marocain est considéré comme l'une des régions les plus sensibles aux instabilités de terrain dans le monde. Afin de réaliser, à titre d'exemple, un plan d'aménagement territorial ou d'entamer des études de recherches scientifiques plus poussées dans une région donnée, un inventaire cartographiant les instabilités de terrain est nécessaire. Ce dernier, fera l'objet du présent travail, et sera généré à partir des outils de télédétection spatiale, principalement grâce au programme Google Earth Professionnel, aussi à travers des observations directes sur le terrain. Les outils SIG viendront ensuite pour le traitement numérique. Les résultats obtenus correspondent à des cartes d'inventaire mentionnant la répartition, la typologie et l'étendue des instabilités de terrain.

## **INTRODUCTION**

Before any study concerning the ground instabilities of a given region, it is essential to proceed to their census and organize them in a well-defined inventory. The latter represents the simple form of their mapping (Hansen, 1984), and makes it possible to define their type insofar as perceptible traces still exist (Varne, 1984).

### **1 AIM OF THE STUDY**

The coastal region, stretching from Tetouan city to Jebha village, is considered among the areas most affected by the different types of instability in the north-western Rif. The ground movements constitute very active phenomena which find in the geological formations of this zone a place of predilection. Taking into account our scientific research concerning the study of the factors and behaviours of ground instabilities, based essentially on heuristic and conceptual approaches, and in the absence of a national database, it was an opportunity to produce an inventory covering the entire region of study.

### **2 METHODOLOGY**

Obtaining our inventory of ground instabilities is based on two essential steps, the first of which consists of a visual analysis of high resolution satellite images, combined with field campaigns for a confirmatory and complementary purpose. Images from the Google Earth Professional program database were the subject of this analysis. The second corresponds to importing the various digital data into GIS tools for the final processing of the inventory.

---

<sup>1</sup> TRIBAK Haytam, Université Côte d'Azur, Nice, France (FRA), haytam.tribak@etu.unice.fr

<sup>2</sup> GASC-BARBIER Muriel, CEREMA, Aix En Provence, France (FRA), Muriel.Gasc@cerema.fr

<sup>3</sup> EL GAROUANI Abdelkader, Université Sidi Mohamed Ben Abdallah, Fès, Maroc (MAR), Abdelkader.elgarouani@usmba.ac.ma

### 3 RESULTS

The results are translated into maps of distribution of ground instabilities in the study region, while mentioning their typologies and their extent. The synthetic cartography presents four main families of instabilities : landslides, rockslides, forms of gullying and collapses of developed slopes considered to be purely anthropogenic movements. These latter can correspond to the different types of movement mentioned above, but also to mudflows, rockflows, sometimes to all the typologies combined. Two types of inventory map have been created ; the general map of instabilities indicating the location of the phenomena (figure 1). Then, four other inventory maps, even more detailed, were generated from the general map in order to present the instabilities as they are actually in the field.

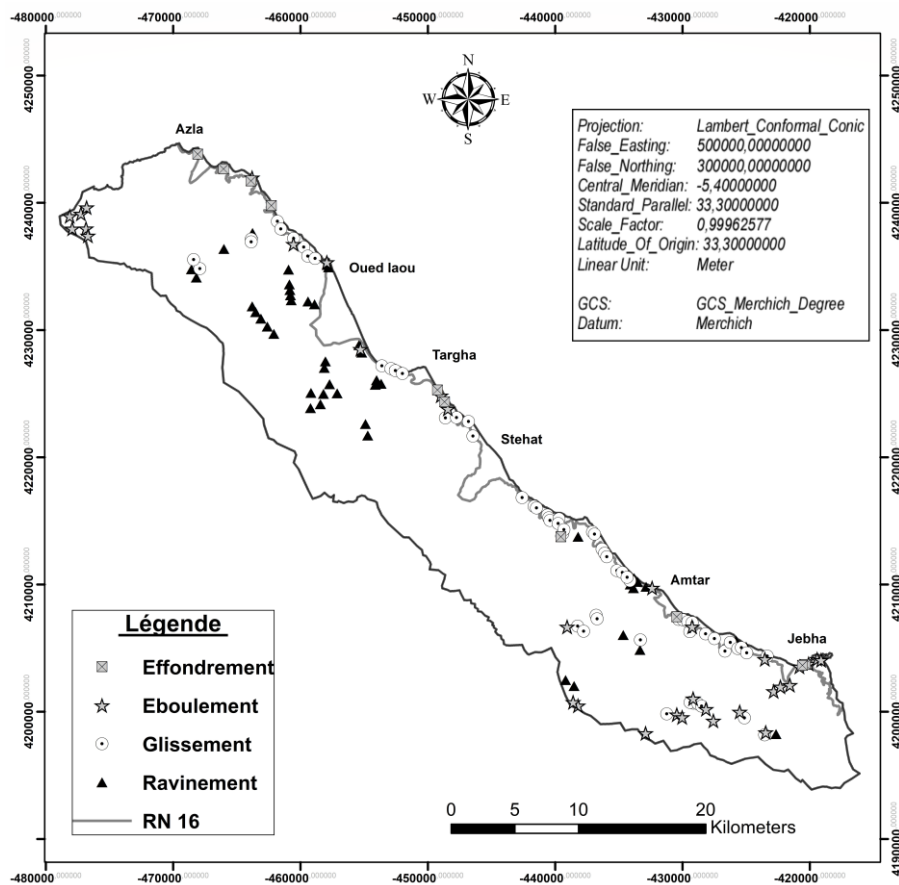


Figure 1 : inventory map of ground instability

### CONCLUSION

The surveys of ground instabilities at the level of the Moroccan Rif, through the spatial analysis of satellite images and field observations, allowed the creation of inventory maps. The latter will be primordial elements for our scientific research of instabilities. They will also participate in interpretative approaches thereafter. On the other hand, they will be part of the national database of ground instabilities and will be used for other applied finality.

### REFERENCES

- Hansen, M.J. (1984) Strategies for classification of landslides. Brunsden, D. and Prior, D.B. (eds.) Slope Instability. John Wiley and Sons, 1- 25p
- Varnes, D.J. (1984) Landslide Hazard Zonation, a review of principles and practice. *IAEG Commission on Landslides*. UNESCO, Paris, 63 p.

## Preventive maintenance and non-destructive monitoring of rock anchors Tools resulting from dynamic tests and their correlation with static tests

Corinne HORB, RINCENT ND Applications, Courcouronnes (FR), corinne.horb@rincent.fr, Jérémie SAUREL, RINCENT Alpes, Montvendre (FR), jeremie.saurel@rincent.com – Jean-Jacques RINCENT, RINCENT SAS, Courcouronnes (FR), jean-jacques.rincent@rincent.com

**Keywords:** anchor, dynamic test, static test, stiffness, force, length, diameter, tools, diagnosis, maintenance, monitoring, prevention.

### RÉSUMÉ

A partir d'essais réalisés sur le site des Petits Goulets à Saint Eulalie en Royans (FR), RINCENT Laboratoires présente les bases des analyses vibratoires menées sur des ancrages et leurs corrélations aux essais statiques.

Sont exposés le calcul des raideurs statiques et dynamiques et la relation entre ces deux paramètres. Des exemples de calcul de longueur et de calcul de diamètre à partir de l'admittance apportent des outils de contrôle complémentaire.

L'équivalence entre raideurs statiques et dynamiques permet de remonter au calcul de la force interne des ancrages. Une baisse ou une augmentation anormale de la rigidité d'un système est un signal concernant le fonctionnement de ce système. Les essais dynamiques non destructifs étalonnés sur des essais statiques sont un moyen de généraliser les diagnostics sur les ancrages et d'améliorer la maintenance.

### ABSTRACT

Based on tests carried out at the Petits Goulets site in Saint Eulalie en Royans (FR), RINCENT Laboratoires presents the basics of vibration analyzes carried out on anchors and their correlations with static tests.

The calculation of the static and dynamic stiffnesses and the relation between these two parameters are exposed. Examples of length calculation and diameter calculation from admittance provide additional control tools.

The equivalence between static and dynamic stiffnesses makes it possible to go back to the calculation of the internal force of the anchorages. An abnormal decrease or increase in the rigidity of a system is a signal concerning the operation of that system. Dynamic non-destructive testing calibrated on static testing is a way to generalize anchorage diagnostics and improve maintenance.

### PRESENTATION

#### 1 STATIC AND DYNAMIC STIFFNESS

The static stiffness is the slope of the stress-strain curve under a given stress, the result is expressed in N / m. This curve is obtained from the tensile tests by steps (NF P 94 444) carried out using a jack and displacement measuring equipment.



Figure 1 : Static step tensile test – Example

The principles of dynamic testing, with instrumentation at the head of the anchor, are as follows :

- Produce a compression wave in the tested element with measuring the force of the impact,
- Measure the velocity of the movement induced on the surface of the tested element,
- Measurements made in time mode are processed in frequency mode.



Figure 2 : Dynamic test – Example

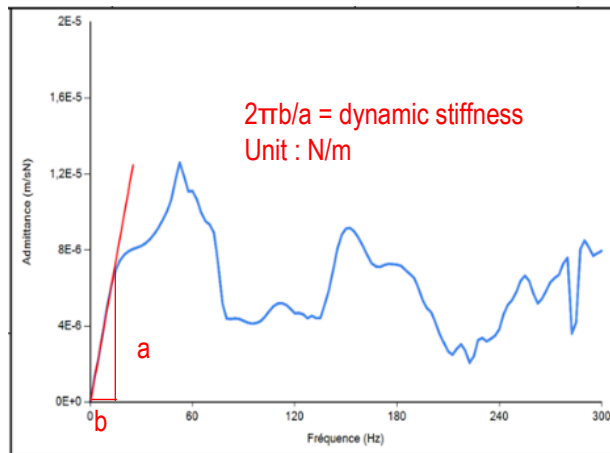


Figure 3 : V/F type curve (frequency)

The final curve is of the V / F type (Velocity / Force) as a function of the frequency.

The dynamic stiffness proportional to the inverse of the slope at the origin is a complex number whose condition of use is linked to this characteristic.

Dynamic stiffness increases as the slope of the curve at its origin decreases.

### 2 RATIO BETWEEN STATIC STIFFNESS AND DYNAMIC STIFFNESS

The ratio between the static stiffness (Rs) and the dynamic stiffness (Rd) is constant for a same element in the same stress situation.

The stiffnesses calculated with the results of static and dynamic tests carried out simultaneously on the same element on this site, anchor n°3, make this observation concrete. The graph in Figure 4 illustrates this.

### 3 TENSILE STRENGTH AND DYNAMIC STIFFNESS

The tensile stress in the anchor has a direct effect on the evolution of dynamic stiffness.

The graph in figure 5 shows the evolution of the dynamic stiffness as a function of the force for anchor n°3.

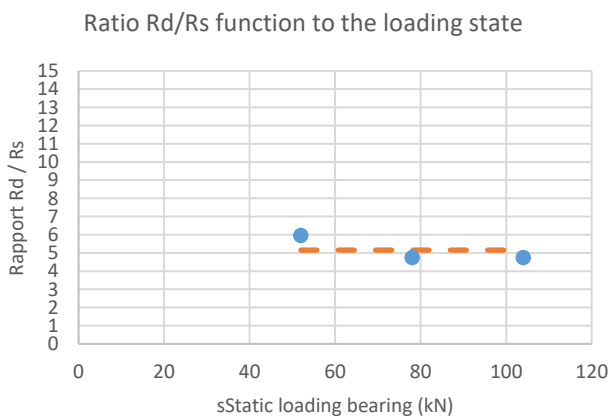


Figure 4 : Graph Rd/Rs (force) – Anchor n°3

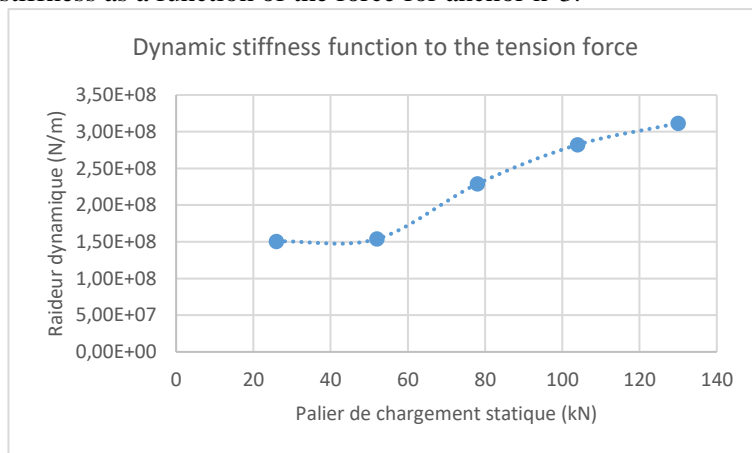


Figure 5 : Graph Rd (force) – Anchor n°3

#### 4 LENGTH OF THE ANCHOR AND DIAMETER OF THE BOREHOLE

The calculated length of the anchor is 2,1 m for a plane wave velocity hypothesis of 4000 m/s, value that corresponds to the length achieved (Figure 6).

The calculated admittance is 5,48E-5 m/sN, which leads to the diameter of the borehole in which the anchor is sealed (Figure 7).

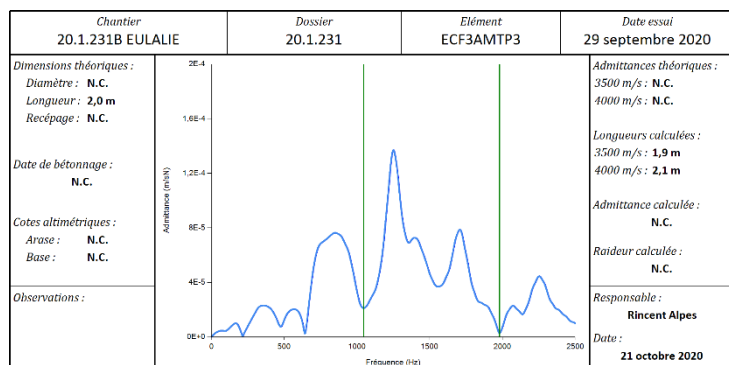


Figure 6 : V/F curve (frequency) – Length

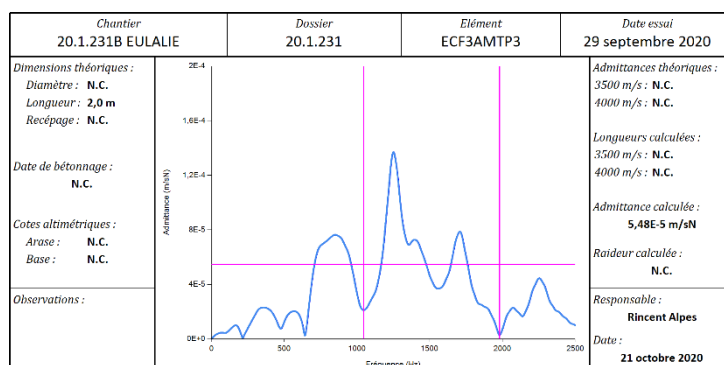


Figure 7 : V/F curve (frequency) – Admittance

#### 5 LOSSES AND INCREASES OF THE LOADINGS

The main parameters which intervene in the evolution of the forces in the anchors are:

- Relaxation of the steels, corrosion,
- The behaviour of the anchor grounds,
- Cyclic loads, vibrations.

The periodic implementation of dynamic tests and the analysis of the dynamic stiffnesses resulting from these tests makes it possible to monitor the evolution of these forces.

#### CONCLUSION

For anchors, increased loads are a problem that non-destructive testing can apprehend. This was one of the objectives of the work done on this site.

The service life of the anchors is linked to the quality of the maintenance carried out and the frequency of follow-up measures.

The techniques, presented and illustrated from a study carried out on site, provide tools for controlling and verifying the sizing of anchors and their operation.

#### REFERENCES

- AFNOR (2002). NF P 94-444, Static tension test on an anchor bonded in rock mass - Maintained axial loading testing.
- DAVIS A.G., DUNN C.S. (1975). From theory to field experience with the non-destructive vibration testing of piles. Ordinary meeting 25 February, 1975, at 5.30 p.m. Written discussion closes 7 March, 1975, for publication in Proceedings, Part 2.
- GUILLERMAIN P. (1979). Contribution to the geotechnical interpretation of the mechanical impedance test of a pile.
- HORB C. (2003). Determination of the forces in the tie rods by non-destructive methods. TP Tech 2003, Module 8 Geotechnical control and monitoring.
- HORB C. (2005). Determination of forces® and lengths of tie rods by means of non-destructive tests. Travaux (821), 41-44.

RINCENT BTP SERVICES (2006). Method and device for determining the tensile stress exerted on a sealed element. Patent OMPI n° WO 2006/010830 A1

ASLI C. (2013). Dynamic analysis of multilayer structures subjected to an impact force. Application to pavements.

MITAINE L., RINCENT J.J. (2015). Innovative non-destructive technique for determining tension in tie rods.

WILQUIN F., HORB C., FENG Z.Q., PORCHER G. (2016). Dynamic non-destructive evaluation of rock anchorage. 3rd International Symposium Rock Slope Stability.

## Modelling Rock Wall Permafrost to Understand Rock Slope Failure

Florence MAGNIN (corresponding author)<sup>1</sup>, Philip DELINE<sup>1</sup>, Pierre-Allain DUVILLARD<sup>2</sup>, Jean-Yves JOSNIN<sup>1</sup>, Alexandre LEGAY<sup>1</sup>, Ludovic RAVANEL<sup>1</sup>

**Keywords:** permafrost, modelling, rock wall, rock slope failure, climate change.

### 1 INTRODUCTION

Rock slope failures are increasingly affecting high mountain rock walls, notably during hot summers (e.g. Ravanel et al., 2017). The common presence of ice in rock fall scars evidences the likely role of permafrost (i.e. ground which temperature is permanently  $\leq 0^{\circ}\text{C}$ ) in rock fall triggering. Laboratory tests and mechanical models suggest that several permafrost-related processes influence bedrock stability (e.g. Krautblatter et al., 2013). Alteration of ice in joints due to the conductive heat transfer from the surface to depth, and advective heat flux by water infiltration in the fractures are thought to be the dominant processes in permafrost degradation (i.e. warming and thawing) causing rock wall destabilization. Water infiltration could also provoke high hydrostatic pressures at perched water table formed by the permafrost body and ice-filled fractures. To assess high mountain rock wall stability, it is thus important to know how permafrost is distributed, evolves, and interacts with hydrological processes. We here present recent developments in modelling rock wall permafrost and how models can help understanding rock slope destabilization at various space and time scales.

### 2 ROCK WALL TEMPERATURE MAPPING AND STATISTICAL OCCURRENCE OF ROCK FALL

Rock wall temperature can be straightforwardly mapped using rock surface temperature (RST) time series that cover at least one year to be computed into mean annual RST (MARST). To do so, a multiple linear regression is fitted with mean annual air temperature (MAAT) during the period of RST measurement and computed solar radiation at location of RST sensors. The regression model can then be implemented in a GIS to map MARST for a given climate period, and permafrost probability (a probability that the MARST is  $\leq 0^{\circ}\text{C}$ ) using a cumulative distribution function and the standard deviation of the regression model.

In the Mont Blanc massif, the MARST map produced by Magnin et al. (2015) was used to assess temperature conditions and recent evolution when observed rock falls occurred (Fig. 1). This assessment was done for 209 rock falls that occurred between 2007 and 2015 and ranging between  $10^2$  and  $60 \times 10^3 \text{ m}^3$ . We extracted the MARST at the detachment locations to then create a RST time series over the recent period (1996-2015) by applying the daily air temperature change to this MARST. The RST time series then forced a 1D transient thermal model (CryoGRID2 model, from Westermann et al., 2013) that simulates temperature-depth (Tz) profiles at daily time step for each rock fall. A similar modelling approach was then applied to 1000 random events drawn at each rock fall location to compare them to the results of the real events and determine the statistical significance of the results. This study showed that rock falls occur after 1 day to 3 weeks of extraordinary high temperature at depth of the scar, which coincides with long-lasting (several days to 2 months) high RST.

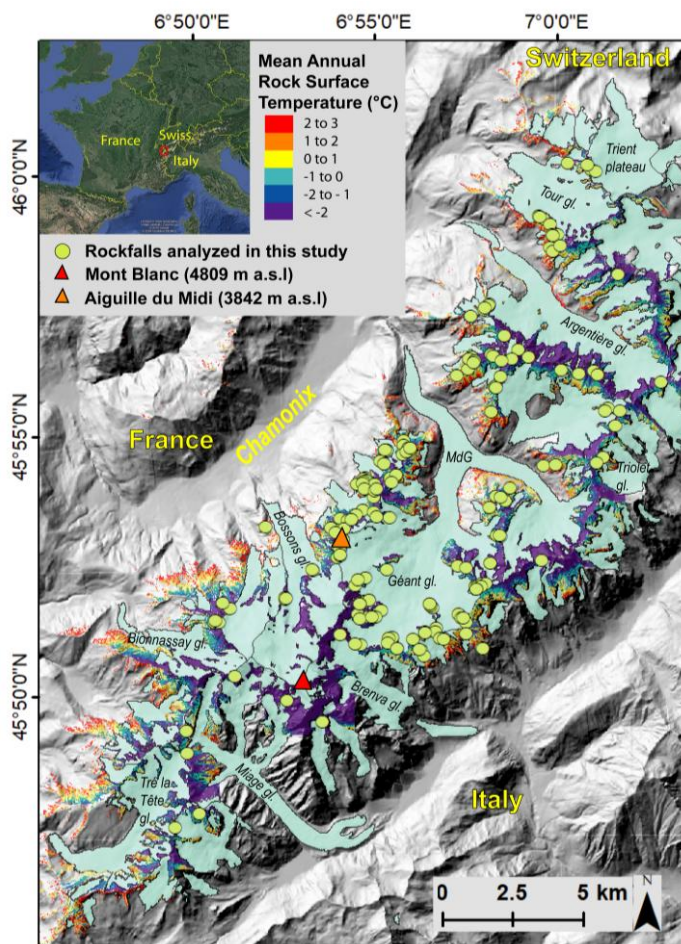


Figure 1: MARST distribution in the Mont Blanc massif overlaid with the rockfalls used in this study.

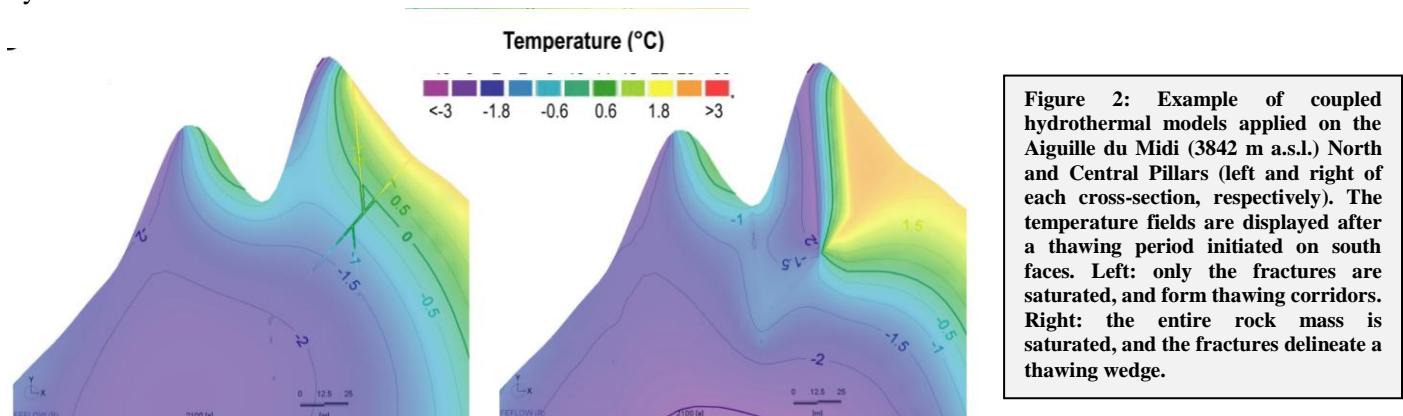
<sup>1</sup> MAGNIN Florence, EDYTEM Lab. (CNRS-Université Savoie Mont Blanc), Le Bourget du Lac, France, [Florence.magnin@univ-smb.fr](mailto:Florence.magnin@univ-smb.fr)

<sup>2</sup> Styx4D, Le Bourget-du-Lac, France, pierre-allain.duvillard@styx4d.com 38

### 3 SIMULATING PERMAFROST EVOLUTION AND CONSIDERING HYDROLOGICAL PROCESSES

By using transient thermal models simulating the conductive heat flow through the rock mass, it can be possible to simulate permafrost evolution over a time period of air temperature records. In alpine rock wall, heat fluxes are generally multidimensional as the sun-exposed faces are up to 8°C warmer than the shaded ones, the heat therefore flows from the warmer towards the colder faces. In addition, even though the ice content is relatively low in bedrock, it has a significant effect on temperature evolution through latent heat consumption and release. 2D models accounting for heat conduction and latent heat processes have been used to assess permafrost evolution at the Aiguille du Midi (3842 m a.s.l.) from the end of the Little Ice Age (1850) to the end of the 21<sup>st</sup> century using the IPSL-CM5A-MR model of the CMIP5 project (Magnin et al., 2017). Comparison of modelled temperature with measured temperature in 10-m-deep boreholes showed that such modelling approach is particularly well-suited to reproduce temperature fields and their changes over time, notably at depth > 8 m.

Nonetheless, the current challenge is to account for hydrological processes that may locally enhance permafrost degradation through heat advection and favour rock falls through hydrostatic pressure. We recently developed a modelling approach to couple thermal and hydrological processes in rock wall permafrost using Feflow® that solves the Darcy law. Our preliminary results show that water infiltration into the fractures provokes thawing corridors, or thawing wedges delineated by connected thawing fractures when the rock mass is fully saturated (Fig. 2). Such models can then be used to image hydrostatic pressure fields and are thus highly promising to develop fully coupled thermo-hydro-mechanical models.



### 4. CONCLUSIONS

Permafrost dynamics and processes may favour rock slope failures. It is thus important to accurately understand them. Various approaches have been developed to model permafrost, depending on the space and time scale of interest. Statistical models have been built using measured RST time series to map permafrost over regional scales. Such maps can then serve the development of 1D transient thermal models that are used to assess permafrost evolution and to determine thermal conditions and dynamics when failure occurs.

2D transient thermal models have been also used to assess past and future permafrost evolution. One of the current challenges is to improve these physic-based models by accounting for hydrological processes that may enhance permafrost degradation and hydrostatic pressures. Such developments are currently in progress at the EDYTEM lab.

### ACKNOWLEDGMENT

The recent developments in modelling were funded by the ANR-19-CE01-0018 *WISPER* project.

### REFERENCES

- Krautblatter, M., Funk, D., Günzel, F.K. (2013) Why permafrost rocks become unstable: a rock–ice-mechanical model in time and space. *Earth Surface Processes and Landforms* 38, 876–887. <https://doi.org/10.1002/esp.3374>
- Magnin, F., Brenning, A., Bodin, X., Deline, P., & Ravel, L. (2015). Statistical modelling of rock wall permafrost distribution: application to the Mont Blanc massif. *Géomorphologie : Relief, Processus, Environnement*, 20.
- Magnin, F., Josnin, J.-Y., Ravel, L., Pergaud, J., Pohl, B., Deline, P. (2017) Modelling rock wall permafrost degradation in the Mont Blanc massif from the LIA to the end of the 21st century. *The Cryosphere* 11, 1813–1834. <https://doi.org/10.5194/tc-11-1813-2017>
- Ravel, L., Magnin, F., Deline, P. (2017) Impacts of the 2003 and 2015 summer heatwaves on permafrost-affected rock-walls in the Mont Blanc massif. *Science of The Total Environment* 609, 132–143. <https://doi.org/10.1016/j.scitotenv.2017.07.055>
- Westermann, S., Schuler, T.V., Gislås, K., Eitzelmüller, B. (2013) Transient thermal modeling of permafrost conditions in Southern Norway. *The Cryosphere* 7, 719–739. <https://doi.org/10.5194/tc-7-719-2013>

## Monitoring unstable slopes with passive RFID

LE BRETON Mathieu<sup>1</sup>, BAILLET Laurent<sup>2</sup>, LAROSE Éric<sup>3</sup>

**Keywords:** RFID, IOT, passive sensors, instrumentation, monitoring, landslide, rockslide, rockfall

### 1 INTRODUCTION

Billions of passive radiofrequency tags are produced by the Radio-Frequency Identification (RFID) industry every year to identify goods remotely. New research and business applications are continuously arising, including recently localisation and sensing for earth science. Indeed, the cost of tags is often several orders of magnitudes below conventional outdoor sensors used in earth science, allowing to deploy up to thousands of tags with minimal investment. Furthermore, passive wireless tags require little maintenance, which fits well for years-long monitoring. This study reviews the earth science applications that are being developed today. In particular, it presents classic tracking technique applied to sediment in rivers and debris flow, and new sensing and localisation techniques for landslides, rockslides and rockfall monitoring.

### 2 DEBRIS FLOW SEDIMENT TRACKING

In geosciences, RFID tags were first used to track the transport of pebbles by rivers (Lamarre et al., 2005). The principle is to insert small tags into pebbles placed in a river bed. The position of these pebbles is then monitored by seasonal measurement campaigns, using a mobile RFID reader. The tags used, operating at 125 kHz by magnetic coupling, are small and work very well in fresh water. This technique has also been used to study the transportation of sediments during debris flows (Graff et al., 2018).

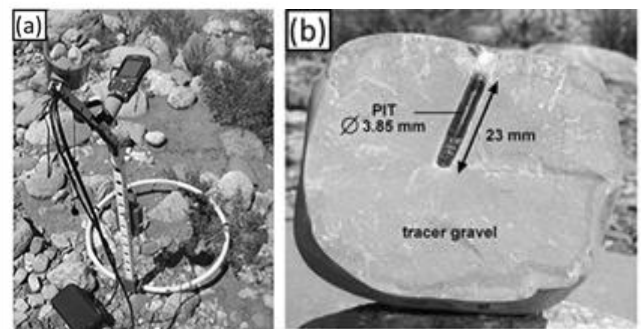


Fig. 1: RFID system for sediment tracking in rivers, with (a) mobile interrogator and (b) tag inserted in a pebble. From (Liébault et al., 2012)

### 3 LANDSLIDE MONITORING

Numerous landslide monitoring technologies exist on the market, such as GNSS, robotic laser tacheometer, optical photography, lidar, radar interferometry, or radio frequency transponder arrays. A landslide was investigated using an 868 MHz passive RFID tag tracking technique. The displacement of about 20 tags was measured continuously by phase difference, and compared to automatic extensometer measurements and tacheometric surveys. This work showed the effectiveness of RFID tracking in measuring displacements of 0.1-5 cm/day, with a range of up to 60 metres (distance between the antenna and the tags) (Le Breton et al., 2019). The method appears to be less sensitive to environmental effects after corrections (Le Breton et al., 2017) than the existing extensometry technique, which makes it a promising monitoring technique. In addition to localisation, RFID tags could also be used for soil moisture sensing (Pichorim et al., 2018).

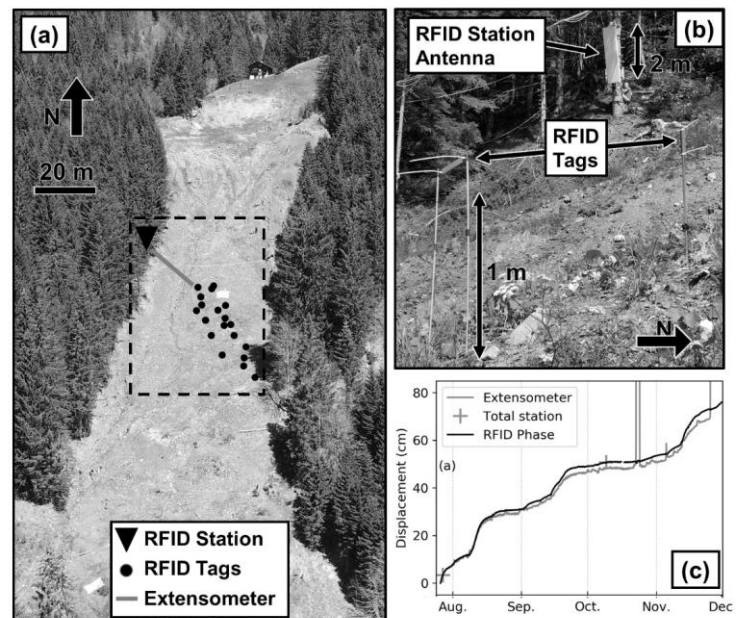


Fig. 2: Continuous monitoring of a landslide displacement with RFID tags. (a) Pont-Bourquin landslide (b) tags on the field (c) displacement measurement on one tag. From (Le Breton et al., 2019)

<sup>1</sup> LE BRETON Mathieu, Géolithe Innov, Crolles, France, mathieu.lebreton@geolithe.com

<sup>2</sup> BAILLET Laurent, Université Grenoble Alpes, ISTERre, Grenoble, France, laurent.baillet@univ-grenoble-alpes.fr

<sup>3</sup> LAROSE Éric, CNRS, Université Grenoble Alpes, ISTERre, eric.larose@univ-grenoble-alpes.fr

#### 4 TOWARDS ROCKFALL AND ROCKSLIDE MONITORING

RFID tags have also been developed for structural health monitoring for civil structures (Zhang et al., 2017), and can be adapted for monitoring unstable rock slopes and unstable rock compartment. First, millimetric to submillimetric displacements can be measured, to monitor crack opening (Caizzzone and DiGiampaolo, 2015). The tilt of unstable boulders on a slope has been monitored with a dense low-cost and low-power wireless sensor network (Dini et al., 2020), and could similarly be monitored with batteryless RFID tilt sensors (Vena et al., 2019) for years.

#### 5 CONCLUSION

RFID technologies and show more and more potential for being used in geoscience applications, to deploy low-cost networks of passive sensors. Identification has become a standard to track riverine sediments, localisation has been proven to work on landslides, and RFID sensors could measure soil moisture or tilt as a complement.

#### 6 ACKNOWLEDGEMENTS

We acknowledge funding and support from the French National Agency for research (ANR) through the LABCOM Geo3iLab project (ANR- 17- LCV2-0007-01), from the Labex OSUG@2020, and from the companies Géolithe and Géolithe Innov.

#### 7 REFERENCES

- Caizzzone, S., DiGiampaolo, E., 2015. Wireless Passive RFID Crack Width Sensor for Structural Health Monitoring. *IEEE Sensors Journal* 15, 6767–6774.
- Dini, B., Bennett, G.L., Franco, A.M.A., Whitworth, M.R.Z., Cook, K.L., Senn, A., Reynolds, J.M., 2020. Development of smart boulders to monitor mass movements via the Internet of Things: A pilot study in Nepal. *Earth Surface Dynamics Discussions* 1–46.
- Graff, K., Viel, V., Carlier, B., Lissak, C., Madelin, M., Arnaud-Fassetta, G., Fort, M., 2018. Traçage sédimentaire d'une lave torrentielle dans le bassin de la Peyronnelle (Queyras, Alpes françaises du Sud). *Géomorphologie : relief, processus, environnement* 24, 43–57.
- Lamarre, H., MacVicar, B., Roy, A.G., 2005. Using Passive Integrated Transponder (PIT) Tags to Investigate Sediment Transport in Gravel-Bed Rivers. *Journal of Sedimentary Research* 75, 736–741.
- Le Breton, M., Baillet, L., Larose, E., Rey, E., Benech, P., Jongmans, D., Guyoton, F., Jaboyedoff, M., 2019. Passive radio-frequency identification ranging, a dense and weather-robust technique for landslide displacement monitoring. *Engineering Geology* 250, 1–10.
- Le Breton, M., Baillet, L., Larose, E., Rey, E., Benech, P., Jongmans, D., Guyoton, F., 2017. Outdoor UHF RFID: Phase Stabilization for Real-World Applications. *IEEE Journal of Radio Frequency Identification* 1, 279–290.
- Liébault, F., Bellot, H., Chapuis, M., Klotz, S., Deschâtres, M., 2012. Bedload tracing in a high-sediment-load mountain stream. *Earth Surface Processes and Landforms* 37, 385–399.
- Pichorim, S., Gomes, N., Batchelor, J., 2018. Two Solutions of Soil Moisture Sensing with RFID for Landslide Monitoring. *Sensors* 18, 452.
- Vena, A., Sorli, B., Saggin, B., Garcia, R., Podlecki, J., 2019. Passive UHF RFID Sensor to Monitor Fragile Objects during Transportation, in: 2019 IEEE International Conference on RFID Technology and Applications (RFID-TA), pp. 415–420.
- Zhang, J., Tian, G.Y., Marindra, A.M.J., Sunny, A.I., Zhao, A.B., 2017. A Review of Passive RFID Tag Antenna-Based Sensors and Systems for Structural Health Monitoring Applications. *Sensors* 17, 265.

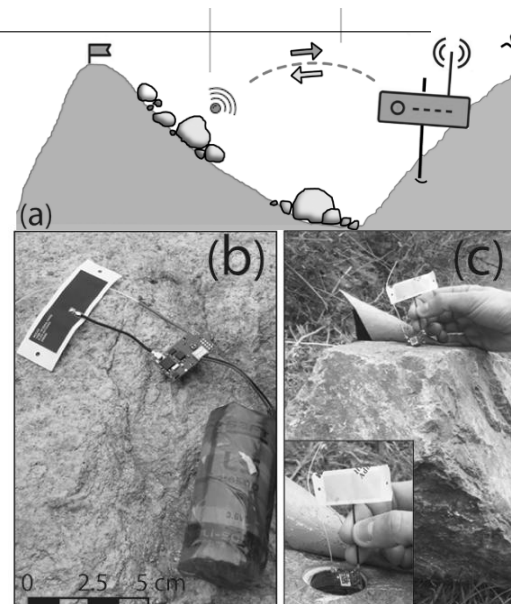


Fig. 3: (a) Monitoring tilt of boulders on a slope with (a) low-power wireless sensors (c) inserted into boulders. From (Dini et al., 2020)

## UNDERSTANDING THE TRIGGERING PROCESSES OF LANDSLIDES WITH INDUCED POLARIZATION

P. VAUDELET<sup>1</sup>, A. Revil<sup>2</sup>, A. Soueid'Ahmed<sup>3</sup>, P-A. Duvillard<sup>4</sup>, A. Coperey<sup>5</sup>

**Keywords:** Landslides, induced polarization, water content, clay content.

### ABSTRACT IN ENGLISH:

Understanding and diagnosing the triggering process of landslides is a major issue for the implementation of preventive measures. Over the past decade, great progress has been made in the induced polarization geophysical method, from field acquisition to the understanding of the underlying petrophysical mechanisms. Today, these advances provide access to essential parameters for the study of landslides, such as water and clay contents as well as permeability. The possibility of imaging these parameters in the underground with a non-intrusive method all over a risky site allows us to develop a new alert tool based on this technique.

### ABSTRACT IN FRENCH:

*La compréhension et le diagnostic des processus déclencheurs d'un glissement de terrain est un enjeu majeur pour la mise en œuvre de moyens de prévention. Durant ces dix dernières années, de grands progrès ont été réalisés sur la méthode de polarisation provoquée, de l'acquisition sur le terrain jusqu'à la compréhension des mécanismes pétrophysiques. Ces progrès donnent aujourd'hui à des paramètres indispensables pour l'étude des glissements de terrain, comme la teneur en eau et la perméabilité. La possibilité d'imager ces paramètres dans le sous-sol de manière non-intrusive sur l'ensemble d'un site sensible ouvre des perspectives pour le développement d'un nouvel outil d'alerte.*

## 1 INTRODUCTION

Hazard anticipation is fundamental to minimize risk. Traditionally, a geomorphological analysis makes it possible to map the potential for landslides, depending on the issues, in order to identify which sites need to be monitored. There are many existing tools, such as LIDAR, interferometry or optic, to survey a ground movement (Jaboyedoff et al., 2012, 2019). The challenge is to develop an approach to alert before the critical limit is reached. The most important risk is related to clay-rich landslides because they lead to rapid movements. Their mechanisms depend on the water content, which, when a critical threshold is exceeded, generating partial or complete liquefaction. Recently, some studies demonstrated that an approach using seismic noise monitoring can detect this threshold (e.g. Le Breton et al., 2021). Our ambition is to propose a method to follow the water content evolution to alert before the mechanism is engaged. In this way, we take advantage of the past decade's progress in induced polarization to characterize and diagnose landslides.

## 2 METHOD

Time-domain induced polarization datasets were acquired on landslide sites in Claix (Isère, France) and New Caledonia (Figure 1).



**Figure 1. Landslides investigated with induced polarization. a. Landslide on a mining site in New Caledonia. b. Landslide in Claix (Isère, France).**

<sup>1</sup> NAGA Geophysics, Le Bourget-du-Lac, France, pierre.vaudelet@naga-geophysics.com

<sup>2</sup> EDYTEM, Université Savoie Mont Blanc, CNRS, Le Bourget-du-Lac, France, andre.revil@univ-smb.fr

<sup>3</sup> NAGA Geophysics, Le Bourget-du-Lac, France, abdellahi.soueidahmed@naga-geophysics.com

<sup>4</sup> STYX 4D, Le Bourget-du-Lac, France, pierre-allain.duvillard@styx4d.com

<sup>5</sup> EDYTEM, Université Savoie Mont Blanc, CNRS, Le Bourget-du-Lac, France, anne.coperey@gmail.com

The inversion was performed with the code described in Soueid Ahmed et al. (2018ab). Petrophysical measurements on samples from the sites validate a recent mechanistic fundamental mechanistic model called the dynamic Stern layer model. This model was applied to interpret the conductivity and normalized chargeability tomograms obtained in the field. Thus, a procedure was developed to image the water content, the cation exchange capacity, and the permeability distribution at the test sites.

### 3 CLAIX RESULTS AND DISCUSSION

Water content, permeability and the cation exchange capacity tomograms obtained in the Claix site are shown on Figure 2. The CEC tomogram exhibits high CEC anomalies corresponding to the presence of plastic clays in the bottom part of the investigated area. The permeability and water content tomograms show that the landslide is associated with a high permeability and water content channel that could have triggered the landslide during an episode of intense rain. These distributions provide some clue regarding the reasons associated with the localization of the landslide. A flow pipe has been identified on the exposed material in the scarp let by the landslide.

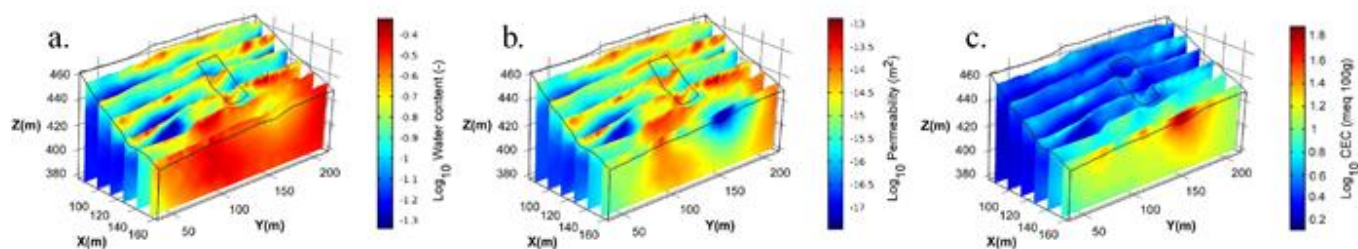


**Figure 2. Induced polarization investigation results on Claix landslide. a. Water content, b. permeability and c. CEC. The thin closed line corresponds to the landslide area. Note that this area is characterized by the presence of a channel with a high-water content.**

### CONCLUSION

The comprehension of petrophysical models allows to interpret induced polarization from the field with a quantitative approach to determine water content, permeability and CEC (associated with the clay content). These parameters are necessary for the understanding of the triggering mechanisms of landslides. Induced polarization appears as a promising non-intrusive geophysical imaging method to monitor crucial change in the soil in order to alert one step ahead. In the future, a 4D approach will be developed to propose a tool for the monitoring sites associated with such geohazards.

### ACKNOWLEDGEMENTS

We thank I-RISK (Research, Development and Innovation platform), the region Auvergne Rhône Alpes (France), and the European FEDER fund for their contribution to this study for their contribution to this study. We thank J. Cardon and F. Abdulsamad for their help in the field.

### REFERENCES

- Jaboyedoff, M., Oppikofer, T., Abellán, A., Derron, M.-H., Loye, A., Metzger, R., et al. (2012). Use of LIDAR in landslide investigations: a review. *Nat. Hazards* 61, 5–28.
- Jaboyedoff, M., Del Gaudio, V., Derron, M.H., Grandjean, G. and Jongmans, D., (2019). Characterizing and monitoring landslide processes using remote sensing and geophysics. *Engineering Geology*, 259, p.105167.
- Le Breton, M., Bontemps, N., Guillemot, A., Baillet, L., & Larose, É. (2021). Landslide monitoring using seismic ambient noise correlation: challenges and applications. *Earth-Science Reviews*, 103518.
- Soueid Ahmed, A., & Revil, A. (2018a). 3-D time-domain induced polarization tomography: a new approach based on a source current density formulation. *Geophysical Journal International*, 213(1), 244-260.
- Soueid Ahmed, A., Revil, A., Jardani, A., & Chen, R. (2018b). 3D geostatistical inversion of induced polarization data and its application to coal seam fires. *Geophysics*, 83(3), 1–59.

# Rockfall trajectory analysis

## Delimiting rockfall runout zones using simulated reach probability maps

Luuk DORREN (corresponding author)<sup>1</sup>, Frédéric BERGER<sup>2</sup>, Franck BOURRIER<sup>3</sup>, Nicolas ECKERT<sup>4</sup>, Charalampos SAROGLOU<sup>5</sup>, Massimiliano SCHWARZ<sup>6</sup>, Markus STOFFEL<sup>7</sup>, Daniel TRAPPMANN<sup>8</sup>, Hans-Heini UTELLI<sup>9</sup>, Christine MOOS<sup>10</sup>

**Keywords:** rockfall hazard modelling, trajectory analysis, reach probability, simulation, silent witnesses

### 1 INTRODUCTION

To come up with realistic predictions of the areas that are potentially endangered by rockfall processes, modelling rockfall trajectories is one of the methods that provide an important information (Volkwein et al., 2011). To account for the many uncertainties in the rockfall process, trajectory simulation models generally use stochastic variables in their algorithms. Since such probabilistic computational algorithms rely on repeated random sampling, the numerical results are presented as probability distributions. In the daily practice, the definition of the realistic runout zone for a given rockfall scenario is mostly based on human interpretation of such simulation results, where extreme long trajectories with low occurrence probability in comparison to the majority of the simulated trajectories are removed from the modelled rockfall runout distribution. Thereby expert judgement can be supported by historical records, mapped deposited rocks (silent witnesses *SW*), and other information recorded in the field (e.g., tree impacts). To do so, rockfall trajectory models provide datasets with the number of passages per cell normalised by the total number of blocks potentially passing through a cell, also referred to as reach probability ( $P_{\text{reach}}$ ). At present, no quantitative basis for the delineation of realistic rockfall runout zones based on  $P_{\text{reach}}$  threshold values exists. This study therefore presents a statistical comparison of simulation-based  $P_{\text{reach}}$  values with field mapped stopping locations of blocks from recent rockfall events.

### 2 METHODS AND MATERIALS

For this study, we used data from 18 different rockfall sites in Europe with a total of 769 mapped *SW* (Table 1). These *SW* correspond to stopping locations of fresh blocks inventoried in the field, meaning that blocks with weathered surfaces as well as those partly buried by material covering the surrounding slope surface were not recorded. We focused at mapping *SW* which, based on our interpretation, corresponded to blocks that resulted from recent rockfall events with return periods of max. 300 years. At the Taesch (CH) study site, all deposited blocks of the rockfall event of August 2013 were mapped. At the Claro, Flaesch, Orvin, Schmitten (all in CH) and Greece (Tithorea) study sites, we mapped all deposited rockfall blocks of multiple recent rockfall events. At six other study sites, we mapped selected blocks of one specific recent rockfall event (Gurtellen (CH) event of May 2006; Varcès (FR) event of Dec. 2008; Veyrier (FR) event of Jan. 2009; Tramin (IT) event of Jan. 2014; Evolène (CH) event of Oct. 2015; Vaujany (FR) rockfall experiments of Oct. 2003). These blocks either had a much larger volume than the surrounding deposited blocks or a longer runout distance compared to the majority of the deposited blocks (i.e., deposited in the lower range of the propagation zone). Lastly, at another six sites, we mapped selected blocks, corresponding to the description above, resulting from multiple rockfall events. We also mapped and recorded field data required for the modelling (terrain roughness, soil types, forest structure) at each site.

With Rockyfor3D we simulated the exact block volumes of the *SW* for each site and extracted the simulated reach probabilities ( $P_{\text{reach}}$ ) at the position of the *SW*. Here we excluded *SW* with a volume  $< 0.05 \text{ m}^3$  and a  $P_{\text{reach}} > 5\%$  from the original dataset, since they were regarded as irrelevant (too small) for a hazard analysis or as not being in the outer runout zone respectively. The threshold of 5% was determined based on a two-step outlier detection according to

<sup>1</sup> DORREN Luuk, Bern University of Applied Sciences BFH – HAFL, Zollikofen, CH, luuk.dorren@bh.ch

<sup>2</sup> BERGER Frédéric, INRAE, Lyon - Grenoble - Auvergne-Rhône-Alpes Centre, FR, frederic.berger@inrae.fr

<sup>3</sup> BOURRIER Franck, INRAE, Lyon - Grenoble - Auvergne-Rhône-Alpes Centre, FR, franck.bourrier@inrae.fr

<sup>4</sup> ECKERT Nicolas, INRAE, Lyon - Grenoble - Auvergne-Rhône-Alpes Centre, FR, nicolas.eckert@inrae.fr

<sup>5</sup> SAROGLOU, Charalampos, School of Civ. Eng., Nat. Techn. Univ. Athens, GR, saroglou@central.ntua.gr

<sup>6</sup> SCHWARZ Massimiliano, Bern University of Applied Sciences BFH – HAFL, Zollikofen, CH, massimiliano.schwarz@bfh.ch

<sup>7</sup> STOFFEL Markus, Dept. of Earth Sciences, Univ. Geneva, CH, markus.stoffel@unige.ch

<sup>8</sup> TRAPPMANN Daniel, BaySF, DE, daniel.trappmann@baysf.de

<sup>9</sup> UTELLI Hans-Heini, Impuls AG, Thun, CH, hans-heini.utelli@impulsthun.ch

<sup>10</sup> MOOS Christine, Interdisciplinary Centre for Mountain Research, University of Lausanne, Sion, CH, christine.moos@unil.ch

Yang (2019) using the median absolute deviation (MAD) as score. We simulated 100 individual block releases per start cell. At all sites, we used digital elevation models with a resolution of 2 x 2 m, except for the site in Greece, where we used a 5 x 5 m resolution DEM.  $P_{\text{reach}}$  in a given cell  $x$  indicates the probability (given in%) that cell  $x$  is reached by a block that has detached from the cliff. Following Dorren (2016), it is calculated by:

$$P_{\text{reach}(x)} = NP_{(x)} \cdot 100\% / (N_{\text{sims}} \cdot N_{\text{sources}(x)}) \quad (1)$$

where  $NP_{(x)}$  is the number of blocks passed through cell  $x$ ,  $N_{\text{sims}}$  is the number of individual blocks simulated from each start cell,  $N_{\text{sources}(x)}$  is the number of source cells “feeding” cell  $x$ . In other words, the reach probability is a measure of the number of blocks passed through a given cell relative to the maximum number of blocks potentially passing through the cell.

**Table 1: Characteristics of the 18 study sites with mapped SW.**  $H_c$  refers to the range of the total cliff heights;  $\phi_{Tr}$  is the range of the mean slope angles in the transit areas;  $L_{Tr}$  is the range of the average lengths of the transit areas;  $n$  represents the number of mapped SW;  $Vol_{\text{max}}$  is the volume range of the mapped SW;  $SW_{\text{des}}$  described which SW we mapped in the field (1 = all deposited blocks of one specific recent rockfall event, 2 = all fresh blocks present at the study site, 3 = selected blocks (for explanation see text) of one specific recent rockfall event, 4 = selected blocks from multiple events).

Country (n sites)	Rocktype	$H_c$ (m)	$\phi_{Tr}$ (°)	$L_{Tr}$ (m)	n	$Vol_{\text{max}}$ (m <sup>3</sup> )	$SW_{\text{des}}$
CH (10)	Limestone, Dolomite Calcschists, Gneiss, Granite	20-400	23-33	65-1750	659	200	1/2/3/4
FR (4)	Limestone	50-350	27-33	190-910	25	33	3 / 4
GR (1)	Limestone	150	28	330	61	38	2
AT (1)	Amphibolite	120	31	300	6	8	4
IT (1)	Limestone	50	29	520	9	72	3
FR (exp. site)	Granite-Gneiss	n.a.	34	190	9	0.9	3

We analysed which slope and forest characteristics influenced  $P_{\text{reach}}$  and tested whether there are significant differences between study sites, as well as between volume classes, based on a one-way analysis of variance (ANOVA) with a logarithmic transformation of  $P_{\text{reach}}$  values. We then fitted a linear mixed effects model (lmm) with terrain variables and rock volumes as fixed effects and the site as random effect.

### 3 RESULTS

In total, we analysed 484 SW with a volume  $> 0.05 \text{ m}^3$  and a  $P_{\text{reach}} \leq 5\%$ . The mean  $P_{\text{reach}}$  was 1.78% (all SW = 2.17%) and the median 1.41% (all SW = 1.25%). 75% of the SW had a  $P_{\text{reach}} \leq 2\%$ .  $P_{\text{reach}}$  is significantly higher for blocks with a volume of 5 - 10 m<sup>3</sup> (Fig. 1). The ANOVA revealed a significant difference between sites, whereby the Tukey post-hoc test showed that only 2 sites in CH (Claro and Taesch) significantly differ from the others. According to the lmm,  $P_{\text{reach}}$  is significantly influenced by the block volume class, the slope roughness and the basal area of the forest. Cliff height, topographic complexity and length of the transit area do not seem to play a role. The lmm explains ~49% of the variance.

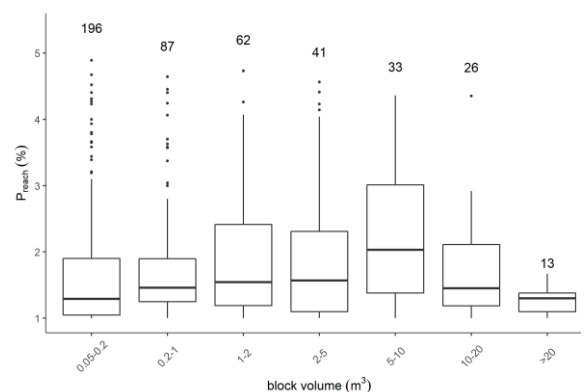


**Figure 1: Distribution of  $P_{\text{reach}}$  values per block volume class.**

### CONCLUSION

We conclude that simulated  $P_{\text{reach}}$  data can be used to delineate the realistic outer range of the runout zone downslope from a rockfall release area. Our results indicate that this range lies in areas where the simulated  $P_{\text{reach}}$  values are larger than 1% and, depending on the rock volume, slope roughness and the type and area of forest cover, smaller than 3%.

### REFERENCES

- Dorren, L. 2016. Rockyfor3D (v5.2) revealed – Transparent description of the complete 3D rockfall model. *ecorisQ paper* (<https://www.ecorisq.org/tool-manuals/rockyfor3d-user-manual>): 33 p.
- Volkwein, A., Schellenberg, K., Labiouse, V. et al. 2011. Rockfall characterisation and structural protection: a review. *NHESS*, 11: 2617–2651.
- Yang, J., Rahardja, S., Fränti, P. 2019. Outlier detection: how to threshold outlier scores? *Proc. Int. Conf. on Artificial Intelligence, Information Processing and Cloud Computing*, Sanya China: pp. 1–6.

# ELANA (Energy Line Angle Normalized Area): un outil d'aide à la cartographie de la propagation des chutes de blocs basée sur la méthode de la ligne d'énergie à différentes échelles

Clara LEVY<sup>1</sup>, Bastien COLAS<sup>2</sup>, Jérémy Rohmer<sup>3</sup>, Frédérique Berger<sup>4</sup>

**Keywords:** angle d'énergie, propagation, chute de blocs, cartographie

Le groupe MEZAP (Méthode d'Evaluation du Zonage de l'Aléa chute de Pierres), pour le compte du Ministère de l'Ecologie propose une évolution des méthodes d'évaluation de l'aléa rocheux dans le cadre de PPR (Plan de Prévention des Risques) ou de PAC (Porté à connaissance). Dans ce cadre, une importante base de données (BdD) d'évènements documentés a été créée afin d'identifier l'impact de la morphologie de versant sur la valeur d'angle de la ligne d'énergie  $\beta$  (rapport BRGM/RP-66589-FR). La valorisation de cette BdD met en évidence une relation entre l'angle d'énergie  $\beta$  et la morphologie d'un profil 2D, représentée par un indice adimensionnel: l'aire normalisée (An). Des lois empiriques reliant  $\beta$  et An ont été proposées. L'outil ELANA valorise cette approche 2D pour la cartographie spatiale de l'aléa de propagation de blocs rocheux.

## 1 ADAPTATION MEZAP DE LA LIGNE D'ENERGIE AVEC L'AIRES NORMALISEE

Afin de comparer la morphologie de profils topographiques variés, le groupe MEZAP a défini l'aire normalisée (An), comme l'aire sous la courbe du profil topographique reliant la position de départ d'un bloc et sa position d'arrêt après la normalisation de ses dimensions par une homothétie de rapport H, H étant la différence d'altitude entre la position de départ d'un bloc et sa position d'arrêt (Fig. 1a). An dépend de la forme générale du versant quel que soit sa hauteur totale, avec  $An < 0,2$  pour des falaises subverticales et  $An > 0,6$  pour des versants réglés. Une 1<sup>ère</sup> base de données de 2800 évènements définis par les couples (An,  $\beta$ ) a permis de mettre en évidence l'impact de la morphologie de versant sur la distribution des angles d'énergie (Fig. 1c) et des lois empiriques reliant  $\beta$  et An ont été proposées pour des qualifier la probabilité de propagation à  $P=10^{-2}$ ,  $P=10^{-4}$  et  $P=10^{-6}$  (Fig. 1c). Plusieurs approches statistiques ont été testées: 1) régression non linéaire de la forme  $\beta = C \exp^{-B \cdot An}$ , 2) transformation des variables pour se ramener à une régression linéaire classique, 3) régression sur les quantiles extrêmes (avec transformation puissance), 4) calage d'une loi de probabilité de type logit-normale. Si les hypothèses des méthodes 1 et 2 n'ont pas pu être validées, elles le sont pour les approches 3 et 4: les lois obtenues pour qualifier la probabilité de propagation sont correctes d'un point de vue statistique et peuvent être utilisées, a priori, pour cartographier l'aléa de propagation. A partir des données de la base MEZAP, enrichie par le projet européen RockTheAlps (FEDER Alpine-Space), INRAe propose une

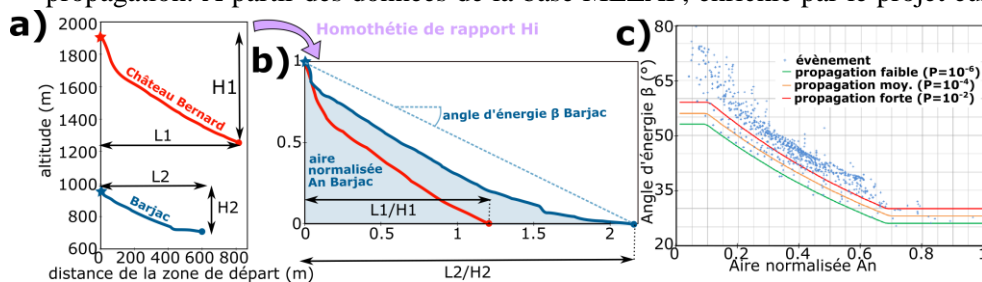


Figure 1 : a) exemple des profils topographiques reliant la position de départ d'un bloc et sa position d'arrêt et b) ces profils après une homothétie de rapport  $H_i$  pour calculer leur aire normalisée  $An$ . c) base de données MEZAP de chutes de blocs (points bleus) avec les lois empiriques proposées pour associer des valeurs d'angle  $\beta$  à différents seuils de passage (probabilité de propagation faible  $P=10^{-2}$ , moyenne  $P=10^{-4}$  et forte  $P=10^{-6}$ ).

approche 2D différente en proposant de choisir à dire d'expert les angles d'énergie d'un site par comparaison avec des profils ayant une forme et une hauteur totale comparables (outil Rock-EU-2D accessible sur la plate-forme PlatRock de l'INRAe).

Certaines précautions sont à adopter lors de l'utilisation de ces lois empiriques : 1) ces lois sont utilisables pour estimer la probabilité

d'atteinte de chutes de blocs. Elles ne sont pas pertinentes pour les éboulements où les interactions entre blocs pendant la propagation ne sont pas négligeables car il existe alors une dépendance de la distance de propagation avec le volume de l'éboulement ; 2) le choix de la valeur d'angle d'énergie pour différentes probabilités relève in-fine de l'expert qui interprètera les valeurs d'angles fournies par profils. Des études complémentaires seront nécessaires pour caractériser la relation entre l'incertitude obtenue sur les angles d'énergie et l'incertitude sur les distances de

<sup>1</sup> LEVY Clara, BRGM, Orléans, FRANCE (ISO 3166-2), c.levy@brgm.fr  
<sup>2</sup> COLAS Bastien, BRGM, Montpellier, FRANCE (ISO 3166-2), b.colas@brgm.fr  
<sup>3</sup> ROHMER Jérémy, BRGM, Orléans, FRANCE (ISO 3166-2), j.rohmer@brgm.fr  
<sup>4</sup> BERGER Frédérique, INRAE, Grenoble, FRANCE (ISO 3166-2), frederic.berger@inrae.fr

propagation. Cela permettra de mieux appréhender la précision cartographique des méthodes utilisant ces lois empiriques pour le zonage de la probabilité de propagation en chute de blocs.

## 2 L'OUTIL DE CARTOGRAPHIE ELANA

ELANA a été développé pour utiliser les lois empiriques 2D présentées ci-dessus afin de cartographier spatialement la probabilité de propagation des chutes de blocs. ELANA utilise les données topographiques d'un Modèle Numérique de Terrain (MNT), ainsi qu'un raster de même dimension où l'utilisateur déclare les pixels qu'il considère comme zone de départ (Fig. 2). ELANA permet d'obtenir le raster des zones de propagation faible, moyenne et fortes à partir des lois empiriques proposées (Fig. 2). Ces lois empiriques étant applicables sur des profils 2D, le logiciel interpole des profils autour de chaque pixel de départ afin de pouvoir déterminer l'emplacement des limites de propagation pour chaque profil. Afin de limiter le temps de calcul, cette opération n'est pas effectuée pour les pixels de départ situés dans la direction de plus grande d'un autre pixel de départ (Fig. 2), ici nommés pixels « aval » par opposition aux pixels conservés pour la suite des calculs, ici nommés « amont ».

Les étapes suivantes de calculs sont :

- la recherche de la direction de plus grande pente autour de chaque pixel de départ « amont » par pas de 1° (Fig. 3a) ;
- la sélection des directions autour de la plus grande pente dans un cône d'ouverture  $2\alpha$  et pour des pentes initiales supérieures à 26° (Fig. 3a).  $\alpha$  est défini par l'utilisateur comme une appréciation de la dispersion latérale des trajectoires. Par ex.,  $\alpha \leq 15^\circ$  pour des versants réglés de pente moyenne supérieure à 30° et/ou chenalisés ;
- l'interpolation de profils topographiques depuis le pixel de départ pour toutes les directions sélectionnées et avec une discrétisation horizontale de la taille de la maille (Fig. 3a) ;
- le calcul des couples  $(A_n, \beta)$  obtenus pour chaque point des profils topographiques (Fig. 3b) et leur comparaison avec les lois empiriques. En chaque point du profil, on précise la probabilité de propagation (forte, moyenne, faible ou nulle, Fig. 3b) ;
- on précise la probabilité de propagation à chaque pixel du « raster de propagation » (Fig. 3d) avec la valeur la plus défavorable obtenue pour tous les profils interceptant le pixel (Fig. 3c). Les résultats sont donc conservateurs vis-à-vis de l'aléa de propagation.

Tout au long du processus des tests sont réalisés afin de vérifier la pertinence ou les limites des calculs réalisés (longueur de profils, résolution spatiale finale, etc.).

## CONCLUSION

ELANA est actuellement en phase de test à diverses échelles et devrait être, à terme, déployé en accès libre sur la plateforme [BRGM VigiRisk](#). D'autres évolutions peuvent d'ores et déjà être entrevues : 1) cartographie « directe » de l'aléa résultant « chute de bloc » en intégrant dans l'analyse l'activité des zones de départ et l'intensité de phénomène redouté, 2) la possibilité pour l'utilisateur de définir ses propres lois empiriques de propagation. Il est rappelé que ELANA demeure un outil d'aide à la cartographie et in fine le choix définitif des emprises de propagation demeure du ressort de l'opérateur-expert.

## REFERENCES

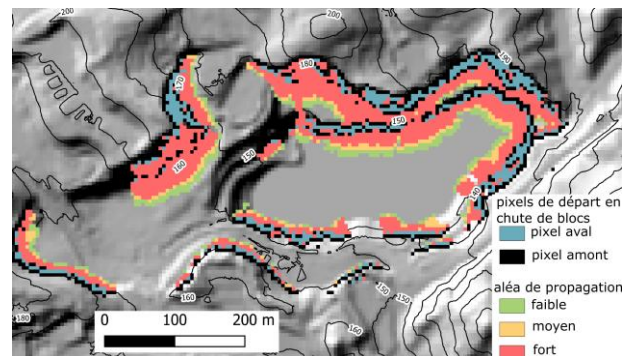


Figure 2 : Exemple des résultats fournis par ELANA à partir du MNT 5 m d'une ancienne carrière et d'un raster de même dimension où l'utilisateur déclare les pixels de départ en chute de blocs. ELANA classe les pixels de départ en pixels « amont » et « aval » et permet d'obtenir le raster des zones de propagation faible, moyenne et fortes à partir des lois empiriques proposées.

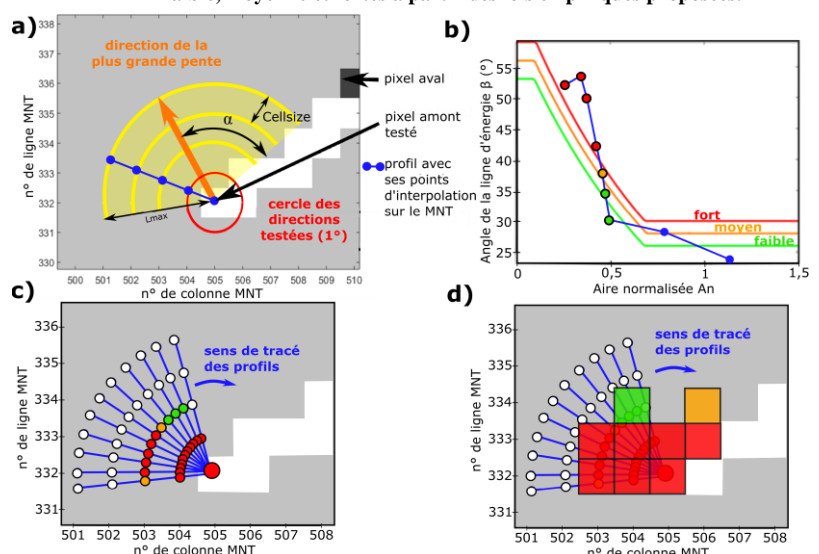


Figure 3 : a) Exemple des étapes d'ELANA pour un pixel de départ en chute de blocs : recherche de la direction de plus grande pente autour du pixel, sélection des directions autour de la plus grande pente dans un cône d'ouverture  $2\alpha$  et exemple de l'interpolation d'un profil topographique de longueur  $L_{max}$ . b) Calcul des couples  $(A_n, \beta)$  pour chaque point du profil et comparaison avec les lois empiriques de propagation. En chaque point du profil, on précise la probabilité de propagation (forte, moyenne, faible ou nulle). c) et d) Reports des probabilités de propagation obtenus pour différents profils dans le raster des probabilités de propagation. La probabilité retenue est la plus défavorable obtenue pour tous les profils interceptant le pixel.

## Influence of scrubs on rockfall dynamics

Adrian RINGENBACH<sup>1</sup>, Andrin CAVIEZEL<sup>1</sup>, Elia STIHL<sup>1</sup>, Marc CHRISTEN<sup>1</sup>, Yves BÜHLER<sup>1</sup>, Andreas STOFFEL<sup>1</sup>, Peter BEBI<sup>1</sup> & Perry BARTELT<sup>1</sup>

**Keywords:** induced rockfall, deadwood, trajectory reconstruction, rock shape, numerical model calibration

Forests have a significant protective function against rockfall. The research focused so far predominantly on standing trees, while the breaking and deflection effects of scrubs are neglected. Shrub forests and other early successional forest types are likely to become more widespread in future due to increasing treeline and natural disturbances. Therefore, it is essential to investigate the scrub-rock-interaction. We present here the results of repeated rockfall experiments with two rock shapes and three mass classes conducted in a dwarf mountain pine stand that transitions into a subalpine spruce stand. The scrubs stop small rock masses. Although larger rocks travelled mostly through the scrub cover, in-situ gyroscope measurements indicate a reduction of the rotational velocities in the dwarf pine scrubs.

### 1 VAL TISCH TEST SITE



Figure 1: UAS-derived orthophoto of the experimental test-site with the release point marked as a green cross and the outlines of the most important soil

The experimental test site Val Tisch (46.61802°N, 9.78649°E) belongs to the municipality Bergün Filisur, Switzerland (Fig 1). The release point is 2232 m a.s.l., followed by an initially steep acceleration zone ( $> 50^\circ$ ) consisting of meadow vegetation. The dense multi-stemmed, subalpine scrub mountain pines (*Pinus mugo Turra subsp. Mugo*) reach 2 - 4 m in height and cover the roughly  $38^\circ$  steep area between 2160 m a.s.l. and 2020 m a.s.l. The adjacent subalpine spruce forest below contains several single, overturned trees and one 0.2 ha large windthrow area resulting from the 2018-storm "Vaia". Laterally, two avalanche tracks limit the forest area. The lower timberline is at 1940 m a.s.l., followed by another 60 meters of pastureland and finally the creek at 1880 m a.s.l.

### 2 ROCKFALL EXPERIMENTS

During summer 2020, we conducted a total of 50 experimental runs with artificial, concrete blocks with masses between 45 and 800 kg and two shapes: the original, equant EOTA<sub>111</sub>-test block (ETAG 027, 2013) and the EOTA<sub>221</sub> version, which is platy and has an axis ratio of 2:2:1. After the deposition points of the rocks have been recorded with a STONEX S800 differential GNSS-device (cm accuracy), the rocks were flown back to the release point with an Airbus H125 Helicopter.

The blocks are equipped with in-situ *StoneNode* sensors, recording rotational velocities up to 4000°/s and accelerations up to 400 g with a sampling rate of 1 kHz (Niklaus, et al. 2017). Together with the recorded video footage (1 BlackMagic 6K from the counter slope and 12 GoPro 7 Black 4K along the

slope) and the pre- and post-experimental UAV-derived orthophotos (eBee+ RTK, WingtraOne PPK or DJI Phantom 4 RTK), the four-dimensional trajectory reconstruction, according to Caviezel *et al.* (2019), is performed.

<sup>1</sup> RINGENBACH Adrian, WSL Institute for Snow and Avalanche Research SLF, Davos Dorf, CH, adrian.ringenbach@slf.ch

### 3 RESULTS AND DISCUSSION

The summarized results in Table 1 show different deposition areas for the different mass classes. With one out of 24 EOTA<sub>45 kg</sub>-runs, only 4.2 % of the lightweight class traversed the scrub mountain pine area. This low ratio suggests a robust protective effect against small rock energies. Within the mass class of 200 kg rocks, we found differences concerning the deposition area between the rock shapes: while no EOTA<sub>111, 200kg</sub> stopped within the scrub mountain pine area, 80 % of the EOTA<sub>221, 200kg</sub>-rocks came to a standstill within this zone. While EOTA<sub>111, 200 kg</sub> and EOTA<sub>111, 800 kg</sub> have nearly the same ratio between depositions in the deadwood section and the creek, EOTA<sub>221, 200 kg</sub> and EOTA<sub>221, 800 kg</sub> differ more.

**Table 1: Deposition Areas for all released rocks taking rock mass and shape into account**

Rock Shape	Mass (kg)	Nr. Runs	Nr. Runs with StoneNode	Deposition Area			
				Scrubs	Deadwood	Forest	Creek
EOTA <sub>111</sub>	45	11	1	10	0	0	1
EOTA <sub>111</sub>	200	6	5	0	4	0	2
EOTA <sub>111</sub>	800	11	9	0	7	0	4
EOTA <sub>221</sub>	45	13	1	13	0	0	0
EOTA <sub>221</sub>	200	5	5	4	1	0	0
EOTA <sub>221</sub>	800	4	4	0	1	2	1
<b>Total</b> (EOTA <sub>111</sub> /EOTA <sub>221</sub> )		<b>50</b> (28/22)	<b>25</b> (15/10)	<b>27</b> (10/17)	<b>13</b> (11/2)	<b>2</b> (0/2)	<b>8</b> (7/1)

Although no ETOA<sub>800 kg</sub> rocks stopped within the scrubs' area, there is still an effect on the rotational velocities visible (Fig. 2). All runs have a decreasing resulting rotational velocity after about 10 s runtime. This corresponds with the time used to travel through the acceleration zone and to enter the pine-area and can thus be attributed to the scrub breaking effect. The rocks that reach the creek (runtimes > 40 s) have a second rotational velocity maximum. However, the slope is less steep below the deadwood section, which corroborates the pines' presumed influence.

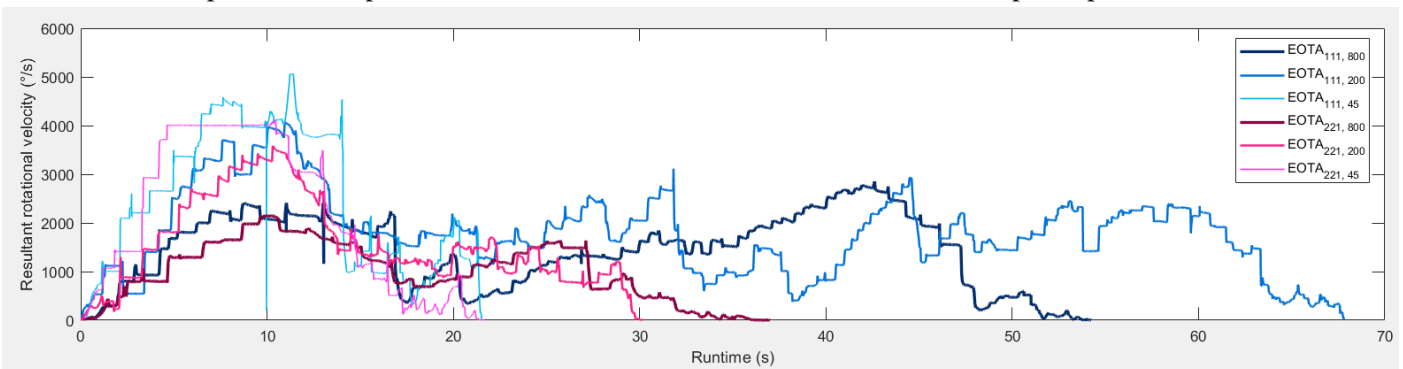


**Figure 2: Resulting gyroscope data plotted against the runtime for one run per shape and mass class.**

### CONCLUSION

With this study, the influence of scrubs is, for the first time, experimentally assessed. Dwarf mountain pines have a significant stopping capacity for small rock masses (< 45 kg). On the upper mass class under investigation, no EOTA<sub>800 kg</sub> rock was stopped by the scrubs independent of the rock shape. Largest variance in results are present in the 200 kg class, where different behaviour between the different rock shapes appears. While the platy EOTA<sub>221, 200 kg</sub> seems to be stopped efficiently by the scrubs, all the equant EOTA<sub>111, 200 kg</sub> rocks cross this area. Nevertheless, we see a reduction of the rotation velocity in the scrubs-area. Further analysis and possibly experiment will yield refined models for energy dissipation due to scrub vegetation. Based on the four-dimensional trajectories, the scrub influence can be calibrated in different rockfall models.

### ACKNOWLEDGEMENTS

The research was partially funded by NRP 73 by the Swiss National Science Foundation (Grant number: 407340\_172415). Further, we thank the municipality Bergün Filisur and all the supporters during fieldwork: Christian Simeon, Simone Ringenbach, Guillaume Meyrat, Gregor Schmucki, Tomaso Baggio, Miguel Sanchez, Jessica Munch, Jens Furrer, Kevin Henzel, Carolin Willibald and Moritz Buchmann.

### REFERENCES

- Caviezel, A. et al. (2019) Reconstruction of four-dimensional rockfall trajectories using remote sensing and rock-based accelerometers and gyroscopes, *Earth Surface Dynamics*, 7, 199–210.
- ETAG 027 (2013) Guideline for European Technical Approval of Falling Rock Protection Kits. <https://www.eota.eu/en-GB/content/etags-used-as-ead/26/>.
- Niklaus, P. et al. (2017): StoneNode: A low-power sensor device for induced rockfall experiments, in: *IEEE Sensors Applications Symposium*, pp. 1–6, 2017.

## Objective comparison of block propagation models using the Platrock platform

Franck BOURRIER (corresponding author)<sup>1</sup>, Vincent Acary<sup>2</sup>

**Keywords:** Rockfall · Model · Propagation · Fields experiments · Calibration

### ABSTRACT IN ENGLISH

The results from the different models available in the trajectory analysis platform Platrock, developed in INRAE Grenoble and freely available, have been compared on a well-documented study site. This analysis emphasized the capacities of trajectory analyses to traduce block propagation but also demonstrated that simulations cannot be relevantly interpreted if they are not accompanied with calibration proofs, sensitivity analysis, and detailed interpretation of the results from the expert in charge of the study.

### ABSTRACT IN FRENCH

Les résultats des différents modèles disponibles dans la plateforme d'analyse trajectographique Platrock, développée à INRAE Grenoble et disponible gratuitement, ont été comparés sur un site d'étude bien documenté. Cette analyse a mis en évidence les capacités des modèles disponibles à traduire la propagation des blocs mais a également démontré que les simulations ne peuvent être interprétées de manière pertinente si elles ne sont pas accompagnées de preuves de calibration, d'analyse de sensibilité et d'une interprétation détaillée des résultats par l'expert en charge de l'étude.

## 1 INTRODUCTION

For most of propagation models, a thorough calibration of the input parameters is not available over the wide range of configurations encountered in practice. Consequently, the parameters choice is strongly depending on expert knowledge. In addition, most of models exhibit substantial sensitivity to some parameters, i.e. small changes of these parameters entail large differences in the simulation results. The quality of trajectory analyses could be substantially improved by the use of several propagation models, calibrated in the site of interest or on similar sites, and by the presentation of sensitivity analyses on the simulation results.

To favour the evolution of the practices towards this direction, a trajectory analysis platform was developed in INRAE Grenoble. This platform, called Platrock, is freely accessible and gathers different types of propagation models on the same environment. 2D and 3D models integrating rocks shape or not have been integrated. The results from the different models available in the platform Platrock have been compared on a well-documented study site.

## 2 PLATROCK TRAJECTORY ANALYSIS PLATFORM

The objective of Platrock development was to contribute to the improvement of trajectory analyses objectivity. The platform is therefore expected to be usable by experts to compare propagation simulations with several models.

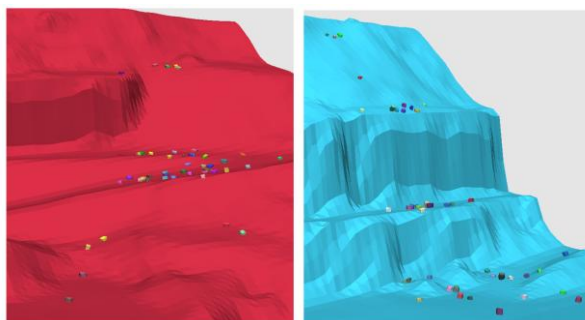


**Figure 1. Blocks stopping points obtained with the 3D model explicitly integrating block shape on the study site**

The terrain can be modelled using multilinear profiles for 2D simulations or digital terrain models (DTM – raster or TIN) for 3D simulations. For both 2D and 3D simulations, two modelling options have been implemented: the block can either be considered as a material point or its shape is explicitly accounted for.

For the material point approach, three classical rebound models based on restitution coefficients have been implemented, as well as a simple algorithm for modelling block rolling motion has been implemented.

<sup>1</sup> BOURRIER Franck, Univ. Grenoble Alpes, INRAE, ETNA, 38000 Grenoble, France - Univ. Grenoble Alpes, Inria, CNRS, Grenoble INP, Institute of Engineering, LJK, 38000, Grenoble, franck.bourrier@inrae.fr

<sup>2</sup> ACARY Vincent, Univ. Grenoble Alpes, Inria, CNRS, Grenoble INP, Institute of Engineering, LJK, 38000, Grenoble, vincent.acary@inria.fr

The model explicitly integrating block shape uses Siconos software, which is dedicated to the simulation of non-smooth dynamical systems (Acary et al., 2019). A specific contact model has been implemented in Siconos for the calculation of the block velocities and percussions at the contact points. This contact model involves normal restitution coefficient, friction, and rolling friction (Acary and Bourrier, 2021). The effect of forest on block propagation was also implemented both in 2D and 3D following the approach proposed in (Toe et al., 2018).

### 3 MODELS COMPARISON

We performed several simulation tests to model block propagation in a study site where exhaustive propagation experiments were performed (Bourrier et al., 2021). The study site, located in a quarry (Authume - France, owner: Pernot S.A), was selected because it offers significant complexity and variability in terms of topography and surface characteristics. Two propagation paths were chosen to favor block propagation that are challenging to model. As such, combinations of gentle slopes and soft soils, favoring block motion almost analogous to rolling, as well as complex topographies, i.e. involving 3D effects and topographical discontinuities, were sought. A total of more than one hundred blocks were released on two propagation paths. The propagation of the blocks was assessed by measuring the block stopping points as well as their kinematics at specific locations of the paths, called evaluation screens.

For each of the propagation paths, both 2D and 3D simulations were done with the different options proposed by the platform. For each option tested, optimal parameters values were first identified by comparison to the experimental results both in terms of propagation distances and block velocities at specific locations of the site. Complementarily, sensitivity analyses around the nominal values calibrated were provided.

### 4 RESULTS

The results show the capacities to obtain relevant results, in terms of distribution of block propagation distances, velocities and passing heights, with the different modelling approaches provided that a sufficient amount of calibration data is available. Despite this statistical adequacy, some models provided unphysical trajectories or were shown unable to traduce some archetypical trajectories. For example, it is very difficult to model typical “pseudo-rolling” block propagation on moderately steep regular slopes with models based on apparent restitution coefficients and that do not integrate a complementary block rolling algorithm. This limitation can be mandatory or not depending on the scale and on the level of accuracy of the analysis. It is more limiting for local studies of the functional efficiency of protection structures than for global hazard analyses at the slope scale, for example. In addition, significant sensitivity of the models to some input parameters is generally observed, especially for material point models based on very simple physical assumptions, such as apparent restitution coefficients. For example, slight changes in soil properties on a ledge can entail blocks stopping on it or not. These results illustrate the difficulties in performing relevant simulations in the absence of calibration data.

### CONCLUSION

The trajectory analysis platform Platrock allows performing 2D and 3D simulations using both material point rebound models and models, based on non-smooth dynamics, that explicitly account for block shape. This platform provides several simulation tools for detailed analyses of block propagation on study sites. Platrock platform is freely available upon request (contact: franck.bourrier@inrae.fr).

The possibilities of the platform have been assessed on a well-documented study site. This analysis emphasized the capacities of trajectory analyses to traduce block propagation. However, the results from these simulations cannot be relevantly interpreted if they are not accompanied with calibration proofs, sensitivity analysis, and detailed interpretation of the results from the expert in charge of the study.

### REFERENCES

- Acary, V., Bonnefon, O., Brémond, M., Huber, O., Pérignon, F., and Sinclair, S. (2019) An introduction to Siconos” Technical report RT-0340-v3, INRIA, <https://hal.inria.fr/inria-00162911>
- Acary, V., and Bourrier, F. (2021) Coulomb friction with rolling resistance as a cone complementarity problem, *European Journal of Mechanics – A/Solids*, 85,104046.
- Toe, D., Bourrier, F., Dorren, L., and Berger, F. (2018) A Novel DEM Approach to Simulate Block Propagation on Forested Slopes, *Rock Mechanics and Rock Engineering*, Vol. 51(3), pp. 811-825, 2018.
- Bourrier, F., Toe, D., Garcia, B., Baroth, J., and Lambert, S. (2021) “Experimental investigations on complex block propagation for the assessment of propagation models quality”, *Landslides*, In press.

## RAMMS Model Updates – Soil Scarring, Trees and Rotational Stability

Marc CHRISTEN<sup>1</sup>, Andrin CAVIEZEL<sup>1</sup>, Adrian RINGENBACH<sup>1</sup>, Jessica MUNCH<sup>1</sup> and Perry BARTELT<sup>1</sup>

**Keywords:** RAMMS, rockfall, numerical modelling, hazard mapping, rock shape, rock trajectories, scarring

The RAMMS::Rockfall model is a three-dimensional, user-friendly simulation tool for rockfall hazard analysis. The model consists of a parallelized computational core (C++) and a graphical user interface (IDL) that facilitates complex, and highly rockfall specific, input and output. The computational core employs hard, non-smooth contact mechanics to simulate the trajectories of falling rocks (Leine et al., 2014).

### 1 THE RAMMS::ROCKFALL MODEL

The graphical user interface of RAMMS facilitates the specification of rockfall scenarios. Point, line and polygon release areas can be specified. Maps and aerial images help define the location of release, soil types and forested areas. Rock size and shape are represented by convex three-dimensional point clouds, see Figure 1. RAMMS contains a tool to generate different rock sizes and shapes from an integrated rock library, consisting of equant, platy and long shaped rock types. Results of thousands of rocks can be analysed in the statistical mode or single rock trajectories can be animated and measured by means of XY-plots in the trajectory mode.

Since the introduction of the first RAMMS::Rockfall model, experiments in real terrain (Caviezal et al., 2019) have been used to make three modelling improvements to the existing simulation tool. These are: (1) the extension of the hard-contact ground-interaction model to include ground deformation and scarring, Figure 2a, (Lu et al., 2019), (2) the replacement of the smeared vegetation model with a discrete tree interaction algorithm, Figure 2b, (Lu et al., 2020) and (3) improved rigid-body time integrators that not only conserve energy but also ensure the stability properties of rotating rocks around the major principle axis (Leine et al., 2021). In this work we will discuss the updated ground-interaction model and the use of an extended intermediate axis theorem to integrate rockfall trajectories. Both have practical significance for rockfall hazard analysis.

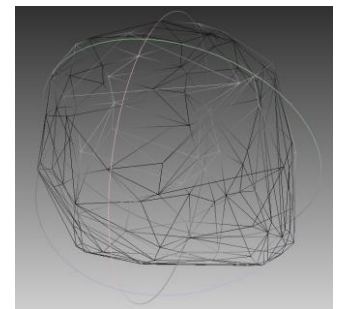


Figure 1: Point cloud of digitized rock measured in the field



Figure 2: (a) Deep ground scars observed in Bilten, Switzerland (rockfall event December 2020, photo by A. Ringenbach). Rock scarring can exist between hard rebounds, indicating that the rocks never completely exit from the scarring drag layer. This leads to long ground scars, in this case of over 50m. (b) Rockfall simulation including measured forest stems and deadwood in Surava, Switzerland. The location of the tree stems can be generated randomly, or measured locations of tree stems can be used.

<sup>1</sup> CHRISTEN Marc, WSL Institute for Snow and Avalanche Research SLF, Davos, Switzerland (CH), christen@slf.ch

## 2 ROCK-GROUND INTERACTION MODEL

Falling rocks experience a wide range of dynamic ground-interaction modes, like bouncing, rolling, sliding and thus scarring. In RAMMS the rock-ground interaction phase is split into two parts – the ground deformation phase (drag contact) and the rebound phase (hard contact) (Figure 3). In the first part the rock enters the ground and dissipates energy by plastic deformation (scarring) of the ground. The magnitude of the dissipation depends on the depth of penetration and mechanical properties of the soil. These are given by two parameters – the soil compactibility (the Me value) and the viscous drag (the Cd value). The soil mechanical parameters governing the energy dissipation have been determined using full-scale rockfall experiments in Switzerland (Caviezel et al., 2019). Different soil types – ranging from soft mountain top soils to hard bedrock – are available for users. The ground phase ends when the soil is compressed to a maximum compaction density and the rock begins to rebound. In this phase, sliding on the compacted soil is possible, inducing shear forces on the rock surface. These forces not only dissipate translational energy, but also induce torques that change the rotational speed of the rock.

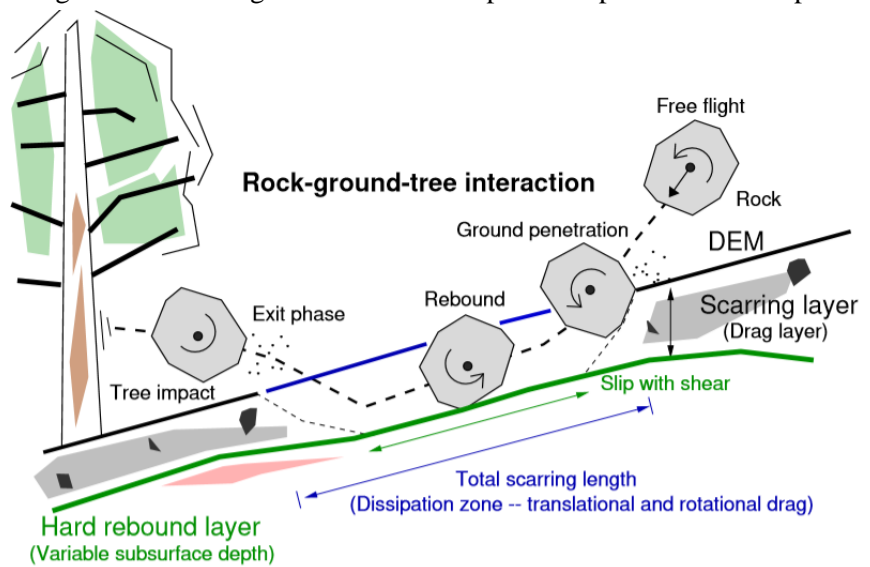


Figure 3: The rock-ground interaction model consists of a scarring layer and a hard-rebound layer. The scar length is the sum of both interactions.

## 3 EXTENDED INTERMEDIATE AXIS THEOREM

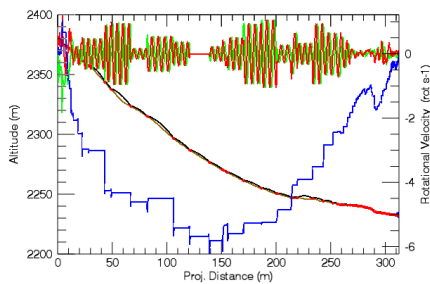


Figure 4: Simulation of a platy-shaped rock. Rotation around principle axis.

The intermediate axis theorem states that the rotation around the major and minor principal axes of a rigid body is stable whereas rotation around the intermediate axis is unstable. The stability of the principal axes is of importance in rockfall since it governs the runout and dispersion of rocks of platy shape (Caviezel et al, 2019). The numerical integration scheme in the first RAMMS rockfall model was not able to represent these stability properties, without a massive reduction in time-step, leading to excessive calculation times. In the updated RAMMS::Rockfall model a new semi-implicit numerical scheme is applied (Leine et al., 2021) that extends the stability properties such that simulations of stable rotations around the principle axes are possible even with large time-steps (Figure 4).

## CONCLUSIONS

Using results from real scale experiments, three important aspects of rockfall modelling have been introduced into the updated RAMMS::Rockfall model: Soil scarring, rock-tree interaction and improved rotational stability properties.

## REFERENCES

- Caviezel, A., Demmel, S., Ringenbach, A., Bühler, Y., Lu, G., Christen, M., Dinneen, C., Eberhard, L., Von Rickenbach, D., and Bartelt, P. (2019) *Reconstruction of four-dimensional rockfall trajectories using remote sensing and rock-based accelerometers and gyroscopes*. Earth Surface Dynamics 7, 1, 199–210.
- Leine, R. I., Schweizer, A., Christen, M., Glover, J., Bartelt, P., and Gerber, W. (2014) *Simulation of rockfall trajectories with consideration of rock shape*. Multibody System Dynamics 32, 241–271.
- Leine, R, G. Capobianco, P. Bartelt, M. Christen and A. Caviezel, (2021) *Stability of 6-DOF rigid body motion: application to rockfall simulation*. Multibody System Dynamics, in revision.
- Lu, G., Caviezel, A., Christen, M., Demmel, S., Ringenbach, A., Bühler, Y., Dinneen, C., Gerber, W., and Bartelt, P. (2019) *Modelling rockfall impact with scarring in compactable soils*. Landslides, 2353–2367.
- Lu, G., Ringenbach, A., Caviezel, A., Sanchez, M., Christen, M., & Bartelt, P. (2020). Mitigation effects of trees on rockfall hazards: does rock shape matter? *Landslides*. <https://doi.org/10.1007/s10346-020-01418-2>.

# Unusual Debris Characteristics from the February 17, 2006, Guinsaugon, Leyte, Philippines, Rockslide

Marte Gutierrez<sup>1</sup>

**Keywords:** Rockslide · Debris Flow · LIDAR · Reconnaissance · Distinct Element Modeling · Runout Distance

## ABSTRACT IN ENGLISH:

This paper presents the results of field reconnaissance and numerical modeling studies of the February 17, 2006 rockslide which occurred in Guinsaugon in the island of Leyte, the Philippines, following several days of extensive rain. The rockslide created a large scarp on the 800-m high Mt. Canabag and generated a large amount of debris consisting of mud and boulders. The debris flow resulting from the slide completely inundated the village of Guinsaugon located at the foot of Mt. Canabag and killed about 1,328 of the inhabitants. The landslide created some very unusual debris response and characteristics that are attributed to the massive energy released during the triggering of the slide, and the topography and presence of water-filled rice fields at the base of slide.

## ABSTRACT IN FRENCH:

Cet article présente les résultats des études de reconnaissance sur le terrain et de modélisation numérique du mouvement de terrain du 17 février 2006 survenu à Guinsaugon dans l'île de Leyte, aux Philippines, après plusieurs jours de pluies abondantes. Le glissement de terrain a créé une importante cicatrice sur le Mont Canabag de 800 m de haut et a généré une grande quantité de débris constitués de boue et de rochers. La coulée de débris résultant du glissement a complètement inondé le village de Guinsaugon situé au pied du Mont Canabag et tué environ 1 328 habitants. Le glissement de terrain a créé une réponse et des caractéristiques de débris très inhabituelles qui sont attribuées à l'énergie massive libérée lors du déclenchement du glissement, ainsi qu'à la topographie et à la présence de rizières remplies d'eau à la base du glissement.

## 1 THE LANDSLIDE

On 17 February 2006, a large-scale landslide (see Fig. 1) occurred in the province of Leyte, an island in the central part of the Philippines. The slide originated on the eastern side of the steep, rock-slope of Mt. Canabag and buried almost the entire village of Guinsaugon, St. Bernard town, resulting in the loss of life of 1,328 people, including 248 school children. The rockslide followed extensive and continuous rain which fell on the area from January 1 to February 17, 2006. The amount of rain is much higher than normal due to the weather phenomenon in the Pacific Ocean known as La Niña, which causes cooling of the water surface temperature in the Pacific Ocean as opposed to the warming of water surface temperature during El Niño years.

The Guinsaugon landslide involved the movement of an extremely large piece of rock on the eastern face of the 800 m high Mt. Canabag, part of the mountain chain that sits on geologic fault running north-south throughout the province. The scarp created by the slide is about 600 m high, 200 m at its deepest part and about 600 m wide at its base. To characterize and understand the nature of the slide and the resulting flow of debris materials, reconnaissance surveys were conducted



Figure 1: View of the large-scale landslide in Southern Leyte.

by a combined US and Philippine team led by the Author. The reconnaissance studies involved LIDAR imaging, photography, compass orientation measurements and fault surface profilometry of the scarp failure surfaces, and interview of survivors who witnessed how the slide unfolded. Using data from the field reconnaissance surveys, modeling using DEM (Distinct Element Method) of the slide were carried out using the computer code 3DEC (Three-dimensional Distinct Element Code) and PFC (Particle Flow Code). The DEM were used to confirm the field observations and to understand the geomechanical process leading the debris flow.

<sup>1</sup> Gutierrez, Marte, Colorado School of Mines, Golden, CO 80401, USA, mgutierrez@mines.edu

## 2 UNUSUAL DEBRIS CHARACTERISTICS

The Leyte rockslide generated about 25 million m<sup>3</sup> of debris consisting of mud and boulders, which were as thick as 30 m in some areas, and with a run-off distance of as much as 3.9 km. Based on the accounts from residents of the area regarding the duration and the distance traveled by the landslide, the flow velocity was approximately 100-140 km/h. The houses along the debris path were believed to have been carried to distances as far as 550-600 m from their original positions. All more than 300 houses and buildings in Guinsaigon, including an elementary school and a church, were destroyed and almost all were completely buried under the debris.

The slide resulted from the usual hydrological and topographical features of and effects on debris spread and sorting with debris materials of difference sizes from big bus-sized boulders to the finer mudflow carried by the rainwater. Mudflow followed the path of water flow. In addition, there were some very unusual phenomena on how the massive debris from the slide initiated and spread. The first distinct characteristics of the debris flow is that very long rubout of about 3.9 km resulting in a very low *Fahrböschung* of about 11°, a value which brings slide closer to that of submarine slides than subareal slides. Other very unusual phenomena were and verified by witnesses who survived the slides include: 1) large bus-sized boulders (Fig. 2) that were observed flying and hopping over hills, 2) isolated large mounds of debris materials (Fig. 3), formation of isolated debris islands that are disconnected from the main debris flow, heated mudflow immediately after the slide which made it difficult to rescue survivors from the debris and recover dead bodies, and basketball-size boulders that float above and sat on top of the mudflow.



Figure 2: Large boulders that were observed to be flying and hopping by witnesses.



Figure 3: Formation of large mounds of debris materials.

## 3 DISCRETE ELEMENT MODELING

Using data from the field reconnaissance study, modeling using DEM (Distinct Element Method) of the slide were carried out using the computer code 3DEC (Three-dimensional Distinct Element Code) and PFC (Particle Flow Code). The DEM confirmed: 1) the role of rainfall-induced pressurization of a fault in triggering the slides, 2) the possibility of flying large blocks, the long runout distance of the debris flow (Fig. 4), and 4) and the lateral spreading of the debris.

## CONCLUSIONS

The massive landslide in Guinsaigon, Leyte, Philippines, on February 16, 2006 was the first major catastrophic disaster of the 21<sup>st</sup> century. It unleashed a huge swath of destruction and casualties on its path. In addition, it exhibited very unusual debris flow characteristics that have never been or rarely observed before. The uncommon debris flow characteristics were attributed to the large amount of energy released by the slide which generated seismic events. DEM simulations verified the triggering of the slide and the eventual long-running debris spreading and flow.

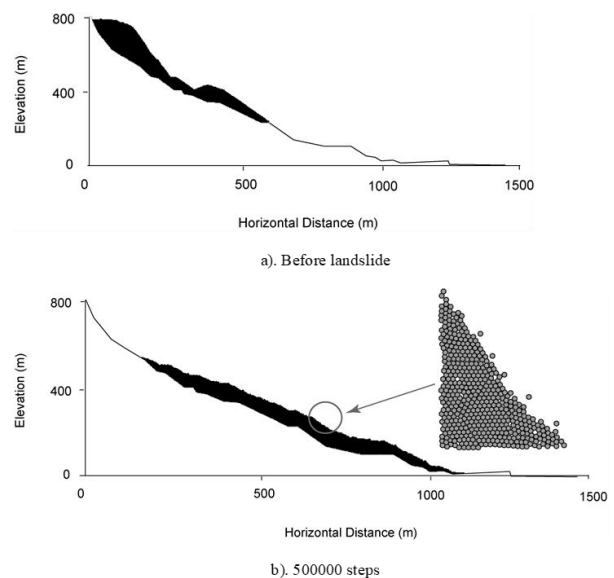


Figure 4: PFC simulation of the debris showing long runout and blocks flying/hopping above the terrain.

# Risk management

## A rockfall risk database for the French Alps

Nicolas Eckert<sup>1</sup>, Robin Mainieri<sup>1</sup>, Franck Bourrier<sup>1</sup>, Florie Giacona<sup>1</sup>, Christophe Corona<sup>2</sup>, V. Le Bidan<sup>3</sup>, A. Lescurier<sup>4</sup>

**Keywords:** Rockfall hazard and risk / observed events / database / French Alps

### ABSTRACT IN ENGLISH:

Rockfall databases including past events and their consequences remain insufficiently developed. In the French Alps, a territory where process activity is significant and stakes are numerous and diversified, related information is dispersed and heterogeneous. In the context of the National Project C2ROP, a first effort to capitalize, standardize and exploit already existing information was conducted. The C2ROP-INRAE database covers the six departments of the French Alps and brings together more than 8000 events in a common geo-referenced environment which includes the date and place of occurrence and the volume of past events. In addition, the textual information available in digital format was analysed to assess the damage caused as completely as possible. Different ways to deepen and extend the C2ROP-INRAE database are proposed and currently investigated.

### ABSTRACT IN FRENCH:

Les bases de données événementielles recensant les chutes de blocs et leurs conséquences restent peu développées. Dans les Alpes françaises, un territoire pourtant propice et où les enjeux sont nombreux et diversifiés, l'information existante est dispersée et hétérogène. Dans le contexte du Projet National C2ROP, un premier effort de capitalisation, d'homogénéisation et d'exploitation de l'existant a été réalisé. La base de données C2ROP-INRAE construite couvre les six départements des Alpes françaises et rassemble d'ores et déjà plus de 8000 événements au sein d'un environnement commun géo-référencé incluant date et lieu d'occurrence et volume des événements. En outre, les informations textuelles disponibles au format numérique ont été dépouillées pour évaluer les dommages occasionnés de façon aussi complète que possible. Des pistes pour approfondir et étendre la base C2ROP-INRAE sont proposées et actuellement en cours d'investigation.

## 1 INTRODUCTION

The National Project C2ROP brought together the majority of operational and academic actors concerned by rockfall risk in France between 2015 and 2020. In response to the insufficient capitalisation of information related to past rockfall events, INRAE has developed, with the help of all concerned stake-holders, a database of rockfall risk at the scale of the entire French Alps. This database currently covers six departments: Alpes de Haute Provence (04), Hautes Alpes (05), Alpes Maritimes (06), Isère (38) and Savoie (73). It brings together all known events within a common geo-referenced environment (GIS). The work carried out includes the critical analysis of data sources (different databases, photographs and archival documents provided by the different stake-holders) and the homogenisation of variables and units, the correction of aberrant information, the elimination of twinned events, etc. These steps are mandatory before any statistical exploitation of the data. In addition, the textual information available in digital format has been analysed to assess the damage caused. This work aims at presenting this original database, known as C2ROP-INRAE, discussing its strengths and weaknesses and proposing perspectives for the future.

## 2 METHODS AND RESULTS

All events have been compiled into a geo-referenced database, with a unique identifier per event. Each event is geo-located as accurately as possible. Different characteristics are provided: date of occurrence (year, month, day), volume, issues affected and damage caused. On 1<sup>st</sup> January 2020, the C2ROP-INRAE database includes 8249 events (Fig. 1). The Alpes Maritimes are, by far, the department the most represented (2716 events), followed by Isère (1664 events) and Savoie (1461 events). Volumes of 1 to 5m<sup>3</sup> dominate, but the empirical frequency of much bigger

---

<sup>1</sup> Université Grenoble Alpes, INRAE, UR ETNA, Grenoble 38402, France, nicolas.eckert@inrae.fr

<sup>2</sup> UMR GEOLAB, Clermont-Ferrand, France

<sup>3</sup> Conseil Départemental de l'Isère, Grenoble, France

<sup>4</sup> Conseil Départemental de la Savoie, Chambéry, France

volumes remains significant. The temporal distribution of events shows a strong seasonality, with a maximum in January (1249 events), more than 500 events per month from October to April, and, by contrast, less than 500 events per month from May to September. Due to the field data collection by stake holders in charge of roads and settlements, locations corresponding to linear stakes (roads, railways) and low elevations are over-represented, whereas, in uninhabited areas, often located at high elevations, rockfall are not recorded. Similarly, the variation in the number of events from one department to another can be explained by the variability of the collection effort and by that of natural activity. Eventually, an increasing temporal trend is obvious, as a direct consequence of the increasingly diverse nature of data sources related to events (e.g. data collection became more and more exhaustive).

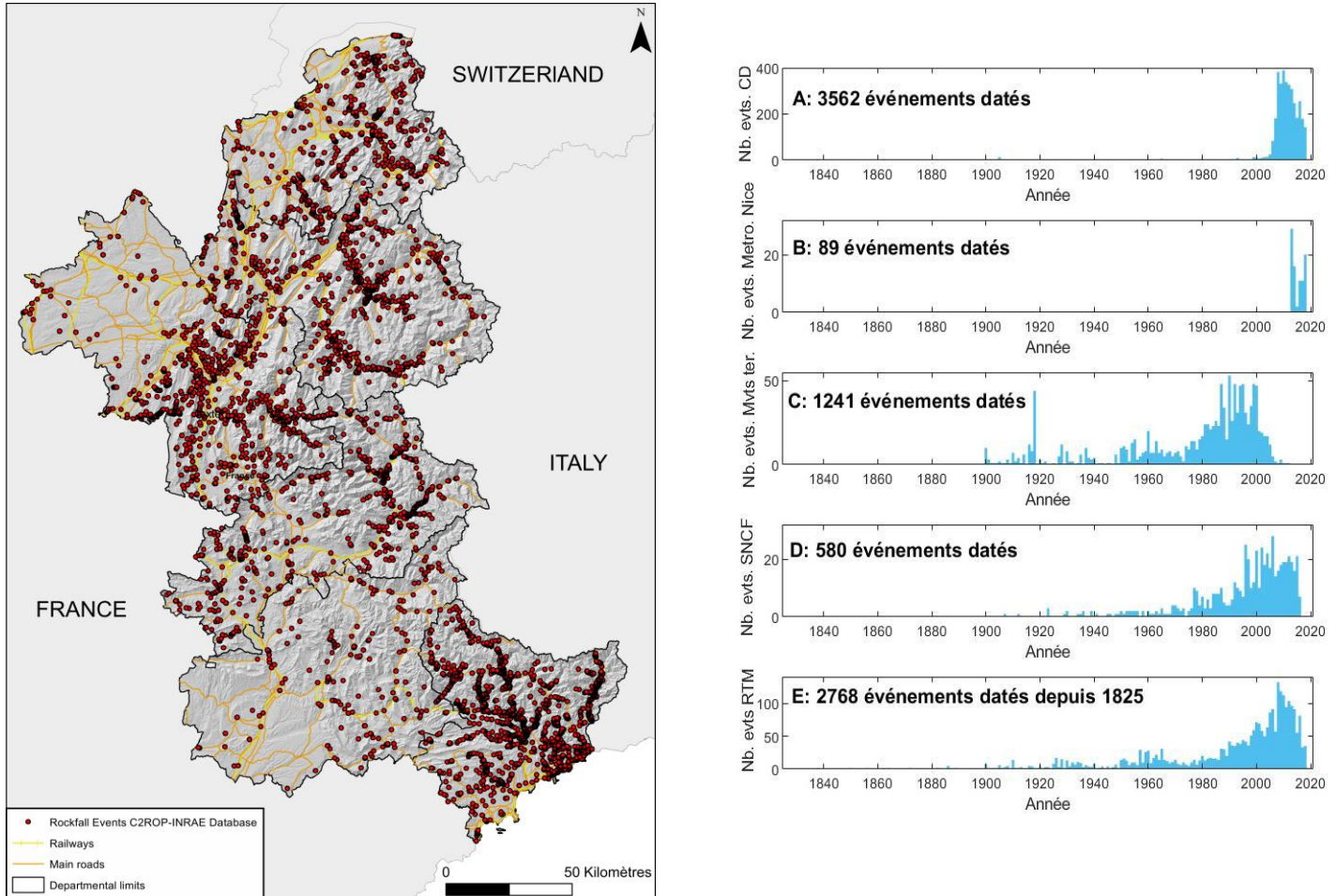


**Figure 1. Spatial (left) and temporal (right) distribution of the 8249 rockfall events included in C2ROP-INRAE database (01/01/2020). Right, rockfall time series are provided for the different stakeholders that collected the data on the field.**

### 3 CONCLUSION AND OUTLOOKS

The C2ROP-INRAE database covers the six departments of the French Alps and already includes more than 8,000 geo-referenced events. The latter includes date, location and volume of the events as well as the damage caused. A rapid analysis of the information collected was proposed: spatio-temporal patterns, distribution of volumes, damage, etc. It highlighted the quantity of information compiled and some of its major characteristics, in particular the very significant effect of data sources (databases and archives available from the different stake-holders in charge of rockfall risk), both in time (gradual increase in fields data collection effort, differentiated according to the origin of the data) and in space (concentration along the linear stakes). However, the C2ROP-INRAE database certainly also includes interesting elements concerning process activity in the French Alps: seasonality and information on the volume of damaging events in particular. Also, it enables us to get close to the reality of the risk, by the location and nature of the main issues at risk. There are perspectives to extend the existing C2ROP-INRAE database. It would be desirable to extend the database to include additional data sources that have not yet been involved: motorway companies, data compiled in the technical appendices of risk prevention plans or even in engineering reports, data from departmental and municipal archives, or even from the press. Finally, a spatial extension beyond the current limits is also possible. In particular, it would be relevant to add the data from the neighbouring departments whose topography remains favourable to rockfall activity. These different outlooks are currently investigated in collaboration with the different stake-holders involved.

# Coastal cliff landslide susceptibility in Essaouira - Morocco

Abdelah KHOUZ<sup>1</sup>, Jorge TRINDADE<sup>2</sup>, Fatima EL BCHARI<sup>3</sup>, Blaid BOUGADIR<sup>4</sup>, Sergio OLIVEIRA<sup>5</sup>, Ricardo GARCIA<sup>6</sup>, Mourad JADOUD<sup>7</sup>

**Keywords:** Rocky coast, Cliff instability, Landslide susceptibility, Geographic Information Systems, Essaouira, Morocco.

## 1 Introduction

Landslides are considered as one of the most damaging natural hazards, which particularly threaten cliff coastal areas. Landslides induce risk for the population and human activities exposed to cliff retreat. Additionally, the human pressure is still increasing on coastal cliff areas, which, are found along 80% of the Earth's ocean coasts (Emery and Kuhn, 1982). As a consequence of the rapid development in these coastal areas, especially as 1.2 billion people globally live in areas within 100 km of a shoreline, and less than 100 m above mean sea level, the area most directly affected by changing sea levels (Marone et al., 2017). Furthermore, climatic change and sea level rise could increase coastal natural processes responsible for its degradation.

The erosion of the rocky coasts, can be related to a wide range of marine and continental processes, as reviewed by Sunamura (1992) and Dong (2009), and a wide range of predisposing factors have been considered: lithology, rock behaviour under stress due to wave impacts and freshwater processes, soil thickness, vegetation cover, cliff exposure to prevailing winds and waves, protective beach width, sea-level rise rates, and also anthropogenic pressures such as footpath location or an increase of artificial areas (French, 2001). In sheltered areas, cliff retreats are mainly driven by subaerial weathering processes (Robinson and Jerwood, 1987; Sallenger et al., 2002).

The West African coast, mostly cut in loose sediments is among the most vulnerable regions of the world, concerning to the effects of coastal erosion and climate change. At the regional level, erosion and flooding, are the most significant hazards, with more than 50% of the coastline classified with a very high level of risk (Jochaud, 2019). Due to its geographical situation at the north-western corner of Africa within moderate latitudes and along the northern border of the African plate, Morocco is exposed to several types of hazards of meteorological origin (Département de l'Environnement, 2005; OCDE, 2015), global climate changes and associated sea-level rise (e.g. Satta et al., 2016), and marine storms (Simonet and Tanguy, 1956, El Messaoudi et al., 2016). These facts surely contribute to conditioning and triggering, landslides and rockfalls (Département de l'Environnement, 2005; Mastere, 2011)

## 2 Study Area

The Essaouira coast area, the study site in this research, is located along the central section of Atlantic Morocco, characterised by a complex of sandy and rocky coast over 134km. This natural morphology is locally interrupted by heavily anthropized coastal areas especially at the city of Essaouira. The cliff coastal sectors are characterized by the presence of many rock falls, debris flows, rock slides and rock topples, which are being the dominant natural hazards responsible for huge constraint for human activities and a safe land use (e.g. Moore and Griggs, 2002).

The assessments of landslide susceptibility aims to evaluate the relative spatial probability of a new landslide occurs in the future (Remondo et al., 2003), and their assessment in a given area should normally be based on the analysis of instability factors. Thus, it is necessary to identify a set of conditions under which landslide have occurred in the past, and to find the critical combinations of preparatory factors for delineating the possible occurrence of further landslides. Nevertheless, a representative and robust landslide inventory is the first step for assessing mass movements susceptibility, hazard and risk (Aleotti & Chowdury 1999, Dai & Lee 2002, Van Westen et al. 2008). Furthermore, they are also mandatory for models that predict landslides based on past conditions. In addition to landslide inventory, susceptibility maps can give the likelihood of occurrence of landslides, which should be take into account in earlier phases of land use planning (Fell et al. 2008). To establish this task for this vulnerable area, there are different methods that manage hillslope instability factors in different manners (Hansen 1984; Corominas et al. 2014).

## 3 Methodology and results

The purpose of this work is to map landslides and zoning susceptible areas for Essaouira coast based on a set of factors that contribute to the instability of the sea cliff. Landslides inventory was supported on bibliographic previous data, medium to high-resolution satellite imagery and aerial photographs interpretation, different scales Digital Elevation Models (DEMs) and field surveys, that allows to mapping 266 landslides.

<sup>1</sup>KHOUZ Abdellah, Laboratory of Applied Sciences for the Environment and Sustainable Development (SAEDD), Higher School of Technology Essaouira, Cadi Ayyad University, Marrakech, Morocco. Centre for Geographical Studies, IGOT, Universidade de Lisboa, Lisbon, Portugal. Universidade Aberta, Lisbon, Portugal [abdellah.khouz@gmail.com](mailto:abdellah.khouz@gmail.com)- [1902243@estudante.uab.pt](mailto:1902243@estudante.uab.pt)

<sup>2</sup>TRINDADE Jorge, Centre for Geographical Studies, IGOT, Universidade de Lisboa, Universidade Aberta, Lisbon, PT, [jorge.trindade@uab.pt](mailto:jorge.trindade@uab.pt)

<sup>3</sup>El BCHARI Fatima, Department of Earth Sciences Polydisciplinary Faculty, of Safi Cadi Ayyad University, Safi, Morocco; [elbchari@uca.ma](mailto:elbchari@uca.ma)

<sup>4</sup>BOUGADIR Blaid, Laboratory of Applied Sciences for the Environment and Sustainable Development (SAEDD) - Higher School of Technology Essaouira, Cadi Ayyad University, Marrakech, Morocco; [b.bougadir@uca.ma](mailto:b.bougadir@uca.ma)

<sup>5</sup> OLIVEIRA, Sergio, Centre for Geographical Studies, IGOT, Universidade de Lisboa, Lisbon, PT, [cruzdeoliveira@campus.ul.pt](mailto:cruzdeoliveira@campus.ul.pt)

<sup>6</sup>GARCIA, Ricardo, Centre for Geographical Studies, IGOT, Universidade de Lisboa, Lisbon, PT, [rgarcia@campus.ul.pt](mailto:rgarcia@campus.ul.pt)

<sup>7</sup>JADOUD Mourad, Geosciences and Environmental Techniques Laboratory, faculty of sciences El Jadida, Chouaib Doukkali University, El Jadida 24000, Morocco; [mourad\\_jadoud@yahoo.fr](mailto:mourad_jadoud@yahoo.fr)

Therefore, after a classification of coastal systems into rocky and sandy systems, terrain units were defined based on the methodology proposed by Marques et al. (2011), according to a morphometric and operational criterion. Lower and upper limits of the terrain units, are defined by the top and bottom of the cliff, respectively, while lateral limits were geometrically drawn perpendicular to the contour lines of the topography, and defined by the segmentation of the ridge line into 50 m wide sections. In total, we had 2975 terrain units, of each 1534 are rocky-tailed units and 1441 sandy units.

The susceptibility assessment model is carried out by classifying the terrain units into two classes: stabilized and non-stabilized (Fig. 1). The classification process is based on the quantification of the percentage of the unstable area of each slope unit. The approach was done individually for each type of slope movement studied, due to the wide range of sizes, as attested by the respective average of the unstable area, which are located more to the south of study area.

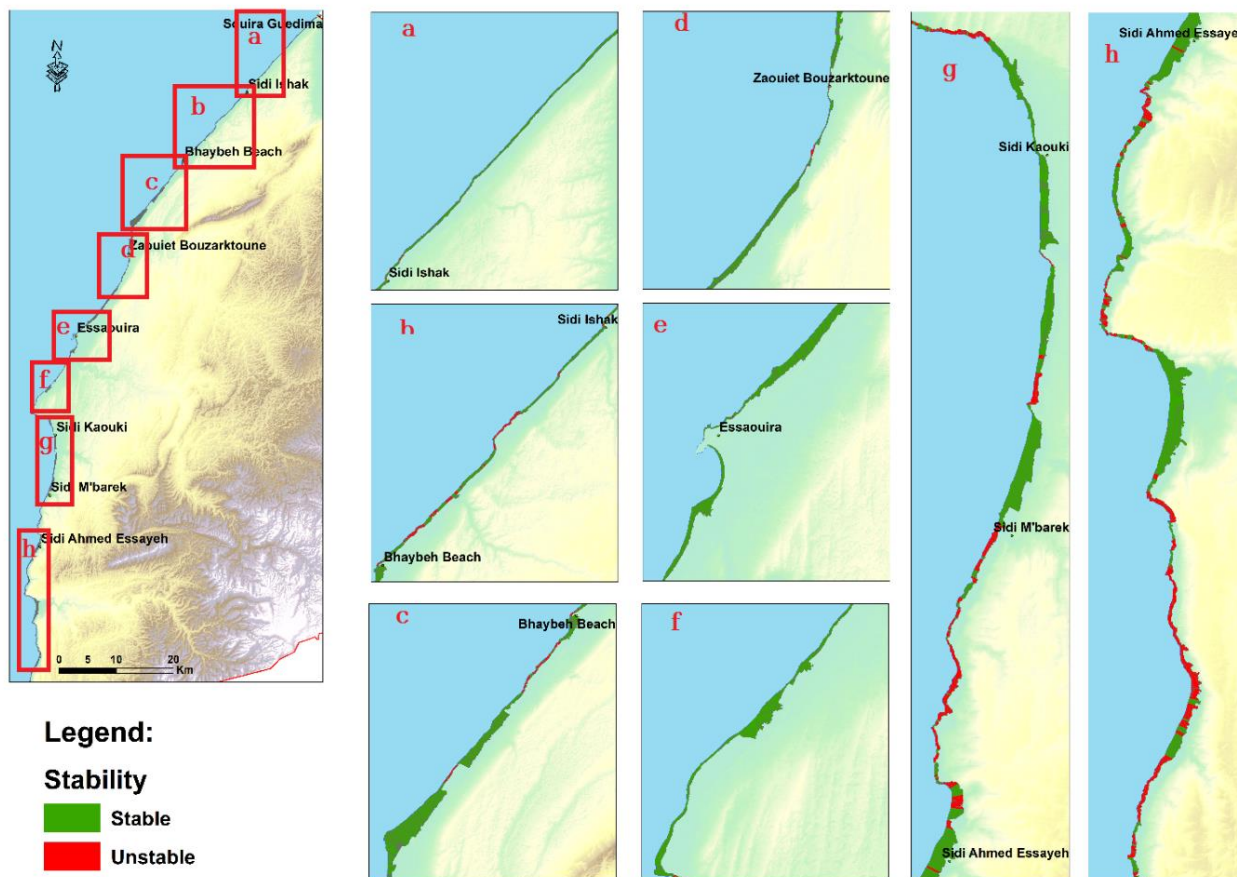


Figure 1: Classification of terrain units regarding geomorphological instability

#### 4 Conclusion

This preliminary approach to landslide susceptibility in the 134 km of coastal area of Essaouira, based in morphological analysis (interpretation of aerial photos, satellite images, and fieldwork) and GIS analyses allowed to identify 737 terrain units as unstable, which means that about 25% of the study area has high problems with cliff stability (48.76 % of the rocky terrain units).

#### REFERENCES

- Aleotti P, Balzeli P, De Marchi D (1996) Le reti neurali nella valutazione della suscettibilita' da frana. *Geologia tecnica e ambientale* 4:37–47
- Ayalew, L., Yamagishi, H., 2005. The application of GIS-based logistic regression for landslide susceptibility mapping in the Kakuda–Yahiko Mountains, Central Japan. *Geomorphology.*, 65, 15–31.
- Corominas J, van Westen C, Frattini P (2014) Recommendations for the quantitative analysis of landslide risk. *Bull Eng Geol Environ* 73: 209–263
- Département de l'Environnement, 2005. Etude pour la réalisation d'une cartographie et d'un système d'information géographique sur les risques majeurs au Maroc. (accessed online 19 March 2019)
- Dong, P., 2009. Cliff erosion—how much do we really know about it. *Environ. Geol.* 58, 815–832.
- El Messaoudi, B., Ait Laâmel, M., El Hou, M., Bouksim, H., 2016. Situations des fortes houles sur les côtes atlantiques marocaines. *Actes Session Plénière Académie Hassan II des Sciences & Techniques, Rabat, 24-25 février 2015*, 79-99.
- Emery, K.O., Kuhn, G.G., 1982. Sea cliffs: their processes, profiles, and classification. *Geological Society of American Bulletin*, 93, 644-654.

- Fell R, Corominas J, Bonnard C, Cascini L, Leroi E, Savage WZ (2008) Guidelines for landslide susceptibility, hazard and risk zoning for land use planning. *Eng Geol* 102:85–98. enggeo.2008.03.022
- French, P.W., 2001. Coastal Defenses: Processes, Problems and Solutions. Routledge, London.
- Hansen A (1984) *Engineering geomorphology: the application of an evolutionary model of Hong Kong's terrain*. *Zeitschrift für Geomorphologie, Supplement band* 51:39–50
- Hungr, O., Leroueil, S., Picarelli, L., 2014. The Varnes classification of landslide types, an update. *Landslides* 11 (2), 167–194.
- Jochaud, Ph, 2019. Coastal hazards in West Africa: improving decision-making at national and regional levels through the promotion of standardized coastal language.
- Marone, E., De Camargo, R., Castro, J.S., 2017. Coastal hazards, risks, and marine extreme events: what are we doing about it? *Physical Sciences, Natural Hazard Science, Hydrology, Atmospheric Sciences, Geophysics*.
- Marques, F., Matildes, R., Redweik, P. (2011) – Statistically based sea cliff instability hazard assessment of Burgau-Lagos coastal section (Algarve, Portugal). *Proceeding of the 11th International Coastal Symposium. Journal of Coastal Research, SI64: 927-931.*
- Mastere, M., Aït Brahim, L., Elfahchouch, N., Guelzim, E., Mansour, M. (2011) Spatiotemporal analysis of landslides using digital photogrammetry and DEM (Teledetection review, in press).
- Moore, L.J., Griggs, G.B., 2002. Long-term cliff retreat and erosion hotspots along the central shores of the monterey bay national marine sanctuary. *Mar. Geol.* 181 (1–3), 265–283.
- OCDE/OEDC, 2016. Etude de l'OCDE sur la gestion des risques au Maroc. Editions de l'OCDE, Paris, 234 p. (accessed online 19 March 2019).
- Remondo, J., González, A., De Terán, J.R.D. *et al.* Validation of Landslide Susceptibility Maps; Examples and Applications from a Case Study in Northern Spain. *Natural Hazards* **30**, 437–449 (2003).
- Robinson, D.A., Jerwood, L.C., 1987. Sub-aerial weathering of chalk shore platforms during harsh winters in southeast England. *Mar. Geol.* 77, 1–14.
- Sallenger, A.H.J., Krabill, W., Brock, J., Swift, R., Manizades, S., Stockdon, H., 2002. Sea cliff erosion as a function of beach changes and extreme wave runup during the 1997-1998 El Nino. *Mar. Geol.* 187, 279–297.
- Satta, A., Snoussi, M., Puddu, M., Flayou, L., Hout, R., 2016. An index-based method to assess risks of climate-related hazards in coastal zones: The case of Tetouan. *Estuarine, Coastal and Shelf Science*, 175, 93-105.
- Mastere, M., 2011. La susceptibilité aux mouvements de terrain dans la province de Chefchaouen (Rif Central, Maroc) : analyse spatiale, modélisation probabiliste multi-échelle et impacts sur l'aménagement et l'urbanisme. PhD Thesis, Université de Bretagne occidentale, 320 p.
- Simonet, R., Tanguy, R., 1956. Etude statistique de la houle dans les différents ports marocains pour la période 1928-1952. *Ann Serv Phys Globe Meteorol, Rabat, XVI*, 109-130.
- Sunamura, T., 1992. *Geomorphology of Rocky Coasts*. Chichester. Wiley, New York 302p.
- Telford, W.M., Geldart, L.P., Sheriff, R.E., 1990. *Applied Geophysics*. Cambridge University Press 26 oct. 1990, 770p.
- Van Westen CJ, Castellanos E, Kuriakose SL (2008) Spatial data for landslide susceptibility, hazard, and vulnerability assessment: an overview. *Eng Geol* 102:112–131
- Varnes, D.J., 1978. Slope movement types and processes. In: Schuster, R.L., Krizek, R.J. (Eds.), *Special Report 176: Landslides: Analysis and Control*. Transportation and Road Research Board, National Academy of Science, Washington D. C., pp. 11–33.

## Digitization and Building Information Modeling of rockfall protection's worksites

Clément GALANDRIN (CAN)<sup>1</sup>, Mickaël BEAUFILS (BRGM)<sup>2</sup>

**Keywords:** digital model, rock fall, protective structures, Building Information Modeling, asset management, working supervision

### ABSTRACT:

The major digital transformation ongoing at the level of infrastructure works in line with the progression from BIM to infrastructure BIM and the speed of evolution of new technologies. Geotechnics and natural risk management cannot ignore this context. CAN is now working to implement new technologies in its processes, such as digital model, augmented reality, immersive view, etc. All those possibilities are investigated in order to improve the technicality and precision of rock falls protection projects and take into account the entire life cycle of protective structures.

### RÉSUMÉ:

Les travaux d'infrastructures connaissent une transformation numérique profonde avec la progression du BIM au BIM infrastructure et l'émergence rapide des nouvelles technologies. La géotechnique ainsi que la gestion des risques naturels ne peut ignorer ce contexte. CAN travaille aujourd'hui sur l'implémentation des nouvelles technologies dans ses process: maquette numérique, réalité augmentée, vue immersive,... autant de pistes de développement explorées afin d'améliorer la technicité et la précision des projets de protection contre les chutes de pierres et de prendre en considération l'ensemble du cycle de vie des ouvrages de protection.

## 1 USES OF DIGITAL MODEL

The use of terrain models with the layout of structures in the form of 3D objects on DTMs is not used in the field of implementation of protective structures, neither in the design nor in construction phase. However, it has been observed for years by the actors of the field that structures such as Rockfall barriers needed adaptations to the terrain to ensure their optimal operation and the safety of the workers implementing them. Plus, the visualization of the structures on the field can be a real added value for the project under environmental or landscape constraints. The development of complete digital models of the structure, that we can call BIM model, allows fine layouts, strongly limiting the risks during the execution and a visual integration of the structure in its environment. The use of tools like Augmented & Mixed Reality is also a suitable mean to interact with such models.

## 2 CREATION & EXPLOITATION OF MODELS

### 2.1 Digital Terrain model

The terrain model is mostly created from data acquired by UAV surveys using photogrammetric modeling or LIDAR scanning. Field acquisition must be carried out methodically, to obtain data set that takes into account the irregularities of the terrain: overhang, angularity... Then, different post-processing are applied during the elaboration of the point cloud to obtain accuracy and file size necessary for its use within the complete model according to its objective: cubature, location of objects, etc... For an increased precision, the objects will be implanted on a centimetric accuracy points cloud. Without having a points cloud, it is possible to extrapolate the terrain from contour lines. The workflow depends on the data source, but it consists in creating a mesh surface from the topographic lines. The model will be less accurate than the points cloud but brings an appreciation of the structure in its 3D environment. This will allow to capitalize on the availability of open data (IGN,...). The georeferencing with high accuracy of these models should enable the creation of databases for the various stakeholders, improving the asset management over time.

### 2.2 Full Digital model

Digital tools can be used to create models at different levels of accuracy according to the evolution of the project: from a summary implementation as a simplified model to a complete work rendering in the form of an assembly of objects in its environment (terrain, protected infrastructure, etc.). It is now possible to go as far as rendering an "as-built" model to the client for the operation and maintenance of his infrastructure.

<sup>1</sup> GALANDRIN Clément, CAN, Mirmande, France (FRA), cgalandrin@can.fr

<sup>2</sup> BEAUFILS Mickaël, BRGM, Orléans, France (FRA), m.beaufils@brgm.fr

The use of CAD softwares allows to design the solution within the 3D models in order to carry out measurements and obtain a fine implantation of the structure according to the irregularities of the terrain. The 3D sketch of the structure brings an added value by making it possible to incorporate as early as possible in the execution studies the specificities of the structure to be built: definition of the linear of the structure, positioning of the anchors, respect of the angles of wire ropes, measurement of the gapfillings. To create those models, different objects types are built, each in different softwares : fixed object such as posts, scalable items like wire ropes. Both are matched with the points clouds in a BIM software and can be shared at the output of the workflow.

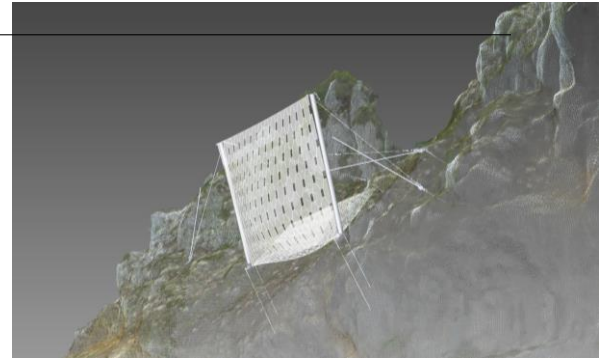


Figure 1: Example of model with gapfilling and anchorages positioning

### 2.2.1 BIM Models Convergence

With the development of BIM, it is possible to set up efficient workflows to create BIM models of protective structures projects. All structures parts are designed as objects, which means attributes and descriptive information can be associated to the geometry as metadata. This opens new perspective, with BIM models offering: a realistic visual rendering that can be adapted to the uses and project phases, possibility for all parties involved to project themselves into the working environment and refine the analyses.

As a Digital Twin of the infrastructure, BIM enables to get instant access to all information regarding it at any stage. Such new capacities, open the door to discussions regarding data exchanges between stakeholders and possible interoperability issues. Although companies such as CAN are working on this subject at their own level, with thoughts on intra-company exchanges in particular. Collaboration have to be organized, relying on the use of common language and practice for data exchange. Standards have to be implemented, such as ISO 19650 series [ISO, 2018] which lay down the concepts of information management during construction projects. Projects like MINnD in France, also aim to extend the OpenBIM standard capacities to properly describe infrastructure projects such as Railways, Road, Tunnel, Bridge and Geotechnics [Beaufils & al, 2019], building on the available standards from building SmartInternational (bSI) and the Open Geospatial Consortium (OGC).

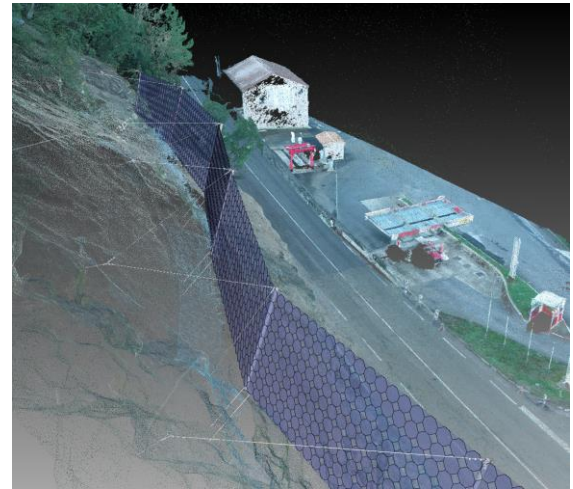


Figure 2 : Example of complete digital model, RN106 Les Salles du gardon (30, France)

## CONCLUSION

Evolution of new digitization and modeling technologies linked to the extension of BIM to infrastructures is an opportunity for the management of gravity-based natural risks, such as rock falls mitigation. The use of BIM models is a new way to ensure a better follow-up of the stakes and solutions at any stages of a project: design, work supervision, working life of structures. Current tools allow to model the protection projects in an efficient way. However a real collective work is to be undertaken between the various stakeholders in order to define the use cases of the digital models and the information linked in, so that digital models are relevant in the field of Natural Gravity Hazards in order to deploy BIM solutions applied and usable by all.

## REFERENCES

ISO 19650 - Part 1 to 5 (2018), Organization and digitization of information about buildings and civil engineering works, including building information modeling (BIM) – Information management using building information modeling.

M.Beaufils & al (2019), Livrable Projet National MINnD saison 1 UC8-1: IFC infrastructures souterraines (UC8) - Standardisation des données géotechniques pour la conception d'infrastructures souterraines.

## FEEDBACK ON THE 4D MONITORING AND ASSESSMENT OF ROCKFALL AND HANGING GLACIER STABILITY (Taconnaz bassin, Chamonix, France)

Johan BERTHET<sup>1</sup>, Pierre-Allain DUVILLARD<sup>2</sup>, Ludovic RAVANEL<sup>3</sup>, Alexandre BARATIER<sup>4</sup>, Philippe BERTHET-RAMBAUD<sup>5</sup>, Laurent ASTRADE<sup>6</sup>, Severin STHALY<sup>7</sup>, Felix BLUMENSCHNEIN<sup>8</sup>, Lorenz MEIER<sup>9</sup>, Felix ROUX<sup>10</sup>

**Keywords:** Rockfall, hanging glacier, outburst flood, high mountain, monitoring

### 1 CONTEXT

Climate change has profound impacts on the high mountain cryosphere, in particular on alpine glaciers. Ice loss and warmer temperatures can amplify glacier instabilities according to site-specific features (*e.g.* morphology, hydrology...) with, in addition, an increase of rockfall frequency/volume due to permafrost degradation. In this context, the characterisation of instabilities that can affect glacier tongue are essential for a quantitative risk assessment in alpine valleys (*e.g.* Vincent *et al.*, 2015). On the 24 nov. 2018, a 42 900 m<sup>3</sup> (+/- 2 200 m<sup>3</sup>) rockfall occurred, resulting in a flow of mixed (rock and ice) debris over 1.85 km in the Taconnaz basin (Chamonix, Mont Blanc massif). This event stopped approximately 165 m upstream of the construction site of a water intake. In this context, an operational monitoring system was set up to anticipate future collapse and flow to reduce the exposure of workers during the summer 2019 and 2020.

### 2 METHOD

Hazard assessment was performed both seasonally and daily. During each summer day, a daily risk assessment report was sent on early morning to the workers, using an automatic deformation analysis based on images of the three glacial tongues (*e.g.* Meier *et al.*, 2018, Giordan *et al.*, 2020). In addition, a trained operator could trigger a warning system in case of imminent hazard.

Seasonal assessment was performed to detect slower but in-depth changes. In June 2020, the worrying advance of the Bossons glacier tongue could be detected. The specific survey of this new risk of glacier destabilisation had consisted in estimating the unstable volume of ice helped with a photogrammetric 3D model and then in simulating ice avalanches with different volume scenarios.

The global approach of the hazard assessment was especially designed to be robust and strong enough to face all types of unpredictable high mountain geomorphic events. On the 1<sup>st</sup> oct. 2019, a small GLOF (Glacial Lake Outburst Flood) occurred on the Taconnaz stream emissary from an inner water pocket located upper on the glacier. It was directly observed by the trained workers on site. We were able to remotely manage the crisis through the combination of the monitoring system, a clear communication with collaborators on site, and the fine knowledge of the site acquired in the recent years.

### 3 FEEDBACK EXPERIENCE

The daily assessment has revealed the complexity of hazards in this high mountain area. We could not be focused on a single process but we had to take into account the wide panel of processes which can occur as well as their interactions: glacier tongue collapse, rockfalls, floods, etc. In the Taconnaz case, the priority was given to the glacial processes, but the qualitative analysis of the time lapse picture was able to give much more information such as water level variations of the torrents or rockfalls (Failletaz, 2019).

Daily observations suggested that we still have a poor knowledge of small events in proglacial and periglacial areas. They were not notified before but they have become noteworthy as new infrastructures, such as hydropower plants, are built in such an environment. The most important events have still to be re-analysed to understand if the daily

---

<sup>1</sup> STYX 4D, Le Bourget-du-Lac, France, johan.berthet@styx4d.com

<sup>2</sup> STYX 4D, Le Bourget-du-Lac, France, pierre-allain.duvillard@styx4d.com

<sup>3</sup> EDYTEM, Université Savoie Mont Blanc, CNRS, Le Bourget-du-Lac, France, ludovic.ravanel@univ-smb.fr

<sup>4</sup> STYX 4D, Le Bourget-du-Lac, France, alexandre.baratier@styx4d.com

<sup>5</sup> ENGINEERISK, Le Bourget-du-Lac, France, philippe.berthet-rambaud@engineerisk.com

<sup>6</sup> EDYTEM, Université Savoie Mont Blanc, CNRS, Le Bourget-du-Lac, France, laurent.astrade@univ-smb.fr

<sup>7</sup> GEOPREVENT, Zurich, Suisse, severin.stachly@geoprevent.com

<sup>8</sup> GEOPREVENT, Zurich, Suisse, felix.blumenschein@geoprevent.com

<sup>9</sup> GEOPREVENT, Zurich, Suisse, lorenz.meier@geoprevent.com

<sup>10</sup> VOLTALIA, Aix-en-Provence, France, f.roux@votalia.com

assessment has missed evidence which could have allowed us to anticipate it. That is how we observed a slow migration of the emissary position in the glacier, one month before the 2019 GLOF. Emissaries positions were especially surveyed in 2020.

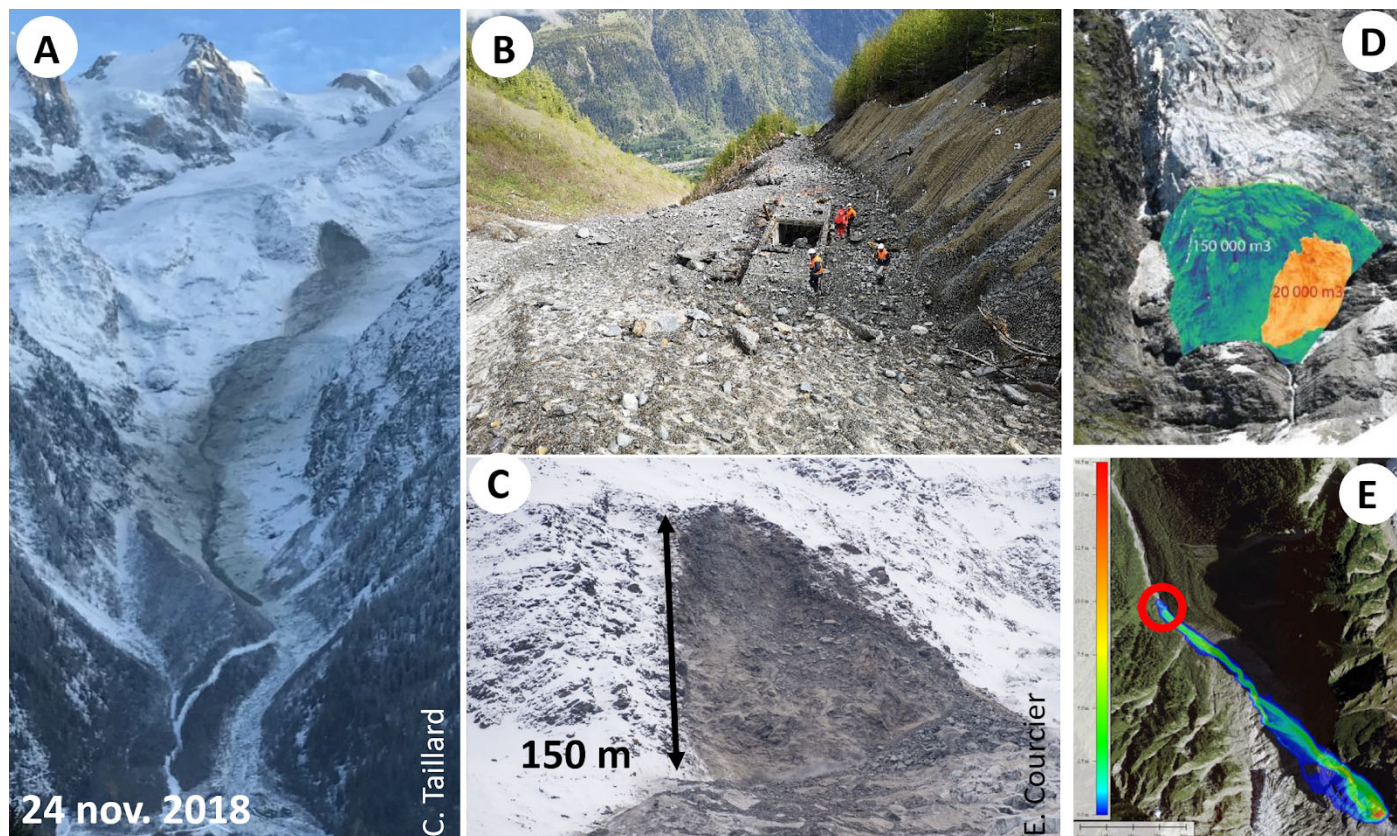


**Figure: The Taconnaz case study since 2018.** A) Rockfall source and related mixed debris flow (snow/ice and rock); B) Water intake in spring covered by the rock debris deposited by the avalanche; C) Rockfall scar of the 24 nov. 2018 event; D) 3D reconstruction of the Bosson glacier tongue volume in 2020. E) Simulation of a destabilization of 20 000 m<sup>3</sup> of ice from the Bossons glacier tongue.

## CONCLUSION

High mountain hazard assessment is really challenging because of the complexity of the processes and their interactions. Even if technological tools are being developed, our feedback underlights that the efficiency of the management still needs to be associated with human analysis with strong specific knowledge and skills.

## Acknowledgements

Authors thank the *Communauté de communes de la Vallée de Chamonix-Mont-Blanc, Benedetti & Guelpa, Voltavia* for the collaboration. We thank E. Mallet, L. Gattini, B. Demilly, C. Gissinger for their help on the field.

## REFERENCES

- Margreth S., Faillettaz J., Funk M., Vagliasindi M., Diotri F., Broccolato M. (2011). Safety concept for hazards caused by ice avalanches from the Whymper hanging glacier in the Mont Blanc Massif. *Cold Regions Science and Technology* 69:194–201.
- Faillettaz J. (2019). Stabilité du Glacier de Planpincieux, Rapport d'expertise. Fondazione Montagna Sicura, 14 p.
- Meier L., Jacquemart M., Steinacher R., Jäger D., Funk M. (2018). Monitoring of the Weissmies glacier before the failure event of september 10, 2017 with radar interferometry and high-resolution deformation camera. *Proceedings, International Snow Science Workshop 2018*. Innsbruck Austria. 661-664.
- Giordan D., Dematteis N., Allasia P., Motta E. (2020). Classification and kinematics of the Planpincieux Glacier break-offs using photographic time-lapse analysis. *Journal of Glaciology* 66:188–202.
- Vincent C., Thibert E., Harter M., Soruco A., Gilbert A. (2015). Volume and frequency of ice avalanches from Taconnaz hanging glacier, French Alps. *Annals of Glaciology* 56:17–25.

## Feedback on four exemplary early warning systems for landslides

Stella COCCIA<sup>1</sup>, Emmanuelle KLEIN

**Keywords:** landslides, early warning systems, risk management, precipitations, local and regional scale

### ABSTRACT IN ENGLISH:

In some contexts, the only solution to manage the risk of slope instability induced by precipitation is to set up an early warning system. Such systems are designed to issue warnings at the right time to enable action to be taken and to guarantee public safety, for landslides can be deployed at the scale of a single slope or at regional scale. Sometimes, local and regional systems coexist in the same area without a real synergy. In order to illustrate the conditions and frameworks in which these different systems operate, this article focuses on four exemplary systems: the Ruines de Séchilienne in France and the Ancona landslide in Italy at the local scale, Norway and Hong Kong systems at the regional scale. This article is based on scientific literature. Note that the scientific observation systems and the monitoring systems, that do not address the issue of response capability, are not included in it.

### ABSTRACT IN FRENCH:

Dans certains contextes, la seule solution pour gérer le risque d'instabilités de pente induites par les précipitations est l'installation de dispositifs d'alerte. Ces dispositifs sont déployés pour produire des alertes en temps opportun afin de garantir la sécurité des populations exposées, pour les instabilités de pente ils sont installés à l'échelle d'un seul versant ou à l'échelle régionale. Parfois, les deux échelles coexistent sur le même territoire sans une réelle synergie. Pour illustrer les conditions et les contextes de ces dispositifs, cet article présente quatre dispositifs emblématiques : les Ruines de Séchilienne en France et Ancône en Italie, à l'échelle locale, la Norvège et Hong Kong à l'échelle régionale. Cet article se base sur la littérature scientifique. A noter que ni les dispositifs d'observation ni les systèmes de surveillance, qui ne prennent pas en compte la capacité de réponse, n'y sont pas inclus.

## 1 INTRODUCTION

Based on the available scientific literature alongside information collected during discussions with the operators responsible for the management of the early warning systems for slope instabilities induced by precipitations in operation in Europe, Ineris wrote a report on these systems. A part of this report has been already presented: general context of early warning systems and their basic components (Coccia and Klein, 2020). Here, we present and compare four exemplary early warning systems: the Ruines de Séchilienne in France and the Ancona landslide in Italy (both at the local scale), Norway and Hong Kong systems (at the regional scale).

## 2 EARLY WARNING SYSTEMS

The first developments in early warning systems for natural risks date back to the 1970s. For this kind of risks, an early warning system is “the set of capacities needed to generate and disseminate timely and meaningful warning information to enable individuals, communities and organizations threatened by a hazard to prepare and to act appropriately and in sufficient time to reduce the possibility of harm or loss”(UNISDR, 2009). Each system is adapted to the site, hazard and affected population. For landslides they can be deployed at the local scale or at regional scale. The so-called local scale (Piciullo et al, 2018 and Pecoraro et al., 2018, etc) is thus applied at the scale of a slope where a single type of landslide can be found. The so-called regional scale (Thiebes and Glade, 2016, etc.) or territorial scale (Piciullo et al., 2018) applies to a region, a municipality or even a whole country. It can thus cover several types of instability at the same time. A non-exhaustive map of 52 early warning systems deployed at local (24) and regional scale (28) was created by Piciullo et al. (2018) and Pecoraro et al (2018) from the scientific literature available without taking into account scientific observation systems (for example the OMIV in France) or the monitoring systems that do not address the issue of response capability. Half of these early warning systems were deployed following a catastrophic event induced by intense rain. At the local level, it is now commonplace to use multi-parameter monitoring systems to track all the physical interactions likely to precede and trigger the feared phenomenon. For regional scale we can also see that the different cases greatly vary in terms of the size of the zones they cover: the systems can cover a region (12 systems), a large metropolis (6 systems) or an entire country (5 national systems). The approach taken is then mainly based on weather monitoring and consists in estimating the probability of occurrence of landslides.

---

<sup>1</sup> COCCIA Stella, Ineris, Nancy, France (54042), [stella.coccia@ineris.fr](mailto:stella.coccia@ineris.fr)

### 3 THE FOUR EXEMPLARY EARLY WANING SYSTEMS

In order to illustrate the conditions and frameworks in which these different systems operate, this article focuses on four exemplary systems: the Ruines de Séchilienne in France and the Ancona landslide in Italy at the local scale, and Norway and Hong Kong systems at the regional scale. Their main components: thresholds, warning level, decisional and organisational algorithm are synthetized in the table 1. In practice, we note that the number of thresholds and warning levels elements greatly varies from one system to another. The decisional and organisational algorithms are thus specific to each system. They can vary in complexity depending on the scale covered by the system and stakes at play. Concerning communication and warning, a great variety of practices can be observed in the local-scale systems. For most of them, warning is almost immediately launched to the affected populations, while in other cases, experts or entities responsible for managing the site (such as the Prefect, or the Mayor in France) receive the information first, and then decide whether to warn or not. Therefore, warning can sometimes be delayed by the time it takes for the experts to verify the facts and dispel any doubts, and, if needed, it can be issued later. In these examples, the warning alerts are almost always issued as the result of a human decision made by an expert or a non-expert decision maker, such as the Prefect in France, for example.

**Table 1: main information about the life and the components of the four exemplary early warning systems**

Layout	Séchilienne (France)	Ancona (Italy)	Hong Kong	Norway
<b>Works from to</b>	1985-now	2009-now	1970-now	2013-now
<b>Number of Thresholds</b>	4	5	2	4
<b>Number of Warning levels</b>	2	5	2	4
<b>Decisional and organisational algorithm</b>	YES	YES	YES	YES
<b>Communication and warning</b>	-	YES	YES	YES
<b>Response capability</b>	-	YES	YES	-

They have developed progressively over the last few decades in line with climate change and the growing urbanisation of at-risk areas. Although they were originally hazard-centered, these systems are increasingly focusing on the affected populations since many now consider response capability to be the key to effective functioning. Unfortunately, the response capability is often little addressed in the scientific literature and in operational feedback.

### CONCLUSION

It is now accepted that these systems have led to a significant decrease in the number of victims of ground movements. We see that there are no completely automated systems; human appraisal is always a fundamental factor in ensuring the effective functioning of these systems. Sometimes, local and regional systems coexist in the same area (like in Italy), which can lead to difficulties in the absence of an overall coordination framework. Synergy between the warning systems is overall poorly developed.

Finally, the lack of effort to disseminate and share knowledge in this domain is regrettable. The experts and the management and warning centres often lack funding and support to widely promote their work to their peers. This explains, for example, the omission of the Séchilienne early warning system in the international review of local systems.

### REFERENCES

- Coccia, S. and Klein E. (2020). Retour d'expérience sur les dispositifs d'alerte appliqués aux instabilités de pente. JNGG (Journées Nationales de Géotechniques et de Géologie de l'Ingénieur), Lyon, 2020.
- Pecoraro, G., Calvello, M., Piciullo, L. (2018). Monitoring strategies for local landslide early warning systems. *Landslides*, DOI 10.1007/s10346-018-1068-z.
- Piciullo, L., Cepeda, J., Calvello, M. (2018). Territorial early warning systems for weather-induced landslides. *Earth science reviews* 179 (2018) 228-247.
- UNISDR (2009). ISDR: Terminology [online]. <http://www.unisdr.org/eng/library/lib-terminology-eng%20home.htm> [Accessed:15 September 2010] US Army Corps of Engineers, 2003.
- Thiebes, B. and Glade, T. (2016). Landslide early warning systems – fundamental concepts and innovative application, in: *Landslides and Engineered Slopes: Experience, Theory and Practice*, edited by: Aversa, S., Cascini, L., Picarelli, L., and Scavia, C., *Proceedings of the 12th International Symposium on Landslides*, Napoli, Italy, 12–19 June 2016, CRC Press, 1903–1911.

## Harmonisation des méthodes de calcul et de justification des soutènements des talus instables – Etude du cas de la route entre Marrakech et Ouarzazate

Imane JABRI<sup>1</sup>, Hicham CHERIFI<sup>1</sup>, Abdessamad JALOUNI<sup>1</sup>, Abdel-Ali CHAOUNI<sup>1</sup>

<sup>1</sup>: Intelligent Systems, Georesources and Renewable Energies Laboratory, Faculty of Sciences and Techniques, Fez, Sidi Mohamed Ben Abdellah University – Morocco.

✉ : [imane.jabri@usmba.ac.ma](mailto:imane.jabri@usmba.ac.ma)  
[i.jabri@mtpnet.gov.ma](mailto:i.jabri@mtpnet.gov.ma)  
[jabri.imane@gmail.com](mailto:jabri.imane@gmail.com)

☎ +212672362073

**Keywords:** Talren, norme, Bishop, éléments finis, soutènement, Talus

### RESUME EN FRANÇAIS:

La présente communication vise à analyser les résultats de l'étude d'aménagement des instabilités de talus entre Taddart et le col de Tichka, faisant partie de l'aménagement de la route nationale n°9 (RN9) reliant les villes de Marrakech et Ouarzazate dans le cadre de la mission type G5 au sens de la norme NF P 94-500 révisée en 2013 et suivant la méthode Bishop (Calcul avec le Logiciel Talren V5). Laquelle étude a été lancée par la Direction Générale des Routes et du Transport Terrestre relevant du Ministère de l'Équipement, du Transport, de la Logistique et de l'Eau du Maroc. Ensuite, un calcul sera mené suivant la méthode des éléments finis. L'objectif étant de comparer les paramètres issus des deux méthodes de calcul et servant au dimensionnement des ouvrages de soutènement des talus instables.

### ABSTRACT IN ENGLISH:

The present communication aims to analyse the results of the slope instabilities developed between Taddart and Tichka, belonging the national road 9, whose connect the cities of Marrakech and Ouarzazate in adequation with the G5 mission as specified in NF P 94-500. The adopted approche consist on comparing three parameters (Bishop method and finite element). Wich study was initiated by the General Directorate of Roads and Transport within Moroccan Ministry of Equipment and Transport. The objectives are being to compare the out-puts derived from both calculation methods and constitutive models, used for the supporting structures dimension for unstable slopes. In the second hand, propose a harmonization guide lines to better choose models and the necessity to adapt a similar Moroccan standars aiming to orient geotechnical desingners.

### 1. PRESENTATION DES ZONES À L'ÉTUDE:

Les 5 zones étudiées sont situées sur le versant Nord du Haut Atlas, approximativement entre 1900 et 2000 m d'altitude NGM (Nivellement Général du Maroc). La route d'origine a été construite entre les années 1920 et 1930. Elle a fait dernièrement l'objet de travaux d'amélioration du niveau de service, y compris le 1er tronçon qui comprend les zones à l'étude. Sur ce tronçon, les travaux d'aménagement comprennent la création d'une troisième voie pour les poids lourds, et ont été réalisés entre septembre 2014 et février 2017, avant la réalisation de la présente étude d'aménagement des instabilités. Ces instabilités analysées sont donc postérieures aux travaux d'aménagements, et donc à la mise en service de ce tronçon, ce qui représente un risqué évident pour la circulation.



**Figure 1 : Photos des instabilités des talus dans les 5 sites à l'étude.**

## 2. CONTEXTE GÉOLOGIQUE

Le site étudié se développe dans des formations métamorphiques de l'Ordovicien fortement tectonisées, dont les composants principaux sont les schistes avec passages gréseux.

## 3. RECONNAISSANCES ET DIAGNOSTICS

Les différentes zones ont fait l'objet de reconnaissances naturalistes, recensant:

- Les limites de la zone instable;
- Les levés structuraux;
- Le mécanisme qui gère l'instabilité.

## 4. APPROCHE D'HARMONISATION ET DE COMPARAISON

L'approche consiste à établir un comparatif technico-économique (Analyse des facteurs de sécurité, des déplacements et des contraintes) selon les out-put obtenus, éventuellement des trois méthodes suivantes:

- méthode des équilibres limites (méthode de Bishop) basée sur le critère Mohr-Coulomb;
- méthode des éléments finis basée sur l'approche de réduction de la contrainte de cisaillement et sur le critère de Mohr-Coulomb;
- méthode des éléments finis basée sur l'approche de réduction de la contrainte de cisaillement et sur le modèle JRM;

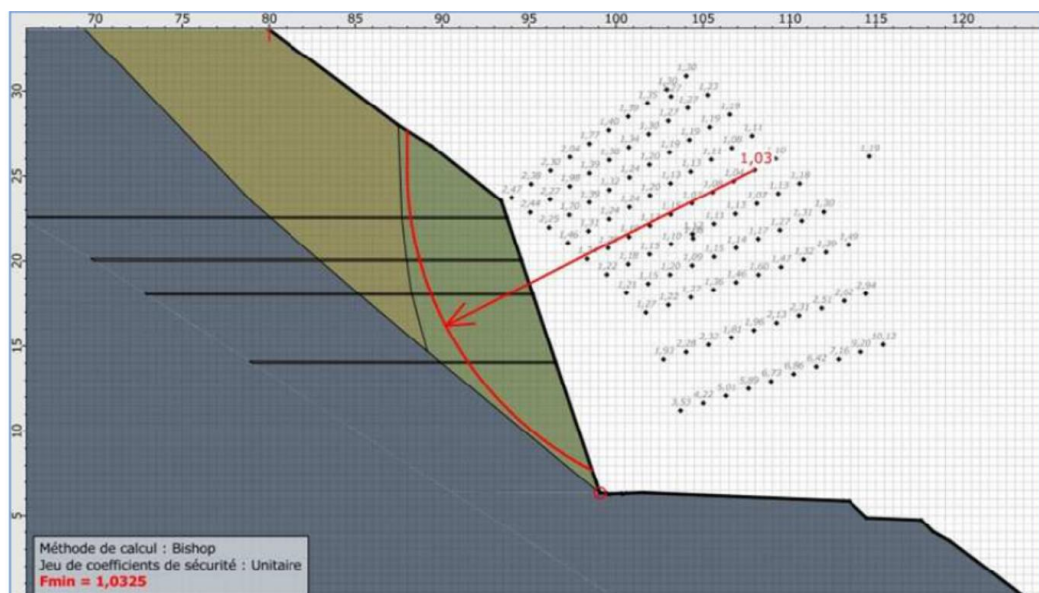


**Figure 2 : Résultats de calcul avec Talren**

## 5. CONCLUSION

Ce travail met en évidence la déficience de la méthode de Bishop dans ce cas de figure qui est particulièrement intéressant en comparaison à la méthode des éléments finis, mais aussi par rapport au modèle de comportement du sol choisi en fonction de la géologie. Ce qui est dû aux lacunes dans le paramétrage qui ne permet pas de paramétrer l'anisotropie des schistes. En effet, les résultats trouvés permettent d'identifier des écarts-types supérieurs à 11% entre les trois approches sur les 5 zones étudiées. Il est à noter que l'approche des éléments finis est plus pessimiste surtout dans le cas de la modélisation via JRM, modèle plus complet par rapport aux autres, d'ailleurs, les résultats des inclinomètres observés pendant 2 ans permettent de confirmer la précision de ce modèle (en comparant les déplacements prévus et ceux observés). Il serait donc judicieux de chercher à harmoniser les pratiques de justification des ouvrages suivant les paramètres disponibles, à l'instar des Eurocodes.

## REFERENCES

- Matsui & San 1992, Dawson et al. 1999;
- Aménagement de la RN 9 reliant Marrakech et Ouarzazate - PROJET D'EXECUTION DES TALUS ENTRE TADDART2 ET LE COL de TICHKA – DIRECTION DES ROUTES-TERRASOL-SETEC (2018)
- Etude géotechnique et expertise des instabilités de terrain sur la RN9 Section Taddart2 – Col de Tichka Province de Ouarzazate – LABORATOIRE PUBLIC D'ESSAIS ET D'ETUDES (2017)
- Expertise des instabilités de talus entre Taddart2 et le col de Tichka – TERRASSOL (2017)

# Quantitative rockfall risk analysis for railway using 2D block propagation simulations

Manon FARVACQUE<sup>1</sup>, Franck BOURRIER<sup>2</sup>, Philomène FAVIER<sup>3</sup>, François CHIROUZE<sup>4</sup>

**Keywords:** Quantitative-Risk-Assessment, Rockfall hazard, Railway, PlatRock platform

Every year, rockfalls reach urbanized areas causing damage to structures and injuring people. In this context, a precise rockfall risk analysis has become essential for authorities and stakeholders. Given the importance of characterizing the risk in an objective and reproducible manner, this study proposes a quantitative risk analysis (QRA) on a linear network (linear section of the French National Railway Company) by accounting for the specificities of the rockfall process.

L'aléa chute de blocs est caractérisé par le détachement brutal d'une masse rocheuse, depuis une paroi (sub)verticale, qui se propage rapidement vers l'aval par rebonds successifs. Ces événements représentent un aléa majeur pour les infrastructures collectives et les habitations, et induisent fréquemment de graves accidents. Dans ce contexte, l'évaluation des risques par une approche de type quantitative (QRA) est devenue incontournable pour l'aménagement des territoires et le choix des mesures de mitigation. Cette contribution vise ainsi à renforcer les bases formelles du calcul du risque dans le domaine des chutes de blocs, et à démontrer sa faisabilité sur un linéaire ferroviaire de la Société nationale des chemins de fer français.

## 1 INTRODUCTION

Rockfall phenomenon is defined as a rock block detachment from a vertical or sub-vertical cliff, travelling down the slope by rapid motions. Some rockfalls have enough energy to reach urbanized areas, causing damages to structure or injuring people. The design and optimisation of both structural and non-structural protective countermeasures based on precise risk analysis is therefore a crucial issue for authorities and stakeholders in rockfall-prone areas.

Quantitative risk assessment (QRA) procedures have been demonstrated to be the most robust tool to quantify rockfall risk. In QRAs, rockfall risk for exposed elements is estimated by including in the analysis each component of risk: the hazard, the exposure and the vulnerability. Hazard integrates (i) the annual probability of occurrence and (ii) the spatial probability and intensity of impacts on structures evaluated through rockfall numerical models.

3D rockfall numerical models have been shown essential to improve risk analysis in spatially distributed situations. However, in practice, most of the existing hazard assessment methodologies estimate reach probability and intensity using 2D rockfall numerical modelling.

The aim of this study is to propose a robust method for quantifying rockfall risk and its consequences for vehicles circulating on railways using 2D rockfall simulations. To this aim, we used the multi-model software platform for the numerical simulation of rockfalls *Platrock*. Our procedure has been illustrated on a real case study, i.e. a linear section of the French National Railway Company.

## 2 STUDY SITE

Rockfall events affect transportation corridors in diverse ways (Mavrouli and Corominas, 2018). For the French National Railway Company, rockfall risk is defined as a probability to derail due to the crash of a moving vehicle on a rock deposited on the railway. In this study, rockfall risk due to such indirect impacts is quantified along a portion of the French National Railway Company, located in Southern France, west of Marseille, in the Bouches-du-Rhône department. This railway section, namely *Aragnols*, is dominated by a 100 m-high sub-vertical cliff made of fractured limestone. Archival records report rockfall events up to the railway and the numerous blocks recorded along the cliff confirm ongoing intense rockfall activity.

## 3 METHODOLOGY

Rockfall risk is generally defined as the combination of hazards with its consequences, expressed in terms of mean damage per year and estimated as:

---

<sup>1</sup> FARVACQUE Manon, Institute for Environmental Sciences, University of Geneva, Geneva, CH, [manon.farvacque@inrae.fr](mailto:manon.farvacque@inrae.fr)

<sup>2</sup> BOURRIER FRANCK, Université Grenoble Alpes, INRAE, UR ETNA, Grenoble, FR, [franck.bourrier@inrae.fr](mailto:franck.bourrier@inrae.fr)

<sup>3</sup> FAVIER Philomène, Université Grenoble Alpes, INRAE, UR ETNA, Grenoble, FR, [philomene.favier@inrae.fr](mailto:philomene.favier@inrae.fr)

<sup>4</sup> CHIROUZE François, SNCF RESEAU-DGII, La Plaine Saint-Denis, FR, [francois.chirouze@reseau.sncf.fr](mailto:francois.chirouze@reseau.sncf.fr)

$$\bar{R}_z = q(z) \times Z \times f \times \bar{d}_z , \quad (1)$$

where  $\bar{R}_z$  represents the expectations of the consequences (or a certain amount of damage) of hazard for the element at risk  $z$ , characterized by an exposure factor  $q(z)$  and a value  $Z$ .  $f$  is the frequency of potentially damageable events (in events/yr) and  $\bar{d}_z$  correspond to the mean damage on element at risk  $z$  evaluated all over the simulations.

Given the sub-vertical outcrops overhanging the railway along Aragnols site, the cliff was considered as a potential rockfall source if its slope angle exceeds a certain threshold (here 51°). On the basis of a digital elevation model (DEM) with 1m resolution, cliff units exceeding this threshold were mapped into a Geographical Information System (GIS) and converted to raster for subsequent trajectographic analyses.

The frequency of rockfall events was assessed from detailed field observations along a representative transect of the Aragnols site. We estimated that the reference period for rockfall events inventoried along this transect should reasonably not exceed 500 years and have been potentially released from a 0.018-hm<sup>2</sup> cliff section. Considering rock blocks > 0.1 m<sup>3</sup> (minimum volume for derailing a train), the rockfall frequency per surface unit,  $\lambda$ , was estimated at 0.56 events/yr/hm<sup>2</sup>.

Numerical propagations of rockfalls were performed for blocks ranging between 0.1 and 5 m<sup>3</sup>, conditional to rockfall volume distribution, using the 2D *shape* model of the platform Platrock. To this aim, we (i) estimated the site-specific rockfall volume distribution from an asymptotic model of the generalized Pareto distribution (GPD; Coles, 2001). For this purpose, 94 block volumes have been recorded along 5-km-long of the linear network in the Aragnols neighbourhood. Similarly, in order to perform numerical simulations, (ii) 2D topographic profiles were defined along the studied site based on simulations of rockfall propagation and runout areas performed through the Rock-EU-Mapping model (also available on the platform PlatRock). In that respect, 16 topographic profiles were extracted following steepest slope directions within preferential rockfall corridors. For each of these 2D profiles, 200 rockfall simulations were performed conditional to the rockfall volume distribution and for simulation parameters calibrated using the distribution of the arrested blocks inventoried along the representative transect. Each profile was also related to its corresponding release surface,  $S$ , estimated from both Rock-EU-Mapping and previous geomorphometric analyses (slope angle threshold), and then related to a rockfall frequency  $f$  as:  $S \times \lambda$ , with  $\lambda$  the rockfall frequency per surface unit and  $S$  the release surface overhanging the profile (in hm<sup>2</sup>).

The distribution of damages on  $z$ , which in this case study corresponds to the intersection between a profile and the railway, was thereafter evaluated as:

$$d_z(Sim) = \begin{cases} 1 & \text{if } Sim \cap z \\ 0 & \text{if } Sim \cap z = \{\emptyset\} \end{cases} , \quad (2)$$

where  $d_z(Sim)$  corresponds to the damage for the train in location  $z$  for rockfall simulation  $Sim$ . Assuming that a moving vehicle, regardless of the volume, inexorably derails after striking a rock deposited on the railway, the damage is thus strictly equal to 0 (no derailment, so that no damage) or 1 (derailment, so that total destruction of the vehicle).

Finally, considering that a moving vehicle has no chance to stop before crashing a block deposited on the railway,  $q(z)$  is equal to 1. The value  $Z$  of the train was not specified in the present study.

## 4 RESULTS

The methodology for risk calculation, as described above, was applied for the 200-m long of the Aragnols railway section. Our approach allows risk to be expressed as the mean annual rate of derailment due to a rockfall event deposited on the railway. Our results were also derived in terms of return period, in order to be compared with an acceptability threshold of 100 years. In details, rockfall return periods lower than this threshold were observed on 8 topographic profiles (50% of the 2D profiles identified along the site). The maximal risk value is estimated at 0.0315 derailment/yr, resulting in a rockfall return period of 32 years.

## 5 CONCLUSION

This study demonstrates the applicability of risk analysis in its quantitative form, and its potential for risk assessment. Our approach, based on 2D rockfall simulations, also shows that such an approach is not a limitation for proposing rockfall risk assessment in a rigorous and comprehensive way. Furthermore, “profile by profile” risk study allows a good assessment of the sections highly subjected to risk along the railway, and thus an optimized planning of protection measures.

**REFERENCES**

Coles, S. (2001). *An Introduction to Statistical Modeling of Extreme Values*. Springer Series in Statistics. Springer London, London. doi:10.1007/978-1-4471-3675-0.

Mavrouli, O., and Corominas, J. (2018). *Quantitative Rockfall Risk Assessment for Roadways and Railways, Landslide Dynamics: ISDR-ICL Landslide Interactive Teaching Tools*, Springer International Publishing, 509—519. doi: 10.1007/978-3-319-57777-730.

Volkwein, A., Schellenberg, K., Labiouse, V., Agliardi, F., Berger, F., Bourrier, F., Dorren, L. K. A., Gerber, W., and Jaboyedoff, M. (2011). Rockfall characterisation and structural protection – a review. *Natural Hazards and Earth System Science*, 11(9):2617–2651. doi: 10.5194/nhess-11-2617-2011.

## Seeking improvements to landslide operational management through case studies

Pauline CHOLLIER<sup>1</sup>, Julien BAROTH<sup>2</sup>, Lucas MEIGNAN<sup>3</sup>, Carine PEISSER<sup>4</sup>, Stéphane LAMBERT<sup>5</sup>

**Keywords:** risk management, uncertainties, case studies, cause effect analysis, landslide, flaws

### ABSTRACT IN ENGLISH:

This communication deals with the management of landslide-related remedial operations. It is based on the collection of data relative to five case studies, provided by departmental councils of the French Northern Alps. The data were analysed in the aim to identify the causes of the difficulties encountered by the stakeholders, in a context of dealing with different types of uncertainties. The aim of this study is to propose improvements to current practices in the management of such operations to be applied in the future.

### ABSTRACT IN FRENCH:

Cette communication porte sur la gestion des opérations de traitement des aléas naturels gravitaires. Elle s'appuie sur les données collectées auprès de quatre conseils départementaux et relatives à cinq cas d'étude. Les données collectées sont analysées dans le but d'identifier les causes des difficultés rencontrées par les gestionnaires de ces sites, dans un contexte de gestion de l'incertitude. L'objectif de l'étude est, dans une phase ultérieure, de proposer des pistes d'amélioration des processus de gestion de telles opérations.

## 1 CONTEXT AND OBJECTIVES

When a slope failure, a rockfall or a debris flow endanger or reach an element at risk such as people, roads, railways or buildings, stakeholders and authorities commit to a process aimed at restoring a satisfactory level of safety. Nevertheless, the good execution of the operational risk management is often disrupted, leading to delays and extra-costs sometimes not affordable. Indeed, as the operational management of landslides combines technical, human, financial and organisational facets, the process efficiency may be altered due to different types of uncertainties such as the un-anticipated evolution of the hazard, an incomplete or late information transmission, a delayed decision making, constraints associated with the environmental conditions, inefficiency of specifically taken countermeasures or uncertainties associated with the collected data describing the hazard.

Upon suggestion from a public service in charge of roads at the department scale, the authors have initiated a research work aiming at improving the operational management of landslides. By contrast with most of the available literature dealing with the improvement of landslide hazards management (Tacnet, 2009; Hantz, 2012), this study starts from a detailed analysis of the practices and flaws based on several cases studies. The data collection and the analysis related to these case studies compose the first step in this work, conducted in the framework of I-RISK.

It constitutes the background of this communication.

## 2 CONSIDERED CASE STUDIES AND METHOD

The five case studies were selected in order to offer a certain variety, considering various criteria, based on case proposals from the four departmental councils of the northern Alps associated with this study (Hautes-Alpes, Isère, Savoie et Haute Savoie). The case studies were selected in relation with methodological specificities of the four departments. One case concerns a rockfall, the four others relate to slope failures, involving different sliding masses. One of the hazards is currently under control while others still evolve. The elements at risk mainly consist of roads with different traffic volumes, and buildings (for one case). The existence of specific constraints impacting the risk management was also a criterion (time, budget, number of actors).

Data were collected from all existing information supports (reports, maps, messages) in addition to interviews with people involved in the considered case management. First, the operation was described along a detailed chronological frame, showing the observations made, the actions taken and decisions made by the different actors.

Second, each case study was analysed in terms of causes and effects (CE) through an Ishikawa diagram (Coccia, 2018). This type of diagram is a representation of the factors that might contribute to flaws in the management. Its main branches were defined as the six main areas of the operational risk management which could be sources of flaws:

---

<sup>1</sup> CHOLLIER Pauline, Insa Lyon, Villeurbanne, France, paulinechollier@orange.fr

<sup>2</sup> BAROTH Julien, Univ. Grenoble Alpes, CNRS, Grenoble INP, 3SR, F-38000, Grenoble, France, julien.baroth@univ-grenoble-alpes.fr

<sup>3</sup> MEIGNAN Lucas, Géolithe, Crolles, France, lucas.meignan@geolithe.com

<sup>4</sup> PEISSER Carine, PARN, Grenoble, France, carine.peisser@univ-grenoble-alpes.fr

<sup>5</sup> LAMBERT Stéphane, INRAE, Grenoble, France, stephane.lambert@inrae.fr

decision making, human resources, information management, elements at risk and risk evaluations, operation-related hazard and, last, regulatory, financial and political contexts. The CE diagram highlights the interrelationships among the possible causal factors and the root causes.

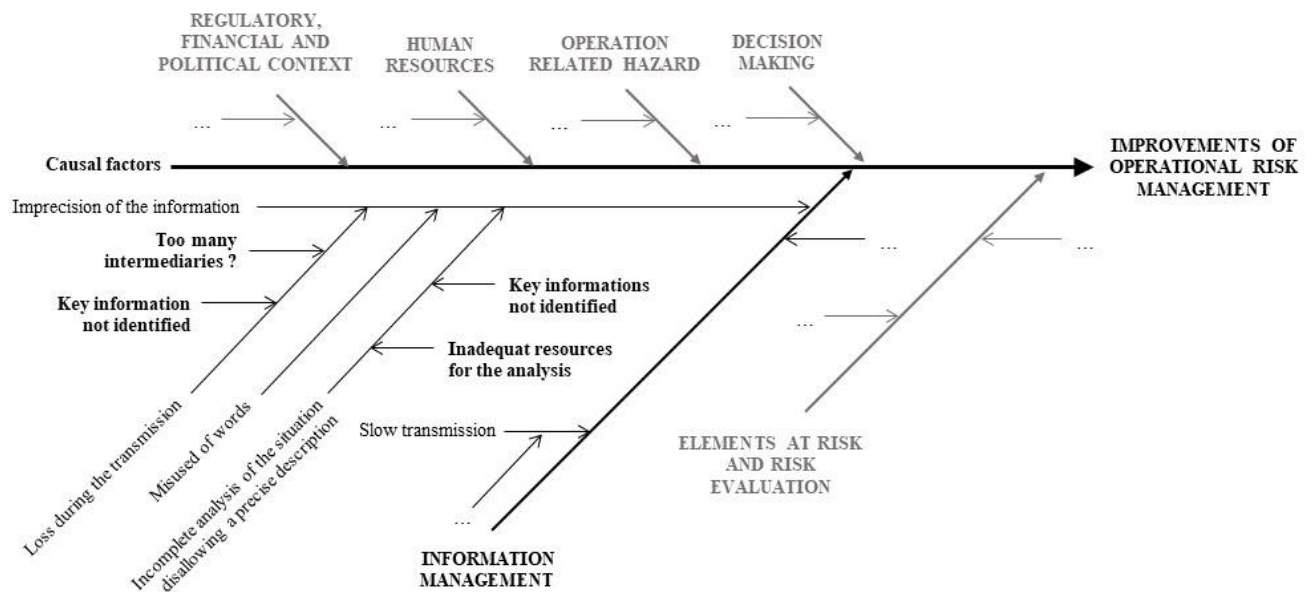


Figure 1: Ishikawa diagram relative to operational landslide risk management – focus on the ‘Information management’ branch

### 3 MAIN RESULTS

The analysis of the five case studies evidenced several root causes of different natures. Some of them are related to technical uncertainties as the hazard qualification or its evolution. Others are linked to human factors such as a deviation from the normal procedure associated to a lack of awareness of an actor (technician, design engineer, decision maker...). The financial, political or regulatory context can also be source of uncertainty. Figure 1 shows the proposed general structure of a cause-effect diagram relative to operational landslide risk management. The information management branch is partly detailed showing the different possible causes of an imprecise information. For example, this could be due to the loss of a piece of information during the transmission. The reasons of this loss can be a lack of identification as a key information or too many intermediates in the transmission process. These last two factors are thus root causes which constitute possible ways of optimisation.

### CONCLUSION

The data collection and analysis allowed a clear and detailed presentation of the successive steps of the operational management of the five case studies, as well as of the interactions between the different actors. The analysis has highlighted various critical points, with influence on the process efficiency, constituting possible ways of improvement. A deeper analysis will be conducted in view of selecting the points to be considered in priority in the next stages of this study, in order to propose tools or methods improving the management of landslides.

### ACKNOWLEDGEMENT

This work is supported by the French National Research Agency in the frameworks of the investissements d’Avenir program (ANR-15-IDEX-02) and of I-RISK supported by Auvergne-Rhône-Alpes Region. The authors would like to thank J.M. Tacnet for his help analysing the collected data.

### REFERENCES

- Coccia, M. (2018) The fishbone diagram to identify, systematize and analyse the sources of general purpose technologies. *Journal of Social and Administrative Sciences*, vol. 4, n. 4, pp. 291-303.
- Hantz, D. (2012) Gestion de l’incertitude et de l’ignorance, dans l’évaluation de la probabilité de déclenchement des éboulements rocheux. *Fiabilité des matériaux et des structures 2012*. Chambéry, France.
- Tacnet, J.-M. (2009) Prise en compte de l’incertitude dans l’expertise des risques naturels en montagne par analyse multicritères et fusion d’information. *Thèse de doctorat en sciences et génie de l’environnement*. Ecole Nationale Supérieure des Mines de Saint-Etienne, France.

# Protection structures

## 5 MJ energy impact test on a slender reinforced soil embankment

Oltion KORINI (corresponding author)<sup>1</sup>, Yassine B. BRAOULI<sup>2</sup>,  
Marion BOST<sup>3</sup>, Patrick JOFFRIN<sup>4</sup>

**Keywords:** rockfall protection, reinforced soil embankment, geosynthetics, horizontal impact

### ABSTRACT IN ENGLISH:

Rockfall hazard in mountainous areas is mitigated using different types of protective structures. Reinforced soil embankments are often preferred over other types of protections due to their lower maintenance requirements. In this study, a slender soil embankment reinforced with Terre Armée technology and vertical faces was built and subjected to a horizontal impact with an energy of 5 MJ. Two systems of reinforcements were installed in the embankment, one for the static stability of the embankment and the other for distributing the effect of the impact in the longitudinal direction. The embankment successfully stopped the impacting block and proved to be an efficient rockfall protection for the considered test conditions. The rapid cameras showed that the embankment was structurally flexible, which is due to the mobilization of the reinforcements even outside the impact position.

### ABSTRACT IN FRENCH:

L'aléa chute de blocs dans les zones montagneuses peut être atténué par différents types de protections. Les merlons en sol renforcé sont souvent préférés aux autres types de protections en raison de leurs besoins en entretien moins importants. Dans cette étude, un merlon en sol renforcé avec la technologie Terre Armée et à parements verticaux a été conçu et soumis à un impact horizontal d'une énergie de 5 MJ. Deux systèmes de renforcements ont été installés dans le merlon, l'un pour la stabilité statique du merlon et l'autre pour répartir l'effet de l'impact dans la direction longitudinale. Le merlon a réussi à arrêter le bloc impactant et s'est avéré être une protection efficace contre les chutes de blocs dans les conditions d'essai considérées. Les caméras rapides ont montré que le merlon était structurellement flexible, ce qui est dû à la mobilisation des renforcements même au-delà de la position d'impact.

## 1 BACKGROUND AND OBJECTIVE

In order to analyse the behavior and performance of reinforced soil embankments subjected to impacts, several experimental studies have been performed (Maegawa et al., 2011; Peila et al., 2007; Yoshida, 1999). Nevertheless, the behaviour of the soil and the reinforcements in dynamic impact conditions remains an open issue.

The construction of the typical trapezoidal reinforced soil embankments in rock slopes is sometimes a difficult task, because their important foundation width requires a significant amount of excavation. The objective of this study is to test the impact resistance of an innovative reinforced soil embankment with vertical facings, which has a reduced foundation width and a higher slenderness compared to the other conventional embankments. The increased flexibility that results from this choice is compensated by the installation of high strength geogrids.

## 2 IMPACT TEST

### 2.1 Design and test conditions

The reinforced soil embankment in this test had a width of 3.3 m, a height of 5.85 m and a length of 15 m. The vertical facings consisted of welded steel mesh panels that were held in position by geosynthetic strips installed in the embankment. In addition, uniaxial geogrid reinforcements (200 kN/m) were placed longitudinally close to the front and back faces for improving the impact resistance of the embankment. The embankment was subjected to a horizontal impact from a 12 400 kg concrete block with a diameter of 1.9 m that travelled at 28.5 m/s when it hit the embankment. This means that the block reached a kinetic energy of about 5 MJ, which is among the highest ones used in the literature for similar structures.

### 2.2 Results

---

<sup>1</sup> KORINI Oltion, Terre Armée, Rueil-Malmaison, France (92500), oltion.korini@terre-armee.com

<sup>2</sup> B. BRAOULI Yassine, Terre Armée, Rueil-Malmaison, France (92500), yassine.bennani@terre-armee.com

<sup>3</sup> BOST Marion, Université Gustave Eiffel, Bron, France (69500), marion.bost@univ-eiffel.fr

<sup>4</sup> JOFFRIN Patrick, Université Gustave Eiffel, Bron, France (69500), patrick.joffrin@univ-eiffel.fr

The embankment resisted the impact by experiencing mainly localized deformation at the impact position (Figure 1a) and an important back extrusion (Figure 1b). The rapid cameras revealed that during the impact, the embankment underwent four phases of deformation: 1) pure block penetration, 2) block penetration plus longitudinal bending, 3) backwards leaning and 4) slight return towards the initial position. The block practically stopped moving with respect to the embankment at the end of the second phase (Figure 2b). In general, the first deformation mechanism governed the response of the embankment. The maximal displacements reached 2.1 m at the front and 1.4 m at the back of the embankment. The geostrip and geogrid reinforcements plus the steel mesh panels were able to prevent the failure of the embankment's downhill face (Figure 1a).



**Figure 1: Deformed shape of the embankment after the impact: a) downhill face; b) uphill face**

The impacting block acceleration measured by a 3D accelerometer showed a peak of 62 g (Figure 2a), which corresponds to a peak dynamic force of 7 542 kN. At the end of the first phase, the block had lost about 75 % of its initial speed and about 94 % of its initial kinetic energy, but it continued to advance during phase 2 and 3 together with the embankment that started to deform structurally. The structural bending deformations that took place after phase 1 affected the whole length of the embankment, which implies that if the embankment was longer, these deformations would be less important.

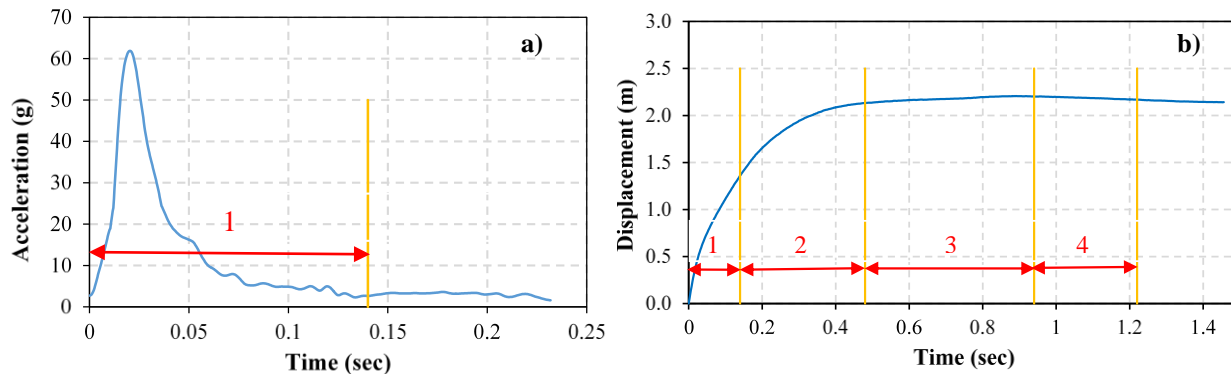


**Figure 2: Impacting block a) acceleration and b) displacement during the phases of the embankment's deformation**

## CONCLUSION

The tested embankment was able to resist a high energy impact despite its relatively low foundation width. Its higher slenderness compared to trapezoidal embankments contributed to a complex response, which consists of a combination of local shearing at the impact position and overall structural bending. The length of this type of embankment is important for its structural behavior because it alters the longitudinal stiffness and also the embedment length of the installed geogrids.

## REFERENCES

- Maegawa, K., Tajima, T., Yokota, T., Tohda, M., (2011). Experiments on rockfall protection embankments with geogrids and cushions. *Int. J. Geomate* 1, 19–24.
- Peila, D., Oggeri, C., Castiglia, C. (2007). Ground reinforced embankments for rockfall protection: design and evaluation of full scale tests. *Landslides* 4, 255–265.
- Yoshida, H. (1999). Recent experimental studies on rockfall control in Japan, in: *Joint Japan-Swiss Scientific Seminar on Impact Load by Rock Falls and Design of Protection Structures*, Kanazawa, Japan.

## A new method for the design of rockfall fences by surrogate modelling

Loïc DUGELAS<sup>1</sup>, Franck BOURRIER<sup>2</sup>, Ignacio OLMEDO<sup>3</sup>, Philippe ROBIT<sup>4</sup>, François NICOT<sup>5</sup>

**Keywords:** rockfall, fences, design, surrogate model, DEM, polynomial chaos expansion, support vector machine

**Résumé en français:** Les métamodèles sont des outils mathématiques permettant de prédire une valeur de sortie d'un modèle numérique très rapidement. Après avoir été calibrés et validés à l'aide du modèle DEM d'un écran souple, ils sont ici utilisés pour analyser le comportement de cet ouvrage. Les métamodèles permettent d'étudier des milliers de configurations d'un ouvrage, et ainsi d'en déterminer les configurations optimales en fonction de paramètres d'entrée auparavant sélectionnés.

### 1 INTRODUCTION

In the context of natural hazard, there is need of protection structures to prevent damages on infrastructures and habitations. Rockfall flexible fences are efficient and cost-effective solutions but their complex behavior under impact is not well known. Numerical models are developed to improve this knowledge, but they are still limited in terms of computation duration to conduct parametric studies. Thus, surrogate models are used to explore the output parameters of these models, and to conduct parametric studies in a reduce computation time.

### 2 GENERAL METHODOLOGY

Using surrogate models is useful to realize quick parametric studies on one output variable. But these models need to be calibrated using simulation results obtained with a Discrete Elements Method (DEM) model of the barrier. Moreover, one surrogate model needs to be calibrated for one output variable (Figure 1).

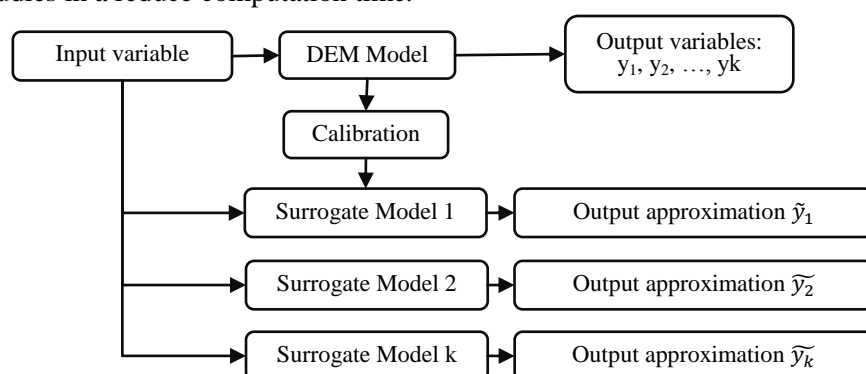


Figure 1 : Methodology used to approximate DEM model results with surrogate models

The method introduced in this study is organized in three steps: setting of the study, surrogate modelling calibration and validation, and exploration with the surrogate models.

### 3 SETTING OF THE STUDY

The studied barrier is the ELITE<sup>®</sup> 5000 kJ category A, developed by NGE Fondations (Dugelas, 2020). The maximum energy the barrier can handle in MEL test conditions is 5000 kJ. It is composed of 3 modules of 11,50m width and 7.00m height. The main characteristics and dimensions are reported Figure 2.

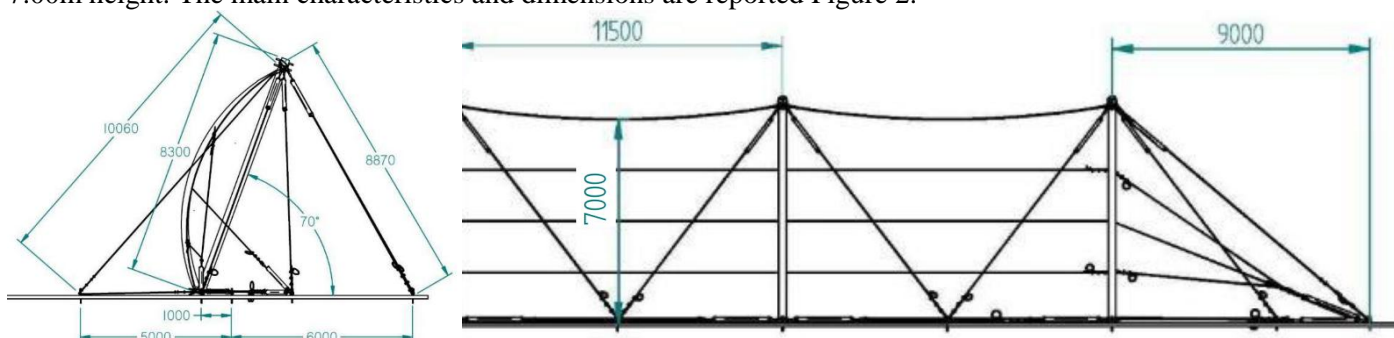


Figure 2 : View of the section and from above of the ELITE<sup>®</sup> 5000 kJ Cat. A barrier (dimensions in millimetres)

This barrier is equipped with 24 energy dissipating devices, divided in four groups according to the cable they are attached to: lower cables (LoC), middle cables (MiC), upstream cables (UpC), lateral cables (LaC). The threshold force of the energy dissipating devices is studied in a range from 50 kN to 200 kN, giving 4 input parameters (the threshold force is the same for all the devices of a group). Both binary parameters (bloc stopped...) and continuous parameters (forces, elongations) are selected for the output parameters.

<sup>1</sup> DUGELAS Loïc, NGE Fondations, Domène, France, ldugelas@ngefondations.fr

<sup>2</sup> BOURRIER Franck, INRAE, Saint-Martin-d'Hères, France, franck.bourrier@inrae.fr

<sup>3</sup> OLMEDO Ignacio, NGE Fondations, Domène, France, iolmedo@ngefondations.fr

<sup>4</sup> ROBIT Philippe, NGE Fondations, Domène, France, probit@ngefondations.fr

<sup>5</sup> NICOT François, INRAE, Saint-Martin-d'Hères, France, francois.nicot@inrae.fr

## 4 SURROAGATE MODELING

### 4.1 Method

Depending on the type of output, different surrogate modeling methods are used. Polynomial Chaos Expansion (PCE) (Blatman and Sudret, 2011; Zuniga and Ko, 2014) is used for the continuous outputs, and the Support Vector Machine (SVM) (Cortes and Vapnik, 1995; Meyer et al., 2017) is used for the binary outputs.

### 4.2 Validation

After calibration against the results obtained with the DEM model of the barrier, surrogate models are validated using a set of results unused for the calibration process. The maximum absolute error in percent (MAPE) between the results obtained with the surrogate model (line in Figure 3) and the DEM model (point in Figure 3) is calculated as a validation value.

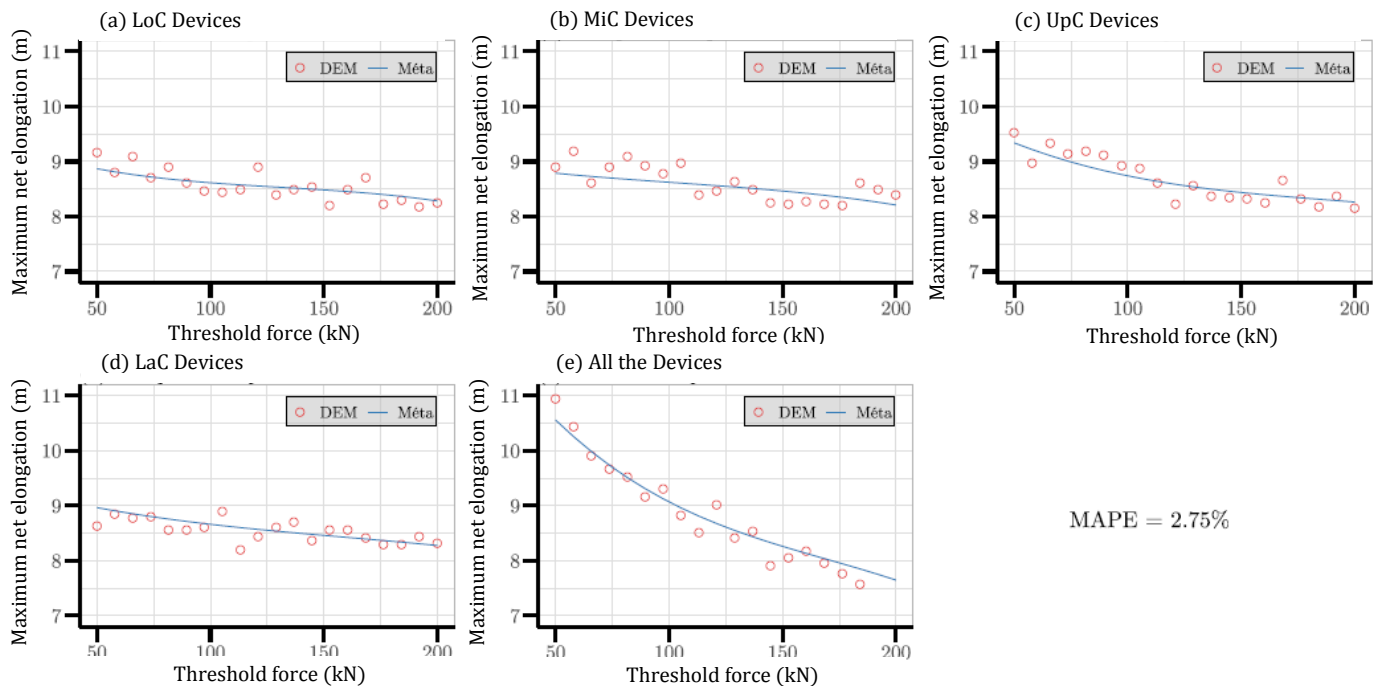


Figure 3 : Comparison between the predict results of the surrogate model (line) and the DEM model results (points) for the maximal elongation of the net

## 5 EXPLORATION

The surrogate models are then used to explore the behavior of the barrier, or as a design tool. Thousands of simulations are run in a short time giving a large overview of the barrier response function of the input parameters. The most prominent ones can be quickly identified with the Sobol' indices (Sobol, 2001) which indicates the sensitivity of an output variable for each input. Into the decision process, the surrogate models are also used to realize a quick selection of the tested configurations by applying limits to the output parameters (maximum force, maximum elongation). This is useful to select acceptable variation ranges for the input parameters.

## 6 CONCLUSION

Introducing surrogate model in the design process of a flexible barrier is a powerful way to explore thousands of configurations in the short time, while parametric studies with the DEM model are time consuming. The exploration with the surrogate models can be improved by the development of a goal function including the technical, normative, field of cost restrictions defined by designer.

## REFERENCES

- Blatman, G., Sudret, B., 2011. Adaptive Sparse Polynomial Chaos Expansion Based on Least Angle Regression. *J. Comput. Phys.* 230, 2345–2367.
- Cortes, C., Vapnik, V., 1995. Support-Vector Networks. *Mach. Learn.* 20, 273–297. <https://doi.org/10.1023/A:1022627411411>
- Dugelas, L., 2020. Stratégies probabilistes appliquées à la modélisation numérique discrète : le cas des filets pare-pierres (PhD Thesis).
- Meyer, D., Dimitriadou, E., Hornik, K., Weingessel, A., Leisch, F., 2017. e1071: Misc Functions of the Department of Statistics, Probability Theory Group (Formerly: E1071).
- Sobol, I.M., 2001. Global sensitivity indices for nonlinear mathematical models and their Monte Carlo estimates. *Math. Comput. Simul.* 55, 271–280. [https://doi.org/10.1016/S0378-4754\(00\)00270-6](https://doi.org/10.1016/S0378-4754(00)00270-6)
- Zuniga, M.M., Ko, J., 2014. GPC: Generalized Polynomial Chaos.

# An innovative Early Warning System for rockfall and debris flow protection structures

Alberto GRIMOD<sup>1</sup>

**Keywords:** rockfall, debris flow, monitoring system, impact, deformation

## ABSTRACT IN ENGLISH:

The abstract describes an innovative monitoring system (Early Warning System) developed to monitor rockfall and debris flow protections, usually installed in remote areas. This new type of device is compact and robust, and it is designed for the alert in rockfall mitigation protections such as rockfall, hybrid and debris flow barriers, simple and secured draperies mesh and nets. The system can be calibrated according to the type of structure and the client needs. It works by detecting the deformations of the net, mesh or barriers once they are impacted. The trigger level is related to a spring. It is possible to adjust it according to specific needs; the standard is 1200 kN.

## ABSTRACT IN FRENCH:

L'article présente un système innovant (Système d'Alerte Précoce) pour le monitoring des protections contre les chutes de blocs et les coulées de boue (débris flow), qui sont généralement installés dans des lieux inaccessibles. Ce dispositif est compact et résistant, et il a été conçu pour envoyer un signal d'alerte dans le cas d'un impact sur des écrans pare-blocs, des barrières debris flow, des grillages ou filets plaqués ou pendu simple, ou des ouvrages déflecteurs. Le système de monitoring peut être calibré en fonction du type d'ouvrage et du besoin du client. Il est en mesure d'envoyer un signal d'alerte en détectant la déformation du grillage/filet ou de la barrière impactée. Le niveau de déclenchement est lié à un ressort. Il est possible de l'ajuster en fonction des besoins (normalement le calibrage est à 1200 kN).

## 1 EARLY WARNING SYSTEM (EWS)

The Early Warning System developed Maccaferri and patented by NESA is an alert system for safeguarding lives, infrastructures and buildings protected by rockfall and/or debris flow mitigation structures, such as rockfall, debris flow and hybrid barriers and simple or secured nets.

The device is designed to operate in environment with high energy impacts and aggressive climatic conditions; moreover, there are not electric connection wires, and/or weak points of breaking.

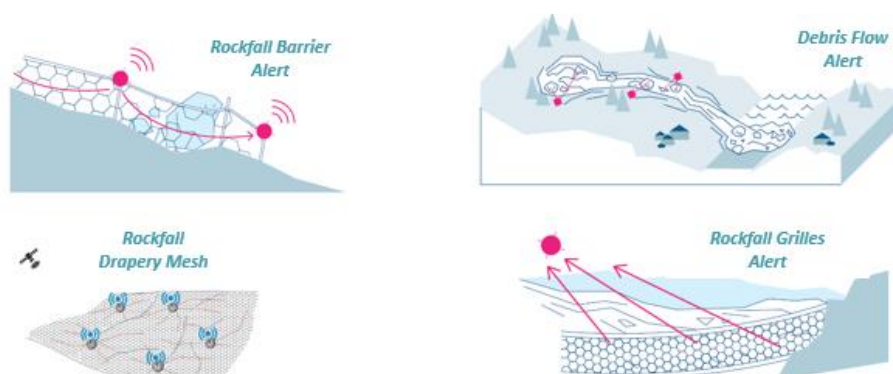


Figure 1: Fields of application

Compared to usual monitoring systems, the EWS present the following advantages:

- Immediate dissemination of essential information, such as alarms and status;
- Simple to install and manage (like a kit);
- Low maintenance required.

The device is installed directly on rockfall mitigation systems. It works by detecting the deformation occurred on the protection structure. It daily transmits the location and the status of the monitored structure. In this way, the final user, can quickly check (on his PC, tablet or smart phone) the location of the system (GPS coordinates) and if it has been impacted or not. There is not a big amount of data transmitted, its simplicity avoids data transmission issues.

<sup>1</sup> Alberto GRIMOD, France Maccaferri, Valence, FRANCE, a.grimod@maccaferri.com

It is tested against impacts (resists up to 16g of acceleration), it works between  $-40^{\circ}\text{C}$  and  $+60^{\circ}\text{C}$  and it is light (8 kg). Moreover, it has 8 batteries with an estimated lifespan of 5 years (each device daily communicates battery level too).

## 2 INSTALLATION ON CE MARKED ROCKFALL BARRIERS

The device can be calibrated to be installed on tested rockfall protection kits (ETAG 027 or EAD 340059-00-0106). The transmitting tool is installed directly on the post and it relates to 8 cables fixed on the interception structure. The cables properly designed according to the deformation parameter measured on full scale tests. By knowing the main deformation characteristics recorded during the full-scale tests (MEL and/or SEL), users can choose to have an alert if the installed rockfall barrier is impacted with a serviceability energy level (SEL) or the maximum one (MEL). The system can be installed on all type of barrier, no matter the energy absorption, the height and the producer. The system can measure local deformations.

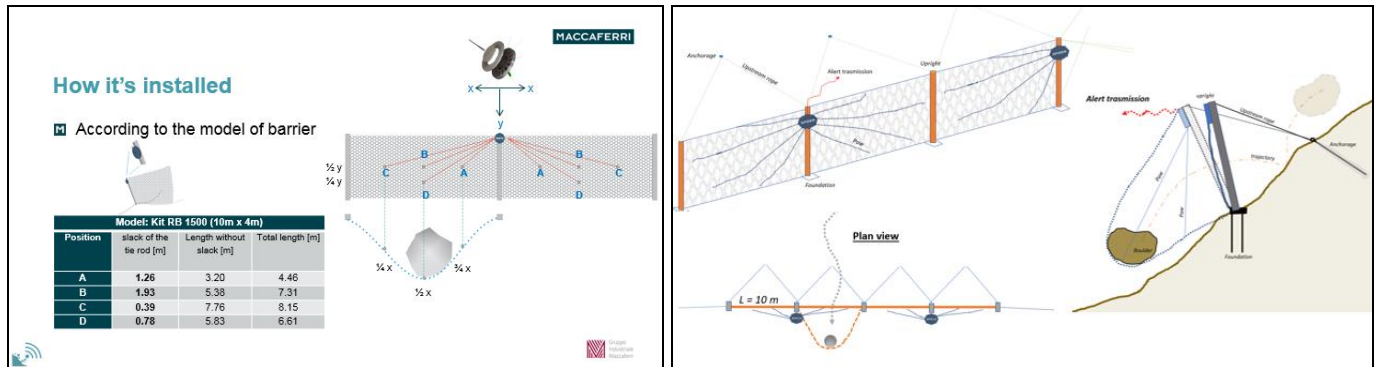


Figure 2: Example of an installation on a RB 1500 barrier

### 2.1 Real case study

The EWS device has been successfully installed on a rockfall barrier ETAG 027 tested and CE marked. The monitoring system was able to transmit an alarm when the barrier was impacted by the calibrated energy, that in this specific case was supposed to be lower than the SEL-1 level.

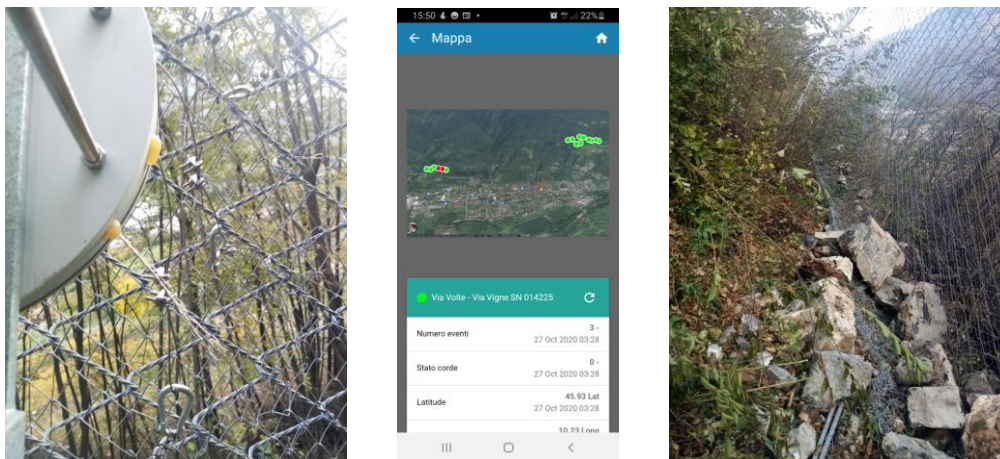


Figure 3: ETAG 027 barrier impacted – LEFT: EWS device installed on the post; CENTER: alert of the impacted barrier on the smart phone; RIGHT: rock boulders impacted against the barrier

## CONCLUSION

A new reliable device to monitor impacts against rockfall and debris flow protection system installed in remote areas. The internal GPS allows the system to identify the event location(s), also mapping the alarmed areas (land registry). Extremely simple to install (no skilled/trained workers required), it does not need any configurations and calibrations on site, and it can be installed on existing structures too. Maintenance and replacing are very quick and easy as well. The tool is an external device installed on the rockfall protection systems without affecting in any way the systems certifications. Moreover, a sophisticated electronic solution inside the device guarantees to the Early Warning System an autonomy of several years with an internal battery only, no auxiliary power supply systems are required.

## Assessment of the robustness of a numerical model of Bloc Armé® rockfall protection walls considering high energies impacts on real-scale structures

Agathe FURET<sup>1</sup>, Jean-Philippe JARRIN<sup>2</sup>, Stéphane LAMBERT<sup>3</sup>, Pascal VILLARD<sup>4</sup>

**Keywords:** numerical modelling, rockfall, protective structure, impact

### ABSTRACT IN ENGLISH:

With the aim of proposing a rockfall protection structure responding to new needs, Géolithe and Géolithe Innov have developed the Bloc Armé® technology to build modular structures optimized regarding footprint, time construction and reparability. In this purpose, a 3D numerical model of the structure was developed and revealed promising in terms of structure response prediction while providing insights into dominating energy dissipative mechanisms. This communication deals with the evaluation of the robustness of this modelled when simulating high energy impacts on real-scale *Bloc Armé* structures, based on the comparison with experimental results.

### ABSTRACT IN FRENCH:

Pour répondre aux nouveaux besoins de structure de protection contre les chutes de blocs rocheux, Géolithe et Géolithe Innov ont développé la technologie Bloc Armé®, permettant de construire des structures modulaires optimisées en termes d'emprise au sol, de temps de construction et de réparabilité. Un modèle numérique en 3D de la structure a montré une bonne capacité à reproduire le comportement de la structure et a permis de mieux appréhender la dissipation d'énergie en son sein. Cette communication s'intéresse à la robustesse du modèle numérique en considérant des impacts à haute énergie sur des structures à échelle réelle, et s'appuie sur la comparaison entre les déplacements du mur issus des simulations et ceux mesurés expérimentalement.

## 1 STRUCTURE AND MODEL DESCRIPTION

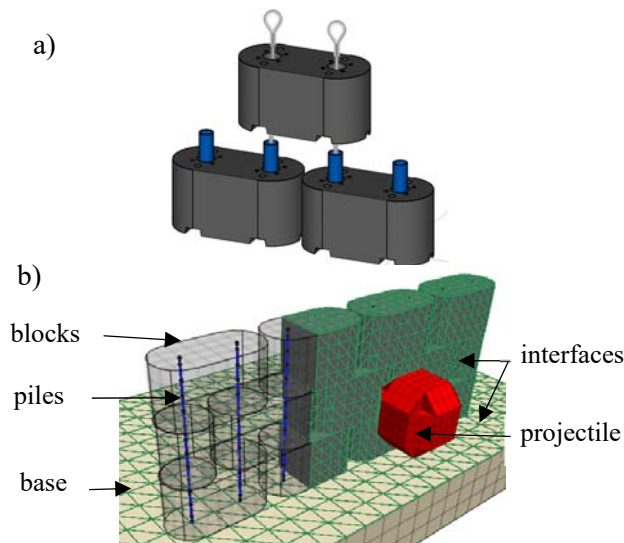


Figure 1: a) Real structure concept b) numerical model

The *Bloc Armé* technology consists of reinforced concrete blocks and a set of metallic reinforcement elements (Figure 1a) forming articulated, self-standing and heavy rockfall protection structures. Tubes and cables are introduced vertically through holes in the staggered blocks. Vertical cables are fixed at base and top of the wall to form a unified reinforcement mesh able to distribute the forces. Gaps between elements allow relative displacements between blocks and give to the wall a certain deformability.

The model (Figure 1b) was developed with *FLAC3D* (Itasca 2017). The concrete blocks are modelled by discrete blocks of continuum media stacked to form the wall, placed on a base. The Mohr-Coulomb constitutive model used for blocks elements allows to consider the energy dissipation by plasticization.

The metallic reinforcements (tubes and cables) are modelled thanks to “*piles*” elements existing in *FLAC3D*. These structural elements transmit forces from one block to the other, increasing the structure mass associated with the impact. The free space between the reinforcement elements and the blocks being a key parameter in the dynamic response of the wall, it is accounting for in the simulation via a specific reinforcement element-block interaction model: the reinforcement element is free to move before it is blocked when it equals the gap existing between elements. In addition, an authorized displacement of 5cm is introduced at top of the wall to consider the slack at top fixation of the cables. “*Interfaces*” are used to manage rigid and frictional contacts between the concrete blocks, the base and the projectile, allowing sliding, detachment and force transfers. The friction angle at the block/block and block/base interfaces have

<sup>1</sup> FURET Agathe, Géolithe, Crolles, France (FR), agathe.furet@geolithe.com

<sup>2</sup> JARRIN Jean-Philippe, Géolithe, Crolles, France (FR), jp.jarrin@geolithe.com

<sup>3</sup> LAMBERT Stéphane, Univ. Grenoble Alpes, INRAE, ETNA, Grenoble, stephane.lambert@inrae.fr

<sup>4</sup> VILLARD Pascal, Univ. Grenoble Alpes, 3SR, Grenoble, France (FR), pascal.villard@univ-grenoble-alpes.fr

been determined by static sliding tests and reduced by 25% for taking into account the dynamic nature of the solicitation. In accordance with Itasca's recommendation, the interfaces normal and tangential stiffness are given high values compared to equivalent stiffness of the neighboring zones, in order to limit the influence of the elastic strain of the interfaces.

## 2 IMPACT SIMULATIONS ON STRUCTURES

Previous simulations demonstrated the model's ability to reproduce the dynamic behavior of walls made of *Bloc Armé*. This work (Furet, 2020) was limited to small scales and to small size walls impacted at moderate energy (<125 kJ). Recent high energy impact tests, conducted on real scale walls, allow to verify the robustness of the numerical model.

Two impacts (500 kJ, mass:2,5t, velocity:20 m/s and 1000 kJ, mass:2,5t, velocity:28,4 m/s) are simulated in a realistic way, by throwing the projectile on the wall with an initial controlled velocity. The conditions are similar to experimental conditions regarding the projectile geometry, mass, velocity magnitude and pre-impact trajectory.

Very similar trends and values are observed between the simulations and the experiments (Figure 2a). These concerns the wall unfolding, the sliding of a significant length of the wall, the maximum displacement (Table 1) and kinematic. The displacement of the top of the wall shows that the model is efficient to replicate the dynamic behaviour, with a maximal displacement reached after 450 ms for a 500 kJ impact (Figure 2b). The main difference concerns the reversible displacement observed at top of the wall, which is partially attributed to the simplification concerning the modelling of tubes displacement in the blocks.

	500 kJ		1000 kJ	
	Exp	Num	Exp	Num
Maximal displacement (m)	0.90	0.96	1.40	1.25
Displaced length (m)	8	8	11	11

Table 1: Experimental and numerical result

The displacement of the top of the wall shows that the model is efficient to replicate the dynamic behaviour, with a maximal displacement reached after 450 ms for a 500 kJ impact (Figure 2b). The main difference concerns the reversible displacement observed at top of the wall, which is partially attributed to the simplification concerning the modelling of tubes displacement in the blocks.

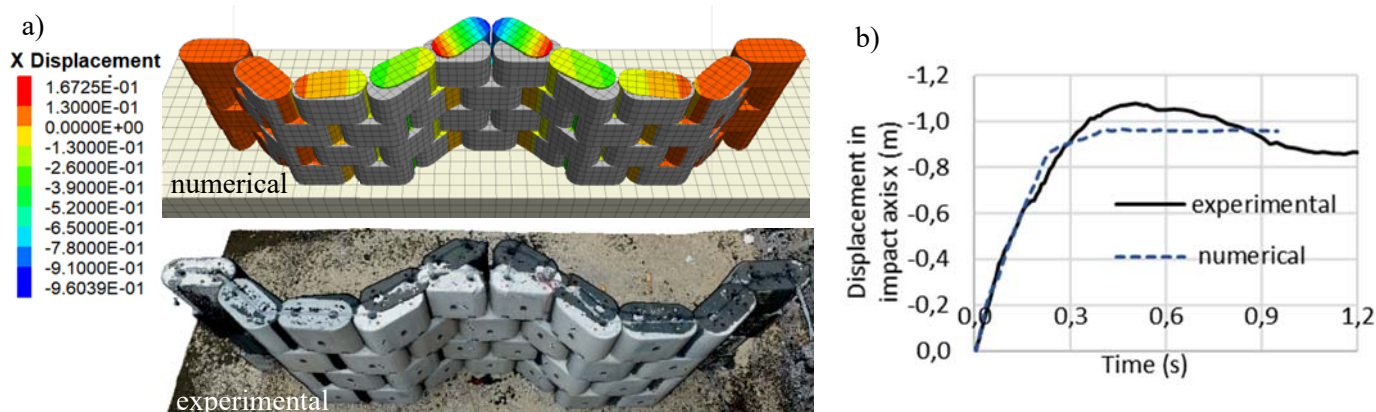


Figure 2: Experimental and numerical comparison for 500 kJ impact a) wall final deformation b) Displacement of the top of the wall

## CONCLUSION

The numerical model reveals efficient in reproducing displacement of real scale walls under high energy impacts. These results are promising in view of using the model as a design tool for rockfall protection structures. The numerical model represents an interesting tool to realize parametric studies aiming to identify the influent parameters. The numerical modelling of *Bloc Armé* walls coupled with gabions facing also impacted at high energy constitute an interesting perspective.

## AKNOWLEDGEMENTS

Authors thank the company Itasca for the IEP partnership they benefited from. The experiments were conducted as part of the Smart-Protect project financed by the Auvergne-Rhône-Alpes region.

## REFERENCES

- FLAC3D Fast Lagrangian Analysis of Continua in 3 Dimensions, Itasca Consulting Group, Inc. User's Guide, Version 3.1. (2017)
- Furet, A., 2020. Modélisations expérimentale et numérique d'ouvrages pare-blocs modulaires : application à la technologie Bloc Armé®. Université Grenoble Alpes.

## Bringing certified rockfall barriers to their realistic limits

Hélène HOFMANN (corresponding author)<sup>1</sup>, Manuel EICHER<sup>2</sup>, Andreas LANTER<sup>3</sup>, Andrin CAVIEZEL<sup>4</sup>

**Keywords:** rockfall barrier, field tests, eccentric testing, snow loads, additional safety

### ABSTRACT:

In the last 30 years, rockfall barriers made of steel wire nets have become established worldwide as a protective solution, are CE certified and the question inevitably arises as to the effect of natural impacts, i.e. impacts from boulders that strike the net at any point, possibly also rotating as they do so. In an Innosuisse-sponsored research project of the WSL Institute for Snow and Avalanche Research SLF together with the industry partner Geobruigg, various field tests are being carried out in the Swiss Alps since 2019, aiming at finding improvements to the capacity of a rockfall barrier outside of the certification standards.

### ABSTRACT :

Au cours des 30 dernières années, les écrans pare-pierres, constitués de filets en acier se sont imposées dans le monde entier comme solution de protection, sont certifiés CE et la question se pose inévitablement de l'effet d'impacts naturels, c'est à dire des impacts des blocs dans le filet en un point quelconque, voire même avec une certaine rotation. Dans le cadre d'un projet de recherche soutenu par Innosuisse, l'Institut pour l'étude de la neige et des avalanches SLF, en collaboration avec le partenaire industriel Geobruigg, divers essais sur le terrain sont menés dans les Alpes suisses depuis 2019, dans le but de trouver des améliorations de la capacité de ces écrans en dehors des normes de certification.

## 1 FROM FAR WEST ROCKFALL BARRIER TESTING TOWARDS GUIDELINES AND THEIR LIMITS

### 1.1 From the beginnings of rockfall testing towards guidelines and standardisation of testing

The first rockfall barrier tests were carried out as early as the end of the 1980s. At the very beginning, for example, wire rope nets were installed in a steel frame and dynamic punching resistance was determined by means of vertical shots in the middle of the net. Experiments were also carried out with rockfall barriers as a system, in which rocks were rolled down a slope into the barrier, hitting randomly a field of it (Duffy & Glover, 2017). Although these tests provided valuable fundamental insights into the performance of such systems, their significance was limited, since no repeatability was given and comparisons between the different protection systems was deemed difficult. The logical consequence was to develop a test method which allowed a real comparison of the different systems based on predefined controllable parameters. Therefore, the two approaches were combined at the end of the 1990s and a rockfall test method was developed. This is still the same approach today in European assessment procedure EAD-340059-00-0106, formerly ETAG 027 (EOTA, 2018). The maximum energy absorption capacity of these flexible barriers has multiplied during this time: from about 1,500 kJ in the mid-1990s to 10,000 kJ in 2018. With such high energies and in some cases higher structures, the question inevitably arises as to the effect of natural impacts, i.e. impacts from boulders that strike the net at any point, possibly also rotating as they do so

### 1.2 Limits of standardized tests

The knowledge about the remaining capacity of rockfall barriers in load cases outside the approval tests is completely different worldwide. In some countries specialized designers are aware of this fact and solve the problem by over-dimensioning the rockfall barriers to ensure the availability of residual capacity outside of the middle field. In other countries however, authorities and/or designers assume that a 1000kJ rockfall system absorbs this energy even in marginal areas or in eccentric hits. Protective solutions are consequently not designed properly. Today's test method, according to EAD-340059-00-0106, means that it is difficult to determine a cost-optimised solution for an adequate protective measure. This research project tries to assess the performance and residual capacity of rockfall barriers over time, after being impacted by various load cases, to improve current knowledge.

---

<sup>1</sup> HOFMANN Hélène, Geobruigg AG, Romanshorn, CH, helene.hofmann@geobruigg.com

<sup>2</sup> EICHER Manuel, Geobruigg AG, Romanshorn, CH

<sup>3</sup> LANTER Andreas, Geobruigg AG, Romanshorn, CH

<sup>4</sup> CAVIEZEL Andrin, SLF, Davos, CH

## 2 RESEARCH AND DEVELOPMENT TAKING ROCKFALL BARRIERS TO THE NEXT LEVEL

### 2.1 Additional tests to assess the effect non-standardized dynamic impacts

The Chant Sura site is situated close to the Flüelapass, in Grisons, in Switzerland. In May 2019 an Innosuisse project was granted for testing fully instrumented rockfall barriers, in natural terrain. Several field campaigns have been undertaken, in which rocks of different shapes and sizes are projected into the netting of the rockfall barrier and its structure (cables and posts). The barrier is equipped with sensors to measure the loading on different elements of the protection system. In addition, the test blocks (up to 3'200 kg) are also equipped with sensors that measure the rotation and the acceleration during the fall and on impact with the barrier. In combination with high resolution drone recordings and video recordings from different viewing angles, the trajectories and velocities of the individual blocks can be reconstructed in detail, enabling further insights into the interaction of all parameters (Sanchez & Caviezel, 2020).



Figure 1: a: rockfall impact on the ground after release; b: eccentric rockfall impact in the netting; c: inspection of the barrier after consecutive impacts

### 2.2 Long term test of barrier for additional load cases in wintertime

Finally, the barrier was left in place since construction and is enduring its second winter without maintenance. A field survey (snow depth and density, loads on cables, posts, etc) was undertaken in the winters 19/20 and 20/21. Currently we are waiting for Spring 2021 and hope to record wet snow slides for completeness.



Figure 2: a: barrier embedded in snow; b: detail on measuring equipment at post head such as rope forces; c: digital device monitoring the barrier's state

## CONCLUSION AND OUTLOOK

The partial evaluation of the data allows an understanding of the remaining capacity of a barrier. The goal is now to assess if additional tests can be carried out in addition to the standardized tests. These additional tests were already under consideration in the 1990s but were discarded, due to the poorer development of sensors and computer technology.

## REFERENCES

- Duffy, J.; Glover, J. (2017) A brief history of rockfall barrier testing. 6th Interdisciplinary Workshop on Rockfall Protection, Barcelona, Spain.
- EOTA (2018) EAD-340059-00-0106-2018 FALLING ROCK PROTECTION KITS, accessed at: [www.eota.eu/en-GB/content/new-eads-published/37/599/](http://www.eota.eu/en-GB/content/new-eads-published/37/599/).
- Sanchez, M.A.; Caviezel, A. (2020) Results of tests at Chant Sura: 13th September and 4th October 2019. WSL Ber. 97, 81 p.

# DEM Modelling of the ELITE rockfall flexible barrier: a new net model introducing sliding

Loïc DUGELAS<sup>1</sup>, Franck BOURRIER<sup>2</sup>, Ignacio OLMEDO<sup>3</sup>, Philippe ROBIT<sup>4</sup>, François NICOT<sup>5</sup>

**Keywords:** Discrete Element Method, rockfall barrier, impact, ELITE, Yade-DEM, sliding

**Résumé en français:** L'écran souple 5000 kJ développé par NGE Fondations est ici modélisé pour en étudier le comportement. Pour ce modèle d'ouvrage, un nouveau modèle de la nappe ELITE intégrant du glissement entre les câbles de la nappe a été développé. Les résultats de simulations d'impacts ont été vérifiés avec les résultats des essais expérimentaux, permettant de valider le modèle DEM de l'ouvrage. Ce modèle a permis d'explorer plus profondément le comportement de l'ouvrage, en particulier la répartition des efforts dans la nappe, ainsi que la distribution de l'énergie dans l'ouvrage au cours de l'impact.

## 1 INTRODUCTION

Natural hazard, and especially rockfall, is frequent in mountainous areas and there is a need of structures to protect infrastructures and habitations from damages. Rockfall flexible fences are one of them (Volkwein et al., 2019), with the advantage of being efficient and cost-effective solution. However, the knowledge of their behaviour under impact needs to be improved. In this purpose, a discrete element method (DEM) model of a flexible fence is developed, allowing a deep analysis of the behaviour of the structure in terms of forces, deformation, or energy. This model is the first to use a model of the ELITE net including sliding.

## 2 THE 5000 KJ ELITE FLEXIBLE BARRIER

The modelled structure is the ELITE 5000 kJ (category A) flexible barrier, developed by NGE Fondations. This barrier was already experimentally tested, and the full-scale tests results are used as assessment data for the model. This flexible barrier is made of 3 modules of 11.50 m width and 7.00 m height. The main geometrical characteristics are in Figure 1.

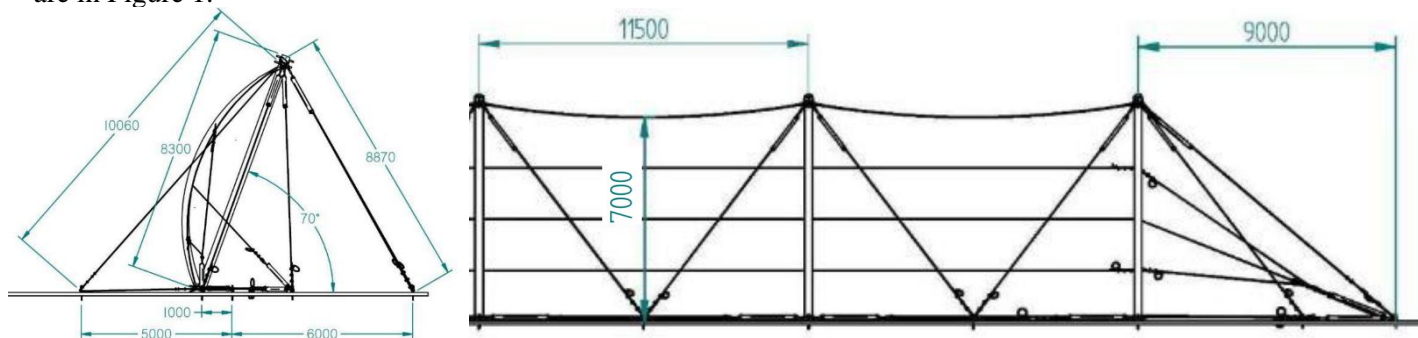


Figure 1 : View of the section and from above of the ELITE® 5000 kJ Cat. A barrier (dimensions in millimetres)

## 3 DISCRETE ELEMENT MODEL

The software Yade-Dem (Šmilauer and others, 2015) is used to model the structure under impact. Each element of the flexible barrier (net, energy dissipating device, poles...) are individually modelled and calibrated. Then, they are gathered to model the complete structure (Dugelas et al., 2019).

### 3.1 ELITE net model

The net is made of a woven cable maintained with rigid clips. Even if a model of this net was previously developed (Bertrand et al., 2012), it

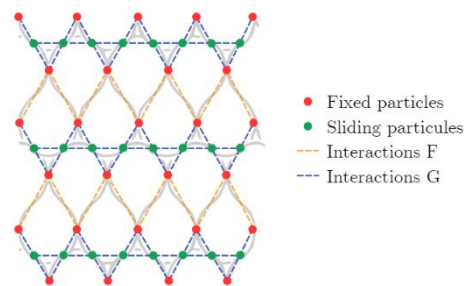


Figure 2 : Illustration of the ELITE net model

<sup>1</sup> DUGELAS Loïc, NGE Fondations, Saint-Priest, France, ldugelas@ngefondations.fr

<sup>2</sup> BOURRIER Franck, INRAE, Saint-Martin-d'Hères, France, franck.bourrier@inrae.fr

<sup>3</sup> OLMEDO Ignacio, NGE Fondations, Saint-Priest, France, iolmedo@ngefondations.fr

<sup>4</sup> ROBIT Philippe, NGE Fondations, Saint-Priest, France, probit@ngefondations.fr

<sup>5</sup> NICOT François, INRAE, Saint-Martin-d'Hères, France, francois.nicot@inrae.fr

has to be improved because of the sliding of the cables observed experimentally at the contact points without clip. A portion of cable between two clips is modelled by 4 particles: 2 at the extremities representing the clips (“fixed particles”), and 2 others representing the contact points with another cable (“sliding particles”). Two types of remote interactions are introduced between these particles to model the mechanical behaviour of the cable: one between two rigid particles (interaction F) and one between a sliding particle and another one (interaction G) (Figure 2).

### 3.2 Energy dissipating devices

The energy dissipating devices are the main element used to dissipate the impact energy. However, their behaviour may be difficult to model because of its variability regarding the solicitation velocity (Castanon-Jano et al., 2017). In this study, both quasi-static and dynamic tests are used to calibrate the energy dissipating devices model.

### 3.3 Complete structure

#### 3.3.1 Experimental validation

The complete structure is assembled, and an impact simulation corresponding to the full-scale experimental test is launched (2h duration). In this test, the structure is impacted by a 12390 kg mass boulder (1.90 m width) with a velocity of 28.41 m/s, giving an impact energy of 5000 kJ. The numerical and experimental results (forces, deflection, energy dissipating devices elongation) are then compared to validate the numerical model. (Figure 3).

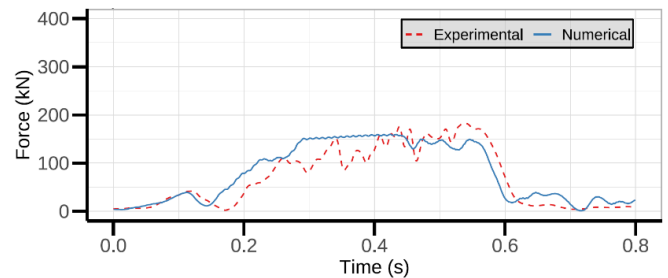


Figure 3 : Comparison of the numerical and experimental evolution of the force into an anchorage

#### 3.3.2 Numerical analysis

The numerical results are then used to explore the behaviour of the structure. Two main points are analysed: the energy repartition during the impact (kinetic, dissipated, stored), and the evolution of the force into the ELITE net (Figure 4).

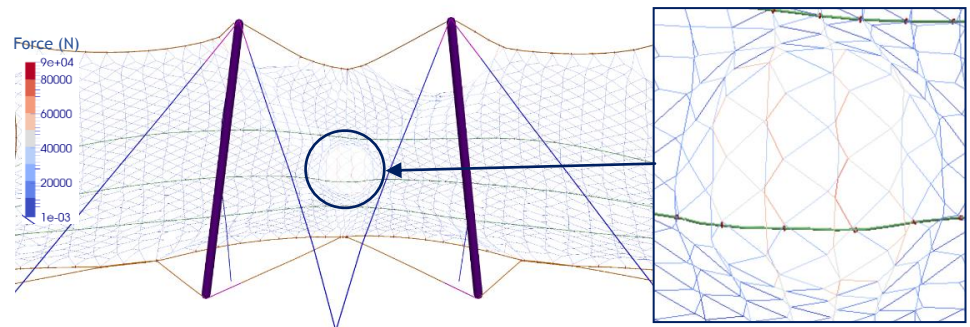


Figure 4 : Example of analysis of the force into the ELITE net

## CONCLUSION

In this study, the simulation of an impact on the ELITE 5000 kJ Category A. barrier was set-up and validated in comparison with the experimental data. This model was then used to make a deep analysis of the behaviour of the flexible barrier. Indeed, this model allows to explore the forces diffusion as well as the repartition of the energy into the structure. This model being now fully validated, it can be adapted to design new flexible barrier using the same components (energy dissipating device, ELITE net...).

## REFERENCES

- Bertrand, D., Trad, A., Limam, A., Silvani, C., 2012. Full-Scale Dynamic Analysis of an Innovative Rockfall Fence Under Impact Using the Discrete Element Method: from the Local Scale to the Structure Scale. *Rock Mech. Rock Eng.* 45, 885–900. <https://doi.org/10.1007/s00603-012-0222-5>
- Castanon-Jano, L., Blanco-Fernandez, E., Castro-Fresno, D., Ballester-Muñoz, F., 2017. Energy Dissipating Devices in Falling rRock Protection Barriers. *Rock Mech. Rock Eng.* 50, 603–619.
- Dugelas, L., Coulibaly, J.B., Bourrier, F., Lambert, S., Chanut, M.-A., Olmedo, I., Nicot, F., 2019. Assessment of the Predictive Capabilities of Discrete Element Models for Flexible Rockfall Barriers. *Int. J. Impact Eng.* <https://doi.org/10.1016/j.ijimpeng.2019.103365>
- Šmilauer, V., others, 2015. Using and Programming, in: *Yade Documentation 2<sup>nd</sup> Edition*. The Yade Project. <https://doi.org/10.5281/zenodo.34043>
- Volkwein, A., Gerber, W., Klette, J., Spescha, G., 2019. Review of Approval of Flexible Rockfall Protection Systems According to ETAG 027. *Geosciences* 9, 49.

## Forest Flexible fences: increasing their energy capacity

Ignacio OLMEDO<sup>1</sup>, Loïc DUGELAS<sup>1</sup>, Philippe ROBIT<sup>1</sup>

**Keywords:** rockfall, forest, tests, protection, flexible fences

### ABSTRACT IN FRENCH:

L'installation d'ouvrages de protection pare-pierres utilisant les peuplements forestiers comme éléments structuraux, appelés écrans forestiers, permettent la sécurisation en réduisant l'impact sur les écosystèmes et les émissions de CO<sub>2</sub> par rapport à des ouvrages de protection classiques. Dans cet optique, la société NGE Fondations propose une gamme d'écrans forestiers ne nécessitant pas des travaux de débardage ni de forage. Afin de valider et optimiser les ouvrages de ce type, un dispositif a été conçu pour la réalisation d'essais d'impact en contexte forestier.

Trois essais d'une énergie d'impact de plus de 500kJ ont été menées sur une structure utilisant uniquement comme points de fixation des arbres. Les blocs impactants ont été arrêtés dans les trois cas. Les observations et mesures ont permis l'analyse des impacts et l'étude de la dégradation de l'ouvrage.

## 1 INTRODUCTION

In a highly competitive domain as rockfall protection, the development of new concepts is a priority for industrials and works companies. At the same time, the environmental crisis leads to focus on environmental respectful and sustainable solutions. Even if technical solutions exist to reduce the environmental impacts of such structures and works, few are economical feasible (Volkwein et al 2011).

Forest rockfall flexible fences appear as a simple and innovative solution to reduce significantly both CO<sub>2</sub> emissions and tree felling and loggings.

Forest rockfall flexible fences are characterized by using standing trees as poles. Thus, trees are used as structural components allowing the interception net to stand. Moreover, foundations are also replaced by trees. In consequence, no foundation works are needed as well as helicopter lifting. Forest fences became a low carbonated solution compared to traditional structures. The lack of foundations and logging tasks makes forest flexible fences installation fast. In the other hand, some conditions should be satisfied in terms of forest density and tree mechanical properties in order to implement such structures. Tree characterisation analysis are needed in order to validate the standing trees properties before works.

After an experimental campaign in 2016 which allowed to study and validate a 100kJ forest fence, in 2020, a similar experimental campaign has been carried out in order to validate a 500kJ model. An experimental device allowing accelerating a bloc before impact the structure has been designed and installed. 3 impacts at >500kJ have been carried out. Experimental data has been collected thanks to the instruments installed.

## 2 METHODOLOGY

The experimental device main component is a 90 meter long zip-line. A 920kg boulder can be lifted on the zip-line. An electric winch allows to translate the bloc to the top of the zip-line when it is lifted. Two mechanical triggers are used to first, start the acceleration of the boulder on the zip-line, and second, to release the bloc from the zip-line before impact on the structure. Three tests at the same impact energy level have been conducted on three identical unimpacted structures.

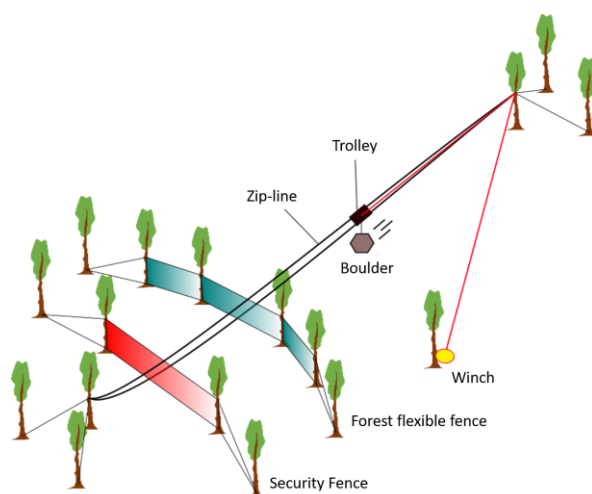


Figure 2: Experimental device

<sup>1</sup> NGE Fondations, St.Priest, France, iolmedo@ngefondations.fr

An accelerometer on the boulder is used to obtain the deceleration and impact forces. A high speed camera has been used to characterize the impact and measure the bloc displacements. Finally, force sensors installed on the wires gave the loading evolutions during the impact. An exhaustive inspection of the protection device has been done after each impact. It provided a qualitative information concerning the structure damage and the values of the energy devices elongation.

### 3 RESULTS

The high speed camera results post-treatment confirms an impact the impact velocity of 34 m/s for two of the impacts (test 2 and 3), leading to an impact energy of 525kJ. The first impact is not considered as the impact location was low and the boulder touched the ground during the impact. The impact force results show that the experimental device allows a good repeatability of the impact conditions.

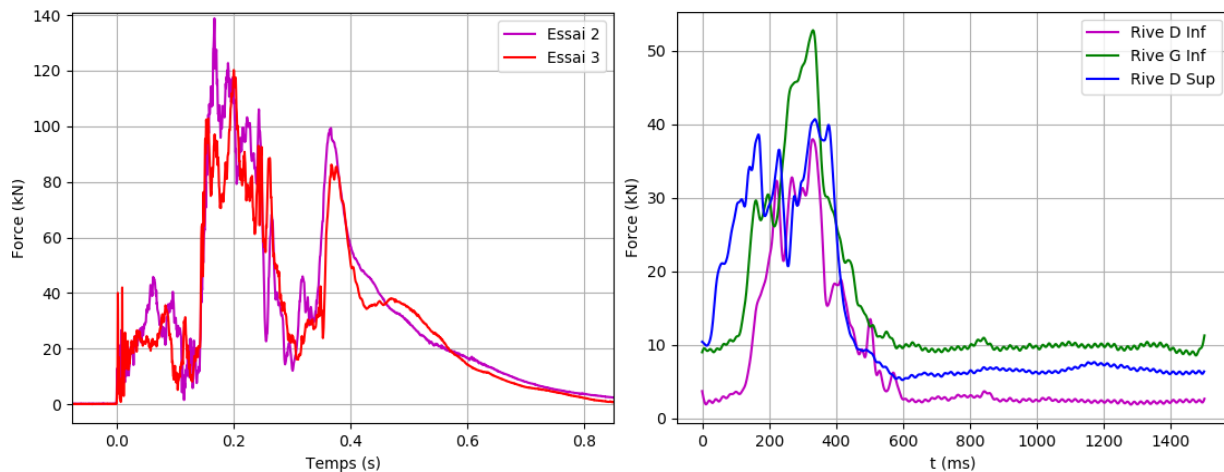


Figure 2: Time evolutions of impact forces for test 2 and 3 (left) and steel wires loading for impact 3 (right)

Force sensors measurements confirm that energy dissipating devices have been activated and loadings on wires and trees have been capped. The maximum loading values measured 53kN which represent 31% of the wire rupture force. The behaviour law of the energy dissipating devices has been characterized by a large quasi static tensile tests campaign (Coulibaly 2018). This allows to estimate the energy dissipation from the devices elongation (Olmedo et al. 2020). These calculations show a total energy dissipation by the energy dissipation devices between 448kJ and 479kJ which represents up to 91% of the total impact energy.

### 4 CONCLUSIONS

Results have shown a good repeatability of sub-horizontal impacts conditions thanks to the zipline. The slight differences between impact 2 and 3 are associated to mounting conditions. The main design objectives have been accomplished. These are the fast structure installation and the validation of the test while reducing the maximum the loading forces on trees. The latter has been achieved by relevant energy dissipation devices activation which leading to an increase of the impact duration. Moreover, no significant damage on the structure has been observed.

### REFERENCES

- Volkwein A. et al (2011). Rockfall characterisation and structural protection - a review. *Natural Hazards and Earth System Science*, Volume 11, Issue 9, 2011, pp.2617-2651. 10.5194/nhess-11-2617-2011
- Jibril Coulibaly. Modélisation numérique discrète du comportement mécanique sous impact des structures d'écrans de filets pare-pierres. PhD. Université Grenoble Alpes, 2017. Français.
- Olmedo,I et al (2020) Étude expérimentale multi-échelle sur les écrans pare-blocs : comportement des ouvrages hors cadre ETAG27. *Revue Francaise de Geotechnique 2020 Vol, 200018s*

## High energy impacts for assessing the Bloc Armé® technology as rockfall protection

Agathe FURET<sup>1</sup>, Julien LORENTZ<sup>2</sup>, Jean-Philippe JARRIN<sup>3</sup>, Pascal SAINTE-MARIE<sup>4</sup>, Stéphane LAMBERT<sup>5</sup>,  
Franck BOURRIER<sup>6</sup>

**Keywords:** rockfall, protective structure, impact, real-scale experiments

### ABSTRACT IN ENGLISH:

This article presents high-energy impact tests on two different real-scale rockfall protection structures employing the *Bloc Armé*® technology. The aim is to emphasize the potential of this recently developed technique while defining the impact strength of the tested alternatives.

### ABSTRACT IN FRENCH:

Cet article présente des essais d'impact réalisés à échelle réelle sur deux variantes d'ouvrages utilisant la technologie *Bloc Armé*®. L'objectif de cette campagne était d'illustrer le potentiel de cette technique et d'évaluer la résistance à l'impact des différentes alternatives considérées.

## 1 INTRODUCTION

Rockfall are frequent in mountainous areas. These events may damage infrastructures and injure or kill people. The growing urbanization and tourism development in areas prone to rockfall, strengthen the need for optimized protection structures with respect to constraints in particular related to the structure footprint, construction time and ease of repair. In this context, the *Bloc Armé*® technology was developed by Géolithe and Géolithe Innov. The technology has already been tested at small-scale (A. Furet et al., 2020) and at real-scale at low energy. This communication deals with the high energy impact response of two different alternatives using this technology, differing by their geometry, design and impact strength. The technology was first tested alone in a specific geometry wall and then coupled with gabion facing.

## 2 EXPERIMENTAL METHODS

### 2.1 Tested structures and impacts tests

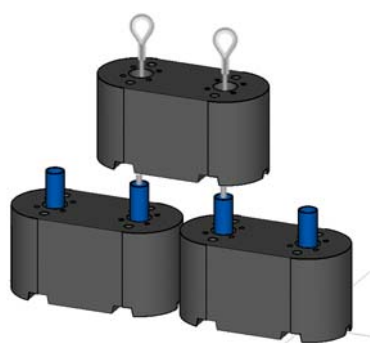


Figure 1: Bloc Armé® concept

The experiments consisted in sub-horizontal impacts by ETAG27-type reinforced concrete projectiles 2500 or 4800 kg in mass with different kinetic energies. These experiments were performed on the pendulum testing facility of the Université Gustave Eiffel test site (Montagnole, France).

The *Bloc Armé* technology consists of reinforced concrete blocks and a set of metallic reinforcement elements (Figure 1) to form articulated, self-standing and heavy rockfall protection structures. Tubes and cables are introduced vertically through holes in the staggered blocks. Vertical cables are fixed at base using bars and at the summit using a cable (Figure 2) to form a unified reinforcement mesh able to distribute the forces. Gaps between elements allow relative displacements between blocks and give the wall a certain deformability.

The modularity of the technology allows its use in different ways. Two different walls 3.2 m in height were submitted to centered impacts at a height of 1.7 m:

- (1) *Bloc Armé* zig-zag wall (Figure 2a), 500 kJ and 1000 kJ impacts in the concavity
- (2) *Bloc Armé* zig-zag wall with a gabion facing (Figure 2b), 2000 kJ impacts in the concavity

<sup>1</sup> FURET Agathe, Géolithe, Crolles, France (FR), agathe.furet@geolithe.com

<sup>2</sup> LORENTZ Julien, Géolithe Innov, Crolles, France (FR), julien.lorentz@geolithe.com

<sup>3</sup> JARRIN Jean-Philippe, Géolithe, Crolles, France (FR), jp.jarrin@geolithe.com

<sup>4</sup> SAINTE-MARIE Pascal, Myotis, Échirolles, France (FR), p.saintemarie@myotis.fr

<sup>5</sup> LAMBERT Stéphane, INRAE, Grenoble, France (FR), stephane.lambert@inrae.fr

<sup>6</sup> BOURRIER Franck, INRIA et INRAE, Grenoble, France (FR), franck.bourrier@inrae.fr

## 2.2 Measurement

In order to evaluate the displacements of the walls, accelerometers and wire extensometers were fixed to the blocks at different positions at the back of the wall. High-speed cameras recorded images at 1000 frames per second in two perpendicular directions. In addition, a topographic survey was conducted based on photogrammetric methods to measure the final deformation of the walls.

## 3 RESULTS

Impacts on the walls made of *Bloc Armé* alone demonstrated a good capacity of the structure to distribute loads. The wall length experiencing sliding was as large as 8 m and 11 m with a maximal displacement of 1 m and 1.45 m during the 500 kJ and 1000 kJ-impacts respectively. The lateral transfer of loads favors energy dissipation by friction and limits the maximal displacement. The impacted blocks fractured. However, we note that complete fracturing and opening of blocks were prevented thanks to the significant reinforcement of the blocks concrete (Figure 2a).

For a 2000 kJ impact, gabion cells (crushed gravel in wire mesh cells) were placed as facing. With this facing, the maximal displacement reaches 1.5m and the structure length experiencing sliding is 11m. Thanks to the gabion facing, no block fractured. Gabions facing improves the structure impact strength by damping the impact force, dissipating energy and distributing loads (Lambert et al, 2020). At this stage, the importance of each mode of action and the specific phenomena are neither precisely identified nor quantified.

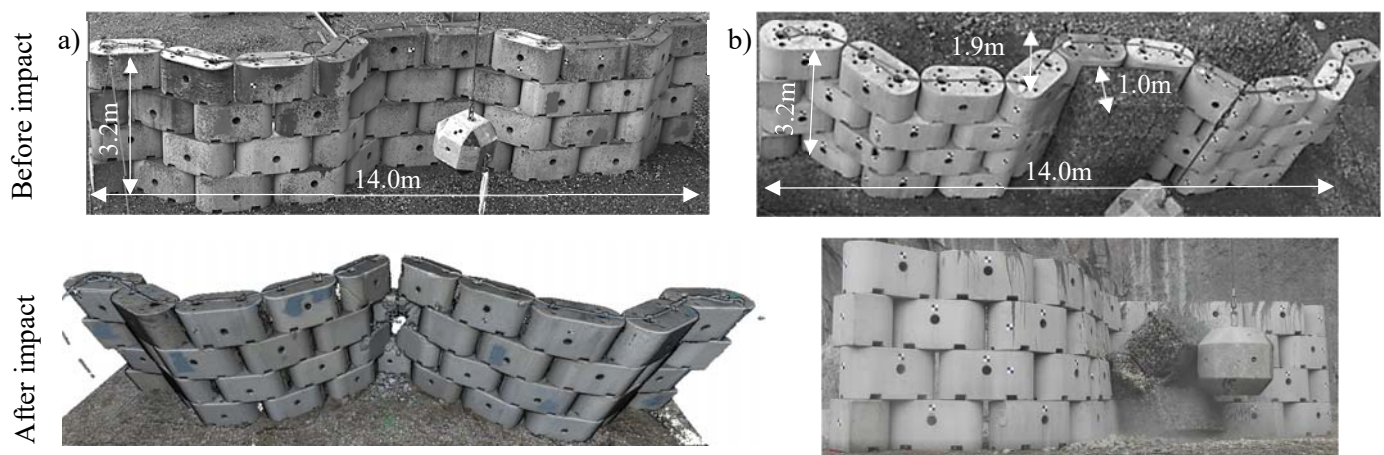


Figure 2: Tested structures before and after impact, *Bloc Armé* wall a) alone at 1000 kJ b) with gabion facing at 2000 kJ

## CONCLUSIONS

The impact tests results show a good capacity of *Bloc Armé* walls to resist high energy impacts. The reinforcement elements distribute loads laterally. The wall resists and the maximum displacement remains acceptable. The campaign proves that complex geometries can be built and that the technology can be easily combined with a granular facing to increase the structure capacity up to 2000 kJ. As a perspective, these first results and measurements constitute interesting data to be analyzed to understand the effect of the facing on the dynamic behavior of the structure.

## ACKNOWLEDGEMENTS

The experiments were conducted as part of the Smart-Protect project financed by the Auvergne-Rhône-Alpes region. The authors thank Université Gustave Eiffel and Cerema for their assistance in conducting the experiments.

## REFERENCES

Furet A., Lambert S., Villard P., Jarrin J-P. et Lorentz J. (2020b). Réponse sous impact de murs pare-blocs, *Revue Française de Géotechnique*, 163, 9 Doi: 10.1051/geotech/2020017

Lambert S., Bourrier F., Gotteland P. et Nicot F. (2020). An experimental investigation of the response of slender protective structures to rockfall impacts, *Canadian Geotechnical Journal*. Doi 10.1139/cgj-2019-0147

## Monitoring debris flow flexible fences for design purposes

Ignacio OLMEDO<sup>1</sup>, Firmin FONTAINE<sup>2</sup>, Stephane LAMBERT<sup>3</sup>, Philippe ROBIT<sup>4</sup>

**Keywords:** debris flow, flexible fences, tests, monitoring

*No abstract required as the paper stands as an extended two-page abstract.*

### ABSTRACT IN FRENCH:

L'utilisation de dispositifs souples pour la rétention/atténuation de laves torrentielles est en croissance dans les zones de montagne, de nouveaux ouvrages de grande taille ont été récemment installés en Europe, Asie et Amérique du Sud. Tels dispositifs, par rapport à des ouvrages classiques en génie civil, présentent l'avantage d'une grande adaptabilité au terrain, installation rapide et moindre cout. Néanmoins, l'analyse de leurs performances en termes de capacités maximales et optimisation en fonction des caractéristiques des écoulements doit être approfondi. Afin de pouvoir calibrer des modèles numériques d'interaction écoulement/ouvrage et optimiser les conceptions futures un chantier pilote est prévu par la société NGE Fondations en collaboration du laboratoire INRAE. Un système d'instrumentation permettant le couplage des données sur l'écoulement et le suivi des efforts et déformation de l'ouvrage a été conçu. Le système sera installé sur un ouvrage dans le torrent du Tuebi (Péone, France), largement suivi par INRAE et l'ONF-RTM. Les travaux de construction en installation de la instrumentation sont prévus pour le premier semestre de 2021. Des résultats sont attendus avant la fin de l'année étant donné que environ 2 évènements du type lave torrentielle sont observés sur ce site par an.

### 1 INTRODUCTION

Flexible fences are increasingly installed for protection against debris flow events. Historically, debris flow mitigation and/or attenuation has been done by check dams (Piton 2015). Lighter solutions like flexible fences can be installed in complement of concrete structures or can be used for smaller debris flow mitigation. Such devices provide a better adaptability to terrain and a faster installation for lower cost.

Debris flow flexible fences designs is mainly done by analytic approaches based on loading models that can be found in the literature (Wendeler 2011, Volkwein 2014). Numerical models including the interactions between flow and structure are also developed (Albaba 2016). These allows simulating the structure behavior including the particularities of such devices like mesh porosity.

However, experimental data enabling the validation of flexible fences for different debris flow characteristics is still needed. Moreover, experimental data should be used to calibrate the numerical models allowing the study of larger loading conditions.

### 2 METHODOLOGY

In order to acquire experimental data, *NGE Fondations* and *INRAE* have designed a monitoring device. A debris flow flexible fence will be set in the Tuebi torrent (Peone, France) (Fig.1). This site is particularly favorable as the slope is homogeneous and for the event's short return periods. Moreover, the Tuebi torrent has been checked for decades (ONF-RTM 2015). Based on these studies, the debris flow volume attended at the chose location is lower than 20.000m<sup>3</sup> for a 10 year of return period event.

---

<sup>1</sup> OLMEDO Ignacio, NGE Fondations, St.Priest, France, iolmedo@ngefondations.fr

<sup>2</sup> FONTAINE Firmin, INRAE, St Martin d'Hères, France, firmin.fontaine@inrae.fr

<sup>3</sup> LAMBERT Stephane, INRAE, St Martin d'Hères, France, stephane.lambert@inrae.fr

<sup>4</sup> ROBIT Philippe, NGE Fondations, St.Priest, France, probit@ngefondations.fr

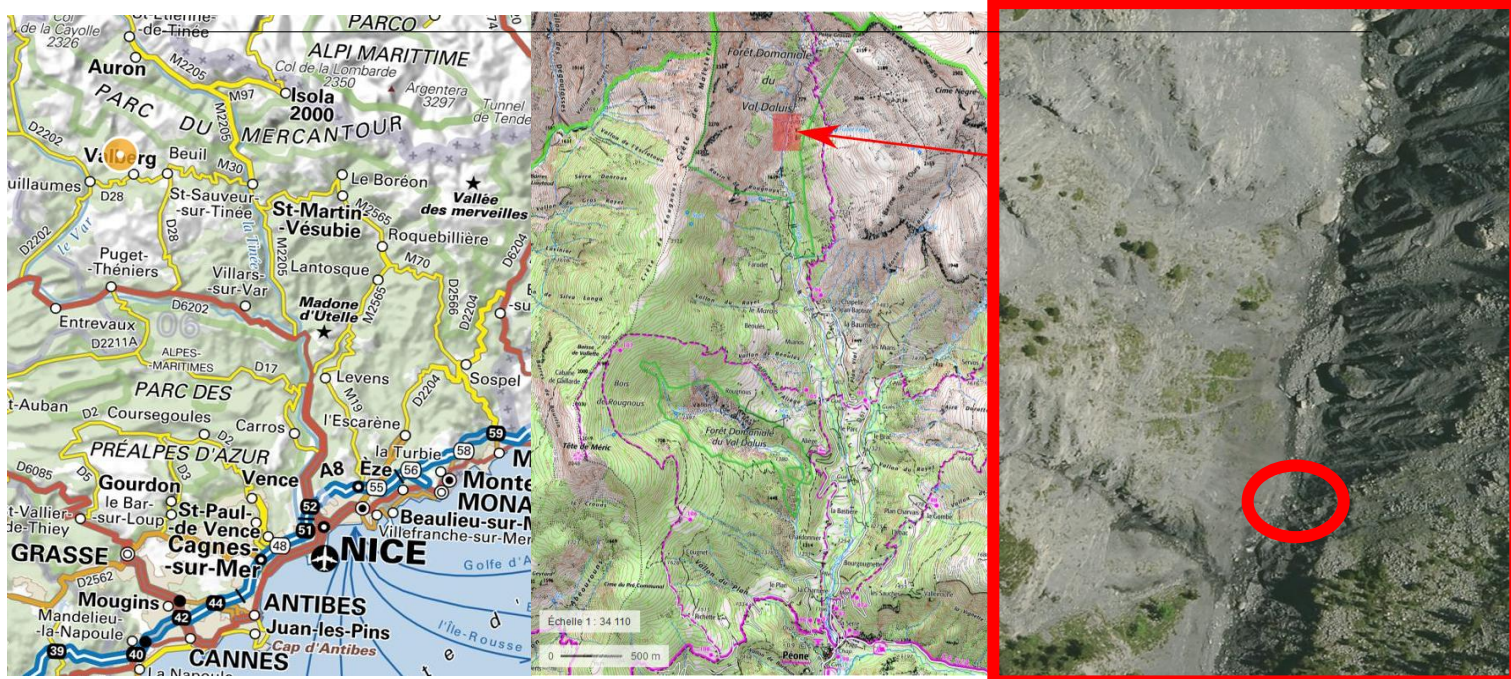


Figure 1: Torrent and structure location

The instrumental set can be dispatched in two main groups: the flow instruments and the structure ones. The former includes a group of geophones for flow velocity measurements and a flow stage for flow height measures. Their recording frequency is 10Hz. A rain gauge is also installed to automatically turn on the instrumental device and trigger the acquisition. The latter includes 10 force sensors installed on the wire rope nets, between the anchors and energy dissipating devices (Fig.2). The recording frequency of the force sensors is 500Hz. Moreover, a displacement sensor is foreseen to record the mid-span upper wire displacement evolution during the flow loading. Two cameras recording at 15 fps will provide extra qualitative information of the debris flow and the structure loading.

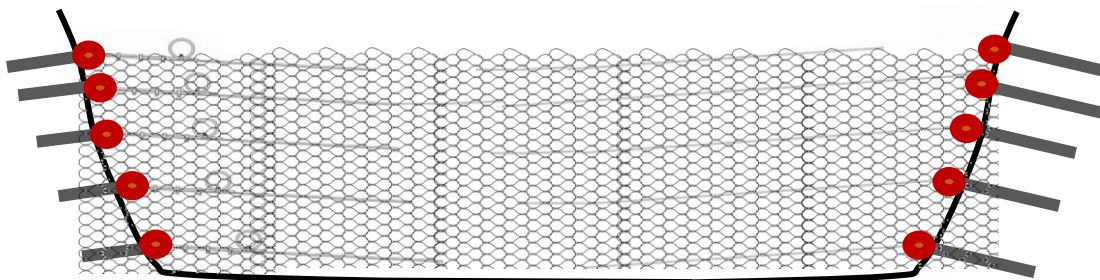


Figure 2: Schema of the structure and the location of force cells on cables supports.

The autonomous monitoring system can be consulted online at real-time and alerts are sent in case of debris flow or heavy rainfalls.

### 3 PERSPECTIVES

Construction works will be carried out during the first semester of 2021. Thus, the monitoring of the torrent and structure should be operating during the summer 2021. Given the frequency of debris flow events on this torrents in between May and October, some data is expected to be obtained during this period. Then, results will be used to explore the flow/structure interaction integrating the particularities of the NGE Fondations structure such as the cable

net and the energy dissipating devices. Experimental data will allow the calibration of the numerical model already developed.

## REFERENCES

Piton,G. (2015) Design of sediment traps with open check dams. American Society of civil engineers DOI: 10.1061/(ASCE)HY.1943-7900.0001048.

ONF-RTM (2015) Etude de bassin de risques : torrents du Tuébi et du Réal. ONF-RTM Nice

Wendeler, C., Volkwein, A., McArdell, B. W., & Bartelt, P. (2018). Load model for designing flexible steel barriers for debris flow mitigation. Canadian Geotechnical Journal, 99, 893-910. <https://doi.org/10.1139/cgj-2016-0157>

Volkwein 2014. Flexible debris Flow barriers: design and application . WSL Berichte Issue 18, 2017, ISSN 2296-3458

Albaba A (2016). Discrete element modeling of the impact of granular debris flows on rigid and flexible structures. PhD. Université Grenoble Alpes.

## Numerical modelling of full-scale rockfall protection structures under dynamic impact using discrete element method

Ali RAFIEE<sup>1</sup>, Pierre PLOTTO<sup>2</sup>, Michel KHATIB<sup>3</sup>

**Keywords:** Rockfall, protection structure, gabion wall, flexible barrier, discrete element method

The main aim of this research is to illustrate the real ability of the Discrete Element Method (DEM) to study retaining structures such as gabion walls, flexible barriers and complex structures in their full-scale configuration. DEM can be used for structures with very complex geometry, and it should be considered that the geometry and inside material characteristics of a protective structure have a fundamental role in its mechanical and dynamic behaviour. This study presents the results obtained for different protective structures under dynamic impact, taking into account their complex geometry while trying to respect their real structures as much as possible, which is one of the innovative aspects of this study. In this short version of the article, the result obtained for a protective gabion wall impacted by a detached block is presented and the results for other complex structures will be presented in the extended version.

### PROTECTION STRUCTURES & DEM ANALYSIS

Retaining structures are used to prevent and reduce damages caused by the instability occurred inside a rock slope because of natural weakness present in this type of medium. Instability and detachment of blocks on a rocky slope can cause significant damage to affected infrastructure and can lead to very high economic and fatal risk. Therefore, one of the key points for securing high risk localities is to design a more precise and adequate protection structure taking into account all the predictable parameters; in a first step related to the expected projectiles, then by knowing better the characteristics and the behaviour of the proposed structure compared to the expected impact (Plassiard & Donzé, 2010). The first phase will be performed by the trajectography investigation, and the protective structure will then be constructed according to criteria and results obtained by this first phase. It should be noted that DEM method can also be employed for this first step by considering all of the detailed geometry and mechanical aspects related to the surface of a rocky slope and the expected removable blocks in order to have more precise results for the design phase of the protective structure.

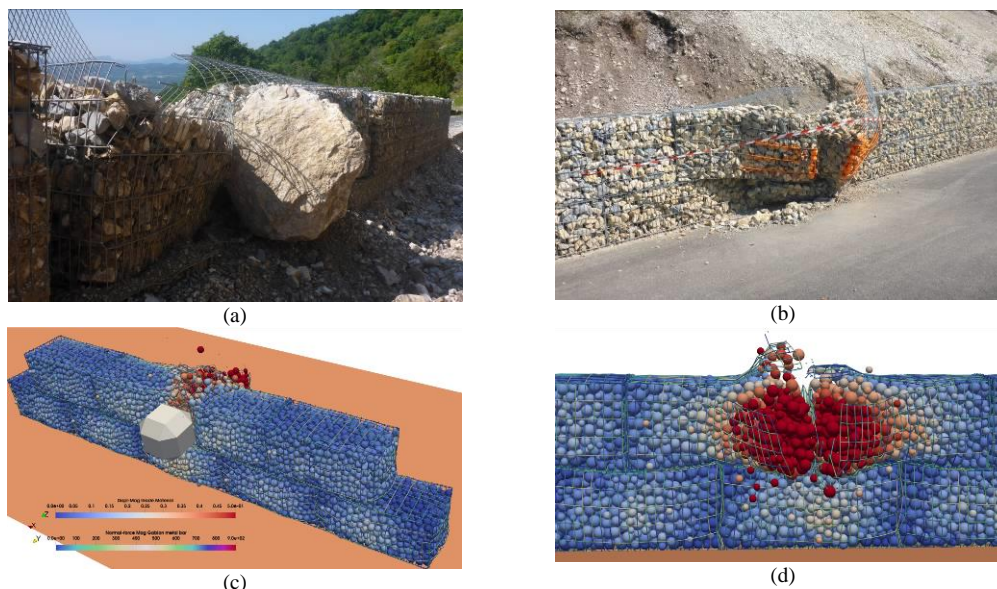


Figure 1: (a & b) impacted gabion wall, (c & d) results obtained by the DEM method

In this short version of article, the results obtained for an impact on a wall in gabion are presented (Figure1). Gabion walls have been used widely around the world in numerous projects for erosion control, soil reclamation works,

<sup>1</sup> RAFIEE Ali, Ginger CEBTP Group, Grenoble, FRA, a.rafiie@groupeginger.com

<sup>2</sup> PLOTTO Pierre, Consultant in Ginger CEBTP Group, Grenoble, FRA, pierre.plotto@imsrn.com

<sup>3</sup> KHATIB Michel, Ginger CEBTP Group, Elancourt, FRA, m.khatib@groupeginger.com

construction of stream channels and retaining structures (Toprak et al. 2016). For this case study, just to show the functionality of an analysis by DEM method, welded gabion boxes are chosen but this method can also be used for hexagonal wire mesh gabions. The mechanical behaviour of gabion cell is generally investigated in some scientific studies for one alone gabion box (Bertrand et al. 2005), in the current study the mechanical and dynamic behaviour of a complete structure made by gabion boxes is simulated. For simulation with a very complex geometry setup, homemade auxiliary codes are developed by which the model can be easily generated for studying with large ranges of scientific and commercial codes. The results presented here are obtained by using the DEM code of Yade (Šmilauer & Chareyre, 2015; Effeindzourou, 2017), for some of other models the code LMGC90 is used (Dubois & Mozul, 2013).

In addition, the results of simulations for a flexible rockfall barrier are shown in Figure 2, the dynamic behaviour of this complex protective structure is also studied by help of DEM method using Yade code with combination some auxiliary codes. The results in detail will be presented on the extended article or on future publications.

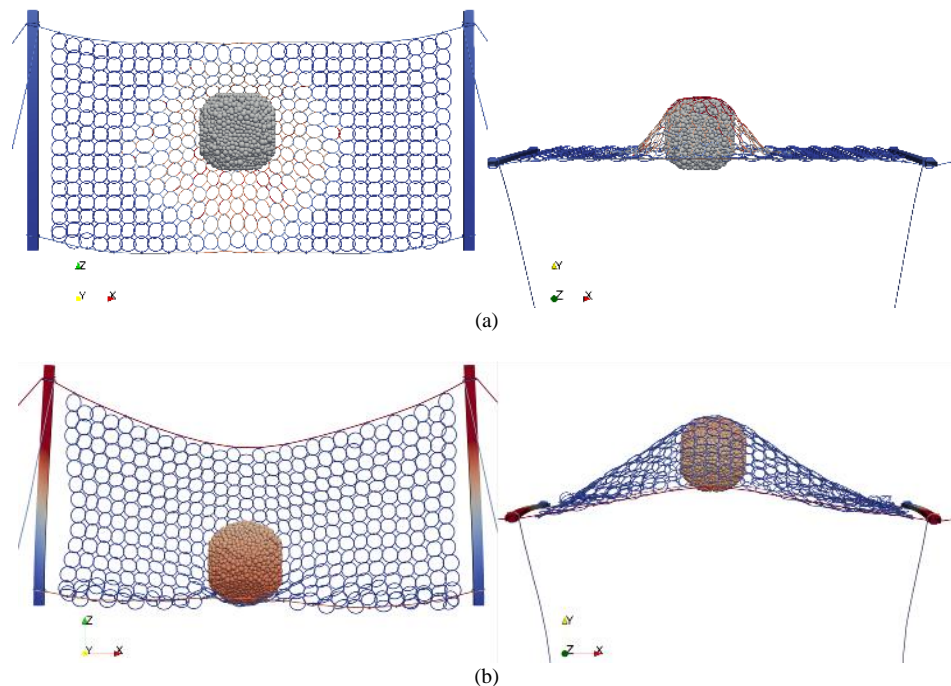


Figure 2:(a & b) snapshots of a flexible rockfall barrier model

## CONCLUSION

The current study focuses on the practical applications of DEM method to investigate and analyse the mechanical and dynamic behaviour of complex protective structures. The comparison of the results obtained by numerical simulation with on-site tests or impacted structures, demonstrates the effectiveness of the technique to better understand the real capacity of the protective structures even for very complex structures. The advantage of using numerical simulation over on-site testing is the ability to perform a wide range of different configurations and to modify loading conditions; of course, to achieve this, the model must be representative of the structure itself.

## REFERENCES

- Bertrand, D., Nicot, F., Gotteland, P., & Lambert, S. (2005). Modelling a geo-composite cell using discrete analysis. *Computers and Geotechnics*, 32(8), 564-577.
- Dubois, F., & Mozul, R. (2013, May). Lmgc90. In *11e colloque national en calcul des structures*.
- Effeindzourou, A., Thoeni, K., Giacomini, A., & Wendeler, C. (2017). Efficient discrete modelling of composite structures for rockfall protection. *Computers and Geotechnics*, 87, 99-114.
- Plassiard, J. P., & Donzé, F. V. (2010). Optimizing the design of rockfall embankments with a discrete element method. *Engineering Structures*, 32(11), 3817-3826.
- Šmilauer V. & Chareyre B. (2015), Dem formulation. In *Yade Documentation 2nd ed.* The Yade Project, DOI 10.5281/zenodo.34044
- Toprak, B., Sevim, O., & Kalkan, I. (2016). Gabion walls and their use. *International Journal Advance Mechanical Civil Engineering*, 3(4).

## Simulation des essais d'arrachement des ancrages passifs par une méthode au module de réaction axial

Jean-François SERRATRICE<sup>1</sup>

**Keywords:** rock bolt, pull-out test, simulation, axial reaction modulus

### ABSTRACT IN ENGLISH:

An axial reaction modulus calculation method is proposed to determine the response of sealed rock bolts subjected to a tensile axial force. The method is applied to the interpretation of tests of instrumented and sealed bolts in hard rock.

### ABSTRACT IN FRENCH:

Une méthode de calcul au module de réaction axial est proposée pour déterminer la réponse de barres scellées soumises à un effort de traction en tête. La méthode est appliquée à l'interprétation d'essais de boulons instrumentés et scellés dans une roche dure.

Le programme d'essais réalisés sur le site de Montagnole compte trente-six essais d'arrachement de boulons scellés au rocher (Ho, 2017 ; Bost et al., 2018). Le plan d'expériences est conçu pour mettre en évidence le rôle de trois paramètres principaux : le diamètre du boulon, le diamètre du scellement et la longueur de scellement. Les expériences apportent des mesures d'effort et de déplacement en tête des boulons. Mais l'originalité de l'instrumentation réside dans l'enregistrement des déformations de la barre d'acier au cours des chargements au moyen de fibres optiques, ouvrant ainsi sur une observation locale des réponses des barres au cœur des scellements. Les chargements sont conduits jusqu'à la limite élastique des barres, sans atteindre la rupture des scellements dans cet environnement de roche résistante et non fracturée à l'échelle des ancrages (calcaires en gros bancs subverticaux du Tithonique).

Les boulons sont scellés dans des trous forés de diamètre  $d_s$  sur une longueur de 2,1 à 2,3 m à partir de la paroi rocheuse et une pente de 14 à 33 ° sous l'horizontale ( $d_s = 64, 76, 90$  mm). Les barres crénelées de diamètre  $d_a$  sont constituées par un acier S500/550 à haute adhérence ( $d_a = 25, 28, 32$  mm). Le scellement est effectué en fond de trou sur une longueur  $l_s$  délimitée par un bouchon ( $l_s = 0,5$  à 1 m). Le scellement gravitaire est réalisé au coulis de ciment malaxé dans les proportions eau/ciment E/C = 0,45. Quelques barres ont été instrumentées au moyen d'une fibre optique en vue de mesurer les déformations du boulon pendant son chargement. La fibre optique est collée dans une engravure ménagée le long d'une génératrice de la barre. Les chargements sont effectués selon la norme XP 94-444 (AFNOR, 2002). Le tableau 1 donne les caractéristiques de deux de ces boulons (essais 3.1 et 13.1).

Tableau 1 : Caractéristiques des essais d'arrachement et paramètres de la simulation

Essai	$d_a$ (mm)	$d_s$ (mm)	$l_s$ (m)	$l_{\text{libre}}$ (m)	$E_a$ (GPa)	$u_{x0}$ (m)	$q_s$ (kN/m <sup>2</sup> )	$F_s$ (kN/m)
<b>3.1</b>	25	64	0,75	2,13	210	0,001	4000	804
<b>13.1</b>	32	76	0,75	2,12	210	0,001	4000	955

La simulation des essais d'arrachement s'obtient avec la résolution du système d'équations liant le déplacement axial  $u_x$  et l'effort normal  $N_x$  à l'abscisse  $x$  le long de la barre, où  $u_r$  est le déplacement imposé par la roche dans la direction  $x$  (ici  $u_r = 0$ ) et où l'effort de cisaillement  $F_x$  par unité de longueur le long du scellement est variable :

$$\frac{du_x}{dx} = \frac{1}{A_a E_a} N_x \quad \frac{dN_x}{dx} = -F_x = -F_s \frac{(u_r - u_x)/u_{x0}}{1 + (u_r - u_x)/u_{x0}} \quad (1)$$

$A_a$  est la section de la barre,  $E_a$  le module d'Young de l'acier,  $u_{x0} = 0,001$  m et  $F_s$  l'effort limite de cisaillement linéique lié à la résistance au cisaillement  $q_s$  du scellement par  $F_s = \pi d_s q_s$ . Dans cette formulation, qui ne dépend que du paramètre  $F_s$  (ou  $q_s$ ), le module de réaction initial tangent est  $k_s = F_s/u_{x0}$  et le coefficient de réaction initial tangent  $G_s = q_s/u_{x0}$ .

<sup>1</sup> SERRATRICE Jean-François, Cerema Méditerranée, Aix en Provence, France, jean-francois.serratrice@cerema.fr

La figure 1 montre les courbes effort-déplacement mesurées pendant deux essais d'arrachement dont les caractéristiques sont reportées dans le tableau 1 (essais 3.1 et 13.1). Les ronds bleus indiquent les mesures obtenues en tête de l'ancrage pour les six paliers de chargement. Les ronds rouges représentent les déplacements en tête de scellement, déduction faite de l'allongement de la longueur libre de la barre. Les losanges verts montrent les déplacements déterminés à partir des mesures de la fibre optique. Deux courbes d'essais sont indiquées sur la figure 1a (essais 3.1 et 3.2). Calculées par intégration depuis le pied de la barre, ces mesures donnent le déplacement relatif dans le scellement. Mais elles ne rendent pas compte du déplacement de la barre en pied.

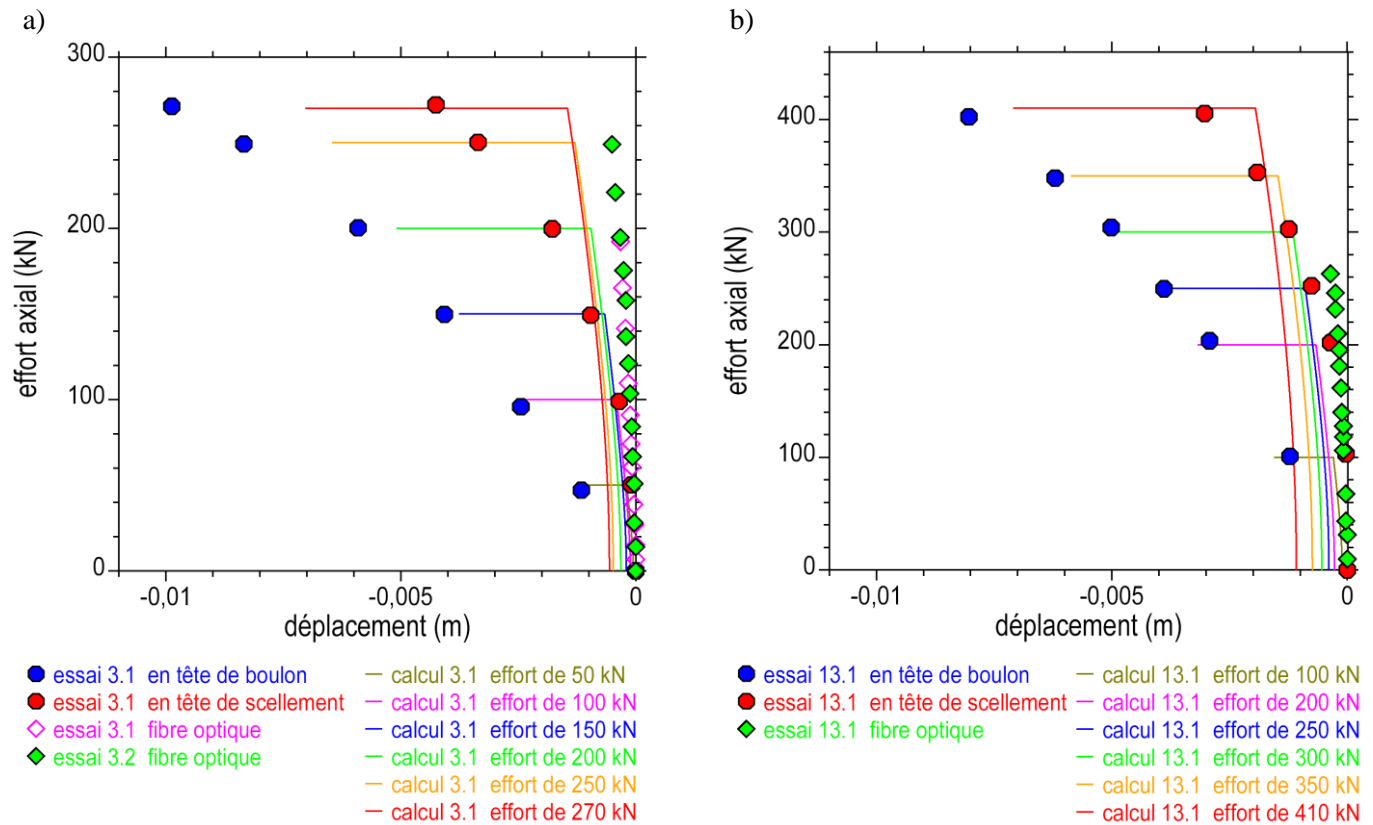


Figure 1 : Comparaison des courbes d'essais d'arrachement effort-déplacement avec les courbes calculées. Mesures globales et locales.  
 a) Essai 3.1. b) Essai 13.1.

Les courbes continues représentent les déplacements calculés par la méthode au module de réaction axial, pour les six paliers de chargement. Les segments horizontaux restituent les déformations de la longueur libre. Les parties sub-verticales des courbes indiquent la réponse de la barre dans le scellement et son déplacement en pied. Ces courbes modélisent raisonnablement bien les mesures de la fibre optique. Pour amener ces courbes théoriques en coïncidence avec ces données expérimentales, il suffit de les translater vers l'origine du plan en faisant abstraction du déplacement calculé en pied. Le paramètre de calcul  $q_s = 4000 \text{ kN/m}^2$  adopté ici permet de rendre compte de la réponse des deux barres d'après les mesures locales de la déformation.

Quand le chargement approche de la limite élastique de l'acier (fin des essais), les mesures globales des déplacements s'écartent des mesures locales en additionnant le déplacement de pied, des déformations non captées par la fibre optique (déformation de la roche, endommagement du scellement, puis décollement), mais aussi des mouvements parasites induits par le dispositif de chargement.

## REFERENCES

Association Française de Normalisation (AFNOR, 2002) Essai statique d'arrachement sous un effort axial de traction, d'un ancrage scellé dans un massif rocheux. Norme NF P 94-444, Décembre 2002, 10 p.  
 Bost M., Ho D.-A., Pruvost C., Khadour A., Joffrin P., Huteau M., Robit P. (2018). Etude paramétrique de la résistance à l'arrachement d'un ancrage passif scellé au rocher. *Actes des Journées Nationales de Géotechnique et de Géologie de l'Ingénieur, JNGG*, Champs-sur-Marne.  
 Ho D.-A. (2017) Comportement axial des ancrages passifs scellés au rocher : étude de l'interface barre scellement et modélisation. Mémoire de thèse. Université de Lyon. 369 p.

# Case studies

## Application of a high-frequency radar for early warning of a rock-fall hazard in the Pitztal valley

Tobias Schöffl<sup>1</sup>, Richard Koschuch<sup>2</sup>, Michael Mölk<sup>3</sup>, Johannes Hübl<sup>4</sup>

**Keywords:** rock-fall, early warning system, high-frequency radar

Due to a rock-fall event on November 12 2020 in Weißwald (part of the municipality St. Leonhard), in the Pitztal (Tyrol, Austria), a helicopter flight was carried out by the Provincial Geological Survey and the Torrent and Avalanche Control Service (WLV). In the course of the flight, a block assembly with a structurally unstable geometry was recognized. Furthermore, an on-site investigation revealed a critical rock-contact of a key block showing signs of obviously contemporary load changes and fractures. At the valley floor a settlement and a federal road (see Figure 1), being the only connection to further villages and a major ski resort, are located. Due to the obviously imminent danger for the road and the residential buildings a closure of the road and an evacuation of the object next to the slope was recommended by experts and executed by the authorities. Thereupon a height difference model, an evaluation of the block sizes (see Figure 2) by a terrestrial laser scan model and a 3D rock-fall simulation were initiated. The results of the analyses and simulations enabled the road administration to design and realize an emergency road alignment well beyond the potential reach of rock-fall events. In order to detect the movement rates of the boulders, an in situ measuring station with six crackmeters was installed by a team of experts (HTB, Trigonos and WLV). To ensure the safety of road users until the completion of the emergency road, an automated early warning system with an alarm function was installed. The system, consisting of a high-frequency radar (HF-radar) from the company IBTP Koschuch and a traffic light system (see Figure 1), was developed in cooperation with the University of Natural Resources and Life Sciences especially for rapid gravitational natural hazards. This system is optimized for a short time of installation and will also serve as a safety measure during the construction of a rock-fall rampart at the foot of the slope. If an event occurs, the traffic lights are switched to red in real time and an SMS is sent to the responsible authorities.

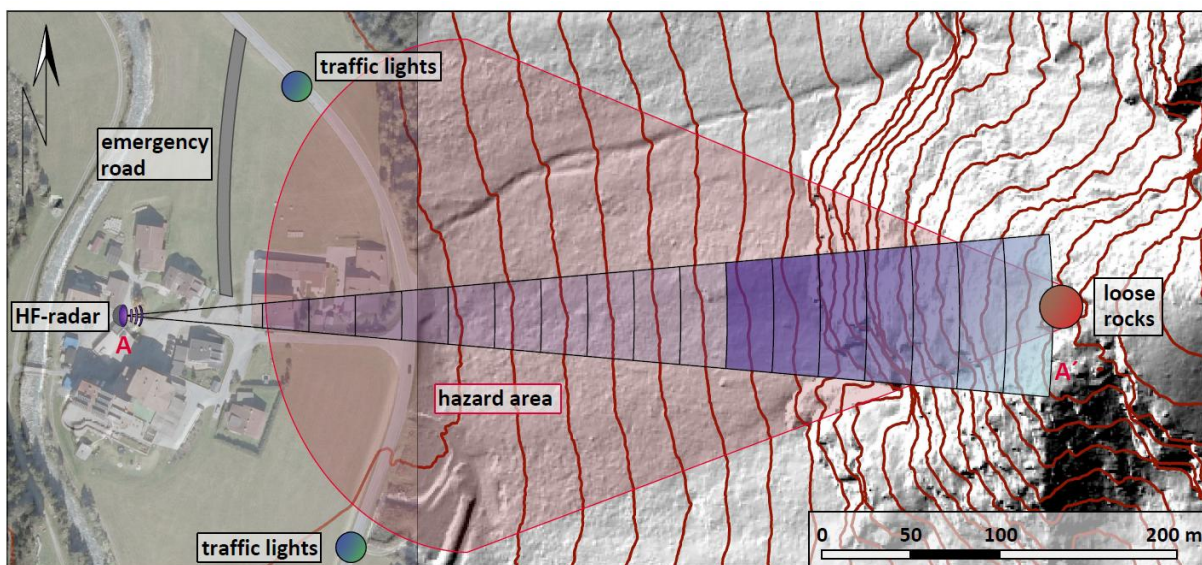


Figure 1: General map of the area of operation ([www.tirol.gv.at](http://www.tirol.gv.at))

The HF-radar has a maximum *range* of 2500 m, where speeds between 1 and 300 km/h can be detected. A lobe-shaped electromagnetic field [W] at the speed of light  $c$  is emitted. The transmission frequency of this field is in the X-band (10.1 - 10.3 GHz). The speed of a target can be calculated using the Doppler effect. The HF-Radar has two

<sup>1</sup> Schöffl Tobias, University of Natural Resources and Life Sciences, Department of Civil Engineering and Natural Hazards, Institute of Mountain Risk Engineering (IAN), Vienna, Austria (AUT), tobias.schoeffl@boku.ac.at

<sup>2</sup> Koschuch Richard, IBTP Koschuch, Leutschach an der Weinstraße, Austria (AUT), office@ibtp-koschuch.com

<sup>3</sup> Mölk Michael, Centre for Geology and Avalanches Innsbruck, Austrian Torrent and Avalanche Control Service (WLV), Innsbruck, Austria (AUT), Michael.moelk@die-wildbach.at

<sup>4</sup> Hübl Johannes, University of Natural Resources and Life Sciences, Department of Civil Engineering and Natural Hazards, Institute of Mountain Risk Engineering (IAN), Vienna, Austria (AUT), johannes.huebl@boku.ac.at

transmission methods. In the first transmission method, a simple pulse is generated via amplitude modulation. In the second method, pulse compression, the phase is modulated by a Barker code sequence (Koschuch, 2015). In both cases the transmission of the signals is pulsed in contiguous series (Skolnik, 2008). The number of pulses transmitted per second is referred to as pulse repetition frequency (*PRF*) [Hz]. The HF-Radar used has a *PRF* of up to 90 kHz. The pulse repetition interval (*PRI*) is the inverse of the *PRF*. The *PRI* [s] consists of the transmission time of a pulse  $\tau$  and the time that elapses until the next pulse is transmitted (Alabaster, 2012). The pulsed transmission method thus irradiates a slope with electromagnetic waves at discrete times. In this process, a range gate length  $r_{RG}$  corresponds exactly to the spatial pulse length and can be divided into multiple range gates (RG). The range gate length is therefore defined as follows:

$$r_{RG} = (c\tau)/2 \quad (1)$$

Shown in Figure 3, the antenna lobe (aperture angle  $\theta$ ) hits the mountain slope over a length of about 220 meters. Therefore, 7 range gates can be used to detect the process. Two parameters are used in the detection algorithm. The reference to the size of a moving object can be made by the received *intensity* [ $W/m^2$ ]. The velocity [m/s] in turn via the received *Doppler frequency spectrum* [Hz]. The HF-radar was calibrated to detect objects moving in the fall line of the slope with the size of  $1 m^3$ . If the blocks start moving, there is an *early warning time* of only about 20-30 seconds before damage can occur. Successful detection must therefore take place in the upper area of the slope (RG15-17). The challenge during the calibration process is not to include detected snow slides in the alarm function.



Figure 2: Loose rocks - total volume about  $300 m^3$

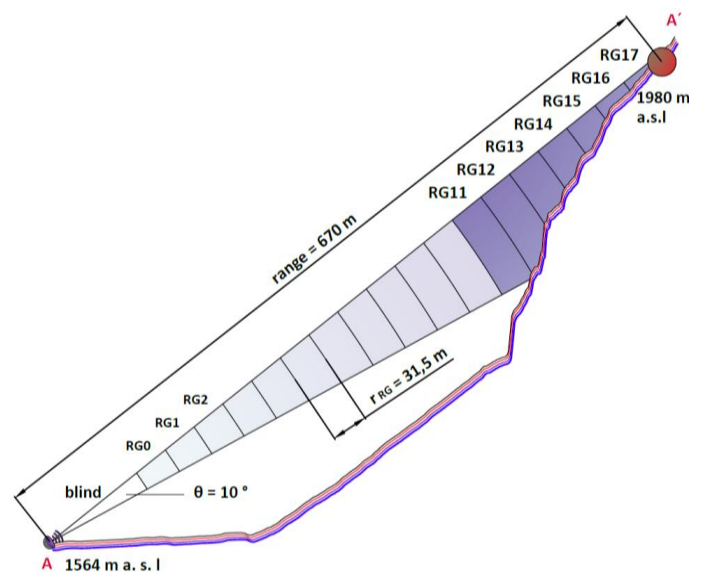


Figure 3: Longitudinal section of the digital elevation profile ([www.tirol.gv.at](http://www.tirol.gv.at)) and the antenna lobe

## CONCLUSION

The use case described here shows that gravitational natural hazards often require immediate action to ensure the safety of settlements, infrastructure and workers performing their duties in the hazard area. Due to the rapidity of the process, sufficient *early warning time* can only be guaranteed if the transmission chain from detection to alerting is automated and a calibration of the sensor to the given situation has been performed. With the experience gained during the calibration process, an optimized threshold algorithm can be used in future deployments. Another very important factor is the reliability of the system in terms of susceptibility to faults. The highest possible redundancy at all levels should therefore always be aimed for. In spring 2021, the system will be specified and optimized for construction site security. It will be expanded to include a stand-alone power supply and a siren.

## REFERENCES

- Alabaster, C. (2012) Pulse Doppler radar: Principles, technology, applications, SciTech Publishing.
- Koschuch, R., Jocham, P., Hübl, J. (2015) One Year Use of High-Frequency RADAR Technology in Alpine Mass Movement Monitoring: Principles and Performance for Torrential Activities. *Engineering Geology for Society and Territory*, 3 (14), pp. 69-72.
- Mölk, M. (2020) AdTLR, Abt. Geoinformation: Steinschlag Weisswald, L16 Pitztal (St. Leonhard i. P): Protokoll Weißwald. Aktenvermerk: 3496/90-2020.
- Skolnik, M. I. (2008) Radar Handbook, Third Edition. New York: McGraw-Hill Education.

## Innovative rockfall alarm system with automatic road closure at Axenstrasse, Switzerland

Severin STÄHLY<sup>1</sup>, Susanne WAHLEN<sup>1</sup>, Lorenz MEIER<sup>1</sup>, Helene HOFMANN<sup>2</sup>, Roger MOOR<sup>2</sup>

**Keywords:** rockfall alarm system, long-term slope monitoring, flexible rockfall protection, rockfall mitigation

The Axenstrasse is a scenic road section along Lake Lucerne with an average traffic volume of 16,000 vehicles a day. It is a major European North-South connection for passenger and goods transport. The road passes below steep mountain cliffs, with an altitude difference of up to 1500 m. The railway is situated below to the road, closer to the lake. The Axenstrasse and railway have been subject to a long history of rockfall and debris flow events (ASTRA, 2020). From 2009 to 2014, a total of 30 days of road closure have been recorded (AXEN, 2016). On 18 July 2019, a large rockfall impacted the road and caused the immediate closure of the route immediately for safety reasons. Large debris accumulations of a previous slope failure have remained in the upper Gumpisch valley and further similar events are likely.

### 1 INNOVATIVE MONITORING AND PROTECTION SYSTEM

In an effort to reopen the important road as soon as possible, an alarm system with automatic traffic control was developed, installed and commissioned within a few weeks so that the road could be re-opened in September of the same year. In addition, structural measures were implemented.

The system combines two different types of technologies: First, sensors for real-time detection of fast movements and second, measurement techniques for long-term monitoring of surface deformation (Fig. 1).

#### 1.1 Monitoring system

For reliable rockfall detection, a combination of long-range Doppler radar technology and high-sensitivity seismic sensors is used to minimize false alarm rates while maintaining high probability of detection. The rockfall radar remotely detects moving debris or large boulders whereas the seismic sensors recognise rockfall based on ground motion. Both technologies work in real time and are independent of visibility conditions (day/night, fog, snowfall).

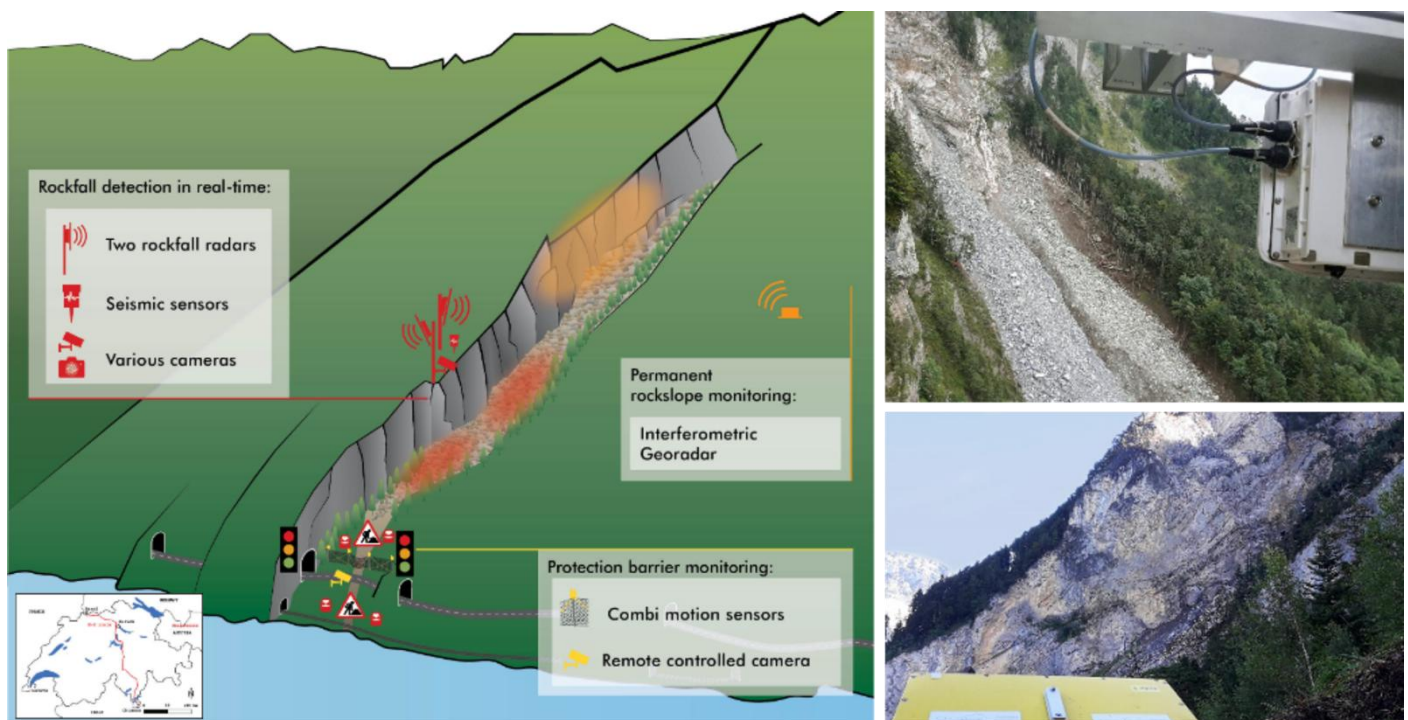


**Figure 1:** Situation of the Axenstrasse as part of the important N-S route through Switzerland. Several rockfall and debris flow events originating from the steep mountain slopes have impacted the road and the railway.

<sup>1</sup> Geoprevent AG, Zurich, Switzerland (CHE), severin.staehly@geoprevent.com

<sup>2</sup> Geobrugg AG, Romanshorn, Switzerland (CHE), helene.hofmann@geobrugg.com

Given the short warning time of around 20-30 seconds, it is vital to close the road immediately once an event is detected. However, many events remain small and never reach the road. In order to avoid unnecessary road closures for minor events, protection nets above the road were equipped with combi-motion sensors to detect an impact of a boulder or the passage of a debris flow. The system automatically reopens the road after 2 minutes, if an event was detected in the upper part, but no impact was recorded in the nets. The sensor fusion approach allows to ensure road safety and simultaneously avoid long closure times of the road.

Long-term slope monitoring has been conducted using an interferometric radar for sub-mm monitoring of the rock face where rockfall initially occurred. Additionally, two deformation cameras monitor the slope of the Gumpisch valley.

## 1.2 Mitigation

As a consequence of the rockfall of July 2019, the Swiss Federal Road Authority (ASTRA) ordered the construction of an earthen dam and flexible rockfall protection systems. The earthen dam should deflect all material (rocks and debris flows) towards the torrent. Additional high-tensile steel flexible rockfall protection barriers of approx. 100 m length, 3.0 m height and an energy dissipation capacity of 100 kJ were installed along the flank of the earthen dam and on top of the dam to prevent any material overtopping the dam (Fig. 2).



Figure 2: Installation of motion sensors on the high-tensile steel flexible rockfall protection barriers installed on the deflection dam.

## CONCLUSION

The example of the Axenstrasse rockfall monitoring and mitigation illustrates how a combination of organizational and structural measures can work for optimal protection and early warning, in order to keep closure times at a minimum and guarantee a sustainable use of this major N-S route. Thanks to the fast installation of the alarming system, the road was only closed for 46 days and could be re-opened for traffic on 12 September 2019. Since installation, the monitoring system has closed the street several hundred times – most of them with automatic re-opening.

## REFERENCES

- ASTRA (2020) Suchergebnisse Axenstrasse Steinschlag. Retrieved December 15, 2020, from: <https://www.astra.admin.ch/astra/de/home/suche.html#Axenstrasse%20Steinschlag>
- AXEN (2016) Initiative "Axen vors Volk – für Sicherheit ohne Luxustunnel". Retrieved December 15, 2020, from: <http://www.axen.ch/fakten-fuer-den-axen/>

## Rock slope cutting works near fragile speleothems: Choranche case study (Vercors, France)

Pierre BOTTELIN<sup>1</sup>, Laurent BAILLET<sup>2</sup>, Alexandre MATHY<sup>3</sup>, Laurent GARNIER<sup>4</sup>, Héloïse CADET<sup>1</sup>, Ombeline BRENGUIER<sup>1</sup>, Rémy ALLIER<sup>5</sup>, David CANTALUPI<sup>6</sup>

**Keywords:** Rock slope cutting; Blasting works; Speleothems; Vibration thresholds

Explosives are widely employed for geotechnical works in areas with outcropping or shallow bedrocks. In mountainous regions such as the Alps, explosives are used every day with various applications: e.g. quarrying, construction sites, rockfall mitigation, rock slope reprofiling, etc. Vibration-sensitive structures such as anthropic constructions (housing, communication infrastructures, ski resorts and lifts, hydraulic dams, ...) or natural stakes (geological features, wildlife, ...) are more and more present near blasting works. Their preservation requires a-priori definition of admissible vibration levels and their monitoring during blasting works.

In our case-study, crucial rock reprofiling works had to be conducted near very fragile and invaluable speleothems. Explosives were fired a few tens of meters far from the speleothems. Our work consisted in establishing admissible vibration thresholds from in-situ blast records, laboratory experiments and dynamic numerical simulations. We also supervised the vibration monitoring system during the reprofiling works.

### 1 STUDY SITE

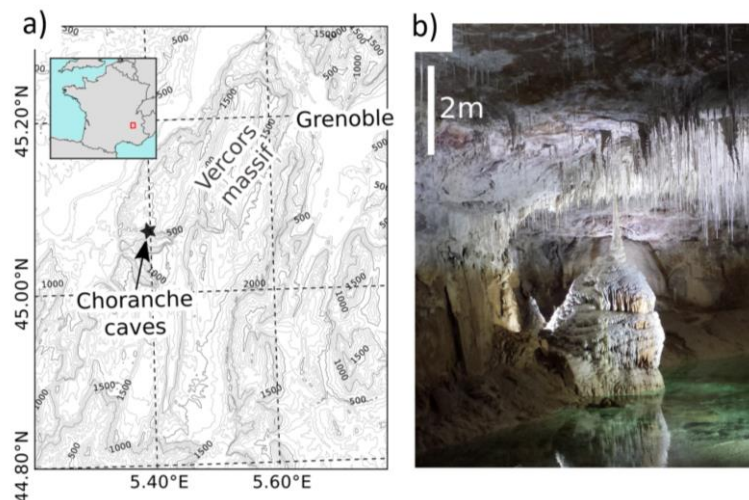


Figure 1: a) Location of the study site. b) Picture of the lake room with soda-straw at ceiling.

Choranche caves are located on the western side of the sedimentary Vercors massif, in the Gorges de la Bourne valley (Figure 1a). The caves host thousands of soda-straw speleothems, including very long and rare specimen (up to 3 m, Figure 1b) dating from ~30,000 years. The caves represent an exceptional geological inheritance (Delannoy, 1986) and welcome about 100,000 visitors per year (Garnier, pers. Comm. 2018). The unique access to the cave consists in a narrow, hanging pedestrian pathway which collapsed in 2018. Rock slope cutting works were hence crucial for access rehabilitation. It required rope-access blasting over about a 100 m long segment, only tens of meters away from the soda-straw room (Figure 1b).

### 2 VIBRATION STUDY

#### 2.1 Laboratory characterization

Static and dynamic properties of Choranche soda-straws were determined with lab experiments. Speleothem geometry, Young's modulus, density and rupture strengths were measured; as well as natural frequencies and damping (Figure 2a and b). Results were found in very good accordance with (Lacave et al., 2003) previous study.

Soda-straws were found behaving as Euler-Bernoulli beams. In situ blast records showed that soda-straws may be excited at modes higher than fundamental frequency ( $f_x > f_0$ , Figure 2b) contrary to most pseudo-static or arbitrary approaches found in the literature (Becker et al., 2006; Cadorin et al., 2001; Gribovszki et al., 2017; Konečný et al., 2015; Lacave et al., 2003).

<sup>1</sup> Association pour le Développement des Recherches sur les Glissements de Terrain (ADGRT), 2 rue de la Condamine, 38610 Gières, France, p.bottelin@adrgrt.org

<sup>2</sup> ISTERre, Université Grenoble Alpes, CNRS, F-38000 Grenoble, France, laurent.baillet@univ-grenoble-alpes.fr

<sup>3</sup> SAGE Ingénierie, 2 rue de la Condamine, 38610 Gières, France, a.mathy@sage-ingenierie.com

<sup>4</sup> SARL Site de la Grotte de Choranche, 2865 route des Grottes, BP7 38680 Choranche, France.

<sup>5</sup> CAN-Travaux d'accès difficile, Relut, 26270 Mirmande, France.

<sup>6</sup> ALPES MINAGES, 102 sentier de la Salle, 74110 Morzine, France.

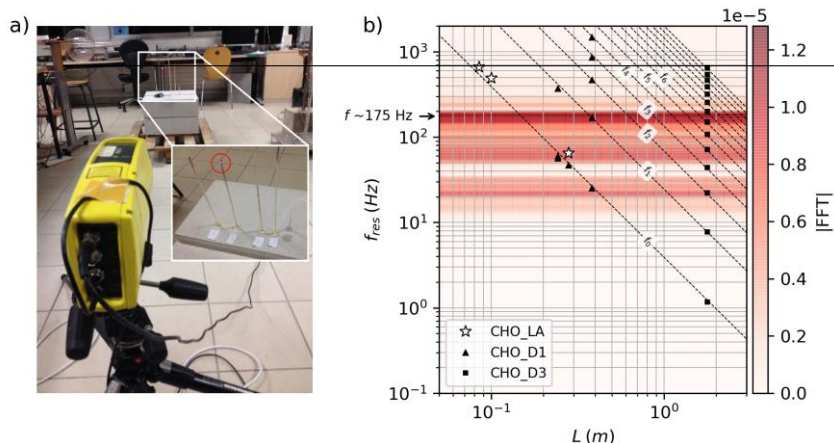


**Figure 2:** a) Lab experimental setup with laser vibrometer (yellow) pointing at speleothem's tip (red laser dot, red circle in inset). b) Soda-straw natural frequencies as a function of speleothem length. Spectral content of blast shot recorded on site is shown as coloured background.

## 2.2 Numerical simulations

A dynamic 2D finite-element code was used to compute the stress endured by the soda-straws during nearby blast shot. Both single shot (black curve, Figure 3a) and delayed blast (grey curve) were simulated. Soda-straw length ranged from 0.025 m to 3.0 m. Speleothems with specific length were found enduring peaks stresses (Figure 3a). This originates from speleothem resonance at various modes ( $f_0$ - $f_4$ ). We note that the highest stresses are undertaken by short speleothems at their fundamental mode. Longer speleothems are exposed at higher modes. Considering the admissible stress derived from lab experiments (dashed red line, Figure 3a), we derived an admissible vibration level expressed as Peak Particle Velocity. We hence set a 2.4 mm/s threshold for delayed shots and 8.6 mm/s for a single shot. Such limits compare well with regulatory thresholds used in literature for fragile assets, but taken into account intense resonance effect in such low-damping structures.

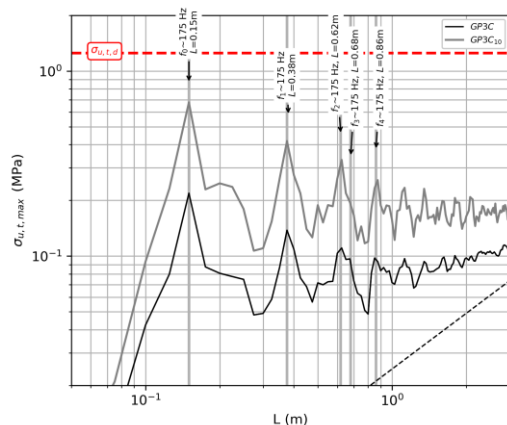


**Figure 3:** Tensile stress as a function of speleothem length, for both single shot (black curve) and delayed shot (grey curve) solicitation. The admissible stress derived from lab tests is shown as red dashed line.

## CONCLUSION

Our study yielded admissible vibration thresholds for speleothems which were monitored and observed during the blasting works, and no damage was observed on the speleothem population. The slope reprofiling hence allowed restoring the access to the caves together with preserving this exceptional geological inheritance. We showed that slender structures such as soda-straw may behave specifically under blasting solicitation, making classic methods obsolete. We believed that similar cases will multiply in the next years across the Alpine area.

## ACKNOWLEDGEMENTS

Full list of acknowledgements can be found in Bottelin et al., *J Seismol* **24**, 573–593 (2020). <https://doi.org/10.1007/s10950-020-09922-7>.

## REFERENCES

- Becker, A., Davenport, C.A., Eichenberger, U., Gilli, E., Jeannin, P.-Y., Lacave, C., 2006. Speleoseismology: A critical perspective. *J Seismol* **10**, 371–388. <https://doi.org/10.1007/s10950-006-9017-z>
- Cadorin, J.-F., Jongmans, D., Plumier, A., Camelbeeck, T., Delaby, S., Quinif, Y., 2001. Modelling of speleothems failure in the Hotton cave (Belgium). Is the failure earthquake induced? *Geologie en Mijnbouw* **80**, 315–322.
- Delannoy, J.-J., 1986. Contribution à l'étude des circulations aquifères dans le géosystème Coulmes-Choranche; Présentation du site expérimental de la Grotte de Coufin. *Revue de Géographie Alpine* **74**, 83–92. <https://doi.org/10.3406/rga.1986.2629>
- Gribovszki, K., Kovács, K., Mónus, P., Bokelmann, G., Konecny, P., Lednická, M., Moseley, G., Spötl, C., Edwards, R.L., Bednárík, M., 2017. Estimating the upper limit of prehistoric peak ground acceleration using an in situ, intact and vulnerable stalagmite from Plavecká priepast cave (Detrek(Hoi-zsomboly), Little Carpathians, Slovakia—first results. *Journal of Seismology* **21**, 1111–1130.
- Konečný, P., Lednická, M., Souček, K., Staš, L., Kubina, L., Gribovszki, K., 2015. Determination of dynamic Young's modulus of vulnerable speleothems. *Acta Montanistica Slovaca* **20**, 156–163.
- Lacave, C., Koller, M., Eichenberger, U., Jeannin, P.-Y., 2003. Prevention of speleothem rupture during nearby construction. *Environmental Geology* **43**, 892–900.

# TEMPERATURE DISTRIBUTION IN A PERMAFROST-AFFECTED ROCK RIDGE FROM CONDUCTIVITY AND INDUCED POLARIZATION TOMOGRAPHY

P-A. DUVILLARD<sup>1</sup>, F. Magnin<sup>2</sup>, A. Revil<sup>3</sup>, L. Ravanel<sup>4</sup>, P. Schoeneich<sup>5</sup>, P. Vaudelet<sup>6</sup>, J. Berthet<sup>7</sup>

**Keywords:** Permafrost, electrical conductivity, temperature.

## ABSTRACT IN ENGLISH:

Geoelectric prospecting is a widely used method for detecting and studying permafrost. The electrical resistivity has been recently combined with induced polarization measurements both in the laboratory and in the field. The use of a recently developed petrophysical model allows the conversion of conductivity and normalized chargeability into temperature. This methodology has been validated and independent modelling and data are used to assess the validity of the approach and discuss application to monitor parameters leading to mass movement.

## ABSTRACT IN FRENCH:

*La prospection géoelectrique est une méthode très utilisée pour détecter et étudier le permafrost. La résistivité électrique, qui a largement fait ses preuves en contexte de permafrost, est de plus en plus combinée à des mesures en polarisation provoquée sur le terrain ainsi qu'en laboratoire. L'utilisation de modèles pétrophysiques récemment développés permet ensuite de convertir les données électriques en données quantitatives comme la température. Cette méthodologie a été testée en haute montagne où des données thermiques permettent de valider les résultats et de discuter leur application pour le suivi de paramètres à l'origine du déclenchement des mouvements de masses.*

## 1 INTRODUCTION

Knowledge about the thermal state of steep alpine rock faces and of rock glaciers and the ice distribution is crucial to assess potential geohazards associated with the permafrost warming. Temperature measurements at the rock surface or in boreholes are however expensive, invasive, and provide spatially-limited information. Electrical conductivity tomography has been broadly used to detect and monitor mountain permafrost since 30 years on rock walls and rock glaciers (e.g. Magnin *et al.*, 2015; Mollaret *et al.*, 2019). Recent studies showed the interest of coupling, at several time and scales, methods of electrical conductivity tomography, induced polarization tomography in the field, in parallel with petrophysical characterization of core samples. The aim of the latter is to develop petrophysical transforms between geophysical observables and parameters of interest such as temperature. The advantages of these geophysical methods are their low cost and their non-invasive character. They provide 2D, 3D, and 4D tomograms/images of the subsurface.

## 2 SITE STUDY

The lower Cosmiques ridge is located at 800 m SSW of the Aiguille du Midi (3842 m a.s.l.), on the northwestern side of the Mont Blanc massif. The ridge is composed by fractured granite from the Hercynian metamorphic series. The extension of the SE face is 50-m-high and stands above the Glacier du Géant. The SE face is sometimes partially covered by snow in spring. The NW face is about 350-m-high, 35° with the vertical, and is highly rugged, allowing heterogeneous snow accumulation during a part of the year.

## 3 METHOD

Geophysical datasets were acquired at the lower Cosmiques bedrock ridge in 2016 and 2019 by conductivity and induced polarization tomography. Three rock surface temperature sensors were installed at a depth of 10 cm in 2016 July in the SE and NW faces and near the refuge foundation.

The conversion of electrical conductivity data into temperature was performed using petrophysical models previously developed (see Duvillard *et al.*, 2018). Electrical conductivity measurements were carried out on a rock sample in order to test the petrophysical model. After saturating the sample with melted snow water collected in the field, electrical conductivity measurements were performed between -15 °C and + 20 °C (see Coperey *et al.*, 2019). The

<sup>1</sup> STYX4D, Le Bourget-du-Lac, France, pierre-allain.duvillard@styx4d.com

<sup>2</sup> EDYTEM, Université Savoie Mont Blanc, CNRS, Le Bourget-du-Lac, France, florence.magnin@univ-smb.fr

<sup>3</sup> EDYTEM, Université Savoie Mont Blanc, CNRS, Le Bourget-du-Lac, France, andre.revil@univ-smb.fr

<sup>4</sup> EDYTEM, Université Savoie Mont Blanc, CNRS, Le Bourget-du-Lac, France, ludovic.ravanel@univ-smb.fr

<sup>5</sup> Institut d'Urbanisme et de Géographie Alpine, PACTE, Grenoble, France, philippe.schoeneich@univ-grenoble-alpes.fr

<sup>6</sup> NAGA Geophysics, Le Bourget-du-Lac, France, pierre.vaudelet@naga-geophysics.com

<sup>7</sup> STYX4D, Le Bourget-du-Lac, France, johan.berthet@styx4d.com

rock surface temperature were also used to force a MATLAB diffusive transient thermal model inside the ridge. Then, the models obtained by conversion of geoelectrical data will be qualitatively compared to thermal data measured directly at the subsurface and the diffusive transient thermal model (Duvillard *et al.*, 2020).

#### 4 RESULTS AND DISCUSSION

Electrical conductivity and normalized chargeability tomograms showed a similar distribution with rather low conductivity values under the NW face and higher values under the SE face (red colours on the figure). This suggests that the presence of permafrost is limited to the NW face with a vertical transition of permafrost below the hut and the absence of permafrost below the SE face. The Mean Annual Rock Surface Temperature (MARST) during the measurement period (from 2016 to 2018 August 15) was  $-3.7^{\circ}\text{C}$  on the NW face and  $+2.4^{\circ}\text{C}$  on the SE face. This is in agreement with suggestion from the petrophysical models and geophysical data, which displays permafrost conditions below the NW face but not below the SE face.

Then, the temperature distribution extracted from the electrical conductivity suggests a temperature of about  $-2^{\circ}\text{C}$  in the NW face, which is consistent with the temperature simulated from a surface temperature sensor from an external data set. This temperature modelling suggests that permafrost is close to the strength limit of ice joints, which could induce possible instabilities in the NW face.

Regarding the geophysical data, sources of errors are associated with (1) uncertainties in the inversion of the geophysical data, (2) uncertainties in the geophysical data and (3) uncertainties in the parameters entering in the petrophysical model. A complete analysis of the uncertainties associated with the two approaches is out of the scope of this paper. This being said, a future investigation will focus on a temperature tomogram that will combine 2-D numerical modelling of the heat equation with the geophysical data to get a balance in terms of combining the two types of information.

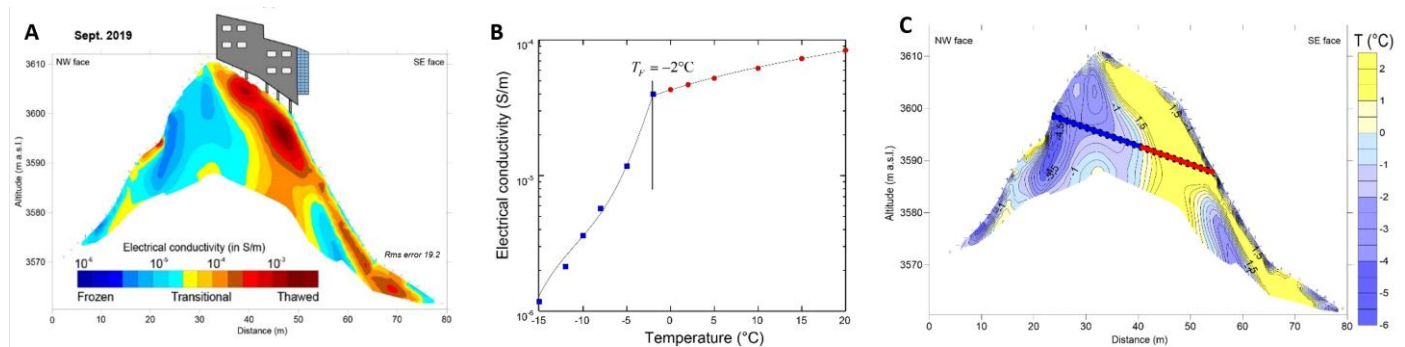


**Figure:** The three steps of Cosmiques hut study (Duvillard *et al.*, 2020). A) Electrical conductivity tomography (in  $\text{S m}^{-1}$ ) of the rock ridge below the Cosmiques hut in 2016; B) In-phase electrical conductivity data versus temperature for a granite core sample and fit of the data with the model from Duvillard *et al.* (2018); C) Distribution of the temperature determined from the electrical conductivity distribution for the 2019 tomogram.

#### CONCLUSION

These recent advances in geoelectrical methods for permafrost characterization show the great interest to use induced polarization and petrophysical models. In the short term, monitoring and repeating profiles over time with induced polarization gives new perspectives to quantitatively characterize the ice / water phase changes. In the future, joint inversion schemes will be developed using temperature data to help the inversion of the geophysical data and to improve the conversion of geoelectric data into temperature or water content.

#### ACKNOWLEDGEMENTS.

Authors thanks the keepers of the Cosmiques hut for the collaboration and all the geotechnical information provided. We thank E. Malet, M. Marcer, M. Rameau, C. Mörtl and G. Marsy for their help on the field.

#### REFERENCES

- Coperey A., Revil A., Abdulsamad F., Stutz B., Duvillard P.A, Ravanel L. (2019) Low frequency induced polarization of porous media undergoing freezing: preliminary observations and modelling. *Journal Geophys. Research*, 124.
- Duvillard P.A., Revil A., Qi Y., Soueid Ahmed A., Coperey A., Ravanel L. (2018) Three-dimensional electrical conductivity and induced polarization tomography of a rock glacier, *J. Geophys. Res.*, 123.
- Duvillard P. A., Magnin F., Revil A., Legay A., Ravanel L., Abdulsamad F., & Coperey A., (2021) Temperature distribution in a permafrost-affected rock ridge from conductivity and induced polarization tomography. *Geophysical Journal International*.
- Magnin F., Krautblatter M., Deline P., Ravanel L., Malet E. & Bevington, A. (2015). Determination of warm, sensitive permafrost areas in near-vertical rockwalls and evaluation of distributed models by electrical resistivity tomography, *J. Geophys. Res.*, 120, 745–762.

Mollaret C., Hilbich C., Pellet C., Flores-Orozco A., Delaloye R., Hauck C. (2019) Mountain permafrost degradation documented through a network of permanent electrical resistivity tomography sites, *The Cryosphere*, 13, 2557–2578.

# Keynotes

## 30 years of Rockfall Engineering research at PoliTO

Valerio DE BIAGI<sup>1</sup>, Monica BARBERO<sup>2</sup>, Marta CASTELLI<sup>2</sup>,  
Maddalena MARCHELLI<sup>2</sup>, Daniele PEILA<sup>2</sup>, Claudio SCAVIA<sup>2</sup>

**Keywords:** Rockfall engineering, Politecnico di Torino, past present and future

Politecnico di Torino is among the leading technical universities in Italy. Although located in a flat area, Torino has deep connections with mountain environments as large part of Piedmont and the surrounding regions are parts of the Alps. The deep connection between the academia and the real world resulted in joint projects with Public Authorities, companies and professionals for solving problems and proposing new engineered solutions to tackle rockfall hazard and risk. With more than 45 MSc theses on hazard analyses and case-studies, design approaches and simulations, and 65 international peer-reviewed papers, rockfall engineering represents an ongoing research activity at Politecnico di Torino. This paper briefly describes the 30 years of works and activities carried out at the university by various research teams.

### 1 INTRODUCTION

Politecnico di Torino is an Italian public university where high level engineering and architecture are taught. Although devoted to the education, research is among the main activities carried on in the university. Many skills merge together and multidisciplinary goals are usually achieved by researchers. Rockfall engineering studies at Politecnico di Torino started in the mid of the Nineties with the preliminary contributions of prof. Giani on rockfall propagation analyses and protection systems. The interests on the topic has grown during the following three decades and, nowadays, many researches of various disciplines are working on such topic: geologists, geotechnical engineers, mining engineers, survey experts, structural engineers, risk managers, geophysics, and so forth. A query on Scopus database provides very interesting results, showing a growing number of publications during the years. The total number of entries in the database in which “rockfall” appears in either the title or the keywords is 65, with a total of nearly 900 citations. Meanwhile, searches on the university library database provide information about MSc theses on rockfall engineering. A total number of 58 dissertation discussed since 2000 is found. Across the last three decades, the major contributions are provided by prof. Daniele Peila (total of 30 papers) on a large variety of facets of the topic. It is interesting to note that the contribution of Prof. Peila appears in approximately half of the indexed documents, meaning his large interests on the topic. In the next section, the research topics and the main research goals achieved by the various teams at Politecnico di Torino are reported and briefly discussed. A short selection of references is reported in the text, while the extended reference list can be found in citations databases.

### 2 RESEARCH TOPICS

#### 2.1 Rockfall risk assessment, reliability analyses and hazard management

Risk assessment is a key topic in the researches carried on at Politecnico di Torino. The first studies were conducted during the FP5-EESD IMIRILAND project devoted to the impact of large landslides in the mountain environment. In this framework, a GIS based approach has been conceived. Following the GIS based framework, a new QGIS tool, named QPROTO implementing the cone method to study the propagation area of rockfall phenomenon, has been delivered (Castelli et al., 2021). Relating to propagation analysis, fragmentation phenomenon has been studied (Marchelli & De Biagi, 2019) as well as the influence of protection forest. In 2010-11 specific studies focusing on quantification and management of rockfall risk in opencast quarrying activities were performed and a new methodology for rockfall risk analysis and management in quarry exploitation was published. Starting from 2013, studies have been devoted to rockfall risk on infrastructures by means of event tree analyses. Various configurations of the approach were proposed, tailored with the type of infrastructure interested by the phenomenon. In recent years, attention was devoted to the reliability analysis of rockfall protection systems, mainly net fences, with the purpose of building a framework for implementing Eurocode philosophy into the design of the net fences (Marchelli et al., 2021). To this purpose, a volume-return period rule was formulated, with details on the accuracy of the outputs (De Biagi et al., 2017). This approach merges observations on past events and evidences at the toe of the cliff through Poisson

---

<sup>1</sup> DE BIAGI Valerio, Politecnico di Torino, Torino, ITA, valerio.debiagi@polito.it

<sup>2</sup> Politecnico di Torino, Torino, ITA

point statistics and Pareto probability distribution. In addition, researches on hazard assessment focused on the quantification of the uncertainties in describing the phenomenon, pointing out some open issues in tackling rockfalls.

## 2.2 Rockfall protection systems: net fences, drapery meshes and embankments

The main contributions on net fences studies are related to the performance of such rockfall protection technologies. In detail, the first activities were devoted to the design of real-scale tests to assess the capacity of net fences. Such results were then implemented in ETAG 027 rules and, recently, in the Italian UNI 11211: 4. The core of the approach lays on the performance (energy and height) based design. In the last decade, the efficiency in time of net time has been investigated with FEM analyses, and in recent years, a quick assessment procedure to evaluate the level of deterioration on existing net fences was produced and a dataset of damages has been organized for future studies on the residual performance. The researches on drapery meshes focused on the design of such protection systems. In detail, Dr Bertolo, a former PhD of Politecnico di Torino, proposed a full-scale test procedure, which is able to permit the evaluation of the global behavior of a draped mesh (Bertolo et al. 2009). Such results later entered in Maccaferri design procedure of drapery meshes. Recently, Marchelli et al. worked on the effects of ageing and environmental actions on such meshes, focusing on maintenance and design for retrofit. The main contribution on the design of rockfall embankments was provided by Prof. Peila who performed full-scale tests on earth compacted and earth reinforced works (Peila et al., 2007). Meanwhile, such tests were numerically simulated through FEM and an energy based design procedure was formulated starting from the FEM simulations. Recently, DEM simulations were performed too.

## 2.3 Vulnerability of buildings

Studies on the vulnerability of buildings subjected to rockfall risk have been carried out by De Biagi and colleagues. The main contributions are devoted to the formulation of a event tree analysis framework to describe local and global effects of rockfall impact against a building. Although the approach was designed for frame RC structures, it can be easily extended to load bearing walls buildings. Recently, simplified formulae have been proposed to quantify the vulnerability of simple residential structures located in hazardous areas (Vallero et al. 2020).

## 2.4 Geophysics and microseismicity for rockfall monitoring,

Interesting applications of fractured rock mass monitoring in complex high altitude environments were performed in the framework of Interred 2007-2013 Alcotra Project no.56 MASSA. Here, a set of instruments to record the microseismicity of the soil was installed at the Carrel hut (3829 m a.s.l., Matterhorn, NW Alps). The results, coupled with temperature measurements provided interesting insights into the effects of permafrost on the stability of fractured rock masses (Occhiena & Pirulli, 2012).

## CONCLUSION

This paper presents a selection of research topics debated and deeply investigated at Politecnico di Torino, where lots of interests are still present and open questions, issues and ideas are formulated and investigated.

## REFERENCES

- Bertolo, P., Oggeri, C., Peila, D. (2009) Full-scale testing of draped nets for rock fall protection, *Canadian Geotechnical Journal*, 46: 306-317
- Castelli, M., Torsello, G., Vallero, G. (2021) Preliminary Modeling of Rockfall Runout: Definition of the Input Parameters for the QGIS Plugin QPROTO. *Geosciences*, 11: 88
- De Biagi V., Napoli M.L., Barbero M., Peila D. (2017) Estimation of the return period of rockfall blocks according to their size, *Natural Hazards and Earth System Sciences*, 17: 103-113
- Marchelli, M., De Biagi, V. (2019) Optimization methods for the evaluation of the parameters of a rockfall fractal fragmentation model. *Landslides*, 16: 1385-1396.
- Marchelli, M., De Biagi, V., Peila, D. (2021) Reliability-based design of rockfall passive systems height, *International Journal of Rock Mechanics and Mining Sciences*, 139: 104664
- Occhiena, C., Pirulli, M. (2012) Analysis of climatic influences on slope microseismic activity and rockfalls: Case Study of the Matterhorn peak (Northwestern Alps), *J. of Geotech Geoenv Eng* 138: 1012-1021
- Peila, D., Oggeri, C., Castiglia, C. (2007) Ground reinforced embankments for rockfall protection: design and evaluation of full scale tests. *Landslides*, 4: 255-265.

Vallero, G., De Biagi, V., Barbero, M., Castelli, M., Napoli, M.L (2020) A method to quantitatively assess the vulnerability of masonry structures subjected to rockfalls, *Natural Hazards* 103: 1307-1325

---

## Conférence Rock Slope Stability 2021 – Chambéry, France

### Proposition de plénière/Keynote Proposal

---

#### **Inspection, assessment and maintenance of rock slopes and excavated caverns of hydroelectric schemes for safety and sustainability**

Inspection, évaluation et maintenance des parois rocheuses et des cavernes des aménagements hydro-électriques pour la sécurité et la pérennité

**Marco Quirion, Judith Bouchard**  
**Hydro-Québec, Montréal, Québec, Canada**

**ABSTRACT:** Hydro-Quebec owns and operates more than 60 hydroelectric powerhouses and out of this number, 8 are excavated underground. From 600 dams owned by Hydro-Québec, 190 are categorized as “large” dams under the ICOLD definition, and the construction of all these hydroelectric schemes required large volume of rock excavations. Also, for many sites, high natural rock slopes are present in the vicinity of the installations. These plants were built over many decades, going from the early 1930s up to the present day. Excavated rock faces and natural slopes are submitted to weathering processes, prominently water, freeze-and-thaw and vegetation, leading to potential slope instabilities or rock falls. In addition, considering climate change, hazards could increase and aging of support systems could be impacted. To insure working personnel safety and long-term sustainability of the facilities, having a framework and an evaluation method for rock faces became essential, especially considering the large number of rock faces in Hydro-Quebec’s facilities. As a starting point, existing rock mass classification methods and rock fall hazard rating systems were thoroughly reviewed. Such systems were not directly applicable for the purpose of rock faces evaluation in the context of existing hydropower facilities. However, these methods serve as a sound basis for the development of an adapted rock slopes evaluation procedure that leads to a condition rating for the slope. It is required to evaluate the quality of the rock mass itself (loose blocks, vegetation, monitoring results, etc.) but also the installed protection systems (rock bolts, steel mesh, fences, etc.). Maintenance of rock faces during facility operations can be very complex and, it should be emphasized that, during the design and construction phases, rock support has to be selected or adapted to rock mass condition to insure safety and sustainability of the rock faces for many years.

**RÉSUMÉ:** Hydro-Québec possède et exploite plus de 60 centrales hydroélectriques et de ce nombre, 8 sont souterraines. Des 600 barrages appartenant à Hydro-Québec, 190 sont classés dans la catégorie des «grands» barrages selon la définition de la CIGB. La construction de tous ces aménagements hydroélectriques a nécessité un grand volume d’excavation dans le roc. De

---

plus, pour de nombreux sites, d'imposants talus rocheux naturels sont présents à proximité des installations. Ces aménagements ont été construits sur plusieurs décennies, du début des années 30 à nos jours. Les parois rocheuses excavées et les talus naturels sont soumis à des processus d'altération, principalement par l'eau, le gel-dégel et la végétation, entraînant des instabilités de pente ou des chutes de blocs. De plus, compte tenu des changements climatiques, la probabilité d'instabilités pourrait augmenter et le vieillissement des systèmes de protection du roc pourrait être affecté. Pour assurer la sécurité des travailleurs et la pérennité des installations, il est apparu essentiel de se doter d'un cadre et d'une méthode d'évaluation des parois rocheuses, surtout compte tenu du grand nombre de parois rocheuses dans les installations d'Hydro-Québec. Comme point de départ, les méthodes existantes de classification des massifs rocheux et les systèmes d'évaluation des risques de chute de blocs ont été soigneusement examinés. De tels systèmes n'étaient pas directement applicables aux fins de l'évaluation des parois rocheuses dans le contexte des installations hydroélectriques existantes. Cependant, ces méthodes constituent une base solide pour le développement d'une procédure d'évaluation des parois rocheuses qui conduit à la détermination d'une cote de l'état de la paroi. Il est nécessaire d'évaluer la qualité de la masse rocheuse elle-même (présence de blocs, végétation, auscultation, etc.) mais aussi les systèmes de protection installés (boulons de consolidation, treillis métalliques, barrières, etc.). L'entretien des parois rocheuses pendant les opérations de l'aménagement peut être très complexe et il convient donc de souligner que, pendant les phases de conception et de construction, la consolidation et la protection superficielle du roc doivent être sélectionnées ou adaptées à l'état de la masse rocheuse afin d'assurer la sécurité et la pérennité des parois rocheuses pour de nombreuses années.

---

# The Cliets, two major rockfalls at the Arly river (2014, 2019, Savoie, France)

Anne LESCURIER<sup>1</sup>, Lionel LORIER<sup>2</sup>

## Abstract

The Arly canyon is a major way for reaching Savoie ski resorts, the Chamonix valley and the Mont Blanc tunnel. This road goes through a narrow and windy canyon and has been historically damaged by numerous rock falls. On a geological standpoint the road goes through highly fractured micashists showing a series of stiff and compliant layers prone to high deformation.

Within the canyon, the Cliets location where rockfalls occurred in 1996 and 2003 shows a wide topple above the road. More recently two major rockfalls occurred at the Cliets in 2014 and 2019 involving volumes of 10 000 and 8 000 m<sup>3</sup>.

The company SAGE achieved for the department de la Savoie a surface displacement monitoring using automatic theodolites and extensometers. This monitoring confirmed the ongoing failure process (topple oriented West / South-West) and allowed triggering alerts and traffic shut down. For each of these rockfalls, experts were able to discriminate between previous transient slope accelerations and the final accelerations preceding these rockfalls.

The failure dates have been forecasted using Fukuzono and Azimi method allowing a traffic shut down nine days and one day before the events. Considering the high probability of a major movement of 10 000 m<sup>3</sup> a tunnel was dug to circumvent the Cliets rockmass. This 240 m length tunnel required building a new bridge on the Arly river. The construction of the tunnel was achieved in an unprecedented short time and showed technical challenges in particular related to the tunnel head and bridge pillars.

<sup>1</sup>CD 73 (Conseil Départemental de la Savoie), Chambéry, France, [anne.lescurier@savoie.fr](mailto:anne.lescurier@savoie.fr), Anne LESCURIER

<sup>2</sup>SAGE (Société Alpine de Géotechnique), Gières, France, [l.lorier@sage-ingenierie.com](mailto:l.lorier@sage-ingenierie.com), Lionel LORIER

# Author Index

- Abbasimaedeh Pouyan, 30, 31  
Acary Vincent, 51, 52  
Allier Rémy, 105, 106  
Astrade Laurent, 65, 66  
Atto Abdourrahmane, 4, 5  
Azemard Pierre, 19, 20
- Baillet Laurent, 40, 41, 105, 106  
Baratier Alexandre, 65, 66  
Baroth Julien, 74, 75
- Bartelt Perry, 15, 16, 21, 22, 49, 50, 53, 54  
Baudin Thierry, 19, 20  
Beaufils Mickaël, 63, 64  
Bebi Peter, 49, 50
- Bennani Braouli Yassine, 77, 78  
Berger Frédéric, 13, 14, 45–48  
Berthet Johan, 65, 66
- Berthet Rambaud Philippe, 65, 66  
Blumenschein Felix, 65, 66  
Bontognali Zeno, 9, 10  
Bost Marion, 77, 78
- Bottelin Pierre, 11, 12, 105, 106
- Bourrier Franck, 45, 46, 51, 52, 79, 80, 87, 88, 91, 92
- Brenguier Ombeline, 105, 106  
Buzzi Olivier, 6–8
- Bühler Yves, 21, 22, 49, 50
- Cadet Héloïse, 105, 106  
Cantalupi David, 105, 106  
Caritg Séverine, 19, 20  
Carrier Aurore, 11, 12  
Cathala Maëva, 13, 14
- Caviezel Andrin, 15, 16, 21, 22, 49, 50, 53, 54, 85, 86
- Chanut Marie-Aurélie, 4, 5  
Chaouni Abdel-Ali, 69, 70  
Cherifi Hicham, 69, 70  
Chollier Pauline, 74, 75
- Christen Marc, 15, 16, 21, 22, 49, 50, 53, 54  
Coccia Stella, 67, 68
- Colas Bastien, 19, 20, 47, 48  
Coperey Antoine, 42, 43  
Corona Christophe, 58, 59  
Couallier Vincent, 25, 26  
Courteille Hermann, 4, 5
- Cunha De Barros Santos Guilherme, 4, 5 117
- Daudon Dominique, 25, 26  
De Biagi Valerio, 111–113  
Deline Philip, 13, 14, 38, 39
- Dorren Luuk, 9, 10, 45, 46  
Dugelas Loic, 79, 80, 87, 88  
Dugelas Loïc, 89, 90
- Duvillard Pierre-Allain, 38, 39, 42, 43, 65, 66, 107–109
- Eckert Nicolas, 45, 46, 58, 59  
Eicher Manuel, 85, 86
- El Garouani Abdelkader, 32, 33  
Elkharrat Kévin, 23, 24
- Farvacque Manon, 71–73  
Fityus Stephen, 6–8  
Fontaine Firmin, 93–95
- Furet Agathe, 83, 84, 91, 92
- Galandrin Clément, 63, 64  
Galichet Sylvie, 4, 5  
Garnier Laurent, 105, 106
- Gasc Muriel, 4, 5, 23, 24, 32, 33  
Giacomini Anna, 6–8  
Giacona Florie, 58, 59  
Grimod Alberto, 81, 82  
Guccione Davide, 6–8  
Guitet Cécile, 19, 20  
Gutierrez Marte, 55, 56
- Halbwachs Camille, 17, 18  
Hantz Didier, 9, 10, 27, 28
- Hofmann Helene, 85, 86, 103, 104  
Homborg Catherine, 23, 24  
Horb Corinne, 34–37  
Hübl Johannes, 101, 102
- Jaboyedoff Michel, 9, 10  
Jabri Imane, 69, 70
- Jalouni Abdessamad, 69, 70  
Janeras Marc, 27, 28
- Jarrin Jean-Philippe, 17, 18, 83, 84, 91, 92  
Joffrin Patrick, 77, 78  
Josnin Jean-Yves, 38, 39
- Khatib Michel, 96, 97  
Khouz Abdellah, 60–62  
Korini Oltion, 77, 78  
Koschuch Richard, 101, 102

- Krebs Nora, 21, 22
- Lafuerza Sara, 23, 24
- Lambert Stephane, 74, 75, 93–95
- Lambert Stéphane, 83, 84, 91, 92
- Lamour Vincent, 30, 31
- Lantada Nieves, 27, 28
- Lanter Andreas, 85, 86
- Larose Eric, 40, 41
- Le Bidan Valentin, 58, 59
- Le Breton Mathieu, 40, 41
- Leblanc Frederique, 25, 26
- Legay Alexandre, 38, 39
- Legoff Elizabeth, 19, 20
- Lescurier Anne, 58, 59, 116
- Levy Clara, 4, 5, 19, 20, 47, 48
- Lorentz Julien, 91, 92
- Lorier Lionel, 116
- Lu Guang, 15, 16
- Magnin Florence, 13, 14, 38, 39
- Mangency Anne, 19, 20
- Manieri Robin, 58, 59
- Martin Rémy, 19, 20
- Mathy Alexandre, 105, 106
- Meier Lorenz, 65, 66, 103, 104
- Meignan Lucas, 4, 5, 74, 75
- Meyrat Guillaume, 21, 22
- Moor Roger, 103, 104
- Moos Christine, 9, 10, 45, 46
- Munch Jessica, 15, 16, 53, 54
- Méger Nicolas, 4, 5
- Mölk Michael, 101, 102
- Nahli Abdeljalil, 30, 31
- Nicot Francois, 79, 80, 87, 88
- Nuñez Amparo, 27, 28
- Olmedo Ignacio, 89, 90, 93–95
- Olmedo-Manich Ignacio, 79, 80, 87, 88
- Palau Joan, 27, 28
- Pedraza Oriol, 27, 28
- Peisser Carine, 74, 75
- Plotto Pierre, 96, 97
- Quirion Marco, 114, 115
- Rafiee Ali, 96, 97
- Ravel Ludovic, 13, 14, 38, 39, 65, 66
- Revil Andre, 42, 43
- Ringenbach Adrian, 15, 16, 21, 22, 49, 50, 53,
- 54
- Robit Philippe, 79, 80, 87–90, 93–95
- Rohmer Jérémy, 47, 48
- Roux Felix, 65, 66
- Sainte-Marie Pascal, 91, 92
- Saroglou Charalampos, 45, 46
- Schwarz Massimiliano, 45, 46
- Schöffl Tobias, 101, 102
- Serratrice Jean François, 98, 99
- Soueid Ahmed Abdellahi, 42, 43
- Stelzenmuller Nickolas, 4, 5
- Sthäly Severin, 65, 66
- Stihl Elia, 49, 50
- Stoffel Andreas, 49, 50
- Stoffel Markus, 45, 46
- Stähly Severin, 103, 104
- Tatin Maxime, 30, 31
- Thibault Thibault, 30, 31
- Thoeni Klaus, 6–8
- Thoraval Alain, 2, 3
- Trappmann Daniel, 45, 46
- Tribak Haytam, 32, 33
- Trouvé Emmanuel, 4, 5
- Utelli Hans-Heini, 45, 46
- Vaudelet Pierre, 42, 43
- Villard Pascal, 83, 84
- Vincent Hugues, 30, 31
- Wahlen Susanne, 103, 104

